

**Canterbury Earthquakes 2010/11 Port Hills Slope
Stability: Risk assessment for Redcliffs**

C. I. Massey
B. Lukovic
G. Archibald

F. Della Pasqua
W. Ries

T. Taig
D. Heron

**GNS Science Consultancy Report 2014/78
August 2014 FINAL**

DISCLAIMER

This report has been prepared by the Institute of Geological and Nuclear Sciences Limited (GNS Science) exclusively for and under contract to Christchurch City Council.

The report considers the risk associated with geological hazards. As there is always uncertainty inherent within the nature of natural events GNS Science gives no warranties of any kind concerning its assessment and estimates, including accuracy, completeness, timeliness or fitness for purpose and accepts no responsibility for any actions taken based on, or reliance placed on them by any person or organisation other than Christchurch City Council.

GNS Science excludes to the full extent permitted by law any liability to any person or organisation other than Christchurch City Council for any loss, damage or expense, direct or indirect, and however caused, whether through negligence or otherwise, resulting from any person or organisation's use of, or reliance on this report.

The data presented in this Report are available to GNS Science for other use after the public release of this document.

BIBLIOGRAPHIC REFERENCE

Massey, C. I.; Della Pasqua, F.; Taig, T.; Lukovic, B.; Ries, W.; Heron, D., Archibald, G. 2014. Canterbury Earthquakes 2010/11 Port Hills Slope Stability: Risk assessment for Redcliffs. *GNS Science Consultancy Report 2014/78*. 123 p. + Appendices

REVIEW DETAILS

This report in draft form was independently reviewed by Dr L. Richards and Dr J. Wartman. Internal GNS Science reviews of drafts were provided by N. Litchfield, J. Carey, D. Mieler and R. Buxton.

Risk calculations were checked by R. Buxton (GNS Science).

CONTENTS

EXECUTIVE SUMMARY	VIII
ES 1 INTRODUCTION.....	VIII
ES 2 INVESTIGATION PROCESS AND FINDINGS	VIII
ES 3 CONCLUSIONS	XI
ES3.1 Hazard	xi
ES3.2 Risk.....	xi
ES 4 RECOMMENDATIONS.....	XII
ES 4.1 Policy and planning	xii
ES4.2 Short-term actions	xii
ES4.3 Long-term actions.....	xiii
1.0 INTRODUCTION	1
1.1 BACKGROUND	1
1.2 THE REDCLIFFS MASS MOVEMENTS	5
1.2.1 Context and terminology	5
1.2.2 Local and random cliff collapse source areas	6
1.3 PREVIOUS WORK AT THE REDCLIFFS SITE	9
1.4 SCOPE OF THIS REPORT.....	13
1.5 REPORT STRUCTURE	14
1.6 METHODS OF ASSESSMENT.....	14
1.6.1 Engineering geology assessment	14
1.6.2 Hazard assessment.....	15
1.6.3 Risk assessment	17
2.0 DATA USED	21
3.0 SITE ASSESSMENT RESULTS	25
3.1 SITE HISTORY.....	25
3.1.1 Aerial photograph interpretation	25
3.1.2 Before the 2010/11 Canterbury earthquakes	26
3.1.3 During the 2010/11 Canterbury earthquakes	27
3.1.4 After the 2010/11 Canterbury earthquakes	28
3.2 SITE INVESTIGATIONS	29
3.2.1 Geomorphological mapping	29
3.2.2 Subsurface trenching and drilling	29
3.2.3 Surface movement	30
3.2.4 Subsurface movement	43
3.2.5 Groundwater	44
3.3 ENGINEERING GEOLOGICAL MODEL.....	45
3.3.1 Slope materials.....	45
3.3.2 Geotechnical properties	48
3.3.3 Rainfall and groundwater response.....	52
3.4 SLOPE FAILURE MODELS	56

3.4.1	Landslide types affecting the site	56
3.4.2	Cliff collapse failure mechanisms	57
4.0	HAZARD ASSESSMENT RESULTS	61
4.1	SLOPE STABILITY (SOURCE AREAS 1–3)	61
4.1.1	Slope stability – Static conditions (deep-seated failures).....	62
4.1.2	Slope stability – Dynamic conditions	68
4.1.3	Slope stability – Summary of results	77
4.2	RUNOUT DISTANCE	78
4.2.1	Potential future source volume estimation	78
4.2.2	Runout modelling	83
5.0	RISK ASSESSMENT RESULTS	91
5.1	TRIGGERING EVENT FREQUENCIES	91
5.1.1	Frequency of earthquake triggers	91
5.1.2	Frequency of rainfall triggers.....	95
5.2	DWELLING OCCUPANT RISK.....	96
5.2.1	Variables adopted for the risk assessment	96
5.2.2	Debris avalanche.....	97
5.2.3	Cliff-top recession.....	104
5.3	ROAD USER RISK	106
6.0	DISCUSSION.....	111
6.1	DWELLING OCCUPANT RISK.....	111
6.2	RISK TO THE ROAD USER.....	111
6.3	RISK ASSESSMENT SENSITIVITY TO UNCERTAINTIES	112
6.3.1	Debris volumes.....	112
6.3.2	Area of cliff-top lost.....	112
6.3.3	Debris runout	113
6.3.4	Other sensitivities and uncertainties.....	113
6.3.5	How reliable are the results?.....	113
7.0	CONCLUSIONS	115
7.1	HAZARD.....	115
7.2	RISK.....	115
7.2.1	Dwelling occupant	115
7.2.2	Road user	116
8.0	RECOMMENDATIONS.....	117
8.1	POLICY AND PLANNING.....	117
8.2	SHORT-TERM ACTIONS.....	117
8.2.1	Hazard monitoring strategy	117
8.2.2	Monitoring alerts and early warning	117
8.2.3	Surface/subsurface water control.....	117
8.2.4	Pavement closure.....	118
8.3	LONG-TERM ACTIONS.....	118
8.3.1	Engineering measures	118

8.3.2 Reassessment.....	118
9.0 REFERENCES	119
10.0 ACKNOWLEDGEMENTS.....	123

FIGURES

Figure 1	Location map.....	3
Figure 2	The Redcliffs mass movement location map showing the assessed source areas 1 and 2.	7
Figure 3	Aerial view of the Redcliffs mass movement area after the 4 September 2010 (Darfield) earthquake and before the 22 February 2011 earthquakes.....	9
Figure 4	Aerial view of the Redcliffs mass movement area after the 4 September 2010 (Darfield) earthquake and before the 22 February 2011 earthquakes.....	10
Figure 5	Aerial view of the Redcliffs mass movement area after the 22 February 2011 earthquakes and before the 13 June 2011 earthquakes.	11
Figure 6	Aerial view of the Redcliffs mass movement area after the 22 February 2011 earthquakes and before the 13 June 2011 earthquakes.....	11
Figure 7	Aerial view of the Redcliffs mass movement area after the 22 February 2011 earthquakes and before the 13 June 2011 earthquakes.	12
Figure 8	Aerial view of the Redcliffs mass movement area after the 22 February 2011 earthquakes and before the 13 June 2011 earthquakes.	12
Figure 9	Aerial view of the Redcliffs rock slope after the 13 June 2011 earthquakes. Photograph taken by C. Massey.....	13
Figure 10	Main features identified at the site from field mapping and the interpretation of historical aerial photographs.....	27
Figure 11	Engineering geological map.	31
Figure 12	Site investigation map.	32
Figure 13	Engineering geological cross-sections 1–6.	33
Figure 14	View to the west onto the main cliff at Redcliffs.....	48
Figure 15	Geological Strength Index plot for volcanic breccia and lava at Redcliffs (modified after Hoek 1999).....	49
Figure 16	Daily rainfalls at Christchurch Gardens and landslides in the Port Hills.	53
Figure 17	Rainfall depth-duration-return period relations estimated for Christchurch Gardens by Griffiths et al. (2009) using recorded rainfall data.....	55
Figure 18	Engineering geological model.	59
Figure 19	Schematic diagram showing the increasing frequency of defects in the slope in response to the successive 2010/11 Canterbury earthquakes.....	61
Figure 20	Example of limit equilibrium and finite element modelling results for cross-section 2 representing assessed source area 2, and adopting model 3 material parameters.	65
Figure 21	Example of limit equilibrium and finite element modelling results for cross-section 4, representing assessed source area 1, and adopting model 3 material parameters.	66
Figure 22	Example of limit equilibrium and finite element modelling results for cross-section 6, representing assessed source area 3, and adopting model 3 material parameters.	67
Figure 23	Modelled Slope/W decoupled displacements of cross-section 4 for the 22 February 2011 earthquake and adopting variable estimates of the material strength.	71

Figure 24	13 June 2011 earthquake, modelled Slope/W decoupled displacements for cross-section 4, and adopting variable estimates of the material strength.	71
Figure 25	Results from the seismic slope stability assessment for cross-section 4, for the 22 February 2011 earthquake, adopting model 1 material strength parameters.	72
Figure 26	Results from the seismic slope stability assessment for cross-section 4, for the 22 February 2011 earthquake, adopting model 2 material strength parameters.	72
Figure 27	Decoupled Slope/W displacements calculated for cross-section 4, for different ratios of yield acceleration to maximum average acceleration of the mass (K_y/K_{MAX}), and maximum acceleration of the mass (K_y/A_{MAX}), for selected slide-surface geometries, and given material shear strength parameter models 2 and 3. A_{MAX} is the peak acceleration of the input earthquake time acceleration history.	74
Figure 28	Relationship between free field peak ground accelerations at Redcliffs and the volume of debris leaving the Redcliffs slope.	78
Figure 29	Proportion and cumulative proportion of volume from cliff collapses in the Port Hills greater than or equal to a given volume.	80
Figure 30	Estimation of landslide volume assuming a quarter-ellipsoid shape.	80
Figure 31	Proportion of debris volume passing a given fahrboeschung angle (F-angle) line, from debris avalanches triggered during the 22 February and 13 June 2011 earthquakes at Redcliffs.	83
Figure 32	The empirical fahrboeschung relationships, expressed as the ratio of height (H) to length (L) for debris avalanche talus and boulder roll (rockfalls), recorded in the Port Hills. N = 45 sections.	84
Figure 33	Range of parameters used to back-analyse the runout of debris avalanches in the Port Hills triggered by the recent earthquakes using the RAMMS software (RAMMS, 2011).	85
Figure 34	Range of parameters for different mass movement processes: a) debris flows, b) snow avalanches, c) snow avalanches, d) ice avalanches, e) debris floods.	86
Figure 35	Mean volume difference between the RAMMS modelled volumes and the actual recorded volumes per 1 m ² grid cell. N = 23 debris avalanches triggered by 22 February and 13 June 2011 earthquakes.	86
Figure 36	Comparison between the RAMMS modelled and the empirical-modelled debris runout (Figure 32, and the actual recorded runout for debris avalanches triggered by the 22 February and 13 June 2011 earthquakes. N = 23 debris avalanches.	87
Figure 37	Debris avalanche hazard maps.	89
Figure 38	Cliff collapse annual individual fatality risk (scenarios A–C).	99
Figure 39	Cliff collapse annual individual fatality risk (scenario B 100% distributed).	102
Figure 40	Results from the debris avalanche risk assessment per scenarios A, B and C (dwelling occupant).	103
Figure 41	Results from the cliff top recession risk assessment, per scenarios A, B and C (dwelling occupant).	105
Figure 42	Road user risk maps (the contribution to road user risk per journey from individual grid cells along the road edges).	107
Figure 43	Road user risk per journey, central source volume estimates.	109
Figure 44	Road user annual fatality risk, central source volume estimates.	109
Figure 45	Risk per journey; lower assumed debris source volumes.	110
Figure 46	Risk per journey; upper assumed debris source volumes.	110

TABLES

Table 1	Assessed mass movement relative hazard exposure matrix (from the Stage 1 report, Massey et al., 2013).	5
Table 2	Risk scenarios used in the modelling of cliff collapses.	19
Table 3	Summary of the main data used in the analysis. LiDAR is Light Detecting and Ranging.	21
Table 4	Summary of observations from aerial photographs used to assess the site history at Redcliffs.....	25
Table 5	Summary of the ground investigations carried out at the site by Aurecon NZ Ltd. (Pletz and Revell, 2013) and Tonkin and Taylor Ltd. (Tonkin and Taylor, 2012a).....	29
Table 6	Measured total cumulate crack apertures (measured normal to the slope), which formed during the 2010/11 Canterbury earthquakes (mainly during the 22 February 2011 earthquakes and less so during the 13 June 2011 earthquakes).	39
Table 7	Measured cumulate crack apertures, horizontal only, which formed during the 13 June 2011 earthquakes, measured by M. Yetton (Geotech Ltd.; Appendix 4).	40
Table 8	Inferred cumulative crack apertures for the 22 February 2011 earthquakes.	40
Table 9	Estimated volumes lost from the cliffs calculated from the terrestrial laser scan (TLS) and LiDAR surveys.....	42
Table 10	Summary of drillhole inclinometer surveys.	44
Table 11	Engineering geological descriptions of the main geological units forming the cliffs (descriptions as per New Zealand Geotechnical Society, 2005).	47
Table 12	Range of adopted bulk soil strength parameters for Redcliffs soils.....	48
Table 13	Range of adopted rock strength parameters (for cross-section 4).....	50
Table 14	Shear wave velocity data and shear modulus used for modelling.	51
Table 16	Annual frequencies of given rainfall in the Christchurch for four main events following the 2010/11 Canterbury earthquakes (rainfalls are calculated daily from 09:00 to 09:00 NZST).....	54
Table 17	Material strength parameters used for modelling for cross-section 4 (similar parameters were adopted for sections 2 and 6, but the actual values used varied due to the different lithostatic stress range of the materials in the slope.	62
Table 18	Example results from slope stability assessment of source area 1 (cross-section 1).	64
Table 19	Results from the dynamic modelling of cross-section 4.....	70
Table 20	Forecast modelling results from the dynamic slope stability assessment for cross-sections 2, 4 and 6, adopting model 3 material parameters, and no water in tension cracks. Estimated displacements are rounded to the nearest 0.1 m.	76
Table 21	The volumes of debris leaving the slope during each of the 2010/11 Canterbury earthquakes and the earthquake's estimated peak ground acceleration, at the Redcliffs site – horizontal (H) and vertical (V) peak ground acceleration (PGA) components are listed separately.	78
Table 22	The estimated volumes of debris leaving the slope for different bands of peak ground acceleration (PGA).	79
Table 23	Example of estimated source volumes (the first digit in the number is significant) and fahrboeschung angles.	81
Table 24	Information used to estimate event volumes contributing to the total risk from non-seismic rockfall triggering events, all sites.....	82
Table 25	The annual frequency of a given peak ground acceleration (PGA) band occurring on rock (Site Class B) for different years from the 2012 seismic hazard model for Christchurch (G. McVerry, personal communication 2014).	91

Table 26	Proportion of the total debris volume per peak ground acceleration band allocated to distributed and local failures, for upper, central and lower estimates of volume (rounded to the nearest 100 m ³).....	92
Table 27	Forecast modelling results from the dynamic slope stability assessment for cross-sections 2, 4 and 6, adopting model 3 material parameters, and no water in tension cracks. Estimated displacements are rounded to the nearest 0.1 m.	94
Table 28	Representative annual event frequency of debris avalanches occurring, and the representative volume of the avalanche, for each time-period band.	95
Table 29	Area of cliff top lost per peak ground acceleration (PGA) band for upper, middle and lower volume estimates.....	104
Table 30	Volume of debris and area of cliff top lost per non-seismic band (based on historical rockfall rates in Massey et al., 2012a).	104
Table 31	Uncertainties and their implications for risk.	114

APPENDICES

A1	APPENDIX 1: METHODS OF ASSESSMENT.....	A1-1
A1.1	HAZARD ASSESSMENT METHOD.....	A1-1
	A1.1.1 Slope stability modelling.....	A1-1
	A1.1.2 Risk assessment.....	A1-6
A1.2	ROAD-USER RISK ASSESSMENT.....	A1-14
	A1.2.1 Background and Context.....	A1-14
	A1.2.2 Risk Modelling Approach.....	A1-15
	A1.2.3 Traffic Parameters on Main Road at Redcliffs.....	A1-16
	A1.2.4 Individual Risk per Journey – Hazard 1 (Impacted/Inundated by Debris).....	A1-19
	A1.2.5 Road user risk per journey and risk parameters derived from it.....	A1-22
A2	APPENDIX 2: RESULTS FROM AIRBORNE LIDAR SURVEYS.....	A2-1
A3	APPENDIX 3: RESULTS FROM TERRESTRIAL LASER SCAN SURVEYS.....	A3-1
A4	APPENDIX 4: RESULTS FROM SURVEYS OF CADASTRAL AND MONITORING SURVEY MARKS.....	A4-1
A5	APPENDIX 5: FIELD MAPPING OF CRACKS FOLLOWING THE MAIN EARTHQUAKES (CARRIED OUT BY M. YETTON, GEOTECH LTD).....	A5-1
A6	APPENDIX 6: RESULTS FROM THE TWO-DIMENSIONAL SITE RESPONSE ASSESSMENT FOR CROSS-SECTION 4.....	A6-1
A7	APPENDIX 7: RAMMS MODELLING RESULTS FOR SOURCE AREAS 1–3. ESTIMATED LANDSLIDE RUNOUT HEIGHT.....	A7-1
A8	APPENDIX 8: RAMMS MODELLING RESULTS FOR SOURCE AREAS 1– 3, ESTIMATED LANDSLIDE RUNOUT VELOCITY.....	A8-1
A9	APPENDIX 9: ROCFALL MODELLING RESULTS FOR CROSS-SECTIONS 2, 4 AND 6.....	A9-1
A10	APPENDIX 10: STERONET KINEMATIC ANALYSIS OF REDCLIFFS DISCONTINUITY DATA.....	A10-1

APPENDIX FIGURES

Figure A1.1	Expanded calculation of the probability of each local source area “scoop” occurring.....	A1-9
Figure A1.2	Main Road section modelled (opposite Redcliffs Park).	A1-14
Figure A1.3	View northwest along the Main Road section assessed for Redcliffs (image taken from Google Earth).	A1-15
Figure A1.4	Possible boulder/road user collision configurations.....	A1-20
Figure A6.1	Amplification relationship between the synthetic free-field rock outcrop input motions (A_{FF}) and the modelled cliff crest maximum accelerations (A_{MAX}) for cross-section 4.....	A6-2
Figure A6.2	Modelled peak horizontal ground acceleration contours for the 22 February 2011 earthquake at Redcliffs, cross-section 4, adopting the 2003 airborne LiDAR slope surface geometry.....	A6-3
Figure A6.3	Relationship between the modelled horizontal and vertical maximum accelerations modelled at the convex break in slope (A_{MAX}) for cross-section 4, using the synthetic free-field rock outcrop motions for the Redcliffs site by Holden et al. (2014) as inputs to the assessment.	A6-4

APPENDIX TABLES

Table A1.1(a)	Estimated westbound traffic on Main Road at Redcliffs.	A1-17
Table A1.1(b)	Estimated eastbound traffic on Main Road at Redcliffs.	A1-18
Table A1.2	Correlation between traffic levels and average speeds/separations.....	A1-18
Table A1.3	Summary of road user numbers and average speeds.....	A1-19
Table A1.4	Road user speeds and times per journey within 2 m cell.....	A1-21
Table A1.5	Calculation of risk parameters of interest from single cell risk per journey.	A1-23
Table A6.1	Results from the two-dimensional site response assessment for cross-section 4, using the out-of-phase synthetic free-field rock outcrop motions for the Redcliffs site by Holden et al. (2014) as inputs to the assessment. PGA is peak ground acceleration.....	A6-1

EQUATIONS

Equation 1	17
Equation 2	51
Equation 3A	A1-10
Equation 3B	A1-10
Equation 3C	A1-10
Equation 4A	A1-11
Equation 4B	A1-11
Equation 5	A1-12
Equation 6	A1-15
Equation 7	A1-20
Equation 8	A1-20
Equation 9	A1-21
Equation 10	A1-21
Equation 11	A1-21

EXECUTIVE SUMMARY

ES 1 INTRODUCTION

This report brings together recent field information on the Redcliffs site and uses numerical models of slope stability to assess the risk to people in dwellings and users of Main Road from cliff-collapse hazards (debris avalanches and cliff-top recession) at the site, over and above those assessed in an earlier cliff collapse study (Massey et al., 2012a).

Following the 22 February 2011 earthquakes, extensive cracking of the ground occurred in some areas of the Port Hills. In many areas, the cracks were thought to represent only localised relatively shallow ground deformation in response to shaking. In other areas, however, the density and pattern of cracking and the amounts of displacement across cracks clearly indicated large mass movements.

Christchurch City Council contracted GNS Science to carry out further detailed investigations of these areas of systematic cracking, in order to assess the nature of the hazard, the frequency of the hazard occurring, and whether the hazard could pose a risk to life, a risk to existing dwellings and/or a risk to critical infrastructure. This work on what are termed mass movements is being undertaken in stages. Stage 1 is now complete (Massey et al., 2013) and stages 2 and 3 are detailed investigations of mass movements from highest to lowest priority.

The Stage 1 report identified 36 mass movements of concern in the Port Hills project area. Four of these were further subdivided based on failure type, giving a total of 46 mass movements including their sub areas. Fifteen of these were assessed as being in the Class I (highest) relative hazard-exposure category. Mass movements in the Class I category could cause loss of life, if the hazard were to occur, as well as severe damage to dwellings and/or critical infrastructure, which may lead to the loss of services for many people.

Redcliffs mass movement area was assessed in the Stage 1 report (Massey et al., 2013) as being in the highest relative hazard exposure category (Class I, involving potential risk to life). Following the 22 February 2011 earthquakes significant localised cracking was noted in the loess (soil) mantling the steep rock slope and in the cliff face at the Redcliffs mass movement.

This report, as part of the Stage 2 investigations, presents the revised risk assessment results for the Redcliffs Class I mass movement.

ES 2 INVESTIGATION PROCESS AND FINDINGS

Detailed investigations of the site and its history were carried out by GNS Science. These investigations have identified several relict landslides (up to 10,000–15,000 m³ in volume) at the site that appear to date from before the time of European settlement (about 1840 AD). Rockfalls are also apparent from the steep rock slope in aerial photographs covering the period 1946–1984. The areas of past failures from the slope coincide with the same areas that failed during the 2010/11 Canterbury earthquakes.

The slopes at Redcliffs were significantly cracked during the 22 February, 16 April, 13 June and 23 December 2011 earthquakes. Up to 24,000 m³ of debris fell from the slope during the 22 February 2011 earthquake and the cliff top recessed by up to 7 m during the 13 June 2011 earthquake.

The relative ground displacements at this site through the 2010/11 Canterbury earthquakes are constrained by the mapping of crack apertures, measured before and after the main earthquakes. The bulk strength of the rock mass forming the slope was weakened by cracking, and in particular, the presence of open surface cracks have made the slope more susceptible to the ingress of run-off water.

The main types of landslide hazard identified at the site are debris avalanches and cliff-top recession, which are a relatively rapid type of landslide involving many hundreds to thousands of boulders. The risk to life of people in dwellings from debris avalanches and cliff top recession hazards associated with the steep rock slope has already been estimated by Massey et al. (2012a).

Further investigation of the site has involved field mapping, ground investigation (comprising subsurface drilling and trenching), laboratory testing, numerical modelling and monitoring (of the features in the field and how they have responded to earthquakes and rain).

The further investigation has identified an additional three potential source areas, where local larger volumes of rock may fall from the cliff, during a triggering event, as single or multiple failures, with the resultant debris travelling further on the valley floor than occurred in the 2010/11 Canterbury earthquakes. This is the reason for the Redcliffs mass movement being included in the Class I (high priority for further investigation) mass movements.

This assessment improves on the original work in Massey et al. (2012a) by taking into account:

1. Large localised failures from three assessed source areas; and
2. Other failures, randomly distributed across the slope.

These three assessed source areas are in addition to the randomly distributed source areas, from which debris could fall from anywhere along the cliff. Numerical models have been used to assess the stability of the Redcliffs slopes, in particular the three potential landslide sources. Analyses have considered both:

- static (without earthquake shaking); and
- dynamic (with earthquake shaking) conditions.

Cliff-collapse hazards

Cliff-top recession and associated debris avalanches pose the greatest landslide hazards and landslide risk to people on the cliff top (Glendever Terrace) and cliff toe. These slope-instability processes form the basis of the hazard and risk assessments contained in this report.

Under current conditions, it is possible for failure of the slope to occur under either static or dynamic conditions. However, it should be noted that material strengths – and therefore the slope factors of safety – may reduce with time (weathering), water content, and further movement of the slope under either static or dynamic conditions.

For non-earthquake triggers, given the relatively low static factors of safety, an increase in pore water pressures in open tension cracks within the overlying loess and joints within the underlying rock mass could lead to instability of the slope under static conditions (i.e., short duration, high intensity rain) especially where antecedent rainfall has been high.

For earthquake triggers, given the relatively low yield acceleration of the slope, it is likely that future earthquakes could generate permanent displacements that could be quite large, and potentially lead to large volumes of debris falling from the slope. Earthquake-induced failures are likely to be larger in volume and the debris travel further, due to the larger volume, than rainfall-induced failures.

Parts of the slope crest have already undergone more than one metre of permanent slope displacement, during the 2010/11 Canterbury earthquakes and this displacement may have reduced the shear strength of critical materials in the slope, making the slope more susceptible to future earthquakes.

Failure volumes and triggering frequencies

The volumes of rock that could fall from the cliff under dynamic (earthquake) and static (non-earthquake, e.g., rain) conditions have been assessed.

The original cliff-collapse risk assessment by Massey et al. (2012a) was based on future failures that were all randomly distributed across the slope face. The results of the engineering geological assessments identified that although many failures were randomly distributed across the slopes, these failures only accounted for a relatively small proportion of the total volume of rock leaving the slopes. Much of the debris leaving the Redcliffs slope (and other similar slopes in the Port Hills), derived from a few non-random (local) failures that involved larger volumes of rock, particularly in areas where the rock mass strength had been weakened as a result of earthquake-induced cracking.

The volumes of material involved in, and the frequency of, cliff collapse from the slopes are assessed. Three source-volume ranges (upper, middle and lower volumes), and seven earthquake event annual frequencies (representing different ranges of peak ground acceleration), and four non-earthquake event band annual frequencies (representing mainly rainfall triggers) have been modelled. All are uncertain and the frequency of the triggering events is particularly uncertain.

Three scenarios have been adopted for modelling the risk to dwelling occupants and users of Main Road to provide an indication of the range of uncertainty associated with the risk estimates. The three scenarios span reasonable ranges of: 1) the assessed total volume that could be generated in a representative event; and 2) the volume of debris that passes a given distance down the slope.

ES 3 CONCLUSIONS

With reference to the assessment area boundary as shown in Figure 2, the conclusions of this report are:

ES3.1 Hazard

1. The strength of the rock mass forming the slope at Redcliffs has been reduced by earthquake-induced fractures and movement and it will continue to weaken over time due to factors such as physical and chemical weathering, wetting and drying and further ground movement. Failures, of volumes of rock greater than those that failed during the 2010/11 Canterbury earthquakes, from the cliff are now more likely to be triggered by future earthquakes or by non-earthquake triggers such as rain. Failure volumes triggered by earthquakes may now be larger than any that fell during the 2010/11 Canterbury earthquakes; they could be more similar in size to past failures (from the same slope) identified from pre-1940 aerial photographs and pre-2010/11 earthquakes slope geometry.
2. Revised debris-avalanche dwelling risk maps (revised from those by Massey et al., 2012a) – incorporating local larger source volumes, and both physically and empirically based debris runout models – have little effect on the original risk estimates.

ES3.2 Risk

ES3.2.1 Dwelling occupant

1. There are very few additional dwellings in the revised debris avalanche or cliff recession zones, within the assessment area, that do not already have “red zone” offers made by the Canterbury Earthquake Recovery Authority and based on the previously assessed cliff-collapse risk.
2. Earthquake-triggered cliff collapses contribute most to the risk.
3. The results show that the most critical uncertainty in the risk assessment is the volumes of material that could be generated at different bands of peak ground acceleration. There is approximately two orders of magnitude difference (a factor of 100 times) in the risk estimates between the upper and lower failure volume estimates (scenarios A and C respectively).
4. The inclusion of the assessed source areas 1–3 in the risk assessment increases the runout and hence the risk further out from the toe of the slope. However, there is little difference between the risk estimates including the local source areas 1–3 and those where the entire debris is distributed randomly across the slope. This is because the volume of debris, and therefore risk, is already high in these areas from distributed failures alone, and so the inclusion of additional debris from source areas 1–3 does not significantly increase the area where people are exposed to high levels of risk.
5. The largest difference between the original risk estimates (Massey et al., 2012a) and those presented in this report is at the cliff crest. The inclusion of earthquake triggered source areas 1–3 increases the width of the cliff top recession risk zone because the annual individual fatality risk bands have widened.

ES3.2.2 Road user

1. The rockfall risk is greatest for the slowest road users (pedestrians, then cyclists), because their slower travel exposes them to risk for longer on each journey.
 - a. The rockfall risk is significantly higher on the side nearest the slope than on the opposite side of the road.
 - b. Based on middle debris volume estimates, individual risk to road users of Main Road at Redcliffs for the section of road assessed is among the highest per journey assessed for Port Hills roads, and comparable to the road risks assessed for the Deans Head mass movement.
 - c. The rockfall risk falls to virtually zero on the far side of the road, and to virtually zero using the lower debris volume estimates modelled in this assessment.
2. The most pressing issue appears to relate to the section of Main Road within the risk zone. This section of Main Road currently has containers placed along the inside of the road, nearest the slope, to protect road users from falling debris. These measures are temporary. The footpath along this section of road is also closed.

ES 4 RECOMMENDATIONS

GNS Science recommends that based on the results of this study, Christchurch City Council:

ES 4.1 Policy and planning

1. Decide what levels of life risk to dwelling occupants and road users will be regarded as tolerable.
2. Decide how Council will manage risk on land where life risk is assessed to be at the defined threshold of intolerable risk and where the level of risk is greater than the threshold.
3. Prepare policies and other planning provisions to address risk lesser than the intolerable threshold in the higher risk range of tolerable risk.

ES4.2 Short-term actions

ES4.2.1 Hazard monitoring strategy

1. Include the report findings in a slope stability monitoring strategy with clearly stated aims and objectives, and list how these would be achieved, aligning with the procedures described by McSaveney et al. (2014). In the meantime, extend the current survey network (by increasing the number of slope monitoring marks) further up the slope (particularly into source area 1), so as to maintain awareness of changes in the behaviour of the slope.
2. Ensure that the emergency management response plan for the area identifies the dwellings that could be affected by movement and runout, and outlines a process to manage a response.

ES4.2.2 Monitoring alerts and early warning

Monitoring the slope for early warning of potentially dangerous trends in groundwater or slope movement as part of a hazard warning system is not recommended. Monitoring alerts for slope deformation and groundwater changes cannot be relied upon to provide adequate early warning as experience from Port Hills and elsewhere shows that deformation and groundwater changes can occur rapidly, with little warning.

ES4.2.3 Surface/subsurface water control

Reduce water ingress into the slopes, where safe and practicable to do so, by:

- a. Identifying and relocating all water-reticulation services (water mains, sewer pipes and storm water) inside the identified mass-movement boundaries (at the slope crest) to locations outside the boundary, in order to control water infiltration into the slope. In particular, a storm water main currently traverses the crest of source area 1; and
- b. Filling the accessible cracks on the slope and providing an impermeable surface cover to minimise water ingress.
- c. Control surface water flow and direct away from mass movement area and into the appropriate storm water system.

ES4.2.4 Pavement closure

1. Maintain the closure of the pavement on the slope-side of the road, and continue to divert pedestrians onto the footpath on the seaward side of the road.
2. It is not known how effective the current temporary containers would be if impacted by a sizable debris avalanche (as per those discussed in this report). The effectiveness of such temporary risk management measures should be reassessed to ensure they are “fit-for-purpose”.

ES4.3 Long-term actions

ES4.3.1 Engineering measures

1. There appears to be reasonable scope to realign the at-risk section of Main Road further away from the bottom of the slope, outside the debris avalanche risk zone.
2. For the section of Main Road within the risk zone, liaise with whoever is responsible for roading in this area to ensure that the debris avalanche risk is taken into account in any road design (or in the design of modifications to the road).

ES4.3.2 Reassessment

Reassess the risk and revise and update the findings of this report in a timely fashion, for example:

- a. in the event of any changes in ground conditions; or
- b. in anticipation of further development or land use decisions.

1.0 INTRODUCTION

This report uses results from recent field investigation and numerical models of slope stability for the Redcliffs site to assess the risks to people in dwellings and users of Main Road from cliff-collapse hazards (debris avalanches and cliff-top recession. This report provides an update from the original risk assessment for Redcliffs presented by Massey et al. (2012a).

1.1 BACKGROUND

Following the 22 February 2011 earthquakes, members of the Port Hills Geotechnical Group (a consortium of geotechnical engineers contracted to Christchurch City Council to assess slope instability in the Port Hills) identified some areas in the Port Hills where extensive cracking of the ground had occurred. In many areas, cracks were thought to represent only localised relatively shallow ground deformation in response to shaking. In other areas however, the density and pattern of cracking and the amounts of displacement across cracks clearly indicated that larger areas had moved systematically *en masse* as a mass movement.

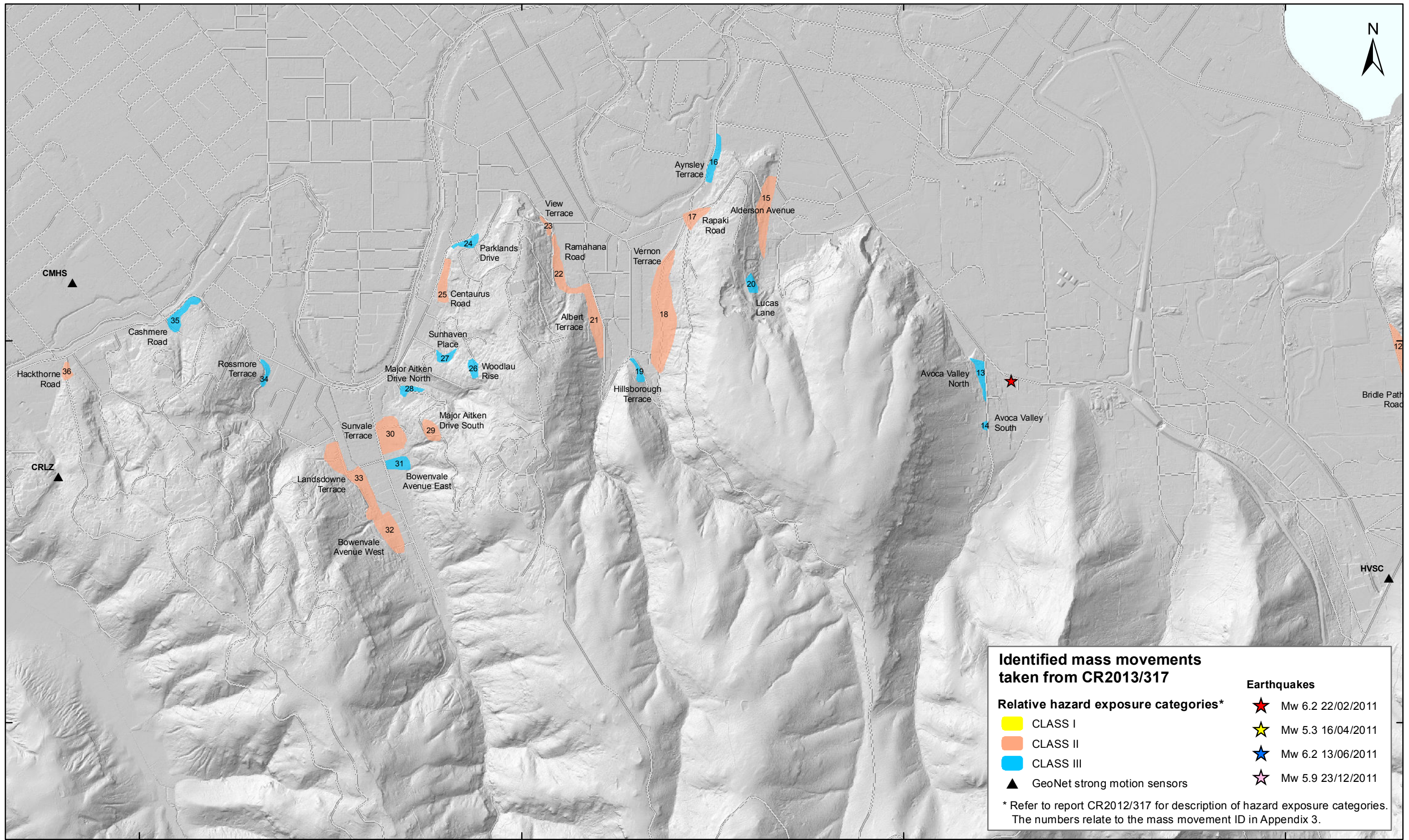
Christchurch City Council contracted GNS Science to carry out detailed investigations of the identified areas of mass movement, in order to assess the nature of the hazard, the frequency of the hazard occurring, and whether the hazard could pose a risk to life, a risk to existing dwellings and/or a risk to critical infrastructure (defined as water mains, sewer mains, pump stations, electrical substations and transport routes). This work is carried out under Task 4 of contract No. 4600000886 (December 2011).

The main purpose of the Task 4 work is to provide information on slope-stability hazards in the Port Hills. This is to assist Christchurch City Council land-use and infrastructure planning and management in the area, as well as to establish procedures to manage on-going monitoring and investigation of the hazards.

The Task 4 work is being undertaken in stages. Stage 1 is now complete (Massey et al., 2013; hereafter referred to as the Stage 1 report) and comprised: 1) a list of the areas susceptible to significant mass movement; 2) the inferred boundaries of these areas (as understood at the time of reporting); and 3) an initial “hazard-exposure” assessment (Table 1) intended only to prioritise the areas with regards to future investigations.

The Stage 1 report identified 36 mass movements of concern in the Port Hills project area. Four of these were further subdivided based on failure type, giving a total of 46 mass movements including their sub areas (Figure 1). Fifteen of these were assessed as being in the Class I (highest) relative hazard-exposure category. The results of their detailed investigation and assessment are presented in Stages 2 and 3, which includes this (Stage 2) report on the Redcliffs mass movement. The Redcliffs study area includes the Glendever Terrace (8) and Balmoral Lane (9) mass movements shown on Figure 1. Mass movements assessed as being in the Class I category may cause fatalities severe damage to dwellings and/or damage critical infrastructure leading to loss of services for many people if the hazard were to occur.

The Stage 1 report recommended that mass movements in the Class I relative hazard-exposure category be given high priority by Christchurch City Council for detailed investigations and assessment.



SCALE BAR: 0 0.5 1 km

EXPLANATION:
 Refer to Appendices 2 and 3 of report CR2012/317 for maps and more details of each mass movement.
 Background shade model derived from NZAM post earthquake 2011c (July 2011) LiDAR survey resampled to a 1 m ground resolution.
 Roads provided by Christchurch City Council (20/02/2012).
 PROJECTION: New Zealand Transverse Mercator 2000

DRW:
BL
 CHK:
CM



LOCATION MAP

**Port Hills
Christchurch**

FIGURE 1

Map 2

FINAL

REPORT:
CR2014/78

DATE:
August 2014

Table 1 Assessed mass movement relative hazard exposure matrix (from the Stage 1 report, Massey et al., 2013).

		Hazard Class		
		1. Displacement* greater than 0.3 m and debris runout	2. Displacement* greater than 0.3 m; no runout	3. Displacement* less than 0.3 m; no runout
Consequence Class	1. Life – potential to cause loss of life if the hazard occurs	CLASS I	CLASS III	CLASS III
	2. Critical infrastructure ¹ – potential to disrupt critical infrastructure if the hazard occurs	CLASS I	CLASS II²	CLASS II
	3. Dwellings – potential to destroy dwellings if the hazard occurs	CLASS I	CLASS II	CLASS III

*Note: Displacements for each assessed mass movements are inferred by adding together the mapped crack apertures (openings) along cross-sections through the assessed mass movements. They are a lower bound estimate of the total displacement, as no account is given for plastic deformation of the mass and not every crack has been mapped.

¹ Critical infrastructure is defined, for the purpose of this report, as infrastructure vital to public health and safety. It includes transport routes (where there is only one route to a particular destination), telecommunication networks, all water related mains and power networks (where there is no redundancy in the network), and key medical and emergency service facilities. Networks include both linear features such as power lines or pipes and point features such as transformers and pump stations.

² This relative hazard exposure category is based largely on an assumption that ‘critical infrastructure’ exists within these areas. Until further assessments are made on the nature of toe slumps and the existence of critical infrastructure in these areas, the relative hazard exposure category of these assessed mass movements has been appropriately assessed as “Class II”. It is likely that many of the assessed mass movements in the Class II relative hazard exposure category (where the hazard class is 2 and the consequence class is 2) would be more appropriately classified as “Class III” following further assessments.

1.2 THE REDCLIFFS MASS MOVEMENTS

The Redcliffs mass movement area is shown in Figures 1 and 2. This mass movement area was assessed in the Stage 1 report (Massey et al., 2013) as being in the highest relative hazard exposure category (Class I). During the 22 February 2011 earthquake, two people were killed from falling rock at Redcliffs; one person was inside a dwelling and another was in their garden, both at the bottom of the slope in the debris runout zone. The risk to life of people in dwellings at the slope crest and toe from debris avalanche and cliff top recession hazards (collectively termed cliff collapse) presented in this report provides an update from the original risk assessment for Redcliffs presented by Massey et al. (2012a).

1.2.1 Context and terminology

This report uses the terms: “cliff-top recession” to describe the result of landslides from the top and face of cliffs, and “debris avalanche” to describe the landslide process that inundates land at the cliff foot (referred to as “toe”) with countless boulders. The two are collectively referred to as cliff collapse.

Debris avalanche refers to a type of landslide comprising many boulders falling simultaneously from a slope. The avalanching mass starts by sliding, toppling or falling before descending the slope rapidly (>5 m/sec) (following Cruden and Varnes, 1996) by any combination of falling, bouncing and rolling.

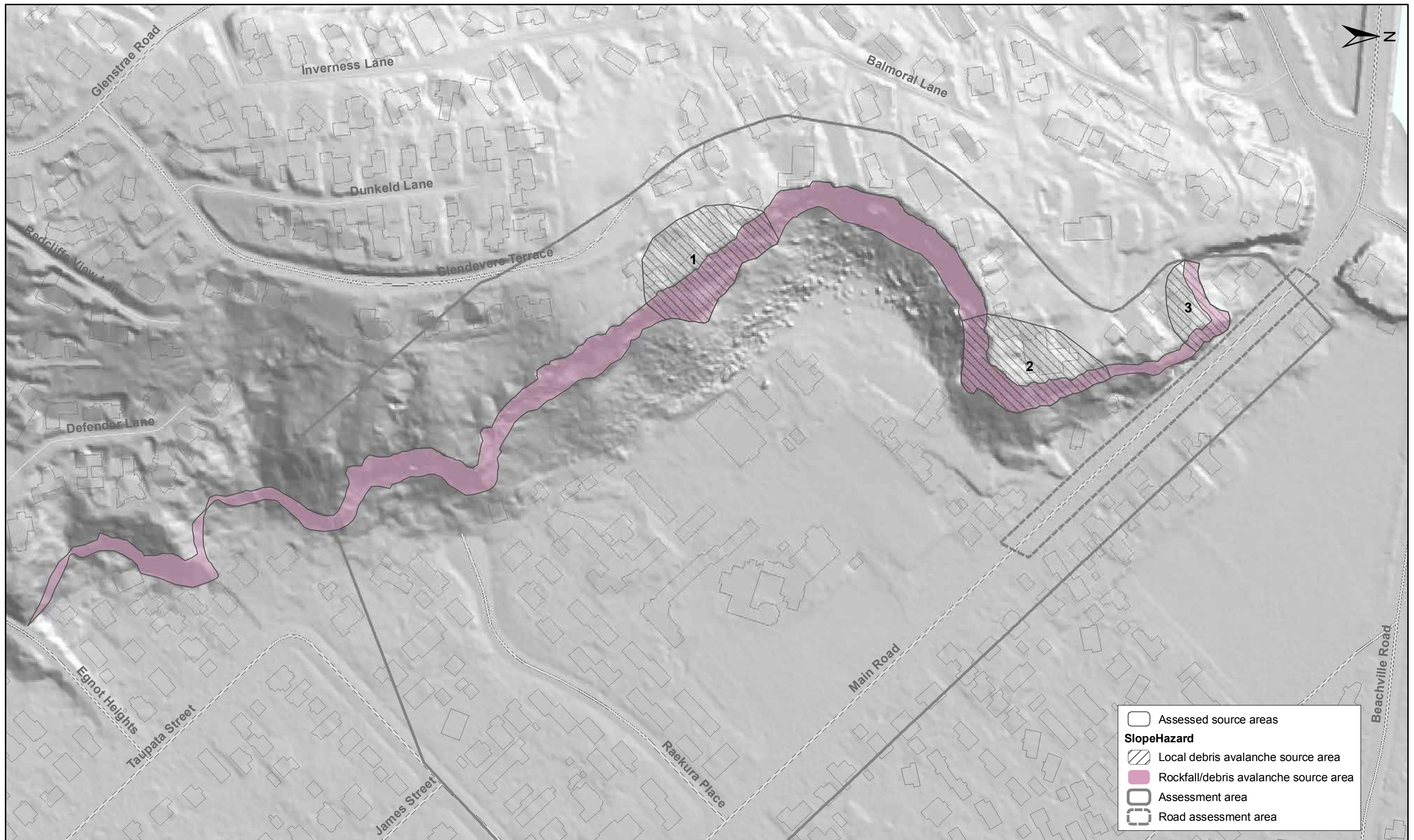
Cliff collapses have been considered separately from the failure and runout of individual boulders, referred to as “boulder rolls”. Although cliff collapses and boulder rolls both can be classified as rockfalls (Cruden and Varnes, 1996), the risk analysis for boulder rolls uses information on the location of each fallen boulder. Mapping individual boulder locations in a cliff collapse is impractical because of the large number of boulders involved. The main reason for the difference is that in a debris avalanche the boulders interact with one another, for rockfalls, involving individual boulders, the boulders behave more or less independently.

1.2.2 Local and random cliff collapse source areas

Further investigation of the site has involved field mapping, ground investigation (comprising subsurface drilling and trenching), laboratory testing, numerical modelling and monitoring (of the features in the field and how they have responded to earthquakes and rain). During the 2010/11 Canterbury earthquakes many rocks fell from these slopes, forming debris avalanches. The majority of failures involved relatively small volumes of debris, which fell from locations distributed randomly over the cliff face. The larger proportion of the total volume of debris that fell from the slopes however, came from a few much larger volume debris avalanches that were localised “discrete” failures of weaker parts of the rock mass.

The original assessment by Massey et al. (2012a) treated all of the debris avalanches as occurring from random locations anywhere on the slope. The original assessment is now superseded by this assessment, which identifies three specific areas (defined as assessed source areas 1–3) on the slope where local cracking and rock-mass deformation has been focused. These areas are potentially more susceptible to failure during a future triggering event, and could result in local larger volumes of debris leaving the cliff, as single or multiple failures, with the resultant debris travelling further on the valley floor than occurred in the 2010/11 Canterbury earthquakes. These three assessed cliff-collapse source areas are additional to the randomly distributed cliff collapse sources, from which debris could fall from anywhere along the cliff during a future event.

This is the reason for the Redcliffs mass movement being included in the Class I (high priority for further investigation) mass movements. The Redcliffs assessment area is shown on Figure 2 and this report presents: 1) annual individual fatality risks for given users of Main Road; and 2) revised annual individual fatality risks for dwelling occupants, within the given assessment area, which take into account the assessed source areas 1–3. Recommendations are provided to assist Christchurch City Council in considering potential options to mitigate the risk.



	Assessed source areas
SlopeHazard	
	Local debris avalanche source area
	Rockfall/debris avalanche source area
	Assessment area
	Road assessment area

SCALE BAR: 0 50 100 m

EXPLANATION:
 Background shade model derived from NZAM post earthquake 2011c (July 2011) LiDAR survey resampled to a 1 m ground resolution.
 Roads and building footprints provided by Christchurch City Council (20/02/2012).
 PROJECTION: New Zealand Transverse Mercator 2000

DRW:
BL
 CHK:
CM, FDP



MASS MOVEMENT LOCATION MAP

**Redcliffs
Christchurch**

FIGURE 2

FINAL

REPORT: CR2014/78	DATE: August 2014
----------------------	----------------------

1.3 PREVIOUS WORK AT THE REDCLIFFS SITE

During the 22 February 2011 earthquakes, within the Redcliffs mass movement area, significant volumes of debris fell from the steep rock slope (debris avalanches), inundating dwellings at the cliff bottom, along with localised recession and cracking of the cliff crest. These have been collectively termed cliff-collapse hazards (Figure 3–Figure 9). Previous investigations of the site comprised:

1. The risk to life of people in dwellings at the cliff top and bottom from cliff top recession and debris avalanche hazards has already been estimated by Massey et al. (2012a);
2. Field mapping of the crack distributions at the cliff crest was carried out by GNS Science and Geotech Ltd., and the results are contained in the Stage 1 report (Massey et al., 2013);
3. Ground investigation of the site has involved drilling of two fully cored drillholes and a third open hole (with no core recovery), and inclinometer monitoring, carried out by Aurecon NZ Ltd, under contract to Christchurch City Council. The results of the drilling are reported by Pletz and Revell (2013); and
4. Ground investigation and field mapping of the site was also carried out by Tonkin and Taylor Ltd, (Tonkin and Taylor, 2012a) under contract to the Earthquake Commission. The ground investigations comprised the drilling of three drillholes (one cored, one open hole and one open barrel), 11 test pits to depths between 2 and 3.5 m below ground level, two cone penetrometer tests and two Scala penetrometers. Three standpipes were installed to measure groundwater levels and one drillhole inclinometer tube was installed.



Figure 3 Aerial view of the Redcliffs mass movement area after the 4 September 2010 (Darfield) earthquake and before the 22 February 2011 earthquakes. Photograph taken by M. Yetton.

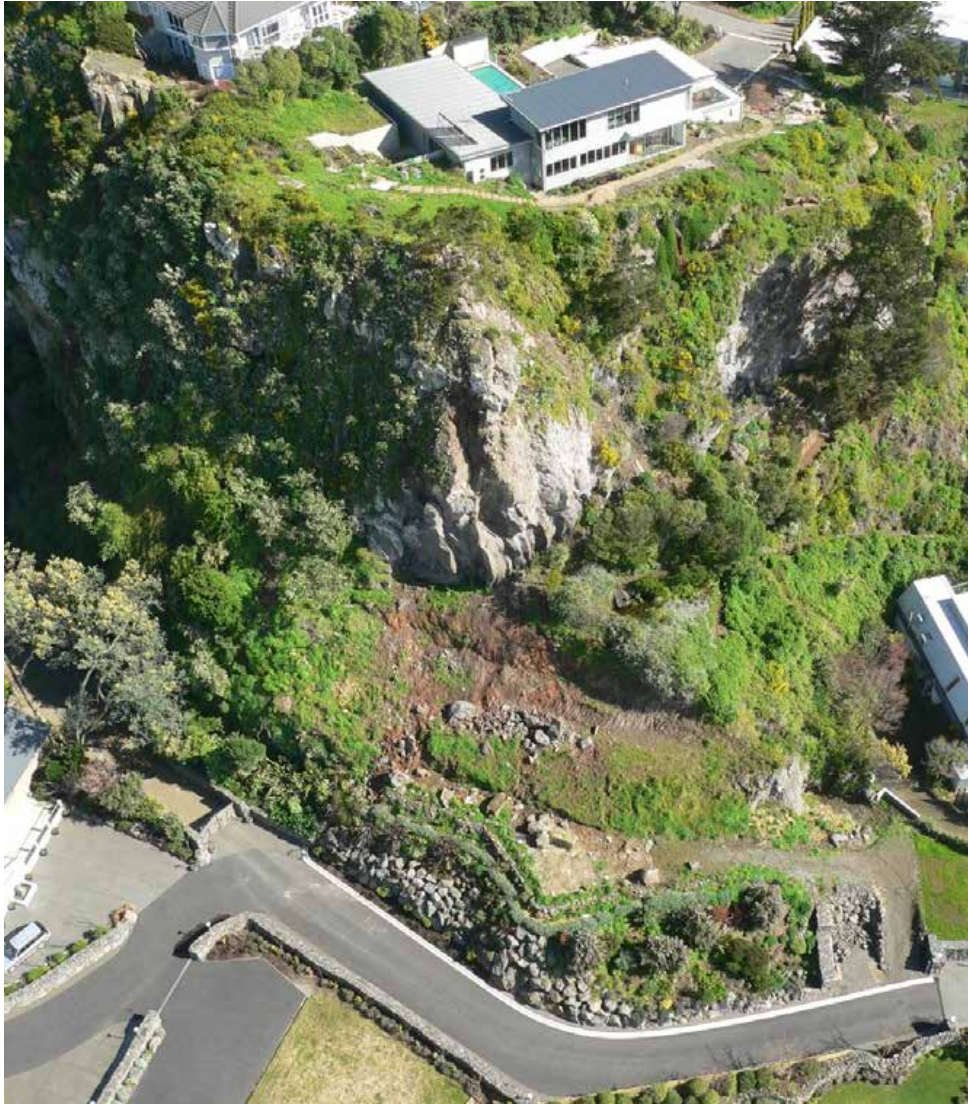


Figure 4 Aerial view of the Redcliffs mass movement area after the 4 September 2010 (Darfield) earthquake and before the 22 February 2011 earthquakes. Photograph taken by M. Yetton.



Figure 5 Aerial view of the Redcliffs mass movement area after the 22 February 2011 earthquakes and before the 13 June 2011 earthquakes. Photograph taken by G. Hancox.



Figure 6 Aerial view of the Redcliffs mass movement area after the 22 February 2011 earthquakes and before the 13 June 2011 earthquakes. Photograph taken by G. Hancox.



Figure 7 Aerial view of the Redcliffs mass movement area after the 22 February 2011 earthquakes and before the 13 June 2011 earthquakes. Photograph taken by G. Hancox.



Figure 8 Aerial view of the Redcliffs mass movement area after the 22 February 2011 earthquakes and before the 13 June 2011 earthquakes. Photograph taken by C. Gibbons.



Figure 9 Aerial view of the Redcliffs rock slope after the 13 June 2011 earthquakes. Photograph taken by C. Massey.

1.4 SCOPE OF THIS REPORT

The scope of this report as per Appendix A of contract No. 4600000886 (December 2011) is to:

1. Estimate the annual individual fatality risk for affected dwelling occupants from cliff collapse hazards (debris avalanche and cliff-top recession) in the study area in Figure 2;
2. Estimate the fatality risk for users of Main Road from cliff collapse hazards for the section of Main Road shown in Figure 2; and
3. Provide recommendations to assist Christchurch City Council with considering options to mitigate life risks, associated with the assessed cliff collapse hazards.

For the purpose of this risk assessment, dwellings are defined as timber framed single-storey dwellings, of building importance category 2a (AS/NZS 1170.0.2002). The consequences of the hazards discussed in this report on other building types, such as commercial buildings, Redcliffs School and the retirement home (30 Raekura Place), fall outside the terms of reference for this report and have not been assessed.

The risk results contained in this report supersede the preliminary results contained in Working Note CR2013/304LR (Massey and Della Pasqua, 2013).

1.5 REPORT STRUCTURE

- Section 1.6 of the report details the methodology.
- Section 2 details the data used in the assessments.
- Sections 3–5 contain the results from the engineering geological, hazard and risk assessments respectively.
- Section 6 discusses the results of the risk assessment and explores the uncertainties associated with the estimated risks.
- Section 7 summarises the assessment findings.
- Section 8 presents recommendations for Christchurch City Council to consider.

1.6 METHODS OF ASSESSMENT

The site assessment comprised three stages:

1. Engineering geology assessment;
2. Hazard assessment; and
3. Risk assessment.

The methodology adopted for each stage is described in detail in Appendix 1, and is summarised in the following sections.

1.6.1 Engineering geology assessment

The findings presented in this report are based on engineering geological models of the site developed by GNS Science. The engineering geological assessment comprised:

1. Interpretation of aerial photographs covering the period 1940–2011, to determine the history of the site.
2. Surveying of cadastral survey marks within and around the study area, to determine the magnitudes of displacement of the slope during the 2010/11 Canterbury earthquakes.
3. Assessment of the results from the surveying of monitoring marks installed on the site by Aurecon NZ Ltd. (under contract to Christchurch City Council), following the 22 February 2011 earthquake. This was undertaken to assess the amount of slope displacement relating to the 22 February, 16 April, 13 June and 23 December 2011 earthquakes.
4. Geological and geomorphological field mapping to identify the materials and processes that have been active within the study area.
5. Construction of an engineering geological map and six cross-sections, based on the results from the aerial photograph interpretation, surveying, field mapping, and the ground investigations carried out by Aurecon NZ Ltd. (Pletz and Revell, 2013), and Tonkin and Taylor Ltd. (Tonkin and Taylor, 2012a). These were used as the basis for the hazard and risk assessments.

1.6.2 Hazard assessment

The hazard assessment method followed three main steps:

Step 1 comprises assessment of the static stability of the slope under non-earthquake (static) conditions, and an assessment of the dynamic (earthquake) stability of the slope, adopting selected slope cross-sections, to determine the likelihood of large-scale cliff collapse, and whether these can/cannot be triggered under static and/or dynamic conditions.

Step 2 uses the results from step 1 to define the likely failure geometries (source areas) of potential failures, which are combined with the crack patterns and slope morphology and engineering geology mapping to estimate their likely volume. Three volumes are defined for each source area (upper, middle and lower volumes), which represent the probable range of potential source areas that could occur within the assessment area.

Step 3 models: 1) the distance the debris travels down the slope (runout); and 2) the volume of debris passing a given location, should the failure occur. Modelling is done for each representative source area, and for the upper, middle and lower volume estimates.

The results from this characterisation are then used in the risk assessment.

1.6.2.1 Estimation of Slope Failure volumes

The original cliff-collapse risk assessment by Massey et al. (2012a) was based on the simulation of potential future cliff collapses that were all randomly distributed across the slope face. The results of the engineering geological assessments identified that during the 2010/11 Canterbury earthquakes, many cliff collapses were randomly distributed across the slopes, however, these only accounted for a relatively small proportion of the total volume of debris leaving the cliff. Much of the debris leaving the Redcliffs cliff (and other similar cliffs in the Port Hills), derived from a few discrete (local) failures that involved larger volumes of rock, particularly in areas where the rock mass strength had been weakened as a result of earthquake-induced cracking.

This assessment improves on the original work by Massey et al. (2012a), by:

1. Taking into account the potential for large local cliff collapses from three assessed source areas;
2. Revising the risk estimates from other cliff collapses that are randomly distributed across the cliff; and
3. Including an assessment of the risk from cliff collapses on users of Main Road.

The volumes of debris that could fall from the cliff under dynamic (earthquake) and static (non-earthquake, e.g., rain) conditions have been assessed.

- Earthquake generated failure volumes:
 - The volumes of material lost from cliffs during the 2010/11 Canterbury earthquakes were estimated using change models generated from airborne LiDAR and terrestrial laser scan surveys. The volumes lost in each earthquake were graphed against the corresponding synthetic free-field rock-outcrop peak horizontal ground accelerations relating to the earthquake (calculated specifically for Redcliffs; Holden et al., 2014). The synthetic free-field rock-outcrop motions

were used because there are no instrumental records at the site, and the existing instrumental records from nearby sites each contain site effects that relate to the instrument site.

- Assessment of the many failures that occurred from the steep rock slopes in the Port Hills during the 2010/11 earthquakes indicates that about 60% of the total volume of debris leaving the cliffs during the 13 June 2011 earthquakes is attributable to a small number of specific local failures of greater than 2,500 m³ in volume.
 - The most likely locations and volumes of three potential large localised failures were estimated based on the assessment of crack distributions, inferred displacements, slope morphology and geology and numerical analyses. The purpose of this exercise was to constrain the likely depth, width and length of the three assessed source areas.
 - Three possible failure volumes were estimated for each assessed source area; a low, middle and upper estimate. This variation in failure volume is intended to reflect the range of uncertainty from the results of the modelling and mapping, e.g., the depth, width and length dimensions.
 - The credibility of these potential failure volumes was evaluated by comparing them against: 1) the volumes of relict failures recognised in the geomorphology near the site and elsewhere in the Port Hills; and 2) the volume frequency distribution of debris that fell from this site and other similar sites in the Port Hills during the 2010/11 earthquakes.
- Non-earthquake generated failure volumes:
 - There are four main sources of information on historical non-earthquake failures for the Port Hills: 1) archived newspaper reports from 1870 to 1945; 2) the GNS Science landslide database, which is “complete” only since 1996; 3) insurance claims made to the Earthquake Commission for landslips which are “complete” only since 1996; and 4) information from local consultants (M. Yetton, Geotechnical Consulting Ltd. and D. Bell, University of Canterbury) which incompletely covers the period 1968 to present. These have been used to estimate the likely process rate of non-seismic rockfalls from the slope. These data are detailed in Massey et al. (2012a).
 - These failure volumes were assumed to be randomly distributed across the slope as per those recorded from sequential terrestrial laser scan surveys of the slope carried out after the 2010/11 earthquakes, during a period when no strong earthquakes occurred.

1.6.2.2 Estimation of debris runout

The distance that debris from debris avalanches travels down a slope is called the runout. The runout distance of debris falling from Redcliffs has been assessed both empirically and numerically. The methods adopted are described in Appendix 1.

For large local failures from the three assessed source areas, the volume of debris passing a given distance down the slope was assessed numerically, using the RAMMS software (RAMMS, 2011). These calculated runout distances were calibrated using data from debris avalanches that occurred from Redcliffs and other similar slopes in the Port Hills, during the 2010/11 Canterbury earthquakes.

For the randomly distributed failures, empirical models were used to estimate the debris runout down the slope. These models were based on the volumes of debris that fell and travelled given distances downslope at Redcliffs during the 2010/11 earthquakes.

1.6.3 Risk assessment

The risk metric assessed in this report is the annual individual fatality risk. The risk is assessed for dwelling occupants and regular road users from the cliff-collapse hazards assessed in this report. The cliff collapse hazards are:

1. Debris avalanches – a type of landside comprising many boulders falling simultaneously from a slope. The rocks start by sliding, toppling or falling before descending the slope rapidly (typically at greater than five metres a second) by any combination of falling, bouncing and rolling; and
2. Cliff-top recession – the result of parts of the cliff top collapsing, causing the cliff edge to move back up the slope.

The quantitative risk assessment uses risk-estimation methods that follow appropriate parts of the Australian Geomechanics Society framework for landslide risk management (Australian Geomechanics Society, 2007). It provides risk estimates suitable for use under SA/SNZ ISO1000: 2009.

Using the Australian Geomechanics Society (2007) guidelines for landslide risk management, the annual fatality risk to an individual is calculated from:

$$R_{(LOL)} = P_{(H)} \times P_{(S:H)} \times P_{(T:S)} \times V_{(D:T)} \quad \text{Equation 1}$$

where:

$R_{(LOL)}$ is the risk (annual probability of loss of life (death) of a person) from debris/earth flows/avalanches;

$P_{(H)}$ is the annual probability of the initiating event;

$P_{(S:H)}$ is the probability that a person, if present, is in the path of the debris at a given location;

$P_{(T:S)}$ is the probability that a person is present at that location; and

$V_{(D:T)}$ is the vulnerability, or probability that a person is killed if present and hit by debris.

The details relating to each of the above input parameters used in the risk assessments are discussed in Appendix 1.

1.6.3.1 Event annual frequencies

The frequency of occurrence of the events that could trigger the assessed cliff-collapse failure volumes is unknown. In place of this lack of information, the ranges of frequencies are defined, and the magnitudes of representative triggering events with these frequencies of occurrence are used to estimate the likely volumes of collapses that are triggered when the triggering event occurs.

- For non-earthquake triggers such as rainfall, rates of debris avalanches, rockfalls and cliff top recession triggered without earthquakes were taken from Massey et al. (2012a). These rates were used to estimate the contribution to total risk from non-

earthquake triggering events. Four representative event-trigger frequencies were used and the volumes of the debris triggered by events with these frequencies were estimated.

- For earthquake events, rates of debris avalanches and rockfalls and cliff-top recession were estimated using the empirical relationship between the volumes of debris leaving the cliffs, and amounts of cliff-top recession recorded during the 2010/11 Canterbury earthquakes, and the synthetic free-field peak ground acceleration of the event that triggered them. Seven representative event-trigger frequencies were used and the volumes of debris triggered by events with these frequencies were estimated.
- For earthquake triggers, the frequency of a given free-field peak ground acceleration occurring is obtained from the New Zealand National Seismic Hazard Model (Stirling et al., 2012), using a modified form of the 2010 version of the National Seismic Hazard Model (Gerstenberger et al., 2011), which takes into account the increased level of seismicity in the Christchurch region.
- For the three assessed source areas – where larger volumes of rock could potentially fall, leading to larger areas of cliff top to be lost – the probability of failure was estimated based on the amount of permanent slope displacement that could occur in response to each of the seven representative events. This was done, adopting the decoupled method (Makdisi and Seed, 1978), by using:
 - a. The relationship between the yield acceleration (K_y) and the maximum average acceleration of the mass (K_{MAX}), derived from back analysing the permanent displacement of the slope during the 2010/11 earthquakes; and
 - b. The New Zealand National Seismic Hazard Model to provide the annual frequencies (return periods) of free-field rock outcrop peak horizontal ground accelerations (A_{MAX}) and therefore the annual frequencies of the equivalent maximum average acceleration of the mass (K_{MAX}).

The methods adopted are discussed in detail in Appendix 1.

1.6.3.2 Scenarios adopted for modelling

Three cliff-collapse risk scenarios have been adopted for modelling (Table 2). The three scenarios are chosen to examine the effect on risk of uncertainties in: 1) the assessed total volume that could be generated in a representative event; and 2) the volume of debris that passes a given distance down the slope.

Table 2 Risk scenarios used in the modelling of cliff collapses.

Volume	Source volume scenario	Runout volume scenario
Earthquake induced volumes		
Total volume generated in a representative earthquake event. Based on the empirical relationship between peak ground acceleration and volume leaving the slope, estimated from slope failures at Redcliffs during the 2010/11 earthquakes.	<ul style="list-style-type: none"> A) The relationship adopted is the mean plus one standard deviation B) The relationship adopted is the mean C) The relationship adopted is the mean minus one standard deviation 	
Local earthquake failures. Representing 60% of the total earthquake volume	<ul style="list-style-type: none"> A) Adopting upper estimates of the source volumes (of assessed source areas 1–3) B) Adopting middle estimates of the source volumes (of assessed source areas 1–3) C) Adopting lower estimates of the source volumes (of assessed source areas 1–3) 	<ul style="list-style-type: none"> A) RAMMS model adopting upper source volume estimates B) RAMMS model adopting mean source volume estimates C) RAMMS model adopting the lower source volume estimates
Randomly distributed earthquake failures. Representing 40% of the total earthquake volume.	<ul style="list-style-type: none"> A) Adopting 40% of the total volume derived from the mean plus one standard deviation relationship B) Adopting 40% of the total volume derived from the mean relationship C) Adopting 40% of the total volume derived from the mean minus one standard deviation relationship 	<ul style="list-style-type: none"> A) Empirical model adopting the mean plus 1 standard deviation relationship B) Empirical model adopting the mean relationship C) Empirical model adopting the mean minus 1 standard deviation relationship
Non-earthquake induced volumes		
Randomly distributed non-earthquake failures. Volume estimated from historical non-earthquake rockfall production rates	<ul style="list-style-type: none"> A) Historical rates multiplied by a factor of two to take into account the increased production rates as the rock mass (post 2010/11 earthquake) is now broken. B) Historical rates C) Historical rates divided by two to take into account any potential overestimate of the historical rockfall rates 	<ul style="list-style-type: none"> A) RAMMS model adopting upper source volume estimates B) RAMMS model adopting mean source volume estimates C) RAMMS model adopting the lower source volume estimates

2.0 DATA USED

The data and the sources of the data used in this report are listed in Table 2.

Table 3 Summary of the main data used in the analysis. LiDAR is Light Detecting and Ranging.

Data	Description	Data source	Date	Use in this report
Post-22 February 2011 earthquake digital aerial photographs	Aerial photographs were taken on 24 February 2011 by NZ Aerial Mapping and were orthorectified by GNS Science (10 cm ground resolution).	NZ Aerial Mapping	Last updated 24 February 2011	Used for base maps and to map extents of landslides and deformation triggered by the 22 February 2011 earthquakes.
Post-13 June 2011 earthquake digital aerial photographs	Aerial photographs were taken between 18 July and 26 August 2011, and orthorectified by NZ Aerial Mapping (0.5 m ground resolution).	NZ Aerial Mapping	18 July–26 August 2011	Used to map extents of landslides and deformation triggered by the 13 June 2011 earthquakes.
Historical aerial photographs	Photographs taken in 1940, 1946, 1975, 1975 and 1984 by multiple sources and orthorectified by NZ Aerial Mapping and GNS Science (at variable ground resolutions).	NZ Aerial mapping and GNS Science	1946, 1975, 1975 and 1984	Used to assess the site history before the 2010/11 Canterbury earthquakes.
LiDAR digital elevation model (2003)	Digital Elevation Model derived from LiDAR survey carried out in 2003; resampled to a 1 m ground resolution.	AAM Hatch	2003	Used as the pre-22 February 2011 ground model.
LiDAR digital elevation model (2011a)	Digital Elevation Model derived from post-22 February 2011 earthquake LiDAR survey; re-sampled to 1 m ground resolution.	NZ Aerial Mapping	8–10 March 2011	To generate change models (between the 2003 and 2011a surveys) to determine the locations, extents and volumes of material leaving the cliffs and where it was deposited.
LiDAR digital elevation model (2011b)	Digital Elevation Model derived from LiDAR survey; resampled to a 1 m ground resolution.	AAM Hatch	May 2011	To generate a model of changes (between the 2011a and 2011b surveys) to determine the locations, extents and volumes of the material leaving the cliffs and where it was deposited.

Data	Description	Data source	Date	Use in this report
LiDAR digital elevation model (2011c)	Digital Elevation Model derived from post-13 June 2011 earthquake LiDAR survey; re-sampled to 1 m ground resolution.	NZ Aerial Mapping	18 July–26 August 2011	Used to generate contours and shade models for the maps and cross-sections used in the report.
Terrestrial laser scan (TLS) surveys	Multiple Digital Elevation Model's derived from surveys following the 22 February, 16 April and 13 June 2011 earthquakes.	GNS Science	Last survey carried out October 2013	To generate models of changes (between surveys) to determine the distribution and volume of material leaving the cliffs at selected areas where surveys were made.
Christchurch building footprints	Footprints are derived from aerial photographs. The data originate from 2006 but have been updated at the site by CCC using the post-earthquake aerial photos.	Christchurch City Council	Unknown	Used to identify the locations of residential buildings in the site.
GNS Science landslide database	Approximate location, date, and probably trigger of newsworthy landslides	GNS Science	Updated monthly	Used to estimate the likely numbers and volumes of pre earthquake landslides in the areas of interest.
Earthquake Commission claims database	Location, date and brief cause of claims made in the Port Hills of Christchurch since 1993.	Earthquake Commission	1993–August 2010	Used to estimate the likely numbers and volumes of pre earthquake landslides in the areas of interest.
Composite seismic hazard model	The increased level of seismicity in the Canterbury region since 4 September 2010 has been quantified using a modified form of the national seismic hazard model.	GNS Science	Updated December 2013	Used to estimate the frequency of occurrence of a given peak ground acceleration.
Synthetic earthquake time/accelerations	Earthquake time acceleration histories for the four main 2011 earthquakes: 22 February, 16 April, 13 June and 23 December.	GNS Science	February 2014	Used as inputs for the seismic site response analysis.
Rainfall records for Christchurch	Rainfall records for Christchurch from various sources, extending back to 1873.	NIWA	1873–present	Used to assess the return periods of past storms triggering landslides of known magnitudes in the Port Hills.

Data	Description	Data source	Date	Use in this report
Drillhole logs	Results from the logging of three drillholes and three scala penetrometers carried out at the site.	Tonkin and Taylor Ltd. (Tonkin and Taylor, 2012a)	2012	Used to generate the engineering geological map and cross-sections.
Drillhole logs	Results from the logging of two drillholes carried out at the site	Aurecon NZ Ltd. (Pletz and Revell, 2013)	September 2013	Used to generate the engineering geological map and cross-sections.
Downhole shear wave surveys	Downhole (in drillhole) shear wave velocity surveys.	Southern Geophysical Ltd. (2013)	February 2014	Used to determine the dynamic properties of the materials in the slope for the seismic site response analysis.
Geotechnical laboratory data	Geotechnical strength parameters for selected soil and rocks in the Port Hills.	GNS Science (Carey et al., 2014)	February 2014	Used for static and dynamic slope stability analysis.
Field work	Field mapping of slope cracking and engineering geology and ground truthing of the risk analyses.	GNS Science and the Port Hills Geotechnical group	22 February 2011–present	Used in generating the engineering geological models of the site. Results from field checks used to update risk maps.
Traffic counts for Main Road (Causeway, Ferrymead/Main Rd junction and Sumner Surf Life Saving club data available for recent years)	Detailed motor vehicle counts at 2-year intervals, by hour of day and day of week, are available for several locations. Data for Redcliffs were taken as the average of figures used for Dean's Head and those used below Quarry Road	Christchurch City Council	2008, 2010 and 2012 surveys	Used to assess total numbers of road users, and to model likely average extent and frequency of delays (and hence extended average time at risk) on Main Road.

3.0 SITE ASSESSMENT RESULTS

The site assessment results and engineering geological conceptual models developed for the site by GNS Science are summarised below.

3.1 SITE HISTORY

3.1.1 Aerial photograph interpretation

Aerial photographs of the site are available for various dates since 1940. Table 4 summarises the photograph details and main features noted.

Table 4 Summary of observations from aerial photographs used to assess the site history at Redcliffs.

Date/scale of photo	Resolution	Comments
1940 1:10,000 (approx.)	Poor resolution	<p>Several large arcuate features – possible relict landslide scars – are apparent in the cliff face. Below these features are what appear to be corresponding accumulations of talus. These features are labelled 1–5 on Appendix 2 Map 1.</p> <p>No dwellings are present at the cliff crest. The area behind the cliff crest appears to be farmland. Several dwellings are apparent at the cliff toe, outside the extent of the pre-2003 talus (Figure 10).</p> <p>Several brighter areas are apparent on the cliff face, these may relate to recent failure of material from the cliff.</p>
30/05/1946 1:5,500 (approx.)	Good resolution	<p>At the northern end of the site there appears to be an area of “hummocky” ground within a subtle concave depression behind the cliff crest. This appears to be consistent with the location of the 2011 loess slump (Figure 10).</p> <p>A possible recent collapse of the cliff edge is apparent in the north east corner of the site (Figure 10).</p> <p>Several relict and recent loess failures, at the cliff crest, are apparent.</p> <p>No dwellings are present at the cliff crest. The area behind the cliff crest still appears to be farmland.</p> <p>A few possible recent boulders are apparent on the surface at the cliff toe.</p>
1973, 1:10,000 (approx.)	Poor resolution	<p>A few dwellings have now been constructed at the cliff crest in the central part of the site.</p> <p>Several possible recent rockfalls are present at the bottom of the cliff (Figure 10).</p> <p>Several brighter areas are apparent on the cliff face, these may relate to recent failure of material from the cliff.</p>
1975, 1:10,000 (approx.)	Poor resolution	<p>No obvious change. Much of the cliff face and toe is in shadow. A few more buildings have been constructed at the cliff crest.</p>
1984, 1:6,000 (approx.)	Good resolution	<p>A few more dwellings have now been constructed at the cliff crest in the central and northern part of the site.</p> <p>Several possible recent rockfalls are present at the bottom of the cliff (Figure 10).</p>

3.1.2 Before the 2010/11 Canterbury earthquakes

- The Redcliffs slopes are part of an abandoned pre-historic coastal cliff. Erosion of the base of the cliff probably ceased 3,500–3,700 years ago (McFadgen and Goff, 2005).
- Several relict (apparent in the 1940 aerial photographs) possible landslide source areas are identified in the slope face with corresponding debris deposited beneath them.
- Using the 2003 LiDAR survey digital elevation model of these slopes, and by projecting the rockslope face at the toe of the slope through the talus to intersect an assumed pre-talus ground surface, it was possible to estimate likely volumes of talus present before the 2010/11 Canterbury earthquakes (Appendix 2). At Redcliffs, the talus totals about 30,000 ($\pm 10,000$) m³, but some of this debris may be wind-blown sand. Some middens excavated from beneath rockfall debris were abandoned some 600 years ago (Trotter, 1975).
- The likely age of the coastal beach surfaces on which this material was deposited may be about 3,500–3,700 calibrated radiocarbon years (McFadgen and Goff, 2005), suggesting rockfall accumulation rates averaging 8.1–8.6 m³/year. If it is assumed that dune sand is largely filling interstices between fallen boulders, the proportion of dune sand may be ignored.
- Estimated debris volumes per possible landslide scar range from 2,400 to 7,300 m³, each of which we assume fell as a result of a single landslide rather than as the accumulation from several smaller landslides (this assumption is justified only as a more conservative option).
- There is no evidence in the aerial photographs (1940, 1946, 1973, 1975, 1984 and 2011) of past quarrying at the site. It appears that none of the rock mass exposed in the cliff has been judged durable enough to be quarried, even as base course for roading, or rip-rap for mitigation of coastal erosion.
- Bell (1992) reports on two failures of the rock slope at Redcliffs, one in 1968 and the other in 1992; both are reported to have been about 50 m³ in volume with rainfall as the trigger.
- There are several possible rockfalls visible in historical aerial photographs (Figure 10).
- A rockfall bund (a barrier constructed of rock fill to prevent rockfalls from passing it) was constructed in 2010 behind the Redcliff School hall (Figure 10).

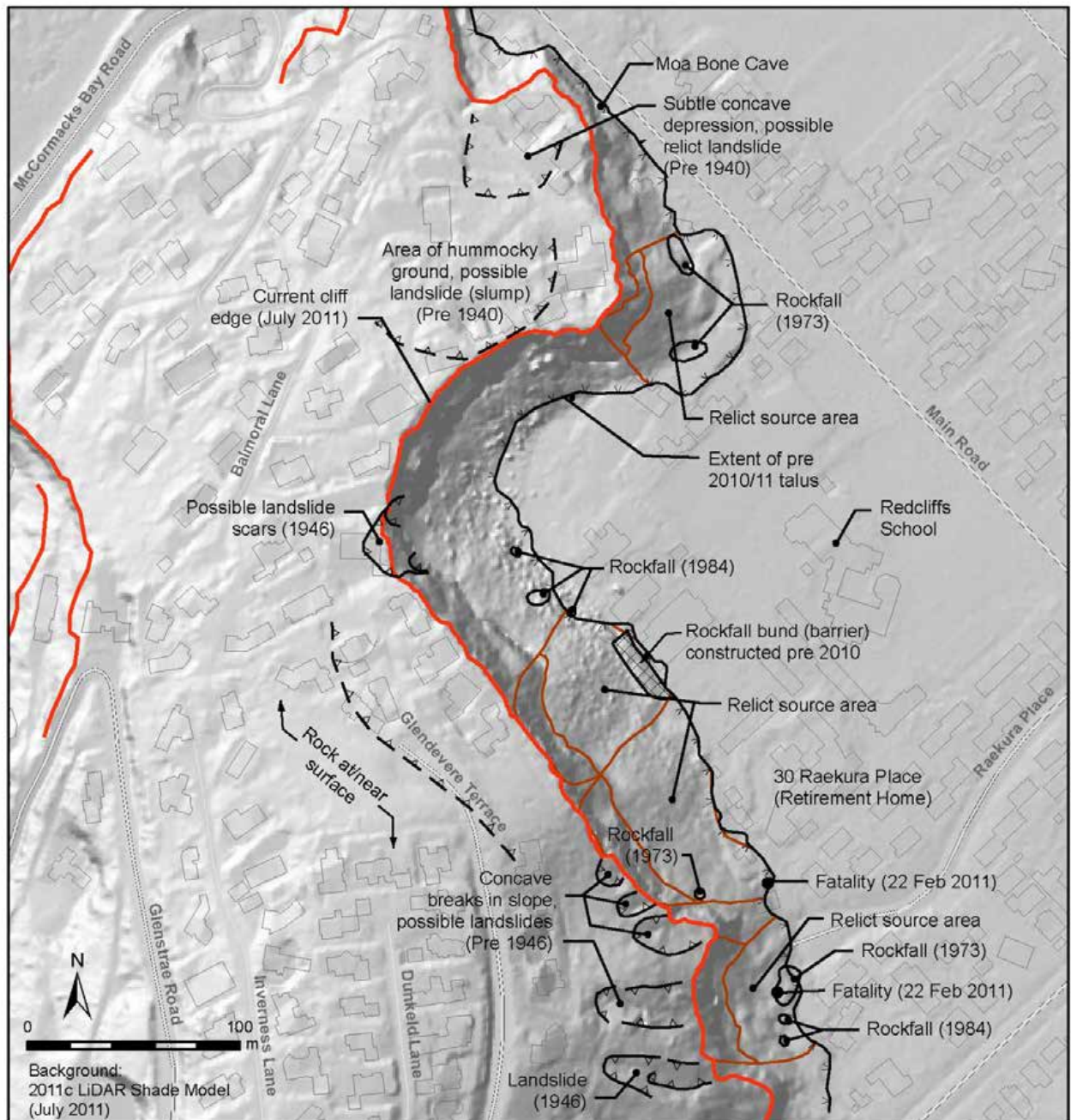


Figure 10 Main features identified at the site from field mapping and the interpretation of historical aerial photographs.

3.1.3 During the 2010/11 Canterbury earthquakes

Summaries of the cliff-top displacements in response to the earthquakes, inferred from crack apertures and limited surveying of cadastral marks, are contained in Tables 5–7. A summary of the volumes leaving the cliffs during the largest 2010/11 Canterbury earthquakes derived from airborne LiDAR and terrestrial laser scan surveys is contained in Table 8.

Assessment results from: 1) airborne LiDAR survey change models are presented in Appendix 2; 2) terrestrial laser scan survey change models in Appendix 3; and 3) surveying of cadastral and monitoring marks in Appendix 4. Results of crack mapping between the main earthquakes, carried out by Yetton (Geotech Ltd.), are contained in Appendix 5.

The main results from these field-based assessments are summarised below:

- *4 September 2010 (Darfield) earthquake*: no mapped displacement of the cliff face or cracking of the cliff top was identified; about 60 m³ of debris fell from the cliff face.
- *22 February 2011 earthquakes* – the cracks, mainly in loess at the cliff crest (shown on the maps in the Stage 1 report and displacements summarised in Tables 5–7), were mainly generated on 22 February 2011 by one or more earthquakes that occurred on this day. Permanent total displacement of the area, inferred from the results of mapping of cracks and measurement of their apertures was between 0.03 and 1.7 m (Table 7). Surveying of cadastral marks, was carried out by GNS Science to allow before and after (the 2010/11 Canterbury earthquakes) measurements to be made (results are presented in Appendix 4). Many of the identified cadastral survey marks were outside the main areas of inferred movement. The displacements of the two survey marks, only marginally within the inferred areas of movement, were about 0.2–0.3 m, and represent lower bound estimates of the total displacement during the earthquakes. During these earthquakes approximately 23,900 (±6,600) m³ of rock fell from the slope (Table 8 and shown graphically in Appendix 2), onto residential and commercial properties at the toe of the slope, killing two people. In some locations the cliff edge receded up to six metres. Many cracks were visible in the cliff face after these events (Massey et al., 2012a). The area behind the rockfall bund, constructed behind the Redcliffs School hall, was completely filled in by debris, and is now incorporated in the debris.
- *16 April 2011 earthquake* – No displacement of the cliff top or opening of the mapped cracks was reported or detected by GNS Science. About 1,180 (±110) m³ of rock fell from the cliff; some of it fell onto vacant dwellings at the cliff toe (Table 8 and Appendix 3).
- *13 June 2011 earthquakes* – Some new cracks, and the reactivation (further opening) of existing cracks, were recorded (in loess) at the cliff crest following these earthquakes (Appendix 5). Horizontal permanent displacement of the cliff crest in response to these earthquakes (inferred from crack apertures) ranged between 0.2 and 0.7 m; vertical displacements were not measured. During this earthquake, about 11,800 (±3,500) m³ of rock fell from the cliff, some onto dwellings and other buildings at the cliff toe, which were unoccupied following the 22 February 2011 earthquake (Table 8 and Appendix 2). The cliff edge locally receded by up to seven metres (Massey et al., 2012a) and many more cracks appeared on the cliff face.
- *23 December 2011 earthquake* – During this earthquake about 1,180 (±130) m³ fell from the cliff, on to unoccupied dwellings at the cliff toe (Table 8 and Appendix 4).
- No survey monitoring marks were installed at the cliff top to record permanent ground movements during these earthquakes.

3.1.4 After the 2010/11 Canterbury earthquakes

- Analysis of survey results for some parts of the cliff top adjacent to Moa Bone cave shows that the cliff edge locally has advanced outward 30 mm since the 2010/11 earthquakes; vertical displacements were not measured. In this area, possible break-out of a shear surface through basalt breccia has been located on the cliff face at the cliff toe. Displacements occurred during the winter of 2013.
- About 460 (±160) m³ of rock fell from the slope face between January 2012 and December 2012 (about 475 m³/year). About 81 (±47) m³ of rock fell from the slope face between December 2012 and November 2013 (about 90 m³/year). No large ground

accelerations were recorded during this interval in the local area. Most of these failures comprised relatively frequent discrete failures that were small in volume (mean volume of about 0.1 m³).

- Many earthquake-induced cracks are apparent on the cliff. Many of these extend from cliff top to cliff bottom and were formed mainly by the 22 February and 13 June 2011 earthquakes.

3.2 SITE INVESTIGATIONS

3.2.1 Geomorphological mapping

The results from field mapping of slope morphology, interpreted surface materials and their genesis, surface deformation mapping and other relevant information are shown in Figure 11.

The site consists of an asymmetric north-tending spur with a very steep eastern flank (cliff face) and a gentler sloping western flank. The width and height of the spur is about 300 m and 80 m respectively. The cliff on the eastern side is about 70 m high, 500 m long with a slope angle ranging from 60° to overhanging in places. The cliff has three main sections based on slope aspect: 1) a southern, northeast-facing cliff; 2) a central, southeast-facing cliff; and 3) a northern north east-facing cliff. The southern and central parts of the cliff are the steepest. Main Road is located at the toe of the northern cliff.

3.2.2 Subsurface trenching and drilling

The ground investigation details are summarised in Table 8 and shown on Figure 12. Geological logs and equipment installation details are contained in the reports by Aurecon NZ Ltd. (Pletz and Revell, 2013; Tonkin and Taylor Ltd., 2012a).

Based on this work the main slope-forming materials and groundwater conditions are summarised below.

Table 5 Summary of the ground investigations carried out at the site by Aurecon NZ Ltd. (Pletz and Revell, 2013) and Tonkin and Taylor Ltd. (Tonkin and Taylor, 2012a).

ID	Source	Type	Depth (m below ground level)	Instrumentation
BH-MB-01	Aurecon NZ Ltd.	Cored hole	35.2	Inclinometer
BH-MB-02	Aurecon NZ Ltd.	Cored hole	41.1	Inclinometer
BH-MB-03	Aurecon NZ Ltd.	Open hole	41.0	Seismometer
BH-BAL-03	Tonkin and Taylor Ltd.	Cored hole (inclined 45°)	35 m	None
BH-GDV-01	Tonkin and Taylor Ltd.	Cored hole	10.0	Inclinometer and standpipe
BH-GDV-02	Tonkin and Taylor Ltd.	Cored hole (inclined 45°)	40.5	None
CPT-GDV-01	Tonkin and Taylor Ltd.	Cone penetration	2.9	Standpipe
CPT-GDV-02	Tonkin and Taylor Ltd.	Cone penetration	4.0	Standpipe
TPB01-02, TPG01-05 and TPY01-04	Tonkin and Taylor Ltd.	Test pits	Variable 2–3.5 m	N/A

3.2.3 Surface movement

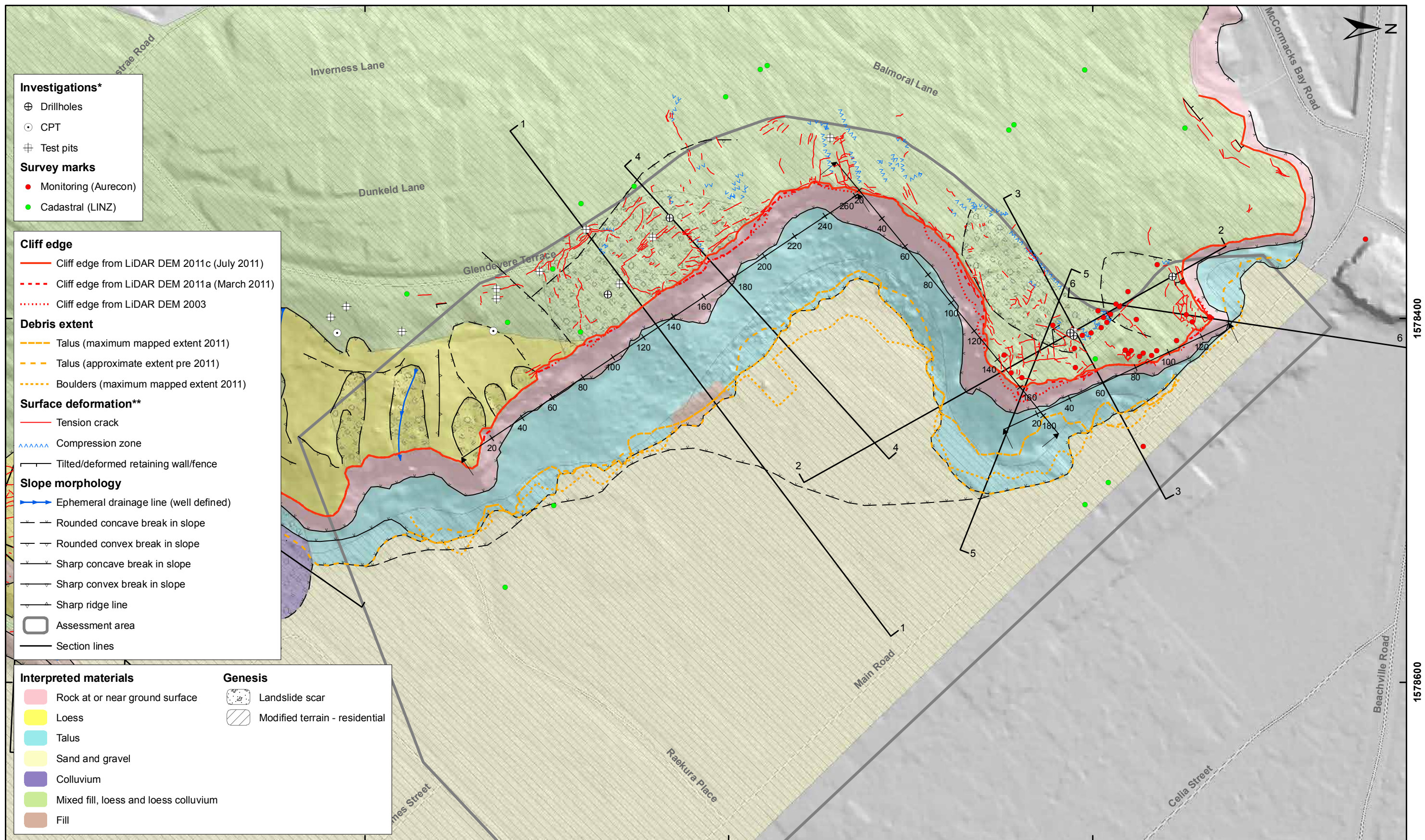
3.2.3.1 Inferred cliff crest displacements from crack apertures

Total displacements of the cliff crest in response to the 2010/11 Canterbury earthquakes have been inferred from the measurement of crack apertures, as there are limited survey data available. Many of the cracks at the slope surface are in loess and fill material. Therefore, the measured crack apertures may not reflect the true displacement of the underlying rock, as the cracks in loess may have formed in response to several different mechanisms, e.g., earthquake induced settlement and or slumping in the loess, as well as permanent displacement of the underlying rock.

The logs from the test pits (Tonkin and Taylor, 2012a) located back from the cliff crest show that cracks in the loess, extend down from the surface, but do not reach bedrock. This would suggest that the presence of cracks in loess do not necessarily imply cracking of the underlying rock. However, field mapping of exposures of loess at the cliff crest also show that cracks formed in the bedrock do not always extend into the loess, or to the ground surface.

Two distinct crack patterns were identified in the loess (and fill) at the cliff crest:

- Set 1 indicates mainly extensional (horizontal) displacements across cracks – occurring well back from the cliff edge – and are inferred to be a function of shallow inelastic response of the loess (and fill) above rock head during shaking (e.g., settlement, slumping).
- Set 2 indicates both horizontal and vertical displacement (up to 1.5 m of cumulative vertical displacement measured), and are located closer to the slope crest. In these areas the thickness of the surficial loess/fill cover over rock is only 1–2 m and therefore unlikely to accommodate settlement of the loess due to earthquake shaking. These cracks are therefore inferred to relate to deeper-seated deformation in the underlying rock mass during shaking.



SCALE BAR: 0 50 100 m

EXPLANATION:
 * For details refer to site investigation map
 ** Taken from report 2012/317
 Background shade model derived from NZAM post earthquake 2011c (July 2011) LiDAR survey resampled to a 1 m ground resolution.
 Roads provided by Christchurch City Council (20/02/2012).
 PROJECTION: New Zealand Transverse Mercator 2000

DRW:
BL
 CHK:
CM, FDP



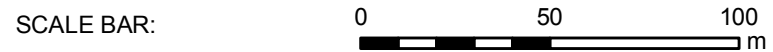
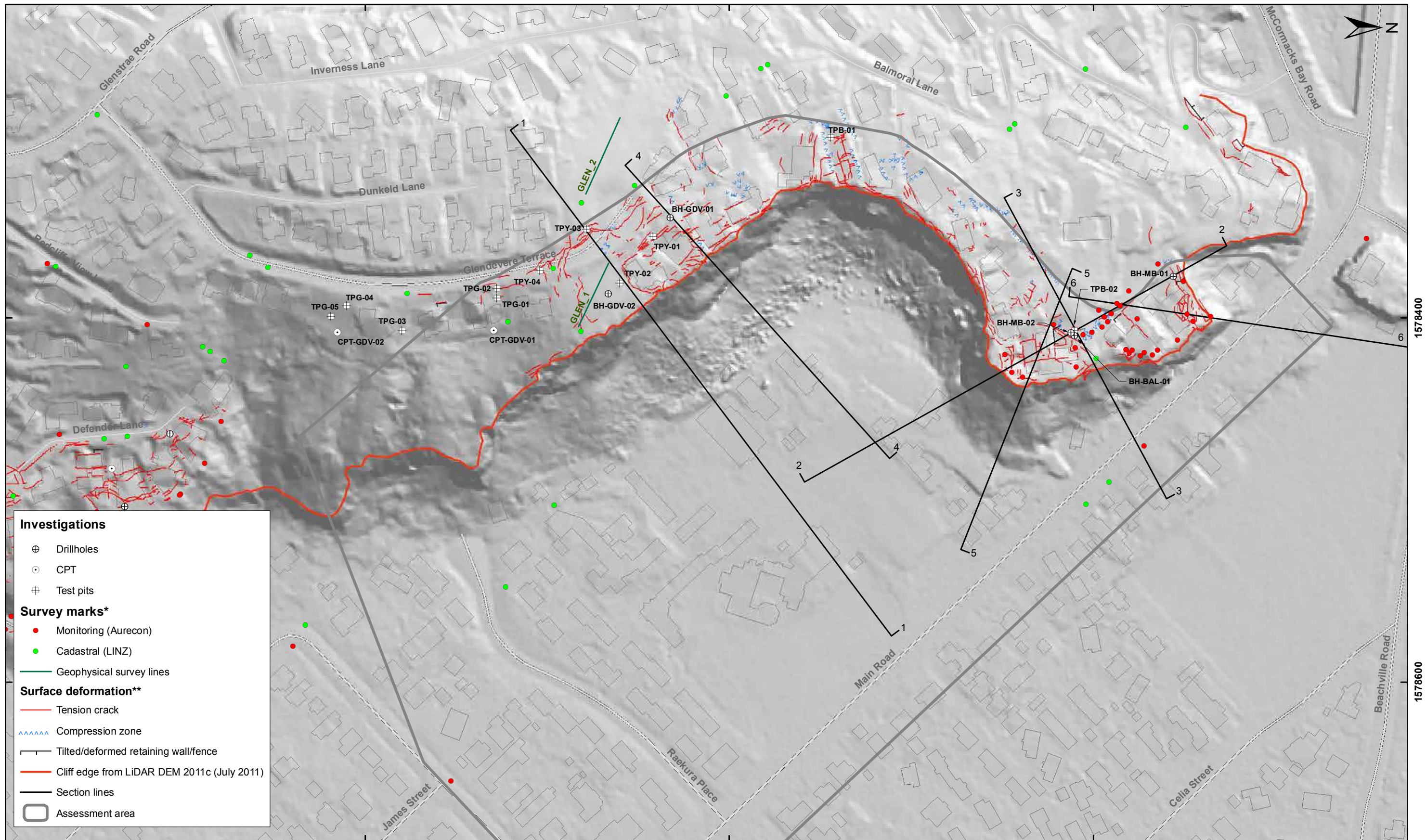
ENGINEERING GEOLOGY MAP

**Redcliffs
Christchurch**

FIGURE 11

FINAL

REPORT: CR2014/78 DATE: August 2014



EXPLANATION:
 * For detail refer to Appendix 4
 ** Taken from report 2012/317

Background shade model derived from NZAM post earthquake 2011c (July 2011) LiDAR survey resampled to a 1 m ground resolution.
 Roads and building footprints provided by Christchurch City Council (20/02/2012).
 PROJECTION: New Zealand Transverse Mercator 2000

DRW:
BL

CHK:
CM, FDP



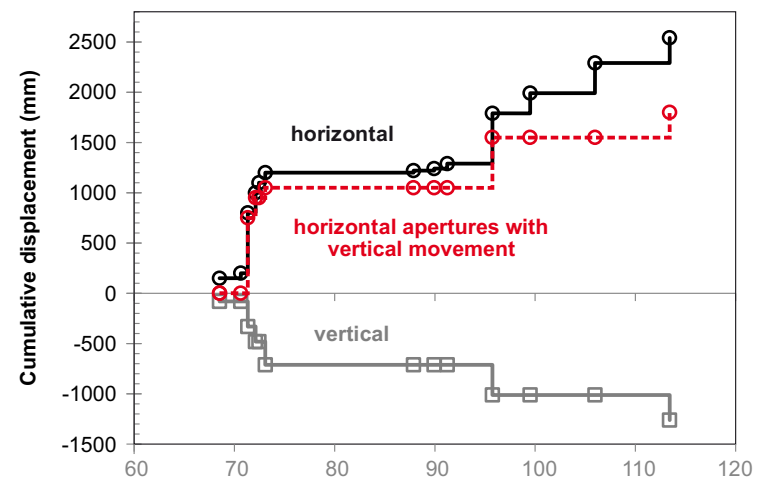
SITE INVESTIGATION MAP

**Redcliffs
Christchurch**

FIGURE 12

FINAL

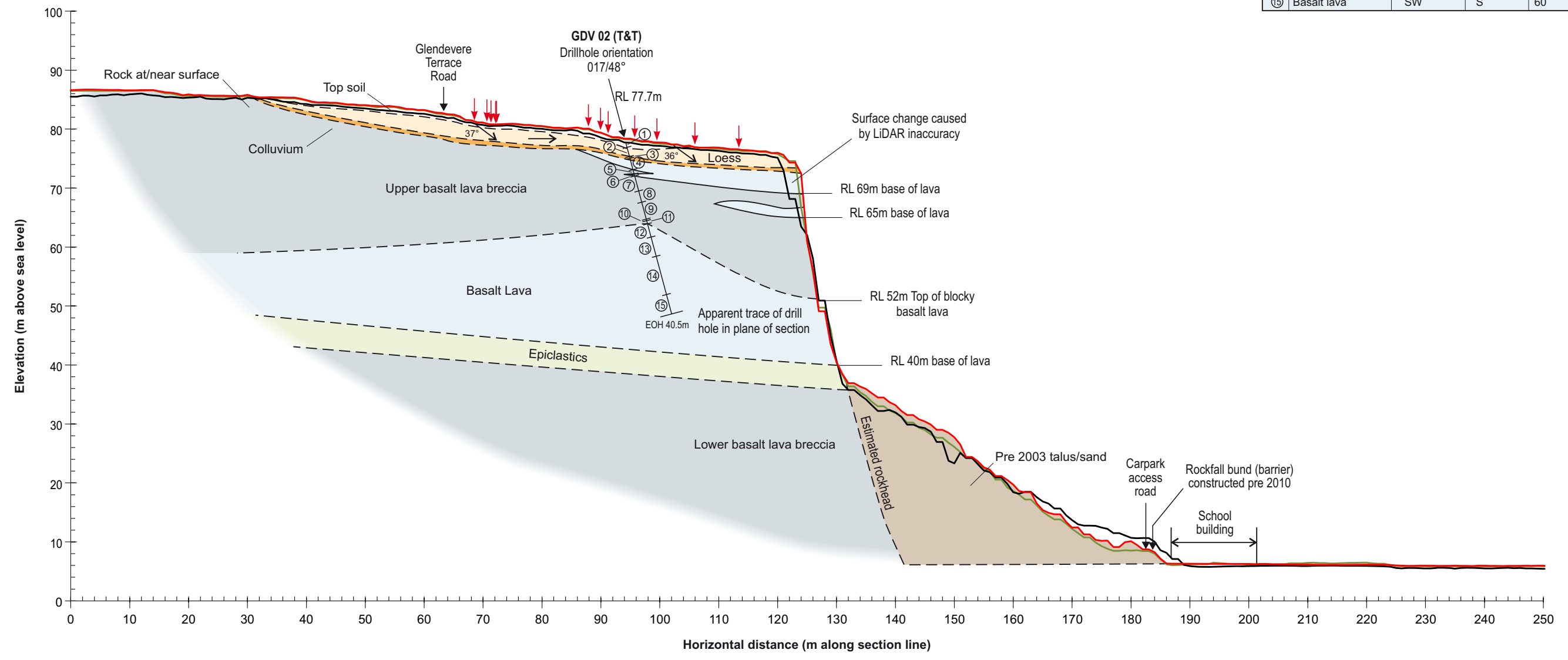
REPORT: CR2014/78 DATE: August 2014



- Material boundary
- - - Material boundary (projected)
- 2011c LIDAR
- 2011a LIDAR
- 2003 LIDAR
- ↓ Tension crack
- Movement direction and angle (from horizontal) inferred from local crack apertures.

GDV 02 (T&T)

	Material type	Weathering	Strength	RQD %
①	Top Soil			
②	Loess			
③	Colluvium			
④	Basalt lava	SW	MS	50-70
⑤	Basalt lava breccia	MW	W	50
⑥	Basalt lava	UW	MS	65-100
⑦	Basalt lava breccia	HW	VW-S	40-80
⑧	Basalt lava breccia	HW	W	50-80
⑨	Basalt lava breccia	HW	VW-W	65-100
⑩	Basalt lava breccia	HW	MS	30-75
⑪	Basalt lava breccia	MW	MS	75
⑫	Basalt lava	SW	S	65
⑬	Basalt lava	SW	S	60-100
⑭	Basalt lava	SW	S	50-90
⑮	Basalt lava	SW	S	60



Weathering (adopting NZGS (2005) terminology): CW completely weathered; HW highly weathered; MW moderately weathered; SW slightly weathered; UW unweathered.
 Rock Strength (field strengths adopting NZGS (2005) terminology): EW extremely weak; VW very weak; W weak; MS moderately strong; S Strong; VS very strong; extremely strong.
 Soil strength (field strengths adopting NZGS (2005) terminology): Coarse soils – VL very loose; L loose; MD medium dense; D dense, VD very dense. Cohesive soils – H hard; VSt very stiff; St stiff; F firm; So soft; VSo very soft.
 RQD: Rock quality designation

DRW:
PC
CHK:
CM/FDP



ENGINEERING GEOLOGY CROSS SECTION R01

**Redcliffs
Christchurch**

FIGURE 13

FINAL

REPORT:
CR2014/78

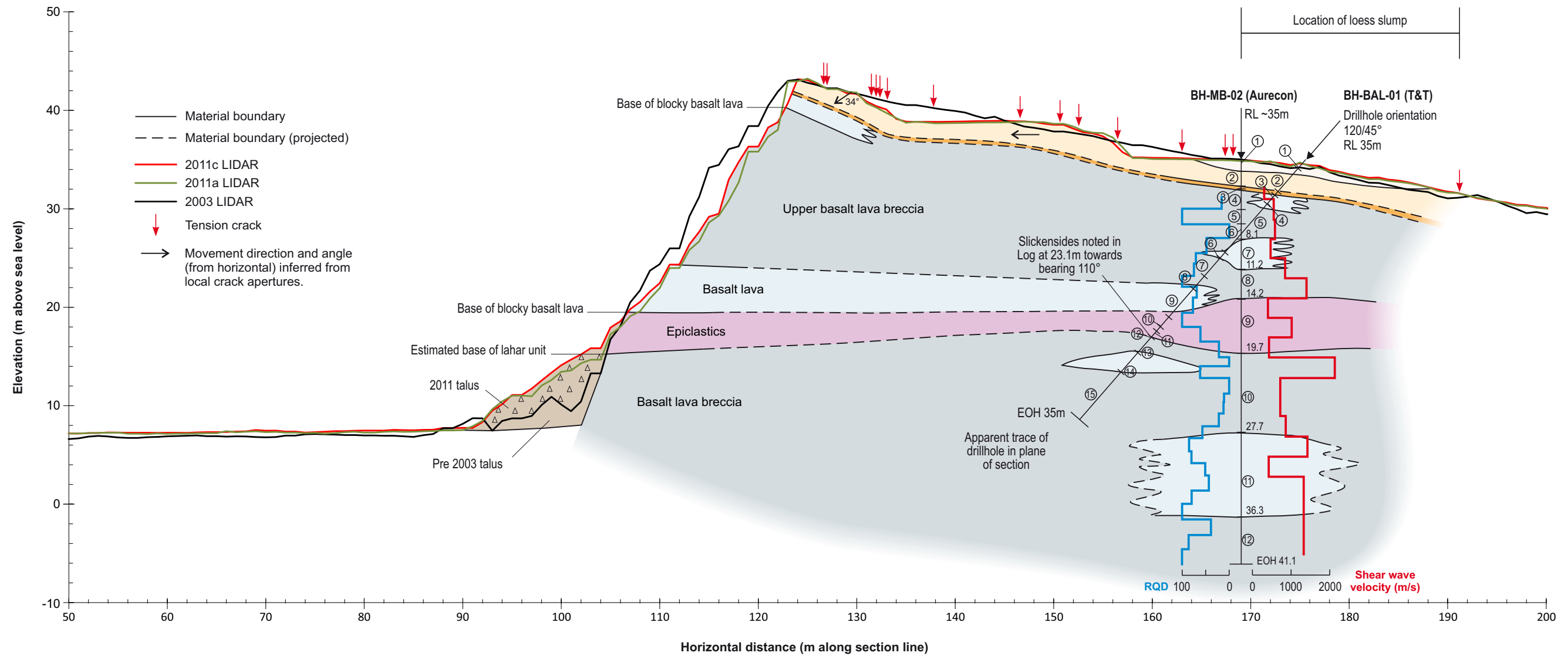
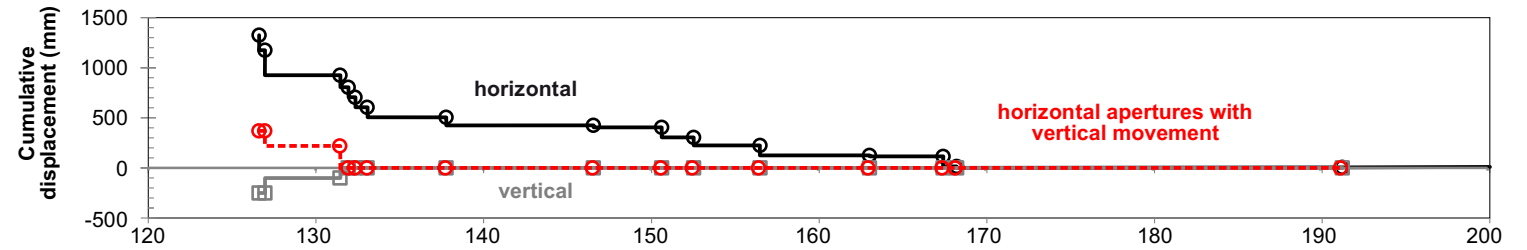
DATE:
August 2014

BH-BAL-01 (T&T)

	Material type	Weathering	Strength	RQD %
①	Top Soil			
②	Loess			
③	Basalt lava breccia	HW	W	
④	Basalt lava	MW	MS	
⑤	Basalt lava breccia	HW	W	
⑥	Basalt lava	SW	VS	
⑦	Basalt lava breccia	MW	MS	
⑧	Basalt lava breccia	HW	EW	
⑨	Basalt lava	MW	VS	
⑩	Pyroclastic breccia	MW	EW	
⑪	Pyroclastics	MW	EW	
⑫	Basalt lava	MW	W	
⑬	Basalt lava breccia	MW	W	
⑭	Basalt lava	MW	S	
⑮	Basalt lava breccia	HW	EW	

BH-MB-02 (Aurecon)

	Material type	Weathering	Strength	RQD %
①	Road/Fill			
②	Loess			
③	Colluvium			
④	Basalt lava breccia	HW	W	0
⑤	Basalt lava breccia	HW	S	92
⑥	No recovery			
⑦	Basalt lava	MW	S	24-71
⑧	Basalt lava breccia	SW	S	71
⑨	Tuff	MW	W	70
⑩	Basalt lava breccia	MW	MS	30-60
⑪	Basalt lava	SV	SW	70
⑫	Basalt lava breccia	MW	MS	0



Weathering (adopting NZGS (2005) terminology): CW completely weathered; HW highly weathered; MW moderately weathered; SW slightly weathered; UW unweathered.
 Rock Strength (field strengths adopting NZGS (2005) terminology): EW extremely weak; VW very weak; W weak; MS moderately strong; S Strong; VS very strong; extremely strong.
 Soil strength (field strengths adopting NZGS (2005) terminology): Coarse soils – VL very loose; L loose; MD medium dense; D dense, VD very dense. Cohesive soils – H hard; VSt very stiff; St stiff; F firm; So soft; VSo very soft.
 RQD: Rock quality designation

DRW:
PC
CHK:
CM/FDP



ENGINEERING GEOLOGY CROSS SECTION R02

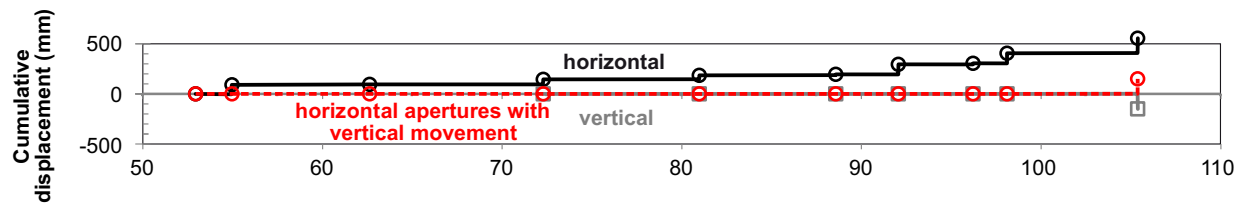
**Redcliffs
Christchurch**

FIGURE 13

FINAL

REPORT:
CR2014/78

DATE:
August 2014

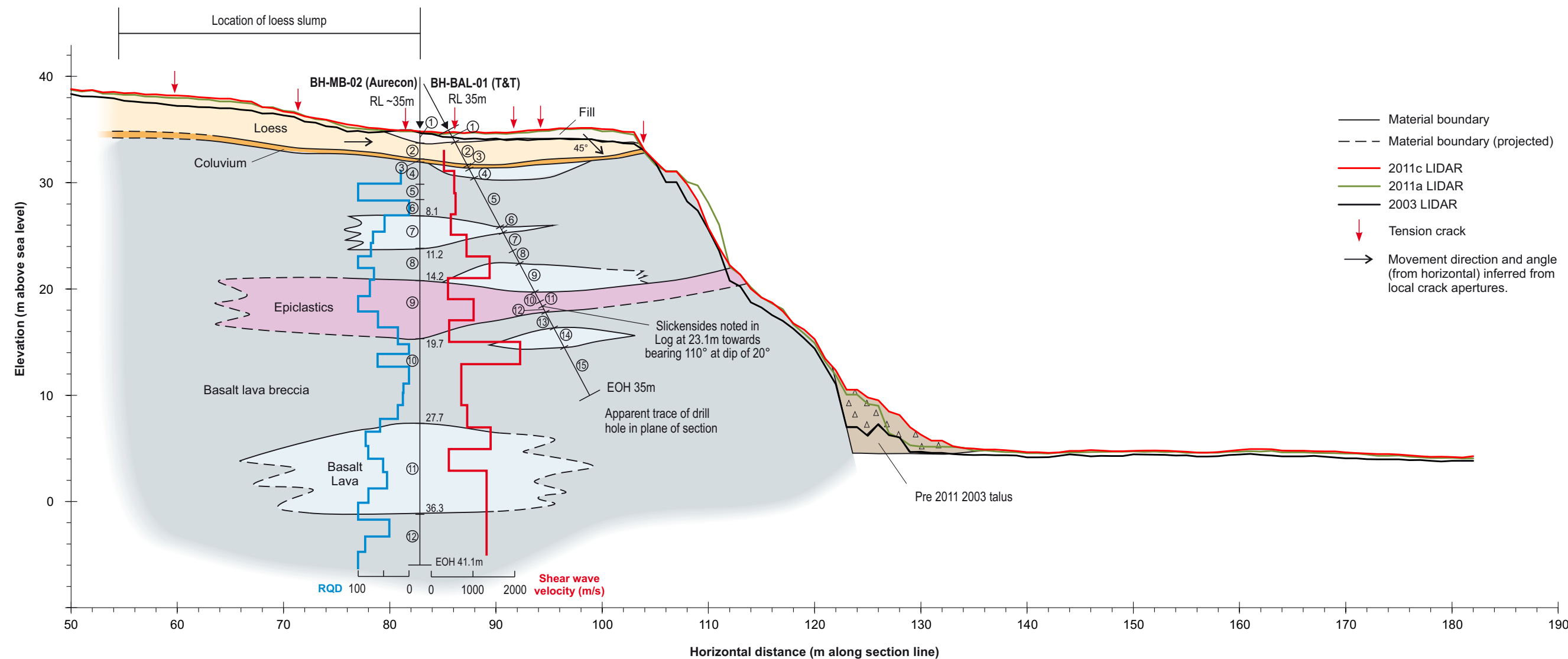


BH-MB-02 (Aurecon)

	Material type	Weathering	Strength	RQD %
①	Road/Fill			
②	Loess			
③	Colluvium			
④	Basalt lava breccia	HW	W	0
⑤	Basalt lava breccia	HW	S	92
⑥	No recovery			
⑦	Basalt lava	MW	S	24-71
⑧	Basalt lava breccia	SW	S	71
⑨	Epiclastics	MW	W	70
⑩	Basalt lava breccia	MW	MS	30-60
⑪	Basalt lava	SV	SW	70
⑫	Basalt lava breccia	MW	MS	0

BH-BAL-01 (T&T)

	Material type	Weathering	Strength	RQD %
①	Top Soil			
②	Loess			
③	Basalt lava breccia	HW	W	
④	Basalt lava	MW	MS	
⑤	Basalt lava breccia	HW	W	
⑥	Basalt lava	SW	VS	
⑦	Basalt lava breccia	MW	MS	
⑧	Basalt lava breccia	HW	EW	
⑨	Basalt lava	MW	VS	
⑩	Epiclastics	MW	EW	
⑪	Epiclastics	MW	EW	
⑫	Epiclastics	MW	W	
⑬	Basalt lava breccia	MW	W	
⑭	Basalt lava	MW	S	
⑮	Basalt lava breccia	HW	EW	



Weathering (adopting NZGS (2005) terminology): CW completely weathered; HW highly weathered; MW moderately weathered; SW slightly weathered; UW unweathered.
 Rock Strength (field strengths adopting NZGS (2005) terminology): EW extremely weak; VW very weak; W weak; MS moderately strong; S Strong; VS very strong; extremely strong.
 Soil strength (field strengths adopting NZGS (2005) terminology): Coarse soils – VL very loose; L loose; MD medium dense; D dense, VD very dense. Cohesive soils – H hard; VSt very stiff; St stiff; F firm; So soft; VSo very soft.
 RQD: Rock quality designation

DRW:
PC
CHK:
CM/FDP



ENGINEERING GEOLOGY CROSS SECTION R03

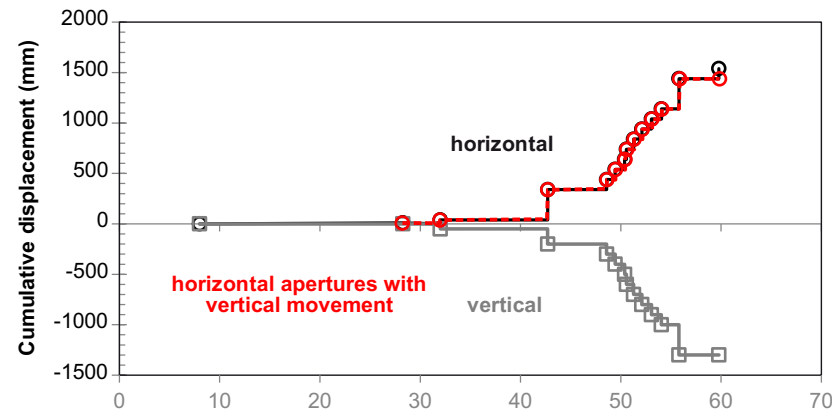
FIGURE 13

**Redcliffs
Christchurch**

FINAL

REPORT:
CR2014/78

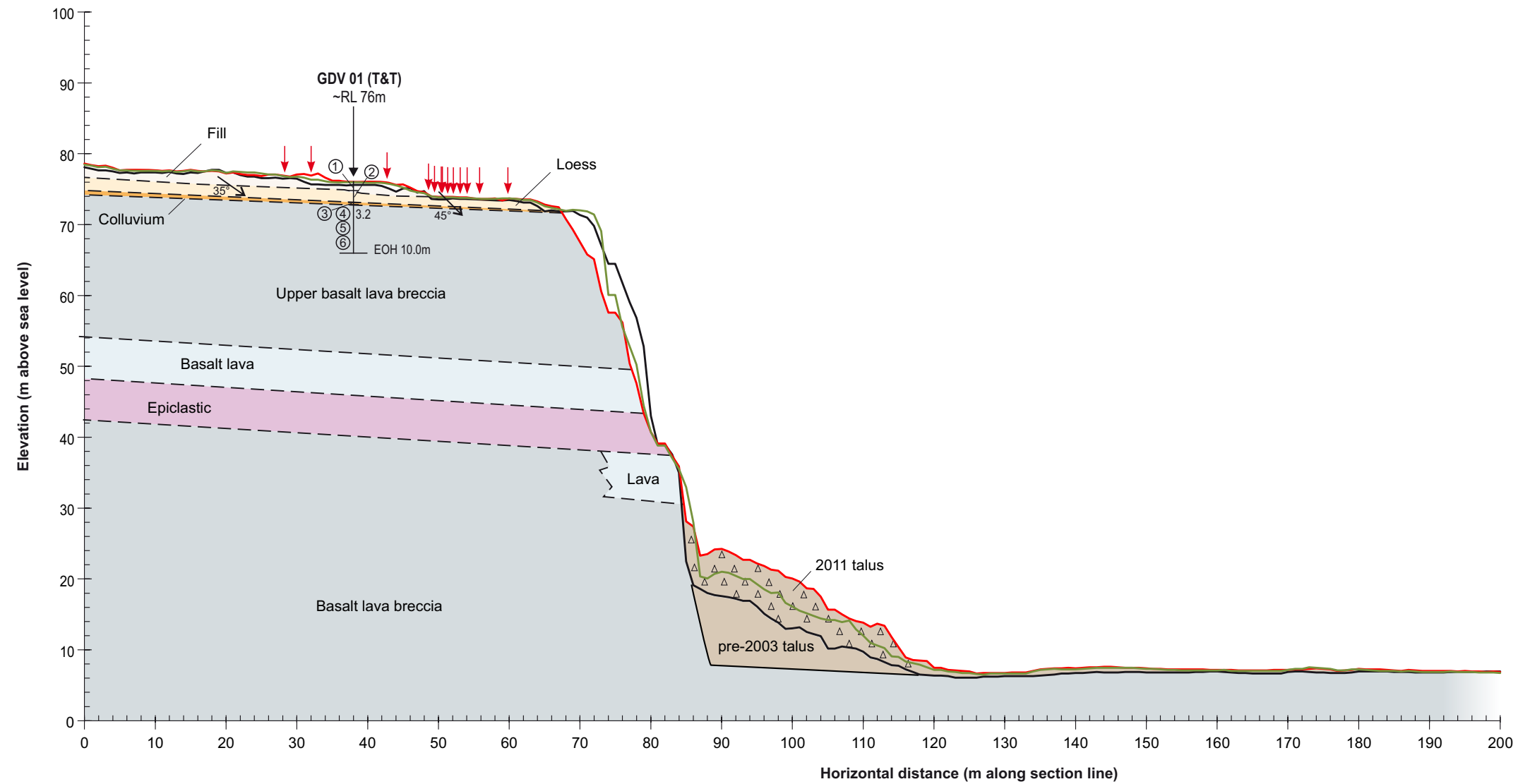
DATE:
August 2014



- Material boundary
- - - Material boundary (projected)
- 2011c LIDAR
- 2011a LIDAR
- 2003 LIDAR
- ↓ Tension crack
- Movement direction and angle (from horizontal) inferred from local crack apertures.

GDV 01 (T&T)

	Material type	Weathering	Strength	RQD %
①	Fill			
②	Loess	M-W		100
③	Colluvium	MW-W	S	100
④	Basalt lava breccia	W	S	100
⑤	Core loss			
⑥	Basalt lava breccia	MW	MS	100



Weathering (adopting NZGS (2005) terminology): CW completely weathered; HW highly weathered; MW moderately weathered; SW slightly weathered; UW unweathered.
 Rock Strength (field strengths adopting NZGS (2005) terminology): EW extremely weak; VW very weak; W weak; MS moderately strong; S Strong; VS very strong; extremely strong.
 Soil strength (field strengths adopting NZGS (2005) terminology): Coarse soils – VL very loose; L loose; MD medium dense; D dense, VD very dense. Cohesive soils – H hard; VSt very stiff; St stiff; F firm; So soft; VSo very soft.
 RQD: Rock quality designation

DRW:
PC
CHK:
CM/FDP



ENGINEERING GEOLOGY CROSS SECTION R04

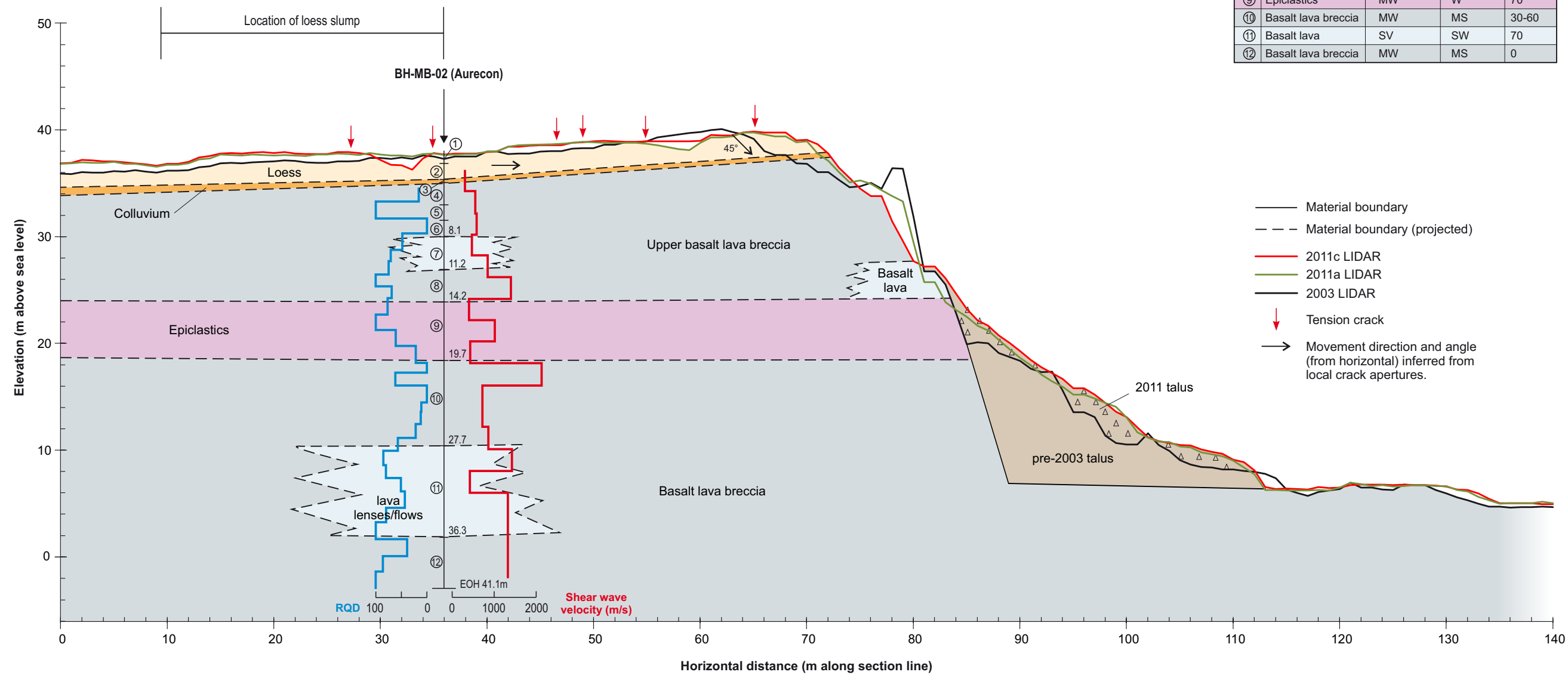
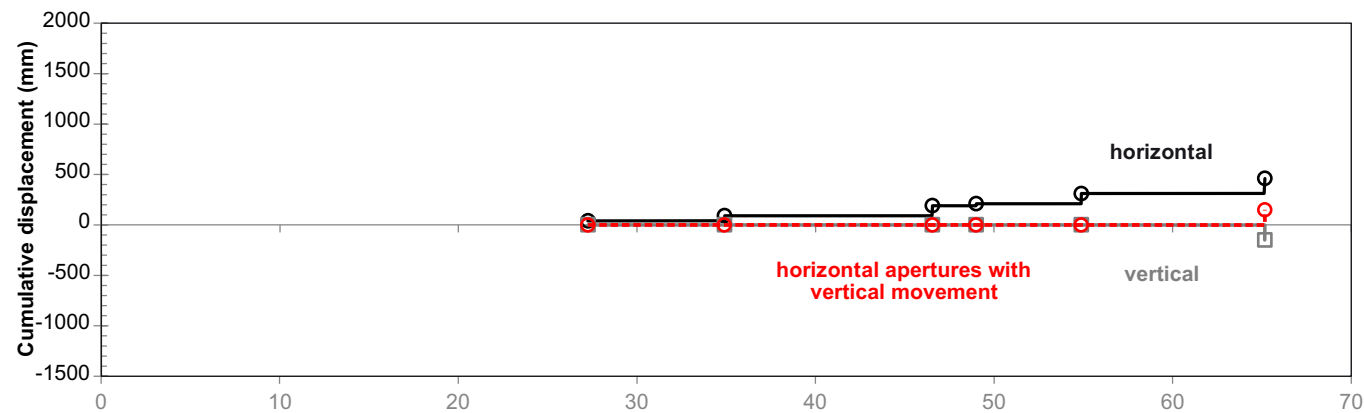
**Redcliffs
Christchurch**

FIGURE 13

FINAL

REPORT:
CR2014/78

DATE:
August 2014



BH-MB-02 (Aurecon)

	Material type	Weathering	Strength	RQD %
①	Road/Fill			
②	Loess			
③	Colluvium			
④	Basalt lava breccia	HW	W	0
⑤	Basalt lava breccia	HW	S	92
⑥	No recovery			
⑦	Basalt lava	MW	S	24-71
⑧	Basalt lava breccia	SW	S	71
⑨	Epiclastics	MW	W	70
⑩	Basalt lava breccia	MW	MS	30-60
⑪	Basalt lava	SV	SW	70
⑫	Basalt lava breccia	MW	MS	0

- Material boundary
- - - Material boundary (projected)
- 2011c LIDAR
- 2011a LIDAR
- 2003 LIDAR
- ↓ Tension crack
- Movement direction and angle (from horizontal) inferred from local crack apertures.

Weathering (adopting NZGS (2005) terminology): CW completely weathered; HW highly weathered; MW moderately weathered; SW slightly weathered; UW unweathered.
 Rock Strength (field strengths adopting NZGS (2005) terminology): EW extremely weak; VW very weak; W weak; MS moderately strong; S Strong; VS very strong; extremely strong.
 Soil strength (field strengths adopting NZGS (2005) terminology): Coarse soils – VL very loose; L loose; MD medium dense; D dense, VD very dense. Cohesive soils – H hard; VSt very stiff; St stiff; F firm; So soft; VSo very soft.
 RQD: Rock quality designation

DRW:
PC
CHK:
CM/FDP



ENGINEERING GEOLOGY CROSS SECTION R05

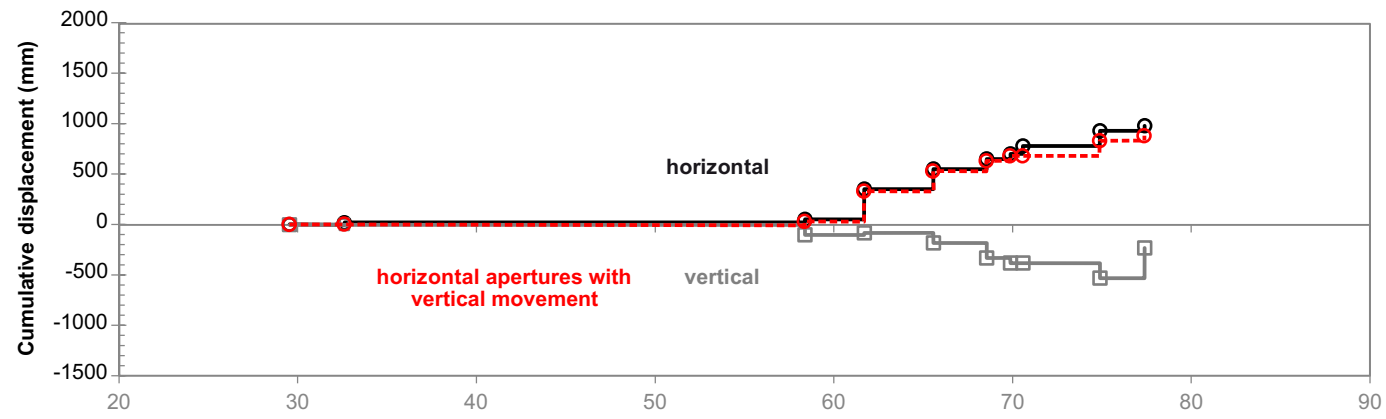
**Redcliffs
Christchurch**

FIGURE 13

FINAL

REPORT:
CR2014/78

DATE:
August 2014

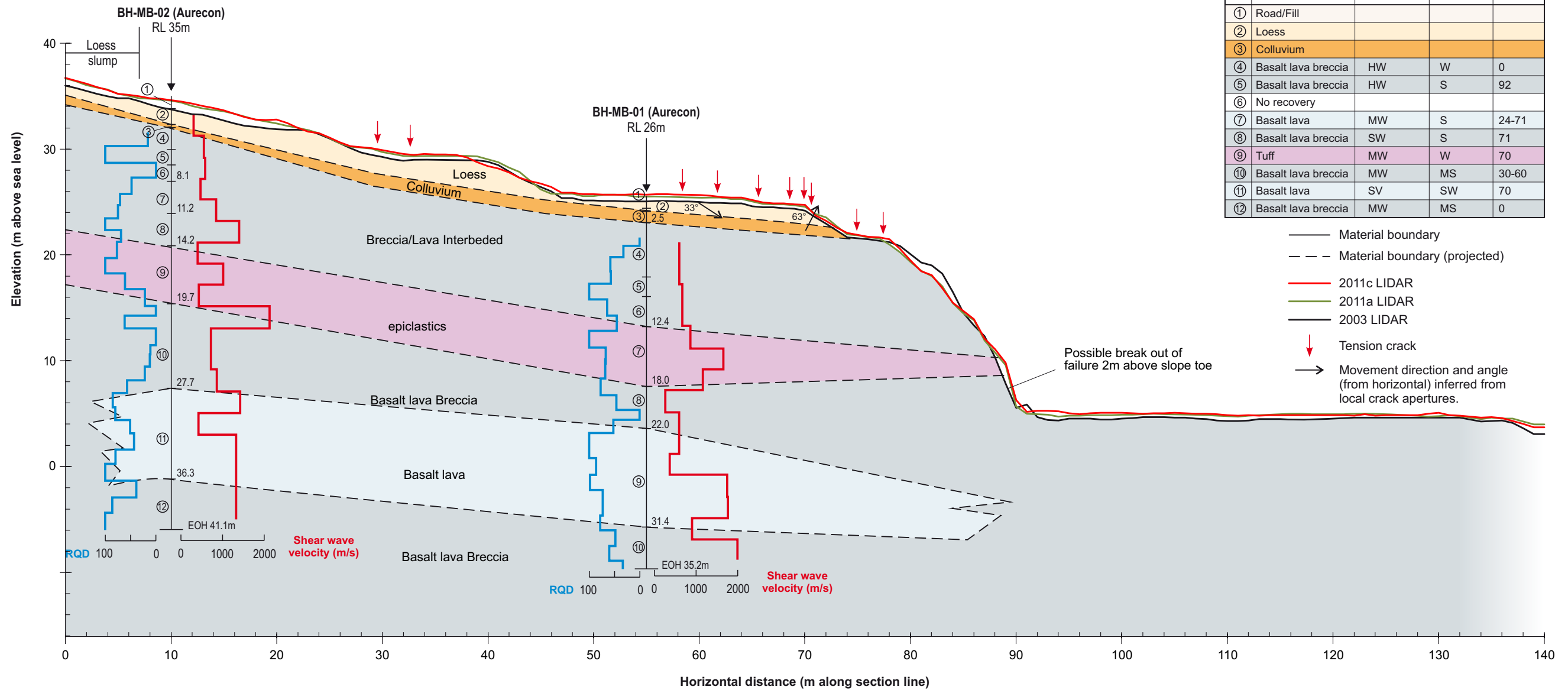


BH-MB-01 (Aurecon)

	Material type	Weathering	Strength	RQD %
①	Road/Fill			
②	Loess			
③	Colluvium			
④	Basalt lava	HW	W-S	0-100
⑤	Tuff	MW	S	60-100
⑥	Basalt lava breccia	HW	S	45-65
⑦	Tuff	HW	W-MS	60-100
⑧	Basalt lava breccia	HW	W-MS	0-50
⑨	Basalt lava	SW	S-VS	100
⑩	Basalt lava breccia	SW-HW	S	30-60

BH-MB-02 (Aurecon)

	Material type	Weathering	Strength	RQD %
①	Road/Fill			
②	Loess			
③	Colluvium			
④	Basalt lava breccia	HW	W	0
⑤	Basalt lava breccia	HW	S	92
⑥	No recovery			
⑦	Basalt lava	MW	S	24-71
⑧	Basalt lava breccia	SW	S	71
⑨	Tuff	MW	W	70
⑩	Basalt lava breccia	MW	MS	30-60
⑪	Basalt lava	SV	SW	70
⑫	Basalt lava breccia	MW	MS	0



- Material boundary
- - - Material boundary (projected)
- 2011c LIDAR
- 2011a LIDAR
- 2003 LIDAR
- ↓ Tension crack
- Movement direction and angle (from horizontal) inferred from local crack apertures.

Weathering (adopting NZGS (2005) terminology): CW completely weathered; HW highly weathered; MW moderately weathered; SW slightly weathered; UW unweathered.
 Rock Strength (field strengths adopting NZGS (2005) terminology): EW extremely weak; VW very weak; W weak; MS moderately strong; S Strong; VS very strong; extremely strong.
 Soil strength (field strengths adopting NZGS (2005) terminology): Coarse soils – VL very loose; L loose; MD medium dense; D dense; VD very dense. Cohesive soils – H hard; VSt very stiff; St stiff; F firm; So soft; VSo very soft.
 RQD: Rock quality designation

DRW:
PC
CHK:
CM/FDP



ENGINEERING GEOLOGY CROSS SECTION R06

**Redcliffs
Christchurch**

FIGURE 13

FINAL

REPORT:
CR2014/78

DATE:
August 2014

Table 6 shows the total inferred displacement across all cracks relative to each cross-section; the number in brackets represents the displacement calculated using only those components with both horizontal and vertical measurements.

The dip of the resultant vectors from the horizontal – adopting only those components with both vertical and horizontal displacement – suggests that the angle of displacement is significantly steeper than the loess/rock interface, and more consistent with displacement of the underlying rock rather than localised slumping of the loess along the loess/rock interface. Also, the loess thickness is only 1–2 m near the cliff edge, where vertical displacements of greater than 0.5 m have been recorded (e.g., 1.5 m in cross-section 4).

Given these uncertainties, the displacements inferred from crack apertures are thought to represent upper bound estimates of the total permanent displacements of the cliff crest during the 2010/11 Canterbury earthquakes.

Table 6 Measured total cumulate crack apertures (measured normal to the slope), which formed during the 2010/11 Canterbury earthquakes (mainly during the 22 February 2011 earthquakes and less so during the 13 June 2011 earthquakes). Cracks measured by GNS Science and M. Yetton (Geotech Ltd). Displacements are inferred from field mapping of tension crack apertures along survey lines. Errors are nominally estimated as being ± 0.01 m (values are rounded to the nearest 10 mm).

Cross-section	Source area	Vertical component (mm)	Horizontal component (mm)	Resultant vector magnitude/dip angle from horizontal		Angle of rockhead (loess/rock interface) (°)
				(mm)	(°)	
1	1	1260 (560) ¹	2540 (750) ¹	2840 (940)	26 (37)	3
2	2	250	1330 (370)	1350 (450)	11 (34)	10
3		150	560 (150)	580 (210)	15 (45)	0
4	1	1300	1540 (1430)	2015 (1930)	40 (42)	4
5		150	460 (150)	480 (210)	18 (45)	3 (into slope)
6	3	230	990 (880)	1010 (910)	13 (15)	5

Values in brackets represent those displacements calculated using only those components with both horizontal and vertical measurements only.

¹ Displacement estimate also excludes the first crack, which corresponds to a local feature within the loess, and is not thought to be related to displacement of the larger cliff.

3.2.3.2 Estimating earthquake displacement of the cliff crest

There are no reliable monitoring data that covers exactly the period of the 2010/11 Canterbury earthquakes. However, it is possible to estimate the likely magnitude of the displacement of the main cracked areas at the cliff crest during the 22 February and 13 June 2011 earthquakes, by subtracting the cumulative inferred displacements from crack apertures as follows:

Total displacement inferred from the mapping of crack apertures over the period corresponding to the two main earthquakes was about 0.2–1.9 m, adopting only those displacements from cracks with measurements of both horizontal and vertical displacements, and recorded along cross-sections 1–6 (Table 6).

Field mapping of the cliff crest was again carried out by Geotech Ltd. following the 13 June 2011 earthquake. This mapping measured pre-existing cracks and any new cracks that may have formed in response to these earthquakes (Appendix 5). These displacements are summarised for each cross-section in Table 7.

Permanent slope displacement of the cliff crest along the cross-sections can be estimated by subtracting the 13 June 2011 earthquake displacements (Table 7) from the total displacements (Table 6), to derive a range of possible displacements that may have occurred during the 22 February 2011 earthquakes. These magnitudes are inherently uncertain (Table 8).

Permanent slope displacement of the cliff crest during the 16 April and 23 December 2011 earthquakes are unknown. Site observations suggest little reactivation of existing cracks with only a few new cracks appearing (Appendix 5).

Table 7 Measured cumulate crack apertures, horizontal only, which formed during the 13 June 2011 earthquakes, measured by M. Yetton (Geotech Ltd.; Appendix 4). Displacements are inferred from field mapping of tension crack apertures along survey lines. Errors are nominally estimated as being ± 0.01 m (values are rounded to the nearest 10 mm).

Cross-section	Source Area	Vertical component (mm)	Horizontal component (mm)
1 and 4	1	Not measured	230–610
2 and 5	2	Not measured	180–200
6	3	Not measured	650–680

Table 8 Inferred cumulative crack apertures for the 22 February 2011 earthquakes. Calculated by subtracting the inferred displacements in Table 7 from the inferred total displacements in Table 6, along corresponding cross-sections.

Cross-section	Source Area	Vertical component (mm)	Horizontal component (mm)
1 and 4	(Source area 1)	750–1430	330–1320
2 and 5	(Source area 2)	370	10–280
6	(source area 3)	880	230–260

3.2.3.3 Surveyed slope displacements

The survey monitoring data are presented in Appendix 4 and summarised below. There are two data sets:

1. Cadastral survey marks (details held by Land Information New Zealand) i.e., property boundaries and roads footpaths etc.; and
2. Monitoring survey marks installed by Aurecon NZ Ltd., for Christchurch City Council, to monitor surface displacement.

Both datasets adopt reference control marks outside the area of landslide movement, but still within the local area. Therefore, regional offsets caused by the tectonic displacements are largely removed from the data.

Cadastral marks (source: LINZ)

Available cadastral survey marks were resurveyed by GNS Science to detect absolute ground movements spanning the earthquake period from before the 22 February 2011 earthquakes (the pre-earthquake survey dates for each cadastral mark vary) to 11 February 2012, and therefore include total displacements of the survey marks in response to the earthquakes within this time period. Only two survey marks are located in the cracked areas behind the slope crest (cadastral survey marks 35 and 42, Appendix 4 Map 2), and therefore do not represent the overall movement of the slope.

The results of this survey are contained in Appendix 4 (Map 2). Vector displacements indicate permanent ground displacements in the order of about 0.2–0.3 m. These are thought to represent lower-bound estimates of the total displacement during the earthquakes, at the cliff crest, as these survey marks were located outside the main areas of cracking.

Monitoring marks (source: Aurecon NZ Ltd.)

The displacements calculated using the Aurecon survey data span the time period 5 November 2012 to 5 April 2013 and there are approximately five observations per mark. Note that the dates covered and the numbers of observations vary per survey mark. The marks are installed only in assessed source areas 2 and 3, and no marks are installed in assessed source area 1.

These data do not span the time frame corresponding to the 2010/11 Canterbury earthquakes. From the survey time series relating to each mark it has been possible to determine the magnitudes and bearings of any displacement over the monitoring period. The only displacements calculated from the monitoring marks that are larger than the associated error (monitoring mark ID's 5 and 17, Map 3, Appendix 4), were:

- Mark 5: 12 mm/year towards bearing 350–355°; and
- Mark 12: 12 mm/year towards bearing 280–290°.

The displacement of monitoring mark 5 is consistent with the field-measured displacement (of 30 mm towards the north) of “tell-tale” survey pegs installed by Geotech Ltd., indicating displacement occurred sometime between November 2012 and April 2013.

The displacement of monitoring mark 17 is consistent with the area of extension and compression at the cliff crest immediately west of assessed source area 2. This movement is not thought to relate to displacement of the rock slope, as the direction of movement is away from the steeper slope. This displacement is inferred to be related to displacement of the mapped slump.

3.2.3.4 Volumes of debris lost from the cliffs

Changes of the cliffs in response to the 2011 earthquakes have been quantified using repeat terrestrial laser scan surveys and LiDAR surveys (Table 9) with field mapping.

Table 9 Estimated volumes lost from the cliffs calculated from the terrestrial laser scan (TLS) and LiDAR surveys.

Change model	Volume leaving slope (m ³)	Area of slope face (m ²) ³	Volume loss per unit area (m ³ /m ²)	Probable trigger
Estimate by PHGG consultants after the 4 September 2010 earthquake	60 (±10)	22,000	0.003	4 September 2010 earthquake (M _w 7.2)
Airborne LiDAR: 2003–March 2011 (2011a) ¹	23,800 (±6600)	22,000	1.08	22 February 2011 earthquake (M _w 6.2)
TLS: 6 March 2011–3 May 2011 ²	1,170 (±110)	22,970	0.05	16 April 2011 earthquake (M _L 5.6)
Airborne LiDAR: March 2011–July 2011 ¹	11,800 (±3500)	22,970	0.51	13 June 2011 earthquake (M _w 6.2)
TLS: 16 June 2011–16 January 2011 ²	1,180 (±130)	22,870	0.05	23 December 2011 earthquake (M _w 6.1)
TLS: 16 January 2011–19 December 2012 ²	440 (±160)	22,870	0.02	No obvious trigger possible rainfall induced
TLS: 19 December 2012–12 November 2013	81 (±47)	22,870	0.004	No obvious trigger possible rainfall induced

¹ Change models derived from airborne LiDAR surveys carried out by AMM Hatch (2003) and New Zealand Aerial Mapping (2011a, March 2011 and 2011c, July 2011); refer to Appendix 2 for details.

² Change models derived from terrestrial laser scan surveys carried out by GNS Science, refer to Appendix 3 for details.

³ Slope surface areas are estimated for each change model using the LiDAR slope surface at the time of the earthquake, and the area where changes to the slope face occurred.

Digital elevation models representing the ground surface at a given time were generated for each data set. For the LiDAR surveys, a 1 m grid (ground resolution) of elevations was generated from filtered scan data points supplied by the contractor. For each of the terrestrial laser scan surveys a 0.1 m grid was generated from the filtered point data. Filtering comprised removal of points representing vegetation and buildings from the supplied point data, thereby creating a “bare earth” or “filtered” point elevation data set. This was undertaken by GNS Science for the terrestrial laser scan survey data, and by the consultants AAM Hatch and New Zealand Aerial Mapping for the LiDAR datasets (these companies were commissioned by other parties, mainly the Earthquake Commission and the Christchurch City Council, to carry out the surveys).

Errors are assessed for each digital elevation model by comparing the modelled surface with the filtered point data used to generate it. Errors in the terrestrial laser scan survey data are generally ± 0.05 – 0.09 m at one standard deviation and for the LiDAR data generally ± 0.1 – 0.3 m (in height) for the New Zealand Aerial Mapping data sets (LiDAR surveys 2011a and 2011c), and ± 0.3 – 0.5 m (in height) for the AAM Hatch data sets.

3.2.4 Subsurface movement

Drillhole inclinometer tubes were used to monitor displacements at depth, assess whether movement was occurring along single or multiple slide-surfaces, and to independently verify the results of surface monitoring. Monitoring is undertaken manually by commercial contract (Geotechnics Ltd.).

Inclinometer tubes were installed in drillholes BH-MB-01, BH-MB-02 (Pletz and Revell, 2013), and BH-GDV-01 (Tonkin and Taylor, 2012a). The inclinometer displacements are monitored at 0.5 m intervals and the inclinometer accuracy is quoted as ± 6 mm over 25 m of tubing (Slope Indicator, 2005). The measurement details are summarised in Table 10.

The inclinometers installed in drillholes BH-MB-01 and BH-MB-02 show no movement of the inclinometer tubes greater than the associated error, and therefore indicate no displacement. However, the inclinometer tube installed in BH-GDV-01 has a deflection between the 2.25 and 3.25 m (below the collar elevation) intervals. The deflection is relatively small, about 2 mm in the A-Axis plot, and is marginally outside the associated error. The monitoring reports received do not indicate what bearing of movement this is towards. The deflection is only recorded in one survey, it is not known if there are more recent survey records.

The deflection occurred between the 25 October 2011 and 24 December 2011 inclinometer surveys (Tonkin and Taylor, 2012a), and corresponds to the base of the loess/volcanic colluvium logged in the drillhole, suggesting displacement along rockhead. This displacement may be related to the 23 December 2011 earthquake. Any deeper-seated displacement of the underlying rock mass forming the cliff would not have been measured by the inclinometer, as the inclinometer base is only 10 m below ground level, compared to a cliff height (cliff crest to toe) of about 70 m.

Table 10 Summary of drillhole inclinometer surveys.

Measuring date	Drillhole ID		
	BH-MB-01 ¹	BH-MB-02 ¹	BH-GDV-01 (Tonkin and Taylor, 2012a)
15/07/2011	N/A	N/A	Base reading
8/09/2011	N/A	N/A	No movement outside error
16/09/2011	N/A	N/A	No movement outside error
12/10/2011	N/A	N/A	No movement outside error
25/10/2011	N/A	N/A	No movement outside error
24/12/2011			About 2 mm in cumulative displacement plot at a depth interval between 2.25 and 3.25 below ground level.
4/04/2013	Base reading	Base reading	No data
5/06/2013	No movement outside error	No movement outside error	No data
21/03/2014	No movement outside error	No movement outside error	No data

¹ Geotechnics Ltd Report 720085.000/RPT (Geotechnics, 2014).

3.2.5 Groundwater

Drill water circulation conditions reported in drilling records (Pletz and Revell, 2013) indicate water losses occurred in drillholes BH-MB-01 and BH-MB02, and were in the range from 10 to 100% (percentage of water flush lost into the ground), but generally between 80 and 100%. BH-MB-01 was reported as being dry by the driller (no water return). Groundwater levels in the Tonkin and Taylor (2012a) drillhole BH-GDV-01 were 0.6–1.8 m below ground level, and ground water was not encountered in CPT-GDV-01 and CPT-GDV-02.

There are three standpipes installed in the assessment area. These were installed by Tonkin and Taylor Ltd in drillhole BH-GDV-01 and cone penetration holes CPT-GDV-01 and CPT-GDV-02. The bottom of the standpipe response zones are reported to be in loess, at depths of between 2.8 m and 3.5 m below ground level.

Monitoring data from the standpipes comprise the manual measurement of water levels in the standpipes. Approximately 3–14 measurements were made over the reporting period 3 August 2011–29 May 2012 (Tonkin and Taylor, 2012a), indicating a poor temporal resolution. No more recent data are available to GNS Science at the time of writing this report. The data show that standpipes CPT-GDV-01 and CPT-GDV-02 were dry at the times they were measured. Measurements from standpipe BH-GDV-01 show water levels in the loess at around 1 m below ground level, with the bottom of the response zone being at about 2.3 m below ground level, for the period 8 August 2011 to about 11 November 2011. The reading made around 9 April 2012 indicated that the standpipe was dry.

It is possible that groundwater is present in the other standpipes, but that the poor temporal resolution has not allowed them to be resolved. Springs and water seepage have been noted (Figure 11). There are also reports of increased storm water flow over the cliff edge due to damaged services.

These data suggest there is some groundwater present at the site but that it is probably confined within the loess at the cliff crest. It should be noted that standpipe BH-GDV-01 is downslope and within about 10 m of a main storm water drain, which appears to be broken. Drilling records indicate that the rock mass, forming the steep rock slope, is predominantly dry with no permanent water table apparent, and that during drilling, circulation of drilling fluids was lost, indicating a highly permeable rock mass.

3.3 ENGINEERING GEOLOGICAL MODEL

An engineering geological map is presented in Figure 11, site investigation map in Figure 12 and cross-sections 1–6 in Figure 13. The map and cross-sections are based on the interpretation of features identified in aerial photographs, field mapping and ground investigation data.

3.3.1 Slope materials

3.3.1.1 Fill

Localised areas of fill relating to the construction of residential homes can be found over much of the site. The depth and extent of these localised areas are unknown, although the inferred boundaries of the fill are shown on cross-sections in Figure 13 (where mapped). The fill, where encountered in drillholes, is described as soft and relatively weak silt with occasional clasts of basalt and concrete. The thickness of the fill, unless encountered in drillholes, is unknown, but it is estimated to be up to several metres in places.

3.3.1.2 Talus

The talus at the toe of the cliff – present before the 2010/11 Canterbury earthquake-induced talus accumulations – comprises several car-sized boulders along with many smaller boulders of volcanic rock that have fallen from the cliff. Much of this material has slaked – due to wetting and drying cycles – indicating that the original rockfall volumes were probably larger than the volume of talus currently present.

The recent accumulations of talus and boulders triggered by the 2010/11 Canterbury earthquakes are shown on Figure 11. Site observations – post-2010/11 earthquakes – indicate that these volcanic materials are already slaking. Sampling for particle size distributions of the talus has not been carried out for health and safety reasons. However, estimates made from photographs and terrestrial laser scan surveys, suggest the majority of the debris comprises boulders of diameter greater than 0.5 m.

3.3.1.3 Loess

The loess mantling the slope within the assessment area is similar to other areas of the Port Hills. It is a relatively cohesive silt-dominated soil with only minor clay mineral content. Its strength is largely controlled by the soil moisture content and this has been well studied, e.g., Bell et al. (1986), Bell and Trangmar (1987), McDowell (1989), Goldwater, (1990), Yetton (1992) and Carey et al. (2014). In some places the loess appears to have been reworked by construction activities for the residential dwellings.

The loess in the main zone of cracking at the cliff crest is unsaturated and relatively strong where exposed. Similarly, the thin layer of loess/volcanic colluvium sometimes present above the bedrock and at the base of the loess does not appear particularly weak or wet. The loess

is highly hygroscopic and when exposed to water (rain) it quickly disintegrates into muddy silt. The thickness of the loess mantling the cliff top inferred from drillhole and trial pit records and from field mapping of exposures, varies between less than 1 m and up to 3 m, but up to 4 m well back from the cliff edge.

3.3.1.4 Colluvium

A layer, of sandy silt containing boulders and gravel with minor clay was logged in drillholes BH-GDV-01, BH-GDV-02, BH-BAL-01, BH-MB-01 and BH-MB-02. Codd and Revell (2013) describe this material as highly variable and dominated by either silts or gravel and cobbles. The thickness of the colluvium varies from about one metre near the cliff crest to less than 0.3 m and less further back from the cliff crest.

Given that all drillholes encountered this material, it has been assumed that volcanic colluvium mantles rockhead and underlies the loess over most of the site. Where exposed in outcrop, the colluvium appears to have slightly higher clay content than those materials described in the drillhole logs. It is thought to represent the deposits of debris from past landslides and other erosion processes. The material derives mainly from weathered volcanic breccia and lava and remobilised loess. In drillholes and field exposures, the colluvium is highly variable. It ranges from gravel to boulder-sized clasts of volcanic basalt with a loess and clay matrix, to remoulded loess with occasional gravel and boulders.

3.3.1.5 Bedrock (volcanic basalt lava breccia and lava)

The cliff face comprises gently dipping (and locally steeply dipping) interlayered variations of four main rock types – in order from the cliff crest to cliff toe: 1) an upper basalt lava breccia that appears generally massive, interlayered with discontinuous and thin blocky columnar-jointed basalt lava flows; 2) blocky columnar-jointed basalt lava flow that is highly variable in thickness (from 10 m to less than 1 m and in some areas is missing completely); 3) epiclastic layer within the basalt-breccia/lava sequence ranging from coarse, poorly sorted conglomerates and sandstones, to tuffaceous clays and silts and rare but prominent palaeosols; and 4) a lower basalt lava breccia that is generally massive and interlayered with discontinuous and thin blocky columnar-jointed basalt lava flows.

The material layering is highly variable both laterally and vertically but the layers are laterally persistent along most of the cliff. Descriptions of the main units are given in Table 11 and shown in Figure 14.

The general dip/dip direction of the volcanic sequence in the north of the site is dip of 10–15° towards dip direction 290–320°, which is well constrained by the rock exposures in the cliff face along Nayland Street (Massey et al., 2012a). This dip becomes less to the south, where it is essentially horizontal and some areas appear to dip out of the slope. However, there are significant variations within the sequences. In the central part of the cliff the trachy basalt lavas form a steeply-inclined dome (possible lava dome) locally dipping into the slope at about 60°.

Discontinuity data derived from photogrammetric surveys of the Redcliffs cliffs and kinematic assessment of the various discontinuity-controlled failure modes is contained in Appendix 10.

Table 11 Engineering geological descriptions of the main geological units forming the cliffs (descriptions as per New Zealand Geotechnical Society, 2005).

Unit name	Description
Basaltic lava breccia	<p>Slightly weathered to highly weathered, light grey to dark grey when slightly weathered to orange or red-brown when highly weathered, massive, brecciated basaltic lava fragments, moderately strong to strong (but varies to weak or very weak when highly or completely weathered), with very widely spaced irregular discontinuities.</p> <p>At all sites basaltic lavas have flowed within thick carapaces of brecciated lava, with the breccia often exceeding the thickness of its source lava (brecciated units may be 2 to >10 m thick.). Breccias are poorly graded, angular lava fragments with a fine to coarse matrix supporting unsorted cobbles, blocks and often 1–5 m diameter megablocks of broken lava. Breccia fragments are often more vesicular and scoriaceous than the source lava, and prone to weathering due to high porosity. Bedding is massive, poorly jointed, with lower boundaries gradational with the source lava and upper boundaries roughly planar. Weathering expression is cavernous and spheroidal, of fine and coarse blocks respectively, and in some cases development of cliff parallel exfoliation joints/cracks. Freshly exposed breccia faces show extensive interstitial clay weathering and deposition of clay within vesicles and between clasts. Most joints are due to recent fracturing of the rock mass during the 2010/11 earthquakes, with very little tectonic discontinuities, if any, apparent. Joints are very widely spaced (>2 m), with their persistence varying from a few metres to tens of metres. Joint surfaces tend to be “fair” to “good” adopting the Geological Strength Index classification (Hoek, 1999).</p>
Basalt lava	<p>Dark greenish grey to black, unweathered to moderately weathered, sometimes vesicular, Basalt, very strong with variably developed columnar joints, widely to very widely spaced (1.5–5 m), typically giving large to very large block sizes that are columnar in shape. Columnar joints are often radial to flow margins, and lavas have gradational contacts with lava breccia at their upper and side margins. Joint faces are generally rough to very rough, stepped or irregular, commonly manganese oxide or calcite coated, and only rarely have clay or silt fill. Joint surfaces therefore tend to be “fair” to “good” adopting the Geological Strength Index classification (Hoek, 1999). Individual flows form lensoidal bodies throughout the cliffs, ranging from 0.5 to 2–4 m thick. Columnar jointing is well expressed where flows are thick, and gives way to thin, platy flow orientated jointing where flows are thin.</p>
Epiclastic deposits	<p>Moderately to highly weathered or oxidised brown to red-brown or yellow-brown thinly bedded Tuff or Tuffaceous Sandstone, intercalated with or grading into fine to coarse pebbly Lapilli Tuffs or gravelly sandstone and conglomerate, with occasional cobble-sized blocks and bombs of basalt, moderately strong to weak, very weak to extremely weak when highly weathered. Rarely jointed, prone to cracking on exposed surfaces and easily eroded. Bedding is thin (0.1–2 m) and discontinuous, disrupted by overlying lavas. In all sites, these layers of red-oxidised pyroclastic and epiclastic paleosol material are found between lava flows and breccias, usually at the top of the preceding lava breccia, and oxidised/baked by the overlying lava flow. The thinly bedded ash and lapilli, with occasional blocks and bombs, is discontinuous due to re-working by water-driven epiclastic processes or re-working by overlying lava flows. The pyroclastic material exposed in the cliffs is often vegetated or a focus for fluid flow, being relatively impermeable compared to the overlying jointed lavas and porous breccias. Contacts are often gradational into lava breccia or lahar/debris-flow deposits.</p>



Figure 14 View to the west onto the main cliff at Redcliffs. (A) is basalt lava breccia, (B) is columnar jointed basalt lava and breccia (C) is the epiclastic layer that generally forms a recessive slope, and the material below this is basalt lava breccia (D). Photograph by C. Gibbons (July 2011). For surveyed boundaries between materials refer to Appendix 3.

3.3.2 Geotechnical properties

Material strength parameters have been assigned based on the results from in-house (GNS Science) laboratory tests and the published results of testing of similar materials from elsewhere in the Port Hills.

3.3.2.1 Loess and colluvium

Material parameters adopted for the loess and loess derived colluvium material in the assessment area are shown in Table 12. These are based on: 1) descriptions of the drillcore materials; and 2) Port Hills soil strength test results reported by Carey et al. (2014) and others.

Table 12 Range of adopted bulk soil strength parameters for Redcliffs soils.

Soil Unit	Unit weight (kN/m ³)	Intact Young's modulus E _i (MPa)	Poisson's ratio	Cohesion c (kPa)	Friction φ (°)	Tensile strength (kPa)
Loess and loess derived colluvium	17	30	0.3	10	30	10

3.3.2.2 Volcanic bedrock

In order to derive rock mass strength parameters for the volcanic breccia, lava and epiclastic that take into account the nature of the discontinuities as well as the intact strength of the material, the Geological Strength Index (Hoek, 1999) was adopted using Rocscience RocLab software.

The Geological Strength Index values adopted for the main materials are shown in Figure 15. Strength tests of Redcliffs rock samples from drillholes BH-MB-01 and BH-MB-02 are shown in Table 13, and are taken from Carey et al. (2014). Mohr-coulomb parameters (cohesion and friction) were derived from Rocscience RocLab software by line fitting over the appropriate stress range of the slope.

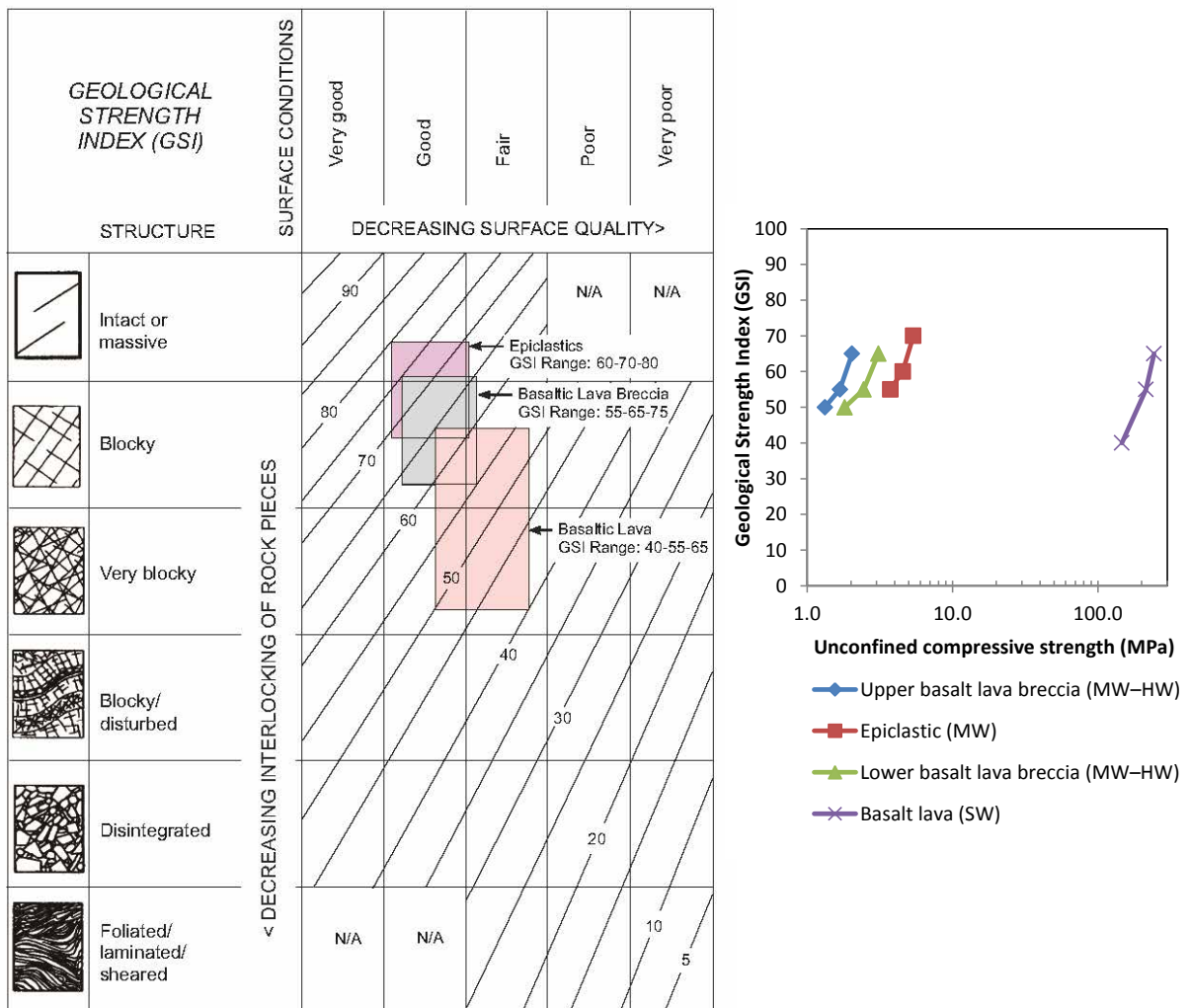


Figure 15 Geological Strength Index plot for volcanic breccia and lava at Redcliffs (modified after Hoek 1999). B) The adopted lower, middle and upper estimates of GSI per given material type plotted against the corresponding lower middle and upper unconfined compressive strength from the laboratory testing (Table 12).

Results from laboratory testing (Carey et al., 2014) show that the upper breccia is weaker than the lower breccia, and that the strength of the breccia is related to its moisture content. The laboratory test results indicate that the samples from the upper breccia had higher moisture contents and lower unconfined compressive strengths to those tested samples from the lower breccia.

Table 13 Range of adopted rock strength parameters (for cross-section 4).

Unit	Range ¹	Laboratory test results						Rock mass parameters derived from RocLab							
		Bulk unit weight (kN/m ³)	Unconfined compressive strength (MPa)	Tensile strength (MPa)	Tangent modulus of deformation (MPa)	m _i ²	Poisson's ratio	Average Slope Height above unit (m)	GSI ¹	Lithostatic stress range (kPa)	Sampling stress tangent (kPa)	Cohesion ³ c (kPa)	Friction ³ φ (°)	Tensile strength (kPa)	Modulus E _M (MPa)
Upper basalt lava breccia	MAX	18.4	2.0	0.4	770	5.0	0.18		65			100	31	21	380
	AVG	18.2	1.7	0.3	600	5.6	0.13	30	55	0–540	270	70	23	11	180
	MIN	18.0	1.3	0.2	430	6.9	0.07		50			64	21	8	132
Basalt lava	MAX	28.0	243	14.7	54,700	16.5	No data, assumed		65			3,100	68	730	13,080
	AVG	28.0	214	11.8	38,800	18.1	0.2	30	55	0–540	270	1,650	69	340	8,450
	MIN	27.0	146	10.6	21,200	13.8			40			670	68	129	3,380
Epiclastic	MAX	19.5	5.4	0.6	1,710	9.5	0.1		70			190	47	50	880
	AVG	18.9	4.55	0.48	1,180	9.5	0.10	30	60	0–540	270	130	38	36	330
	MIN	18.2	3.7	0.4	640	9.4	0.1		55			120	37	20	260
Lower basalt lava breccia	MAX	19.5	3.1	0.5	1,550	5.7	0.4		65			250	26	26	880
	AVG	18.8	2.5	0.4	1,390	6.1	0.3	70	55	540–1,260	900	160	14	22	500
	MIN	18.0	1.8	0.3	1,230	7.0	0.2		50			146	13	15	380

¹ MIN, AVG and MAX represent the range (minimum, average, maximum) of test results and field measurements.

² The m_i values shown, represent the range in the ratio of unconfined compressive strength to tensile strength, derived from tested samples of basalt lavas and basalt lava breccias (Carey et al., 2014), and not the ratio of unconfined compressive strength to tensile values shown in the table.

³ Mohr-coulomb parameters (cohesion and friction) were derived from RocLab by line fitting over the appropriate stress range of the slope.

3.3.2.3 Shear Modulus

The *in situ* shear moduli of the materials were derived from:

1. Results from the downhole shear-wave velocity surveys carried out by Southern Geophysical Ltd. (Southern Geophysical Ltd., 2013) based on the survey results from drillholes BH-MB-01 and BH-MB-02 carried out by Aurecon NZ Ltd. at the site; and
2. Results from the dynamic probing of the loess and loess colluvium carried out by Tonkin and Taylor for the Earthquake Commission at Clifton Terrace (Tonkin and Taylor, 2012b).

The range of shear moduli for the different materials was calculated by using the relationship between the shear wave velocity and material density:

$$G = \rho \cdot V_s^2 \quad \text{Equation 2}$$

Where ρ is the density of the material and V_s is the shear wave velocity.

The shear-wave velocity profiles carried out by Southern Geophysical Ltd. (Southern Geophysical Ltd., 2013) in drillholes BH-MB-01 and BH-MB-02 are shown on cross-sections 2, 3, 5 and 6 in Figure 13 and are summarised in Table 14.

Table 14 Shear wave velocity data and shear modulus used for modelling.

Material Unit	Shear wave velocity range ¹ (m/s)	Bulk density (kN/m ³)	Source of data	Shear modulus range (MPa) ¹
Loess/colluvium	300–400	17	Tonkin and Taylor (2012b) and Southern Geophysical Ltd. (2013)	150–270
Upper basalt lava breccia	300–640	18	Southern Geophysical Ltd. (2013)	160–740
Basalt Lava	400–950	28	Southern Geophysical Ltd. (2013)	450–2,530
Epiclastic	850–1,160	19	Southern Geophysical Ltd. (2013)	1,370–2,560
Lower basalt lava breccia	300–640	19	Southern Geophysical Ltd. (2013)	170–780

¹ Rounded to the nearest 10 m/s for shear wave velocities, and 10 MPa for shear modulus.

In addition to the downhole (drillhole) shear-wave velocity surveys, Victoria University of Wellington carried out two seismic refraction lines at the cliff crest (shown on Figure 12) (Woelz, 2012). Interpretation of the results indicate that along line Glen_1, there are three layers, but only two along line Glen_2. The data are summarised in Table 15.

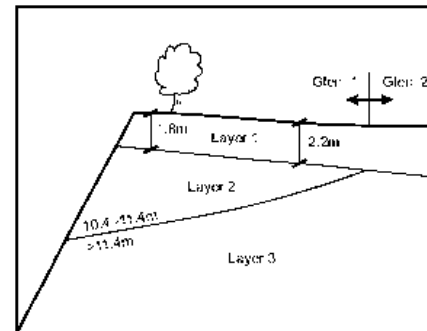
The results from both seismic refraction lines show that there is a lower velocity layer near the surface, which is coincident with the depth of the loess interpreted from nearby drillholes and mapping of the cliff face. Along line Glen_1 there is a second relatively low velocity layer beneath the loess extending to a depth of about 11.4 m, which corresponds to the basalt breccia, interpreted from drillhole logging and cliff-face mapping. In line Glen_2 this layer is

missing, although the geological sequence should be similar to that at Glen_1. The second layer in line Glen_2 is similar in velocity to the third layer along line Glen_1 and is also thought to be the same breccia as layers 2 and 3 along line Glen_1.

Seismic refraction line Glen_1 is closer to the cliff face and within the main zone of mapped surface cracking. It is possible that the recorded P-wave velocities in line Glen_1, associated with the basalt breccia, reflect increased fracturing of the rock mass near the cliff edge.

Table 15 Preliminary layer interpretations of seismic refraction lines Glen_1 and Glen_2 (Woelz, 2012).

Details	Glen_1	Glen_2
Layer 1 depth of base (m below ground level)	1.8–2.1	1.5–2.2
Layer 1 velocity (P-wave) m/s	180–380	510–570
Layer 2 depth of base (m below ground level)	10.4–11.4	-
Layer 2 velocity (P-wave) m/s	590–1,070	-
Layer 3 depth (m below ground level)	>11.4	>2.2
Layer 3 velocity (P-wave) m/s	1,580–1,920	1,580–1,920



Clarke (2012) carried out additional analysis of the seismic refraction data in Woelz (2012) to try to determine the depth of the loess across the site. Results indicate the loess thickness varies between 2.1 and 3.8 m. The results also show at the southern end of line Glen_1, the P-wave velocity of the rock underlying the loess increases. From the field mapping of the cliff face it is apparent that this part of the seismic line, nearer the cliff edge, corresponds to several thin and localised basalt lava layers within the overall sequence of basalt breccia.

3.3.3 Rainfall and groundwater response

In general groundwater has two main effects on the stability of rock slopes that need to be considered: 1) rising groundwater within the slope rock mass leading to an increase in pore pressures in joints and a reduction in the effective stress of the materials; and 2) infiltration from high intensity and prolonged rainfall, leading to increased water pressures in tension cracks and open joints. The first effect is not thought to be the main one affecting the slope at Redcliffs, as the materials forming the slope are relatively free-draining and there is a limited catchment area above the slope. The second effect is thought to be the most important from a stability perspective, as the open tension cracks in the overlying loess would allow water to readily infiltrate any open cracks in the underlying rock mass. It should be noted that there is currently no monitoring of groundwater levels within the rock mass.

The relationship between rainfall and landslides in the Port Hills has been summarised by McSaveney et al. (2014). Heavy rain and long-duration rainfall have been recognised as potential landslide triggers on the Port Hills for many years.

A long historical landslide record, which includes rockfalls, has been gathered by searching “Paperspast” (<http://paperspast.natlib.govt.nz>). This electronically searchable record of daily and weekly newspapers has been searched over the period 1860–1926, but its landslide information is very incomplete, being only what newspapers of those times considered to be “newsworthy”.

A list of Earthquake Commission claims for landslide damage was examined for the period 1997–2010 and a Geotechnical Consulting Ltd. landslide investigations list covers the period 1992–2009. Any duplicate records for the period 1997–2009 contained in the data sets were removed. These records, though incomplete with respect to all of the landslides that occurred over those intervals, may be approximately complete with respect to the episodes of rain associated with landslide occurrences that damaged homes and urban properties (Figure 16).

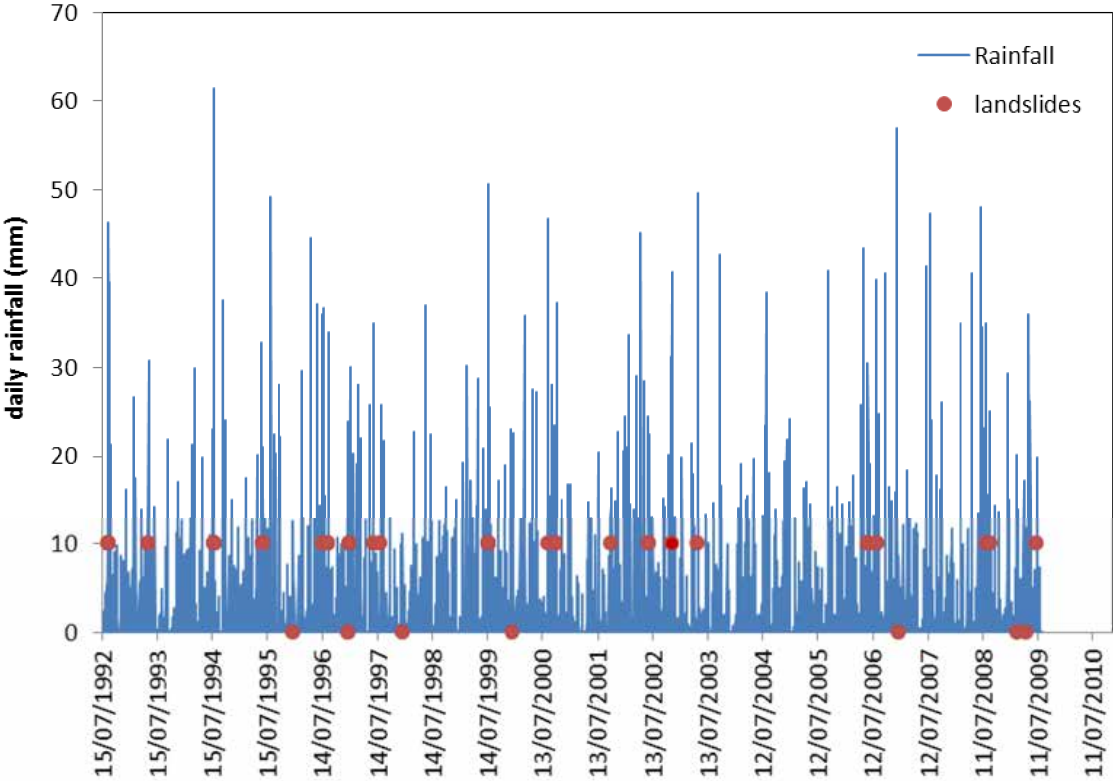


Figure 16 Daily rainfalls at Christchurch Gardens and landslides in the Port Hills. Daily rainfalls at Christchurch Gardens and landslides in the Port Hills investigated by Geotechnical Consulting Ltd, or listed by the Earthquake Commission as causing damage to homes. Landslides without rain are plotted at 0 mm, all others are plotted at 10 mm of rain (the minimum rainfall for triggered landslides).

McSaveney et al. (2014) conclude that the comparison of the record of damaging landslides (including rockfalls) and daily rainfall for the period 1992–2010 shows that:

1. Landslides can occur without rain, but the probability of landslides occurring increases with increasing intensity of rainfall;
2. Landslides occurred much more frequently on days with rain, but there were many rainy days when no landslides were recorded; and
3. As the amount of daily rainfall increased, a higher proportion of the rainy days had recorded landslides.

Following the 2010/11 Canterbury earthquakes there have been two notable rainfall events (Table 16):

- 11–17 August 2012: occurred at the end of winter following a long period of wet weather. During this period a total of 92 mm of rainfall was recorded at the Christchurch Gardens. The maximum daily rainfall (24 hourly rainfall recorded 9 am–9 am) during this period occurred on 13 August 2012 and totalled 61 mm.

- 3–5 March 2014: occurred at the end of a period of dry weather. During these three days, a total of 118 mm of rain was recorded at the GNS Science rain gauge installed at Clifton Terrace in the Port Hills (approximately 2 km west of Deans Head). The maximum daily rainfall (24 hourly rainfall recorded 9 am–9 am) during this period occurred on 5 March 2014 and totalled 89 mm.

The frequency of high-intensity rainfalls in Christchurch has been well studied (e.g., Griffiths et al., 2009, Figure 17, and McSaveney et al., 2014). Griffiths et al. (2009) use rainfall records for the period 1917–2008 from gauges all over Christchurch. McSaveney et al. (2014) use a composite rainfall record, for the period 1873–2013, mainly from the Christchurch Gardens gauge, but substituting averages for other nearby stations where gaps in the Christchurch Gardens data exist.

The annual frequencies estimated for four recent heavy rainfall events, including the two notable events are given in Table 16. Rainfall depth-duration-return period relations for Christchurch Gardens and Van Asch Street, Sumner are taken from Griffiths et al. (2009) and for Christchurch Gardens from McSaveney et al. (2014).

Table 16 Annual frequencies of given rainfall in the Christchurch for four main events following the 2010/11 Canterbury earthquakes (rainfalls are calculated daily from 09:00 to 09:00 NZST).

Date	Total rainfall (mm)	Station	Max daily rainfall/date	Annual frequency Christchurch Gardens Griffiths et al. (2009)	Annual frequency Christchurch Gardens McSaveney et al. (2014)	Annual frequency Van Asch, Sumner Griffiths et al. (2009)
11–17 August 2012	92	Christchurch Gardens (CCC/NIWA)	61 mm, 13 August 2011	92 mm = no data available 61 mm = 0.5 (once every 2 years)	92 mm = 0.4 (once every 2.7 years) 61 mm = 5 (5 times per year)	N/A
3–5 March 2014	118	Clifton Terrace (GNS Science)	89 mm, 5 March 2014	N/A	N/A	118 mm = 0.1 (once every 10 years) 89 mm = 0.1 (once every 10 years)
3–5 March 2014	141	Christchurch Gardens (NIWA)	130 mm 5 March	141 mm = 0.05–0.02 (once every 20–50 years) 130 mm = 0.02–0.01 (once every 50–100 years)	141 mm = 0.05 (once every 20 years) 130 mm = (>0.01) less than once every 100 years	N/A
18 April 2014	68	Lytelton (NIWA)	68 mm	N/A	N/A	68 mm = 0.5 (once every 2 years)
29 April 2014	20	Clifton Terrace (GNS Science)	20 mm	N/A	N/A	Greater than 0.5 (occurs frequently every year)

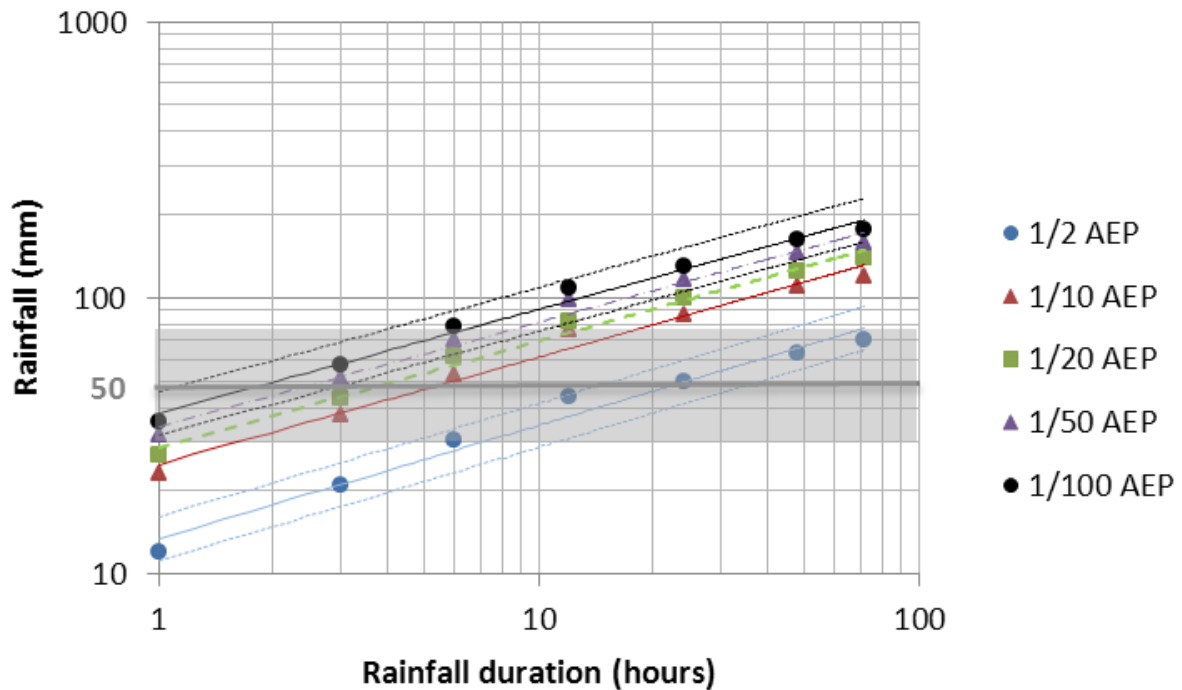


Figure 17 Rainfall depth-duration-return period relations estimated for Christchurch Gardens by Griffiths et al. (2009) using recorded rainfall data. Error limits of 20% are shown by dotted lines for the 1/2 and 1/100 AEP curves. Shaded area covers the range of 30–75 mm of rainfall over which the expected number of soil landslides in the Port Hills rises from very few to many. Rockfalls can occur without rain, but the probability of rockfalls occurring increases with increasing intensity of rainfall.

Bell (1992) reports on two failures of the rock slope at Redcliffs, one in 1968 and the other in 1992; both are reported to have been about 50 m³ in volume with rainfall as the trigger. The failure in 1968 was reported by Bell (1992) as being triggered by the “Wahine storm”. During this storm about 156 mm of rain fell over three days (10–12 April 1968), with the largest daily rainfall of 81 mm occurring on the 11 April 1968 (rainfall records are from the Christchurch Gardens gauge).

This rainfall is comparable to the 3–5 March 2014 rainfall. Laser scan surveys covering this period were carried out, but the data are not available at the time of writing this report, although field observations indicate many small failures of rock occurred from the slope. Results from earlier terrestrial laser scan surveys (between January 2012 and November 2013) indicate considerable volumes of material (90–480 m³/year) continue to fall from the slope, during periods when no notable earthquakes occurred, although the rates may be decreasing (e.g., 480 m³/year in 2012 to 90 m³/year in 2013).

Regardless of the rainfall data sets used, the rainfall data suggest that the heavy rainfalls recorded in the Port Hills following the 2010/11 Canterbury earthquakes are unexceptional. Although the three-day rainfall of 118 mm had an annual frequency of 0.05–0.1 (once every 10 years), it occurred at the end of summer when the ground would have had a seasonally low water content.

However, given the historical rates of rainfall triggered rockfall for the slope of about 5–6 m³/year (although the maximum recorded rate is about 50 m³/year in any one year, estimated from historical data in Massey et al., 2012a), the current rates of rockfalls triggered by rainfall are considerably higher. These increased rates are not unexpected, as the rock mass forming the slope has been considerably degraded by earthquake-induced cracking.

The historical and recent rainfall-induced rockfalls from the slope tend to be local and relatively small in volume (mean volumes of discrete failures tend to be $<0.1 \text{ m}^3$ based on the results from terrestrial laser scan surveys), and are randomly distributed across the slope.

3.4 SLOPE FAILURE MODELS

3.4.1 Landslide types affecting the site

Based on the aerial photograph interpretation, engineering geological mapping, cross-sections, and site observations and measurements of the impacts of the 2010/11 Canterbury earthquakes, there are several landslide types that could affect the slopes in the study area. These could occur under either static or dynamic conditions.

Four potential landslide types have been identified that could affect the site:

1. Debris avalanches – ranging from a single rockfall to many thousands of cubic metres of rock falling from the cliff.
2. Cliff-top recession, deformation and cracking – in response to deformation of the rock mass in the slope.
3. Slumping of loess (and fill) at the cliff crest. The slump features, thought to be predominantly in loess, may also reactivate during or shortly after very wet weather.
4. Earth/debris flows originating in loess above the cliff crest. Rain or snowmelt and ingress of water through tension cracks can wet the fill, loess and loess colluvium at the crest of the slope overlying rock head, causing loss of strength leading to earth/debris flows. To date (post-2010/11 earthquakes), such flows have been relatively small at this location ($<10 \text{ m}^3$) with limited runout of debris down the cliff face.

Based on the past performance of the cliffs in the study area, cliff-collapse hazards (cliff-top recession and debris avalanches) pose the greatest landslide hazard and therefore landslide risk to people at the cliff crest and cliff toe. These slope-instability processes form the basis of the following hazard and risk assessments, and their potential source areas are shown on Figure 18.

3.4.1.1 Cliff collapse

The majority of past failures at Redcliffs have been cliff collapses comprising debris avalanches of various volumes. Results from the terrestrial and airborne laser scan surveys and field mapping of the rock face suggest that about 80% of the material that fell from the cliffs during the 2010/11 earthquakes originated from the basalt breccia (Massey et al., 2012a), the weakest of the materials forming the cliff.

The large arcuate features (possible relict landslide scarps inferred from the aerial photograph interpretation and field mapping) are also predominantly in this material. Failures during the recent earthquakes also occurred in other materials forming the slope, mainly the basalt lava, although these failures tended to be smaller in volume than those in the basalt breccia.

Most of the discrete slope failures that occurred during the 2010/11 Canterbury earthquakes had their failure surface above the epiclastic layer, with the bottom (toe) of the failure surfaces corresponding to the top of the main basalt lava unit and extending into it. However, cracks have now been mapped in the slope face that extend from the cliff crest, through the

basalt lava and epiclastic layers, and into the underlying basalt breccia unit. Failures in the basalt tend to be controlled primarily by the columnar-joint pattern, where blocks tend to topple and slide out of the face.

Assessment of the terrestrial laser scan change models indicates that many of the larger discrete failures, although occurring predominantly in basalt breccia, fell from the upper parts of the slopes, suggesting that these areas were more unstable during the earthquakes (Massey et al., 2012a). The localisation of failures in the upper part of the slope, although related to the geological units, may also result from amplification of ground shaking at the slope crest, caused by the shape of the slope.

The static strength of the rock slope and its loess mantle at the slope crest is considered to have been weakened from its pre-earthquake state by earthquake-induced cracking and deformation of the rock-mass. The newly exposed slope is considered to be more prone to failure than was the former slope which had had many hundreds of years to shed its less stable material after the penultimate earthquake sequence.

The field evidence supporting the possibility of larger local failures comprises the presence of relict (pre-2010/11 Canterbury earthquakes) failure scarps on the cliff face and corresponding debris at the cliff toe, and large discrete cliff failures that occurred at other similar cliffs during the 2010/11 earthquakes. The largest, with a failure volume of about 35,000 m³, occurred at Shag Rock Reserve during the 13 June 2011 earthquake (Massey et al., 2012a).

3.4.2 Cliff collapse failure mechanisms

3.4.2.1 Static conditions

Potential failure mechanisms occurring at Redcliffs under static conditions comprise:

- Ravelling of loose rock from the cliff. This is on-going and occurs during rain and at other times without an obvious trigger. Ravelling has involved (to date) only small volumes of rock (and soil) and has occurred randomly across the slope. However, the post-earthquake accumulation rate of debris at the base of the cliff for 2012 was about 480 m³ per year, reducing to 90 m³/year in 2013 (based on terrestrial laser scan surveys).
- Larger, non-seismic debris avalanches could occur from this slope if rock mass strength continues to deteriorate as a cumulative result of effects such as water ingress, cycles of wetting and drying and movement in future earthquakes.

3.4.2.2 Dynamic conditions

The magnitude of permanent earthquake-induced displacement of the cliff crest, and the volume of debris that could fall from the cliffs, depends on the magnitude and duration of earthquake-induced ground accelerations and the critical yield acceleration of the cliff.

Failure mechanisms that occur at Redcliffs under dynamic conditions are:

- Permanent cliff displacement in future strong shaking – similar to those that occurred during the 2010/11 Canterbury earthquakes, However, these may be larger than those recorded during the 2010/11 earthquakes, because of the accumulated strength degradation of the rock mass behind the cliff caused by the earthquake-induced cracking and deformation. Localised cracking of the loess above rock head can also occur.
- It is expected that future strong earthquakes will trigger further cliff collapses and rockfall volumes could be larger than those triggered during the 22 February, 16 April, 13 June and 23 December 2011 earthquakes.

Engineering geological mapping, aerial photograph interpretation and measurements of cracking, deformation and the volumes of debris leaving the slope during the 2010/11 Canterbury earthquakes, suggests that it is possible for larger cliff collapses (larger in volume than those triggered recently at this site during the earthquakes) to occur at the site. Three potential source areas have been identified, where the crack patterns suggest larger failures could occur. If these were to occur, their debris could travel further downslope than the debris from previous failures.

4.0 HAZARD ASSESSMENT RESULTS

4.1 SLOPE STABILITY (SOURCE AREAS 1–3)

For assessed source areas 1–3, the engineering geological cross-sections in Figure 13 were used as the basis of the numerical slope stability modelling. Geotechnical material strength parameters used in the modelling are from Tables 11 and 12. Models using variable shear strength parameters for the key materials were run to assess the sensitivity of the slope – along a given cross-section – to failure, and to take into account the on-going degradation of the rock mass in response to earthquake-induced fracturing.

Stability assessments were carried out adopting three different geotechnical material strength parameter models. Strength reduction was simulated by reducing the Geological Strength Index values to simulate the observed increased fracturing of the rock mass through the 2010/11 Canterbury earthquakes (Figure 19). The condition of the rock mass at the onset of the 2010/11 earthquakes was inferred from photographs of the cliff taken (by M. Yetton, Geotech Ltd.) immediately after the 4 September 2010 (Darfield) earthquake.

The parameters relating to the different models are presented in Table 17. All models were assessed using the current slope surface geometry, derived from the LiDAR survey 2011c.

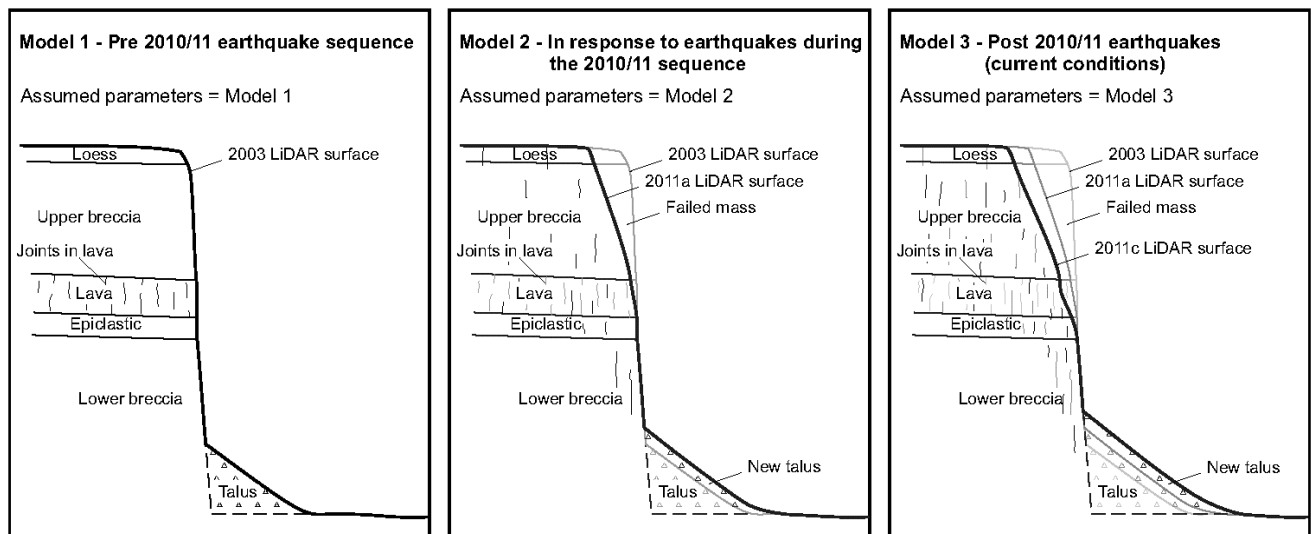


Figure 19 Schematic diagram showing the increasing frequency of defects in the slope in response to the successive 2010/11 Canterbury earthquakes.

Earthquake-induced cracks are unlikely to extend far back from the slope face near the toe of the slope, but are likely to extend further back from the slope face with increasing height from the toe. This is mainly because the amplification of shaking at the cliff crest is substantially greater than at the cliff toe.

Table 17 Material strength parameters used for modelling for cross-section 4 (similar parameters were adopted for sections 2 and 6, but the actual values used varied due to the different lithostatic stress range of the materials in the slope.

Model	Description	Earthquake	Material	Cohesion (c) (kPa)	Friction (ϕ) (degrees)
1	Average parameters (pre-22 February 2011 earthquake)	22 Feb 2011 13 Jun 2011	Loess	10	30
			Upper lava breccia	100	31
			Epiclastic	190	47
			Lava	1,650	69
			Lower lava breccia	250	26
2	Lower parameters (pre-13 June 2011 earthquake)	22 Feb 2011 13 Jun 2011	Loess	10	30
			Upper lava breccia	70	23
			Epiclastic	130	38
			Lava	670	68
			Lower lava breccia	160	14
1a	Average parameters, lava assumed to be breccia	22 Feb 2011 13 Jun 2011	Loess	10	30
			Upper lava breccia	100	31
			Epiclastic	190	47
			Lava (same as upper breccia)	100	31
			Lower lava breccia	250	26
2a	Lower parameters, lava assumed to be breccia	22 Feb 2011 13 Jun 2011	Loess	10	30
			Upper lava breccia	70	23
			Epiclastic	130	38
			Lava (same as upper breccia)	70	23
			Lower lava breccia	160	14
3	Post 2010/11 earthquakes (post 13 June 2011 earthquake)	22 Feb 2011 13 Jun 2011	Loess	10	30
			Upper lava breccia	64	21
			Epiclastic	120	37
			Lava	670	68
			Lower lava breccia	146	13

4.1.1 Slope stability – Static conditions (deep-seated failures)

Table 18 shows the results from the assessment, and graphic examples of stability assessment outputs are shown for cross-sections 2, 4 and 6 in Figure 20–Figure 22 for failures through the rock mass. Failures through the loess at the cliff crest and failure of the loess slumps (Figure 18) have not been modelled.

If a slope has a static factor of safety of one, then the slope is assessed as being unstable. Slopes relating to structures designed for civil engineering purposes are typically designed to achieve a long-term factor of safety of 1.5 under drained conditions, as set out in the New Zealand Building Code.

Results from the stability assessment indicate that under current conditions the factors of safety of the assessed cross-sections 2 and 4 are less than 1.5 adopting model 3 material parameters, and about 1.5–1.9 for cross-section 6.

Under current conditions it is possible that deep-seated failure of the rock mass for cross-sections 2 and 4 (adopting the assessed slide surfaces in Figure 20–Figure 22) could occur without an earthquake, given the relatively low factors of safety and sensitivity of the slope to surface water infilling tension cracks. However, it should be noted that material strengths – and therefore the slope factors of safety – could reduce with time, and the occurrence of future large earthquakes. It should also be noted that the stability assessment results presented are for deep-seated slide surfaces through the rock mass. However, much of the slope face appears unstable and rocks fall from the slope with no apparent trigger, indicating that parts of the slope face are only marginally stable to unstable, with factors of safety much less than those assessed for the deep-seated failures.

Table 18 Example results from slope stability assessment of source area 1 (cross-section 1).

Cross-section	Representative source area	Material strength parameter model (Table 17)	Tension crack condition	FoS ¹ SLIDE	SRF ² PHASE ²	Pseudostatic yield acceleration (g)
2	2	1	Dry	2.3	-	-
		2	Dry	1.5	-	-
		3	Dry	1.4	1.6	0.3
		3	Filled	1.3	-	0.2
4	1	1	Dry	1.7		
		2	Dry	1.2		
		3	Dry	1.1	1.0	0.1
		3	Filled	1.0		<0.1
6	3	1	Dry	2.8		
		2	Dry	2.1		
		3	Dry	1.9	1.9	0.5
		3	Filled	1.5		0.4

Note: In the modelling, the role of defects on the stability of the rock mass have been taken into account by reducing the intact strength of the rock using the Geological Strength Index, therefore the modelling assumes the different units to be homogenous. The given factors of safety represent the overall stability of the larger slope for those slide surfaces shown in Figure 20–Figure 22. They do not represent the localised stability of each potential area or rock-block that could fall from the slope, as such failures are on-going.

¹ FoS is the factor of safety derived using the General Limit Equilibrium method of Morgenstern and Price (1965).

² The finite element model was also used for comparison. Where the slope has been assessed using the finite element model, the stability of the slope is assessed in terms of the stress reduction factor Note the shear strength reduction method is used to determine the Stress Reduction Factor (SRF) or factor of safety value that brings a slope to the verge of failure (Dawson et al., 1999).

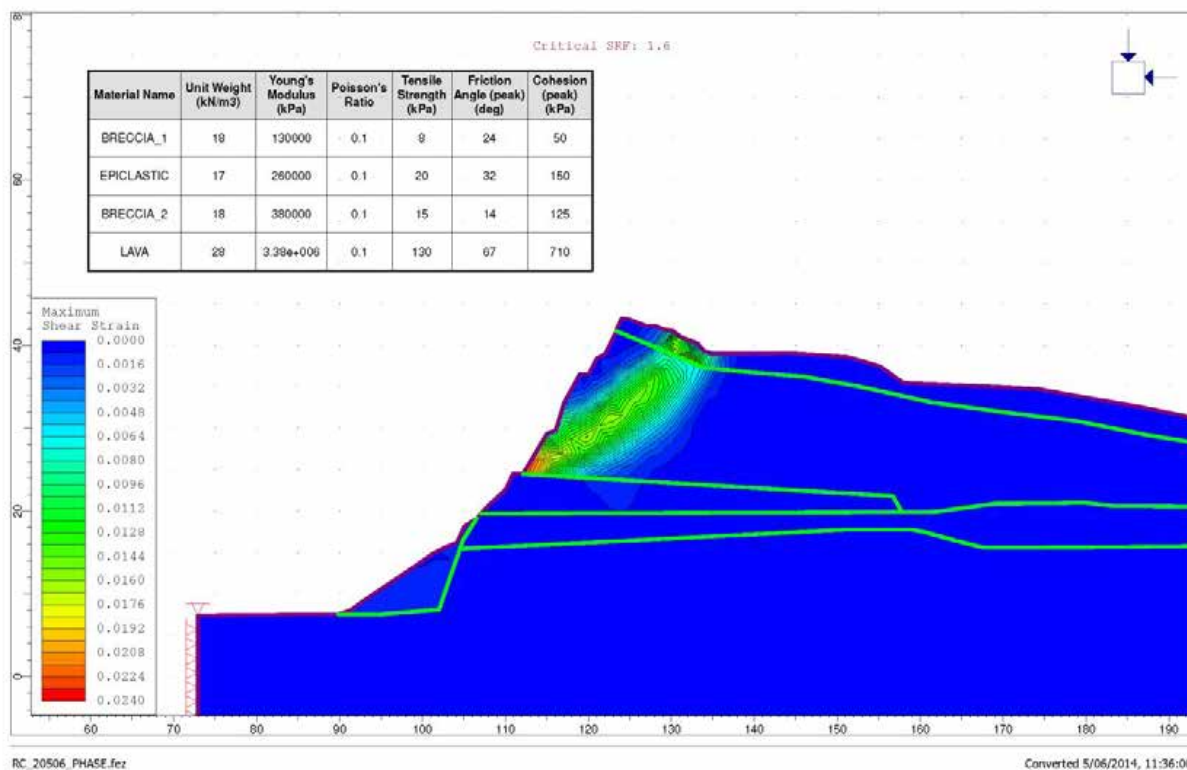
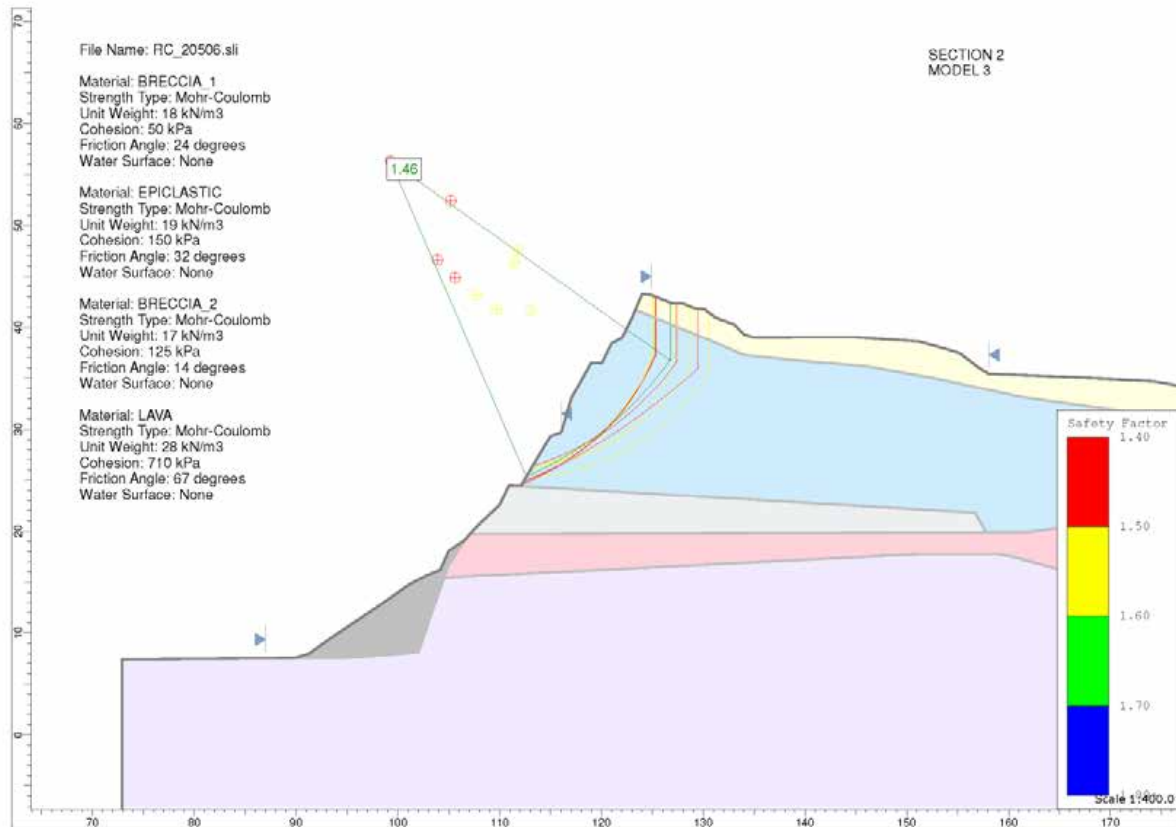


Figure 20 Example of limit equilibrium and finite element modelling results for cross-section 2 representing assessed source area 2, and adopting model 3 material parameters.

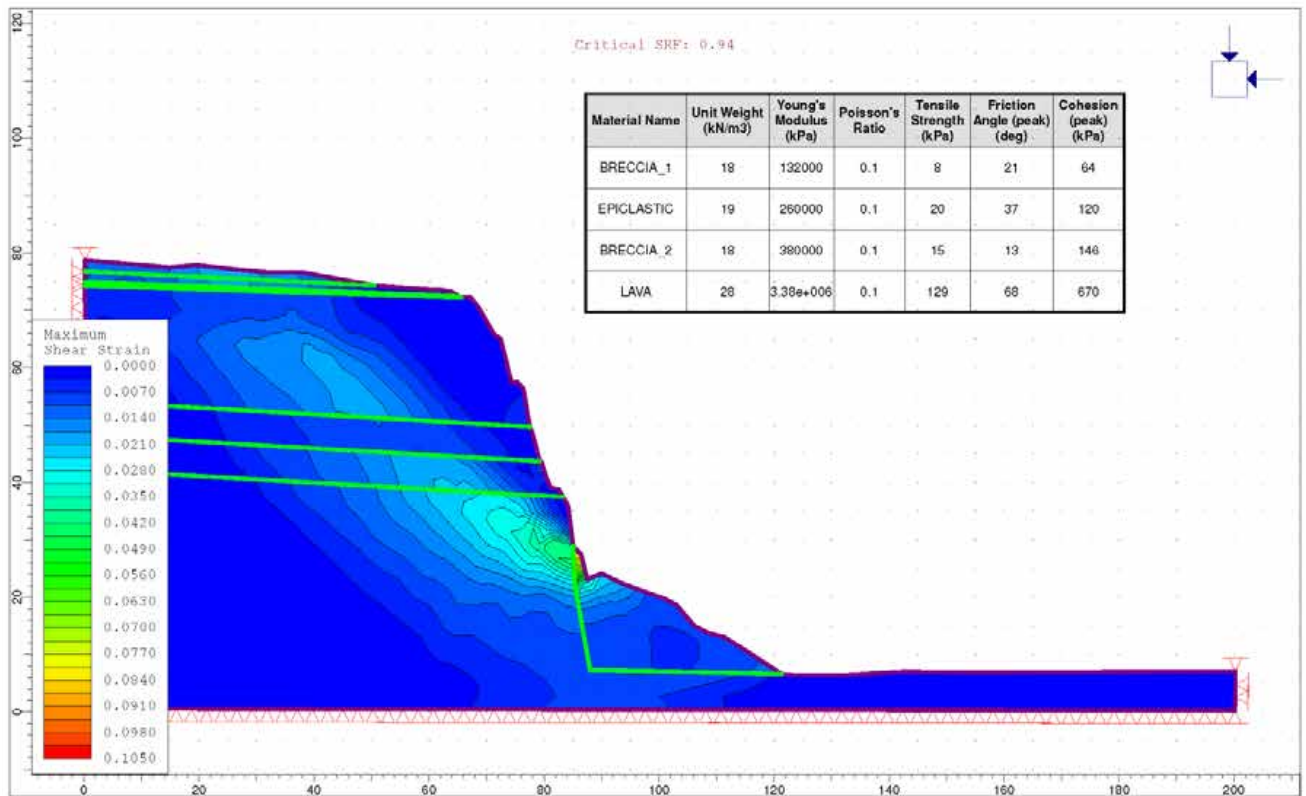
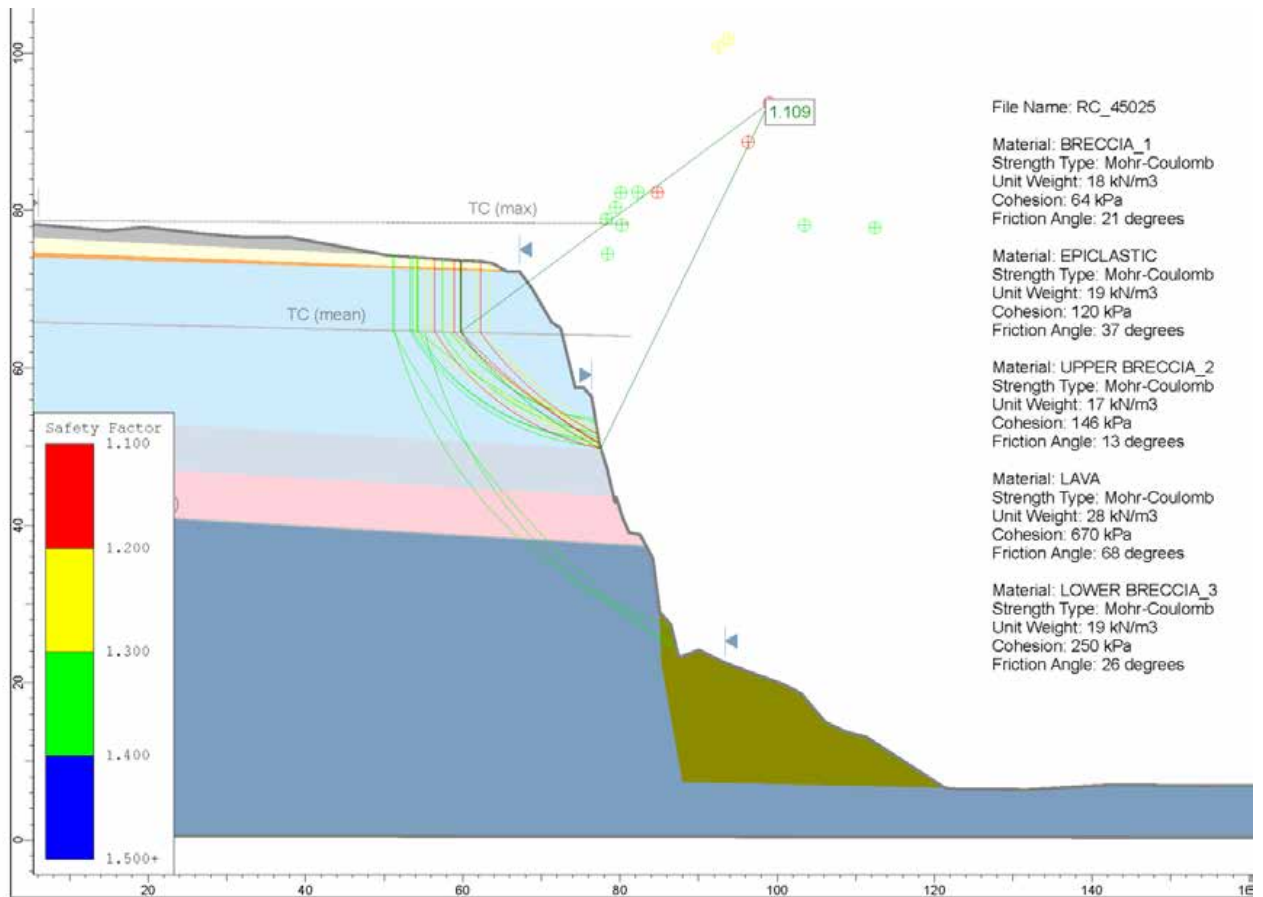


Figure 21 Example of limit equilibrium and finite element modelling results for cross-section 4, representing assessed source area 1, and adopting model 3 material parameters.

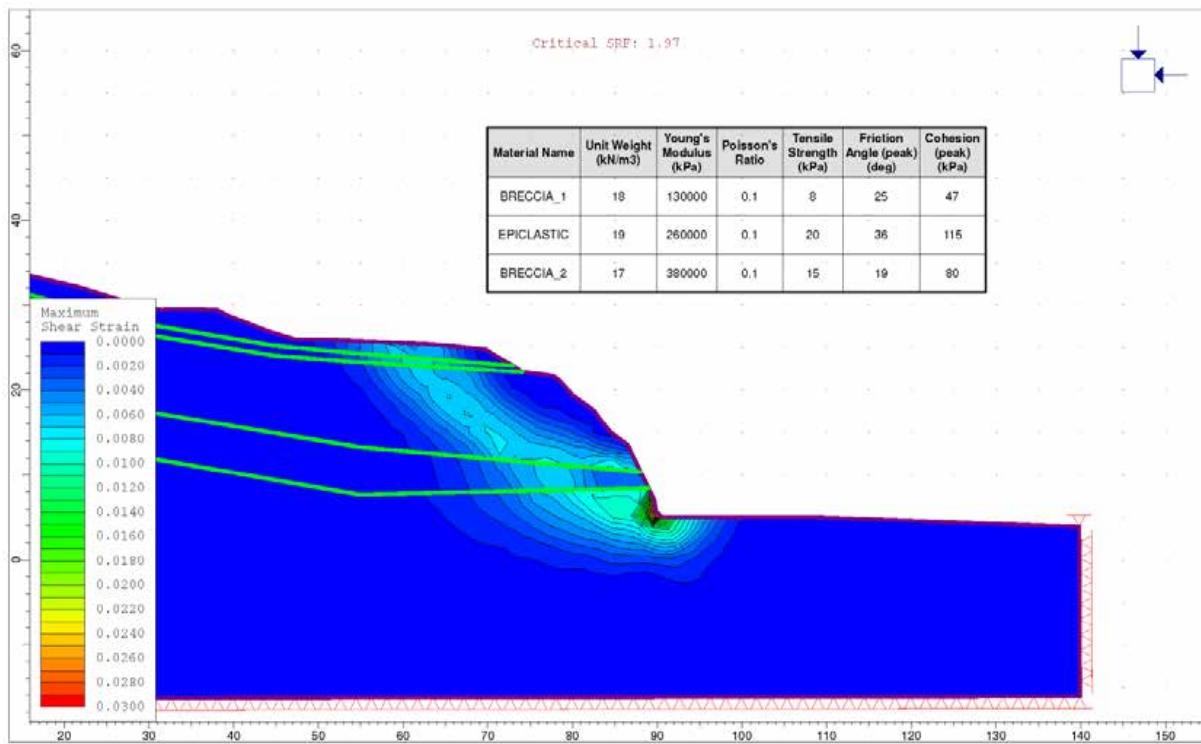
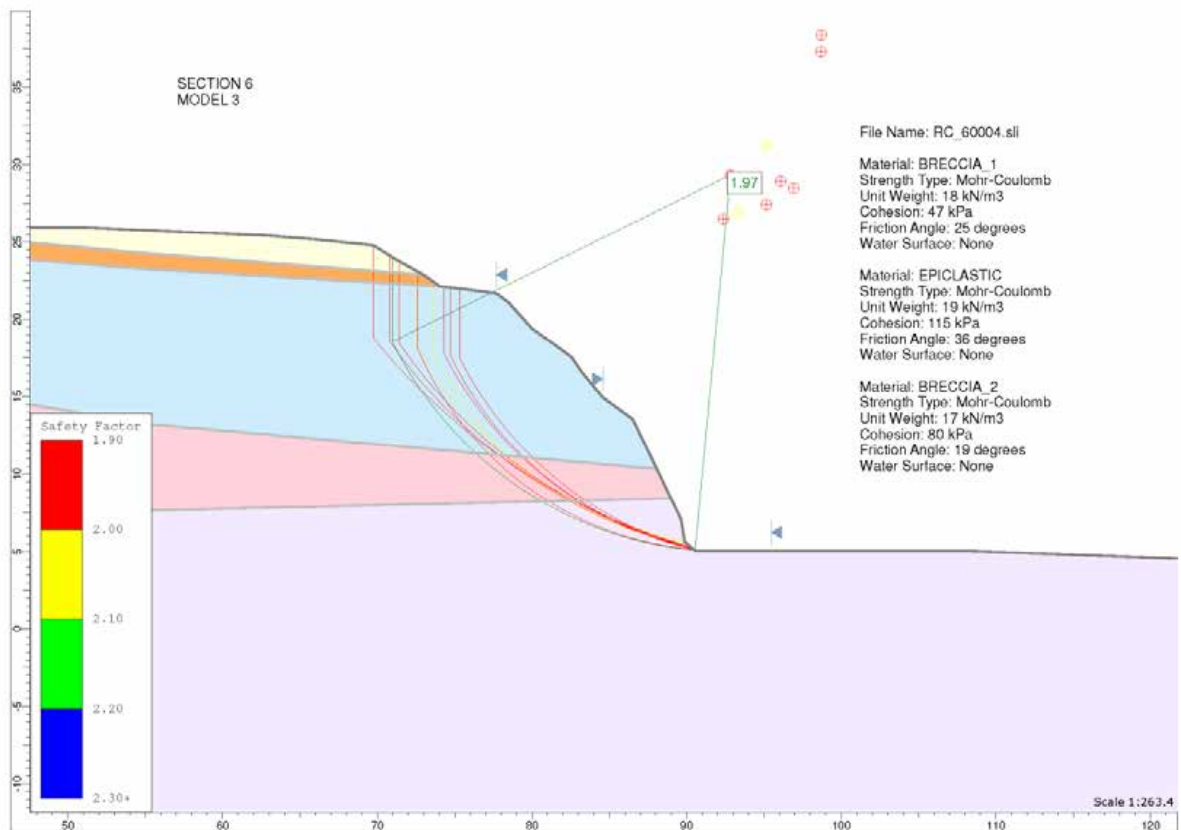


Figure 22 Example of limit equilibrium and finite element modelling results for cross-section 6, representing assessed source area 3, and adopting model 3 material parameters.

4.1.1.1 Model sensitivity to groundwater

The sensitivity of the slope factor of safety to transient changes in ephemeral ground water (pore pressure) has been simulated by modelling pore pressures acting within tension cracks, where the tension cracks are assumed to extend from the surface to the base of the basalt lava. Results are shown in Table 18.

The results show that the inclusion of water filled tension cracks within the model decreases the factor of safety for all cross-sections by 7–21%. The largest decrease is for cross-section 6. It should be noted that the stability model (Slide) used for modelling, can only model one water-filled tension crack. In reality there would be many water-filled tensions cracks and so these results do not fully reflect the impact of water filled tension cracks on slope stability.

4.1.1.2 Model sensitivity to slope geometry

The sensitivity of the slope factor of safety to changes in the slope geometry was assessed by adopting the different slope-surface geometries from the LiDAR surveys for cross-sections 2, 4 and 6, where material from the cliff fell off during the 2010/11 earthquakes, causing the slope geometry to change.

Results show that as material falls from the cliffs the factors of safety increase slightly as the slope angles reduce. Typically the increase in the factor of safety, for cross-sections 2, 4 and 6, is 5–10% between the slope geometries derived from the 2011a and 2011c LiDAR surveys, assuming material parameters are kept constant. However, any increase in stability caused by reducing slope angles, may be counterbalanced by fracture-induced weakening of the rock mass.

4.1.2 Slope stability – Dynamic conditions

Dynamic stability assessment comprised: 1) back-analysing the performance of the slope during the 2010/11 Canterbury earthquakes to calibrate the models and check that the calculated displacements were consistent with the displacements inferred during the earthquakes; and 2) using the calibrated models to forecast the likely magnitudes of future displacements under given levels of peak ground acceleration.

Cross-section 4 (representing assessed source area 1) has been assessed under dynamic conditions, assuming a drained slope, using the decoupled method. The likely yield accelerations for cross-sections 2 and 6 (representing source areas 2 and 3) were assessed using the pseudostatic method.

4.1.2.1 Amplification of ground shaking

The first stage of the assessment was to calculate the maximum acceleration at the slope crest (A_{MAX}) to quantify amplification effects caused by topography and or contrasting materials. The slope crest is defined as the convex break in slope between the lower steeper slope and the upper less steep slope. Results from the dynamic site response assessment are contained in Appendix 6.

Results from this assessment suggest that modelled peak acceleration at the slope crest (A_{MAX}) varies approximately linearly with the peak ground acceleration of the free-field input motion (A_{FF}) for the horizontal motion component, but non-linearly for the vertical motion component. The relationship between horizontal and vertical component values of A_{MAX} is strongly non-linear. Over the range of modelled peak horizontal accelerations, the peak

ground acceleration amplification factor (S_7) for cross-section 4 is about 2.6 (± 0.1) for horizontal motions and 3.3 (± 0.3) for vertical motions, times the input free-field peak accelerations. The input peak accelerations are those derived from the out-of-phase synthetic free-field rock outcrop earthquake time acceleration histories described by Holden et al. (2014).

The results suggest that the modelled ground accelerations increase with increasing height above the toe of the slope, but that the peak horizontal accelerations (for all modelled earthquakes) concentrate around the convex break in slope, defined as A_{MAX} .

4.1.2.2 Back-analysis of permanent slope deformation

Earthquake-induced permanent displacements were calculated using the decoupled method (Makdisi and Seed, 1978) and the Slope/W software. The failure mechanism assessed was failure of the slope through the rock mass. A range of slide surfaces were assessed adopting the “block search” and “semi-circular” functions. Permanent displacements was estimated along each slide surface, where the displacing mass was treated as a rigid-plastic body and no internal plastic deformation of the mass was accounted for, and the mass accrued no displacement at accelerations below the yield acceleration.

The out-of-phase synthetic rock outcrop earthquake time acceleration histories from the 22 February and 13 June 2011 earthquakes were used as inputs for the modelling, as permanent coseismic displacement of the Redcliffs slopes were inferred during these events, and large volumes of materials fell from the slopes. Variable material strength parameters were used for the main materials present, adopting model parameters 1–3 (Table 17).

For these assessments, the displacements inferred from crack apertures are assumed to represent the coseismic permanent displacement of the slope, along cross-section 1, during the 22 February, 13 June and 23 December 2011 earthquakes. The results from each modelled scenario were then compared to the inferred coseismic permanent slope displacements for each earthquake.

For the assessments the slope surface at the time of the earthquake was used adopting the LiDAR survey data. For example, back-analysis of the 22 February 2011 earthquake, uses the slope surface from the 2003 LiDAR survey, and back-analysis of the 13 June 2011 earthquake uses the 2011a LiDAR survey. All forecast modelling uses the 2011c LiDAR slope surface model.

The results from the modelling of the 22 February and 13 June 2011 earthquakes, adopting the parameters listed in Table 17, are summarised in Table 19. Figure 23–Figure 25 show the results for the different models.

Table 19 Results from the dynamic modelling of cross-section 4. Total inferred coseismic displacements are from measurements of crack apertures. Yield accelerations and permanent displacements are calculated from the decoupled assessment and represent the modelled slide surface with the lowest yield acceleration for the given material parameters and failure mechanism. Those rows highlighted in grey represent the material parameters that give the best correlation between the modelled and recorded permanent displacements, for a given earthquake and failure mechanism. Modelled displacements are rounded to the nearest 0.1 m.

Material parameter model (Table 17)	Earthquake	Lowest yield acceleration (g)	Min. modelled coseismic displacement (m)	Max. modelled coseismic displacement (m)	Total inferred coseismic displacement (m)
1	22 February 2011	0.68	0.5	0.6	0.3–1.3
1a	22 February 2011	0.29	0.7	1.1	0.3–1.3
2	22 February 2011	0.19	0.7	1.7	0.3–1.3
2a	22 February 2011	0	18.8	26.2	0.3–1.3
3	22 February 2011	0.15	0.9	2.4	0.3–1.3
1	13 June 2011	0.66	0.0	0.0	0.2–0.6
1a	13 June 2011	0.39	0.0	0.0	0.2–0.6
2	13 June 2011	0.23	0.2	0.2	0.2–0.6
2a	13 June 2011	0.01	2.1	2.4	0.2–0.6
3	13 June 2011	0.15	0.6	0.7	0.2–0.6

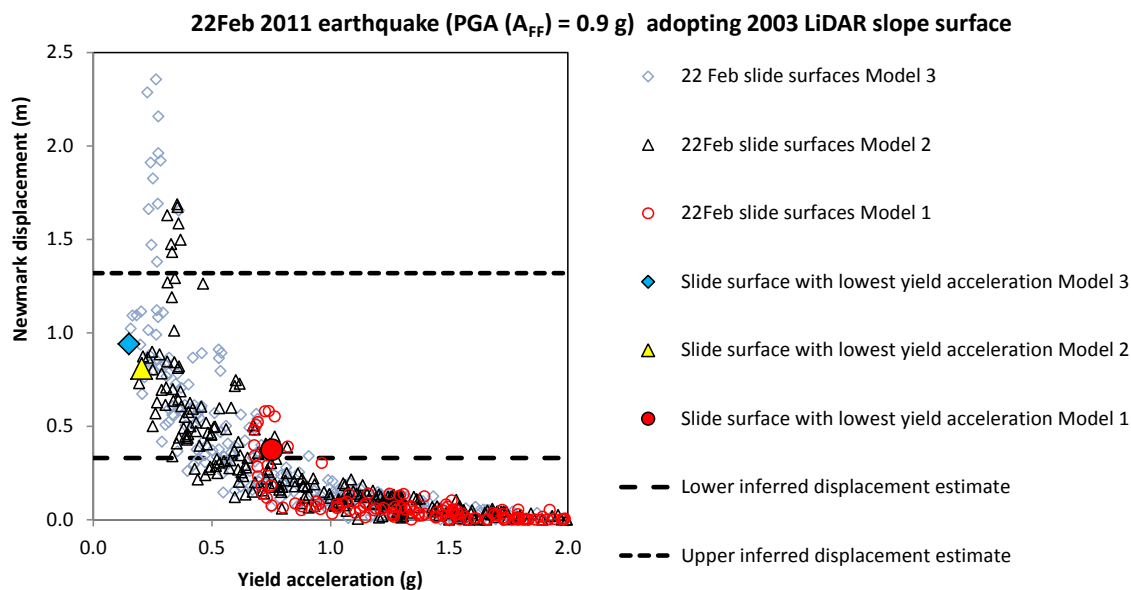


Figure 23 Modelled Slope/W decoupled displacements of cross-section 4 for the 22 February 2011 earthquake and adopting variable estimates of the material strength. Each datapoint represents a modelled slide surface and the corresponding estimate of its displacement as a result of the 22 February 2011 earthquake – adopting the synthetic free-field rock outcrop earthquake acceleration time histories. A_{FF} is the peak horizontal ground acceleration of the free field motion used in the assessment. The dashed lines represent the total inferred coseismic permanent displacement of the slope along the cross-section during the given earthquake.

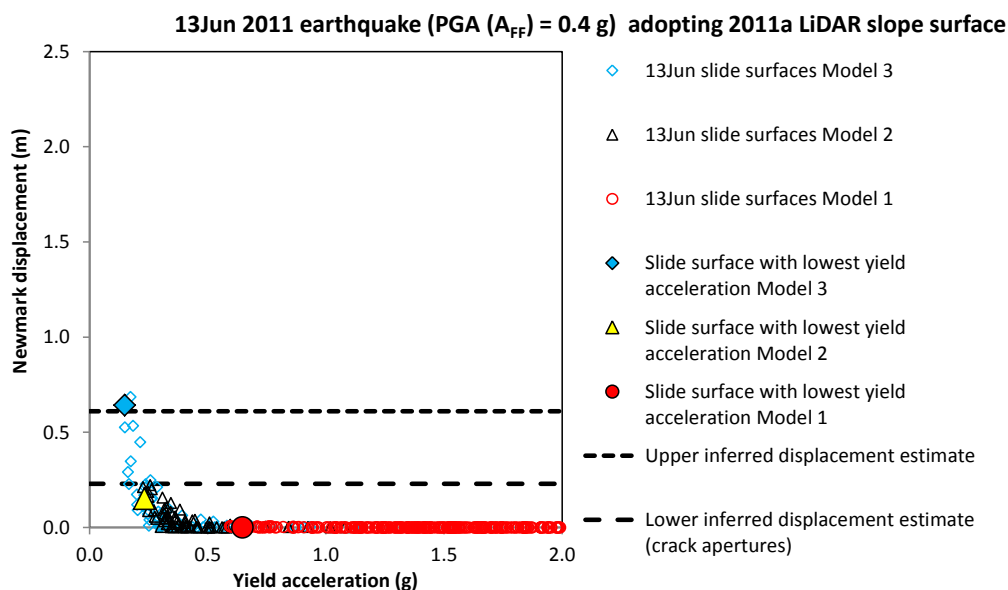


Figure 24 13 June 2011 earthquake, modelled Slope/W decoupled displacements for cross-section 4, and adopting variable estimates of the material strength. Each datapoint represents a modelled slide surface and the corresponding estimate of its displacement as a result of the 13 June 2011 earthquake – adopting the synthetic free-field rock outcrop earthquake acceleration time histories. A_{FF} is the peak horizontal ground acceleration of the free field motion used in the assessment. The dashed line represents the inferred coseismic permanent displacement of the slope along the cross-section during the given earthquake.

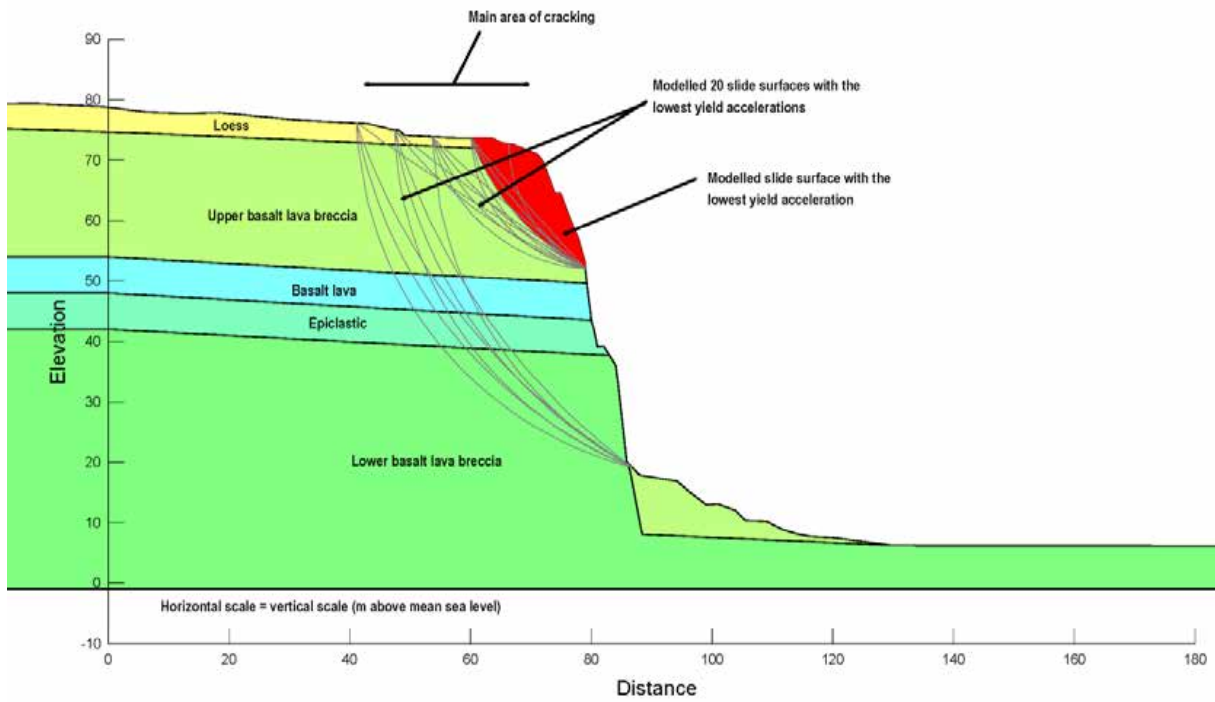


Figure 25 Results from the seismic slope stability assessment for cross-section 4, for the 22 February 2011 earthquake, adopting model 1 material strength parameters.

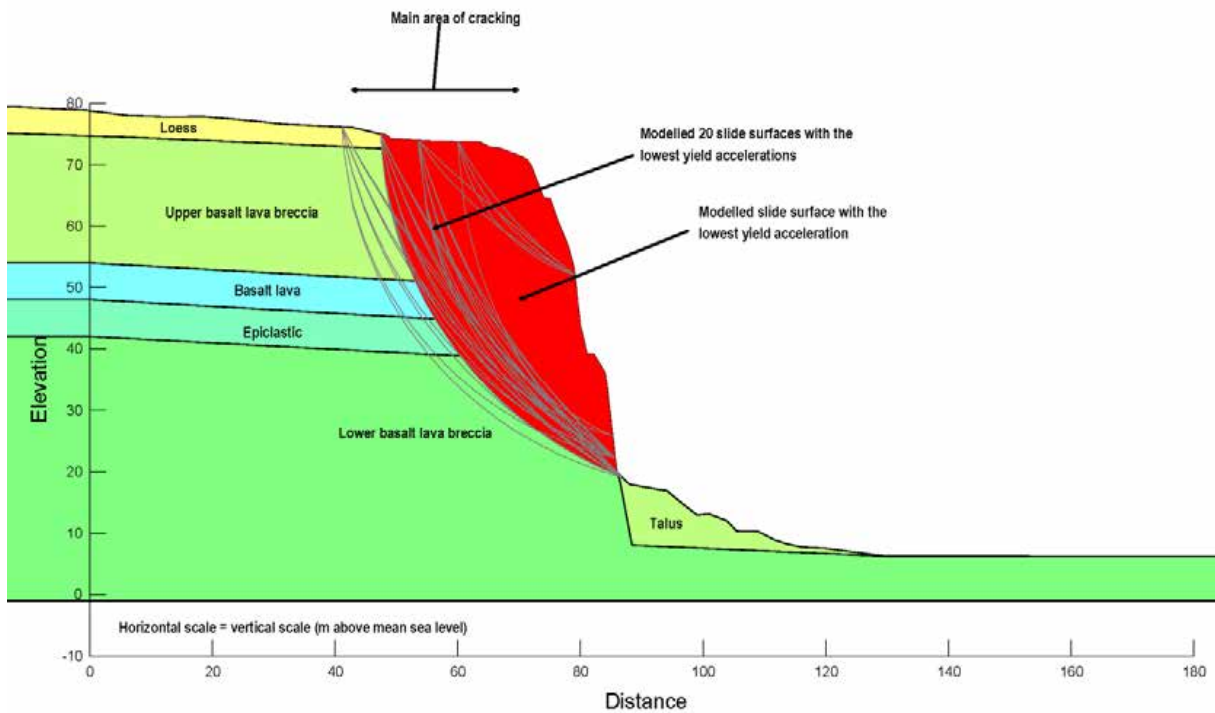


Figure 26 Results from the seismic slope stability assessment for cross-section 4, for the 22 February 2011 earthquake, adopting model 2 material strength parameters.

The results show that:

- A good correlation between the inferred permanent coseismic displacements from crack apertures and modelled displacements of the slope for the 22 February 2011 earthquakes was obtained adopting material parameter models 1 and 2.
- A good correlation between the inferred permanent coseismic displacements from crack apertures and modelled displacements of the cliff for the 13 June 2011 earthquakes was obtained adopting material parameter models 2 and 3.
- The slide surfaces with the lowest yield accelerations adopting the upper range of material strength parameters (model 1) were mainly in the upper lava breccia, indicating a lower factor of safety of the upper part of the cliff.
- When the material strength parameters were degraded (i.e., adopting model 2 material strength parameters) the slide surfaces with the lowest yield accelerations are those that extend to the cliff toe, although the yield accelerations of the slide surfaces in the upper breccia are still low. These observations are consistent with the current slope condition, where recent cracks extend down from the crest to the toe.
- The slope material strength parameters may be reducing after each significant earthquake, as a result of the earthquake-induced fracturing and displacement of the rock mass.
- There is a good correlation between the locations and shape of the slide surfaces derived from the limit equilibrium and finite element static stability modelling, and those from the dynamic modelling.

4.1.2.3 Forecast modelling of permanent slope deformation

Permanent displacements, from the decoupled assessment of results from the 22 February and 13 June 2011 modelled earthquakes, were calculated for a range of slide-surface geometries with different ratios of yield acceleration (K_y) to the maximum average acceleration of the failure mass (K_{MAX}) for a given slide surface. The maximum average acceleration (K_{MAX}) was calculated for each selected slide surface by taking the maximum value of the average acceleration time history from the response to the synthetic earthquake. About 10-20 slide surfaces (with the lowest value of critical yield acceleration K_y) were chosen to represent the results from each earthquake input motion, adopting different estimates of the shear strength of the main materials (models 2 and 3 in Table 17).

The results from the assessment are shown in Figure 27 for those slide surfaces shown in Figure 25 and Figure 26. The results show that between K_y/K_{MAX} values of 0.1 and 0.5, and K_y/A_{FF} values of 0.3 and 0.9, the data are well fitted to a straight line (exponential trend line) in semi-log space. The coefficient of determination (R^2) is 0.89 for K_y/K_{MAX} and 0.82 for K_y/A_{FF} , and includes all of the plotted data ($N = 79$). The lower coefficient of determination for ratios of K_y/A_{FF} is not unusual as Newmark (1965) displacements are highly sensitive to the high frequency components of the input motions, which can vary from event to event. By comparison, K_{MAX} "filters" the higher frequency components, and thus is less sensitive to the input motion characteristics.

The peak ground acceleration of the input motion (A_{FF}) does not take into account amplification effects caused by the slope geometry (Appendix 5). From the data in Figure 27, the mean ratio of K_{MAX} to A_{FF} for cross-section 4 is 2.2 (± 0.3 at one standard deviation), meaning that K_{MAX} is on average 2.2 times greater than the peak horizontal ground acceleration of the input motion, assuming a linear relationship.

For ratios of K_y/A_{MAX} in Figure 27, the estimated magnitudes of displacement are consistent with those reported by Jibson (2007), where these data plot between the ranges for earthquakes of M6.5–7.5 as reported by Makdisi and Seed (1978) and plotted by Jibson (2007).

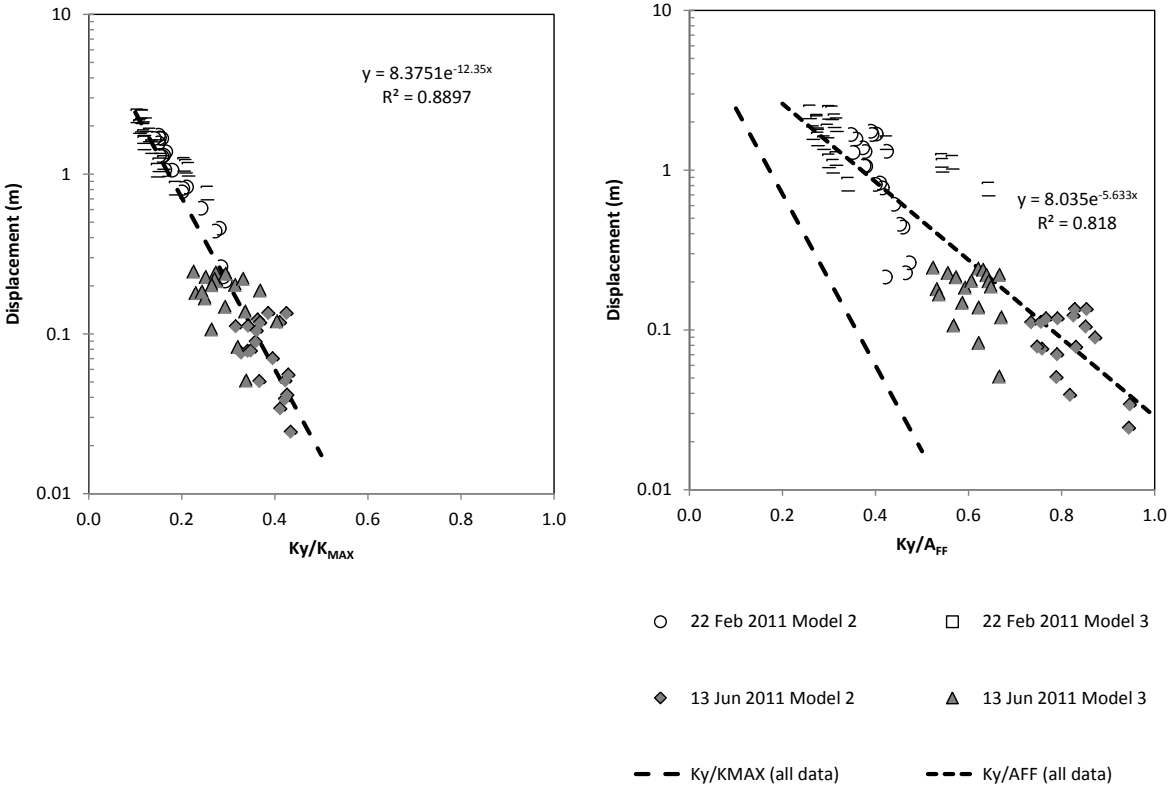


Figure 27 Decoupled Slope/W displacements calculated for cross-section 4, for different ratios of yield acceleration to maximum average acceleration of the mass (K_y/K_{MAX}), and maximum acceleration of the mass (K_y/A_{MAX}), for selected slide-surface geometries, and given material shear strength parameter models 2 and 3. A_{MAX} is the peak acceleration of the input earthquake time acceleration history. Synthetic rock outcrop time acceleration histories for the 22 February and 13 June 2011 earthquakes were used as inputs for the assessment (N = 79). The dashed lines are exponential trend lines fitted to the semi-log data. The formula and the coefficient of determination (R^2) for the trend lines are shown.

The results from the decoupled assessment show that the magnitude of permanent slope displacement during an earthquake will vary in response to:

1. the shear strength of the rock mass at the time of the earthquake;
2. pore pressures within tension cracks and the rock mass, at the time of the earthquake; and
3. duration and amplitude of the earthquake shaking.

For cross-section 4, the relationship between the yield acceleration and the maximum average acceleration (from Figure 27) has been used to determine the likely range of displacements of a given failure mass with an adopted yield acceleration (K_y) at given levels of peak free field horizontal ground accelerations (A_{FF}) and the equivalent maximum average ground acceleration (K_{MAX}). For cross-sections 2 and 6, the pseudostatic method of assessing the yield acceleration of each cross-section was used (the results are shown in Table 18), and the K_y/K_{MAX} relationship (Figure 27), established for cross-section 4, was used to determine the likely magnitude of permanent displacement in a future earthquake. This has been done using the seven earthquake event bands, used to represent the range of earthquake events the slopes could be subjected to in the future.

The results are shown in Table 20. Conservative yield accelerations have been adopted, assuming material parameter model 3, to take into account the possibility that the current shear strength of the materials is now degraded as a result of the past movement and cracking.

Displacement of the slide mass will not occur at maximum average accelerations (K_{MAX}) less than the critical yield acceleration. However, the critical yield acceleration depends upon the strength of the slide surface at the time of the earthquake.

Table 20 Forecast modelling results from the dynamic slope stability assessment for cross-sections 2, 4 and 6, adopting model 3 material parameters, and no water in tension cracks. Estimated displacements are rounded to the nearest 0.1 m.

		Earthquake event band	1	2	3	4	5	6	7
		Peak ground acceleration range of band (g)	0.1–0.3	0.3–0.5	0.5–0.8	0.8–1.2	1.2–1.6	1.6–2.0	2.0–3
		Representative free field peak ground acceleration (A_{FF}) for each band (g)	0.2	0.4	0.65	1.0	1.4	1.8	2.5
		Adopted K_{MAX} to A_{FF}¹ ratio	2.5 (mean plus 1 standard deviation)						
Cross-section	Adopted yield² acceleration (K_y) (g)	Representative equivalent maximum average acceleration (K_{MAX}) of each band (g)	0.4	0.9	1.4	2.2	3.1	4.0	5.5
2	(0.3)	Estimated permanent displacement (m)	0.0	0.2	0.8	1.7	2.7	3.5	4.5
4	0.2	Estimated permanent displacement (m)	0.0	0.3	1.2	2.3	3.3	4.1	5.0
6	(0.5)	Estimated permanent displacement (m)	0.0	0.0	0.1	0.6	1.2	1.9	2.9

¹ A_{FF} represents the peak horizontal ground acceleration of the free field input motion, rounded to the nearest 0.1 g.

² Where shown in brackets, the yield acceleration was calculated using the pseudostatic slope stability method.

4.1.3 Slope stability – Summary of results

The main results from the static and dynamic stability assessment for assessed source areas 1–3 are:

1. Under current conditions, it is possible for failure of the trial slide surfaces to occur under either static or dynamic conditions. Material strengths – and therefore the slope factors of safety – may reduce with time (weathering), water content, and further movement of the slope under either static or dynamic conditions.
2. Under static and dynamic conditions the slide surfaces with the lowest factors of safety and those with the lowest yield accelerations (K_y), are those associated with small failures at the crest and face of the slope, especially when water-filled tension cracks are included.
3. The most critical modelled slide surfaces are those with the lowest factors of safety and yield accelerations passing through the rock mass from slope crest to toe
4. Seismic site response assessment suggests that the peak ground amplification factors between the peak synthetic rock outcrop free-field accelerations and the modelled peak accelerations at the cliff crest vary between 2.6 for horizontal motions and up to 3.2 for vertical motions and that the relationship is non-linear.
5. Given the relatively low static factors of safety (1.4 and 1.1 for cross-sections 2 and 4 respectively), an increase in pore water pressures in open tension cracks within the overlying loess and joints within the underlying rock mass could lead to instability of the slope under static conditions (i.e., short duration high intensity rain).
6. Given the relatively low yield acceleration of the slope (estimated to be about 0.2 g for cross-section 4), it is likely that future earthquakes could reactivate the slope, leading to permanent displacements that could be quite large. The magnitude of any coseismic permanent displacements will depend upon:
 - a. The shear strength of the materials at the time of the earthquake;
 - b. The pore pressure/water content conditions within the slope at the time of the earthquake; and
 - c. The duration and amplitude of the earthquake shaking at the site.
7. Earthquake-induced failures are likely to be larger in volume and the debris travel further, than rainfall-induced failures.

It is inferred that parts of the cliff crest have already undergone more than one metre of permanent slope displacement during the 2010/11 Canterbury earthquakes. Given the thin layer of loess/fill above rock (1–2 m), the magnitude of displacement inferred from the sum of crack apertures suggest that failure/movement of the underlying rock has occurred. This displacement may have reduced the shear strength of critical materials in the slope, making the slope more susceptible to future earthquakes. In addition, there may be an unknown amount of further displacement that the slopes may be able to undergo before failing catastrophically (i.e., where the magnitude of displacement causes the failure mass to break down to become a mobile failure).

4.2 RUNOUT DISTANCE

4.2.1 Potential future source volume estimation

4.2.1.1 Earthquake volumes

The total volumes of cliff-collapse debris likely to be generated in an earthquake representative of each peak ground acceleration band was determined from the relationship between the volumes of material leaving the cliffs during the 2010/11 Canterbury earthquakes (per square metre of cliff face), and the calculated free field rock outcrop peak ground acceleration at the Redcliffs site (Holden et al., 2014) (Table 21 and Figure 28).

Table 21 The volumes of debris leaving the slope during each of the 2010/11 Canterbury earthquakes and the earthquake's estimated peak ground acceleration, at the Redcliffs site – horizontal (H) and vertical (V) peak ground acceleration (PGA) components are listed separately.

Earthquake	PGA H (m/s/s)	PGA V (m/s/s)	Origin ¹	Volume leaving slope (m ³)	Source slope surface area (m ²)	Volume/slope area (m ³ /m ²)
4 September 2010	3.3	1.5	GeoNet LPCC	60 (±10)	22,000	0.003
22 February 2011	8.6	6.4	Synthetic	23,800 (±6,600)	22,000	1.08
16 April 2011	0.5	0.2	Synthetic	1,170 (±110)	22,970	0.05
13 June 2011	3.7	2.7	Synthetic	11,800 (±3,500)	22,970	0.51
23 December 2011	1.6	1.2	Synthetic	1,180 (±130)	22,870	0.05

¹ With the exception of the 4 September 2010 earthquake, peak ground accelerations were taken from the synthetic time acceleration histories (free field rock outcrop motions) derived from earthquake source modelling for the Redcliffs site (Holden et al., 2014). For the 4 September 2010 earthquake the instrumental record (maximum single component) from the GeoNet station LPCC was used.

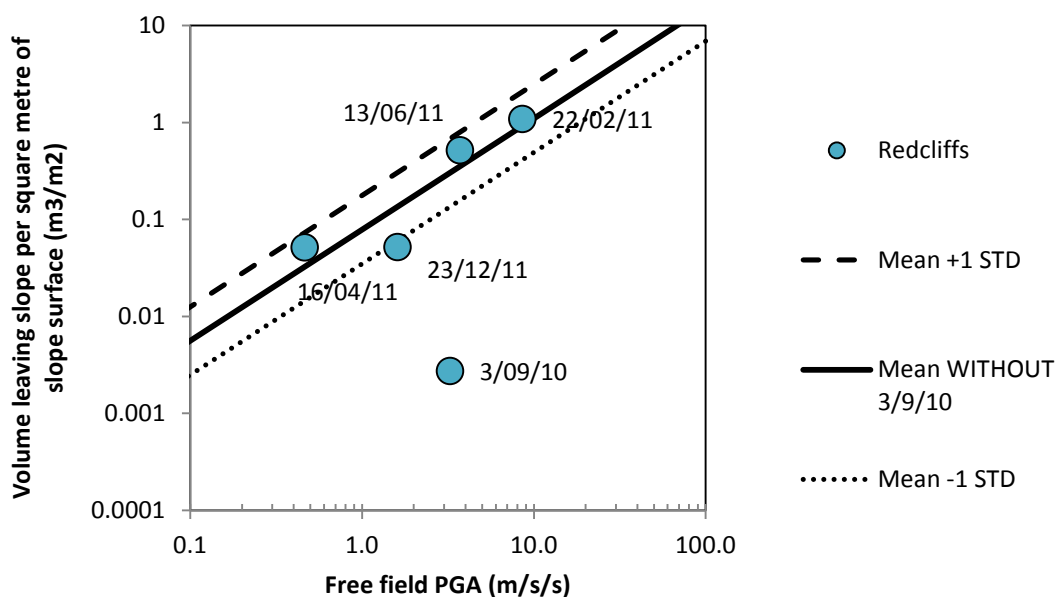


Figure 28 Relationship between free field peak ground accelerations at Redcliffs and the volume of debris leaving the Redcliffs slope.

The observed rockfall volumes correlate well with horizontal peak ground accelerations, with the exception of the 4 September 2010 earthquake. The data are well fitted by a power law, with a coefficient of determination (R^2) of 0.8, if the 4 September 2010 earthquake data is removed, and an R^2 of 0.2 if left in, indicating a poor correlation. In the 4 September 2010 earthquake much smaller volumes were generated (at all Port Hills sites) than for the other, later earthquakes. This difference is presumed to be because of the more fractured nature of the rock slopes following the 22 February 2011 earthquake (consistent with ground observations and measured cracks).

The ground conditions are likely to have weakened further after the 22 February 2011 earthquake. Earthquake induced fracturing and strength degradation of the rock during each subsequent earthquake will have caused further deterioration to rock-mass quality, but the amount of degradation likely in each earthquake is not known.

The 4 September 2010 datapoint is treated as anomalous and was not included in the correlations used to estimate rockfall production as a function of peak ground acceleration.

Seven peak ground acceleration bands are chosen for the assessment and the volumes generated in each band have been estimated from the relationship shown in Figure 29, adopting the mean, the mean minus one standard deviation and the mean plus one standard deviation, as the middle, lower and upper volume estimates respectively (Table 22).

Table 22 The estimated volumes of debris leaving the slope for different bands of peak ground acceleration (PGA). STD is the standard deviation of the mean based on the correlation in Figure 28.

PGA Band (g)	0.1–0.3	0.3–0.5	0.5–0.8	0.8–1.2	1.2–1.6	1.6–2.0	2.0–3
Midpoint of PGA band (g)	0.2	0.4	0.65	1	1.4	1.8	2.5
Midpoint of PGA band (m/s/s)	1.96	3.92	6.38	9.81	13.73	17.66	24.53
Upper volume: MEAN +1 STD (m ³) ¹	8,735	19,349	33,776	55,370	81,460	108,687	158,445
Middle volume: MEAN (m ³) ¹	3,893	8,624	15,054	24,678	36,307	48,442	70,619
Lower volume: MEAN -1 STD (m ³) ¹	1,735	3,844	6,709	10,999	16,182	21,591	31,475

¹ Only the first digit in the number is significant.

Analysis of the volume and frequency distribution of discrete failures that fell from the cliffs during the 13 June 2011 earthquake shows that the total volume of material leaving the cliff will be dominated by infrequent and local large failures. In the case of the 13 June 2011 landslide volumes, one landslide accounted for about 60% of the total volume of all of the surveyed cliff collapses in the Port Hills. At Redcliffs, there were three discrete local cliff collapses of volumes between 1,000 and 2,000 m³ per failure (total volume of about 5,000 m³) which accounted for about 42% of the total volume of debris leaving the slope in response to the 13 June 2011 earthquake.

The 13 June 2011 cliff-collapse data shows that 40% of the total failure volume came from many small randomly distributed failures and 60% from a few very large local failures, with a change in rate at a failure volume of about 2,500–3,000 m³ (Figure 29).

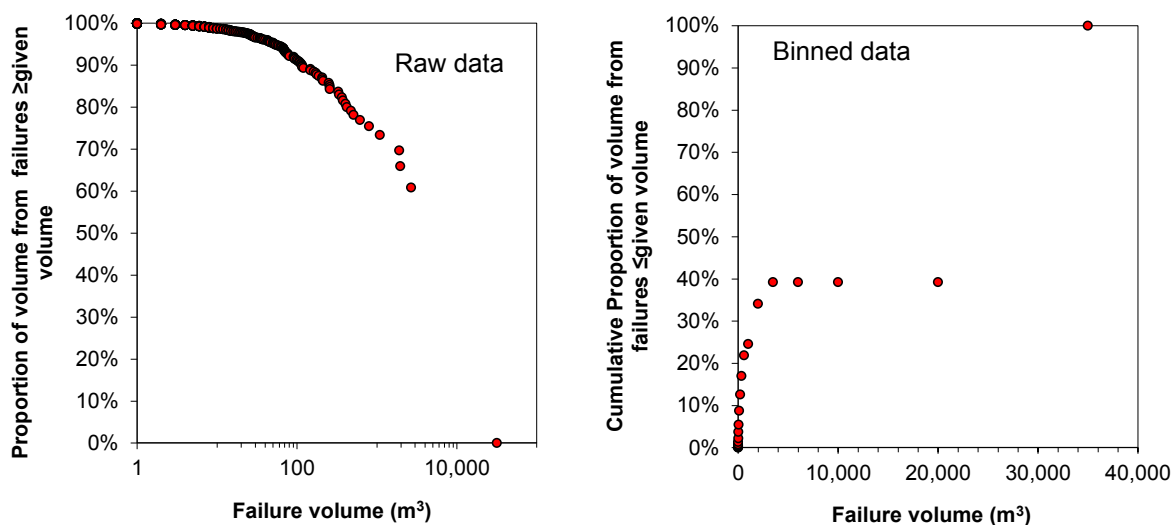


Figure 29 Proportion and cumulative proportion of volume from cliff collapses in the Port Hills greater than or equal to a given volume. Data from the 2011 cliff collapse volumes triggered by the 13 June 2011 earthquakes, derived from terrestrial laser scan change models of Richmond Hill, Shag Rock Reserve and Redcliffs. The different plots represent raw data and binned data.

Local sources (assessed source areas 1–3)

The likely locations and volumes of potential source areas (1–3) have been estimated based on:

1. Numerical stability analysis results;
2. Mapped crack distributions relating to the 2010/11 Canterbury earthquakes; and
3. Engineering geology and morphology of the slope.

Three possible failure volume estimates – lower, middle and upper range estimates – have been calculated for each potential source area. The variation in failure volumes reflects the uncertainty in the source shape (depth, width and length dimensions) estimated from site conditions and the modelling.

Volumes were calculated by estimating the shape of any future failures as quarter-ellipsoids (half-spoon shaped) (following the method of Cruden and Varnes, 1996) (Figure 30). Estimated volumes are shown in Table 23.

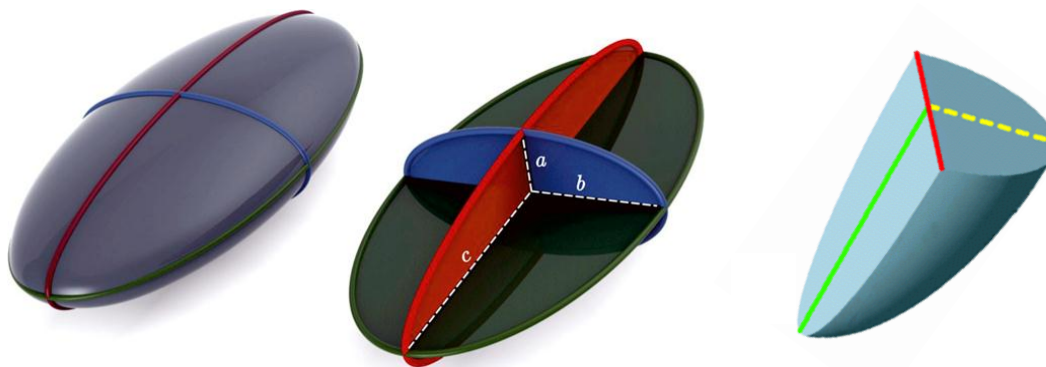


Figure 30 Estimation of landslide volume assuming a quarter-ellipsoid shape.

Table 23 Example of estimated source volumes (the first digit in the number is significant) and fahrboeschung angles.

Assessed source area	Source volume estimate	Volume (m ³)	Fahrboeschung ¹ angle – talus (°)		Fahrboeschung angle – boulder roll (°)	
			Mean	Mean – 1 STD	Mean	Mean – 1 STD
1	LOWER	7,700	38.6	33.0	38.6	33.0
	MID	12,800	38.0	32.4	38.0	32.4
	UPPER ¹	25,000	36.9	31.4	36.9	31.4
2	LOWER	3,700	39.5	33.9	39.5	33.9
	MID	9,400	38.4	32.8	38.4	32.8
	UPPER	18,300	37.6	32.0	37.6	32.0
3	LOWER	1,800	40.4	34.7	40.4	34.7
	MID	2,500	40.0	34.3	39.3	34.3
	UPPER	4,300	39.3	33.7	39.3	33.7

¹ For descriptions of the fahrboeschung angles used in the report refer to Section 4.5.

The credibility of these potential failure volumes has been evaluated by comparing them with estimated volumes of individual debris avalanches that fell from the slopes at Richmond Hill Road, Shag Rock Reserve and Redcliffs (Massey et al., 2012a) during the 13 June 2011 earthquakes (Figure 31). These volumes were derived from the terrestrial laser scan change models.

The estimated potential failure volumes of assessed source areas 1–3 are within the upper volume range of data from relict failures and those that fell in the 13 June 2011 earthquakes. This suggests that such failure volumes could occur, but they are likely to be very infrequent and few in number during a single strong earthquake.

4.2.1.2 Non-earthquake volumes

Non-earthquake volumes and rates of cliff collapse were taken from Massey et al. (2012a) and are based on historical data. The historical data used to infer these rates is summarised in Table 24.

Table 24 Information used to estimate event volumes contributing to the total risk from non-seismic rockfall triggering events, all sites.

Time period (years)	Type of events	Description
<1–15	Rainstorms/frosts that occur frequently.	Cliff collapses tend to be small and localised from events with this high frequency of occurrence. Estimated volumes of events derived using Earthquake Commission claims, local consultant files and the GNS Science database.
15–100	Rainstorms with larger intensities and durations that occur once every 15 – 100 years on average.	Cliff collapses occur but their volumes tend to be limited and localised. Estimated volumes of events derived using historical newspapers and consultant reports.
100–1,000	Rainstorms with very large intensities and durations that occur once every 100 – 1,000 years on average.	Cliff collapses will be widespread. Estimated volumes of events derived using old newspaper reports.
1,000– 10,000	Rainstorms with extreme intensities and durations exceeding Cyclone Bola (1988) and the Manawatu storm (2004) that occur once every >1,000 years on average.	These events might trigger a large number of cliff collapses over a wide area and may be large in volume. However, cliff collapse risk would be low compared with risk from flooding or debris flows.

4.2.2 Runout modelling

4.2.2.1 Randomly distributed cliff collapses

For distributed cliff collapses triggered by earthquakes and for non-earthquake cliff collapses, the volume of debris passing through each 2 m by 2 m grid cell was estimated using the volumes of material that passed a given fahrboeschung angle from debris avalanches triggered by the 22 February and 13 June 2011 earthquakes, at Redcliffs. The values contained in Massey et al. (2012a) have been revised based on reassessment of the LiDAR data sets. Results are presented in Figure 31.

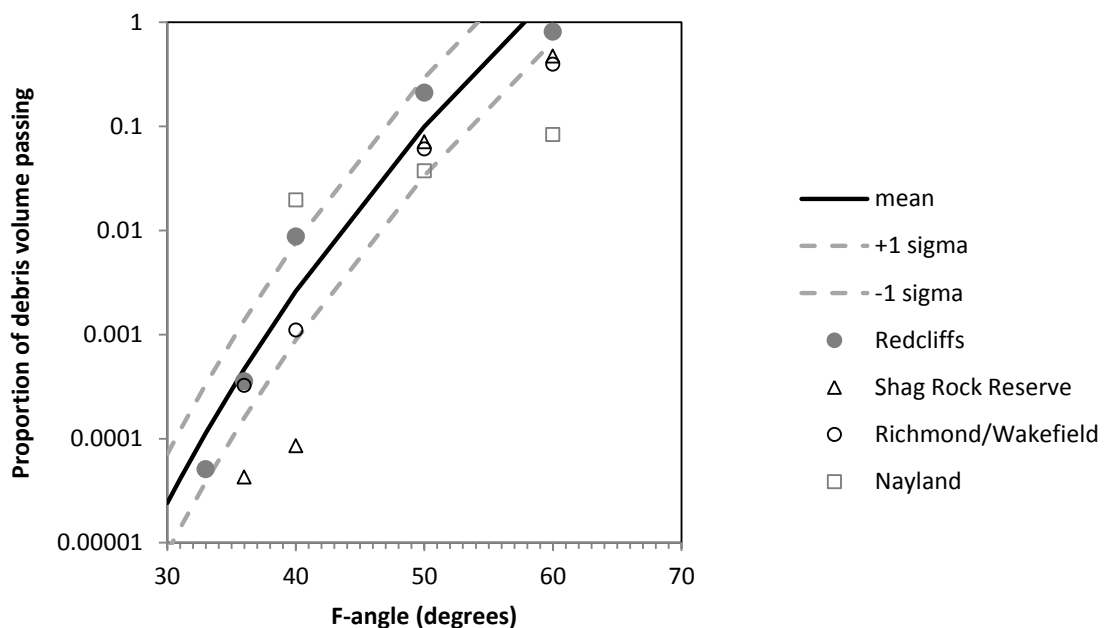


Figure 31 Proportion of debris volume passing a given fahrboeschung angle (F-angle) line, from debris avalanches triggered during the 22 February and 13 June 2011 earthquakes at Redcliffs. Trend lines are fitted to Redcliffs data only. Data from Shag Rock Reserve, Richmond Hill/Wakefield Avenue and Nayland Street are also shown for comparison.

For these randomly distributed cliff collapses, the volume of debris passing through a given 2 m by 2 m grid cell below the slope was derived from the relationship in Figure 31, based on the Redcliffs data only, for each volume estimate (lower, middle and upper). For the risk assessment the volume was converted into an equivalent number of boulders, where 1 m³ of debris comprised about 15 boulders.

4.2.2.2 Local cliff collapses (assessed source areas 1–3)

The runout of debris from the assessed source areas 1–3 was assessed both empirically and numerically.

For local cliff collapses the maximum volume of debris passing through a given 2 m by 2 m grid cell below the source was derived from the RAMMS model outputs for each assessed source area (1–3) for each volume estimate (lower, middle and upper). For the risk assessment the volume was then converted into an equivalent number of boulders, as per the randomly distributed debris volumes.

The runout distances estimated from RAMMS were checked using empirical runout relationships measured from discrete debris avalanches that occurred in the Port Hills during the 2010/11 Canterbury earthquakes.

Empirical method

The procedure followed for estimating the empirical run-out distance, in terms of the fahrboeschung angle, is detailed in Appendix 1.

A total of 45 sections through specific debris avalanches triggered by the 22 February and 13 June 2011 earthquakes have been assessed. For each section the fahrboeschung for “talus” (where the ground surface is obscured by many boulders) and “boulder roll” (individual boulders) have been defined based on field mapping. The results are shown in Figure 32 as ratios of H/L where H is the height of fall and L is the length, or runout distance, of the mapped rockfalls and debris avalanche deposits (talus).

These fahrboeschung relationships are based on debris avalanches that fell from cliffs in the wider Port Hills area during the earthquakes, and not just from the Redcliffs site. They therefore reflect all of the different types of slope shape that could affect the debris avalanche runout.

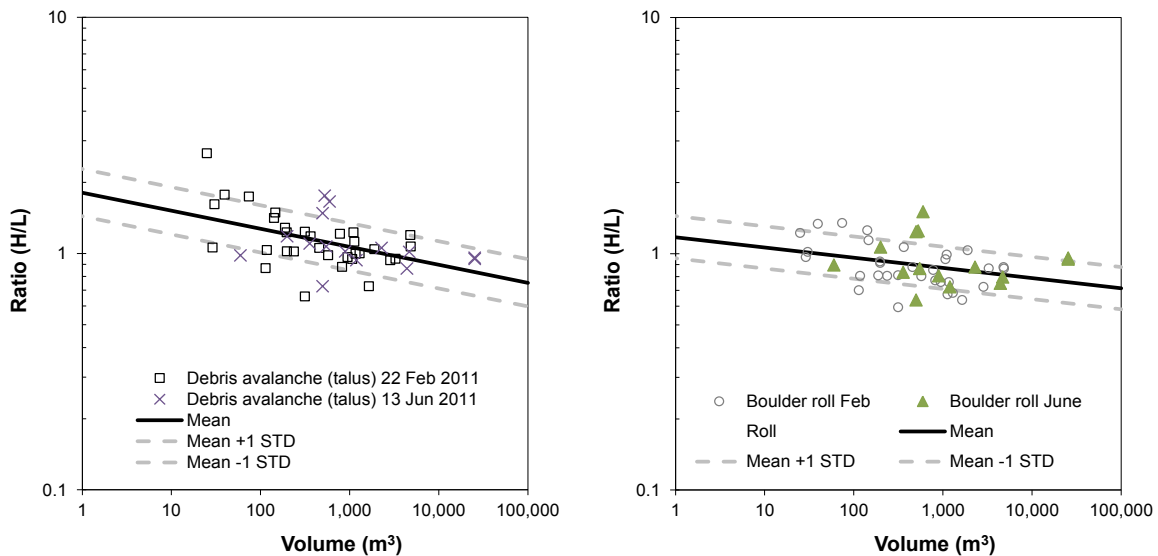


Figure 32 The empirical fahrboeschung relationships, expressed as the ratio of height (H) to length (L) for debris avalanche talus and boulder roll (rockfalls), recorded in the Port Hills. N = 45 sections. Errors are expressed as the mean \pm one standard deviation (STD).

The results show that for very large failure volumes, the fahrboeschung angles – and therefore runout distances – are the same for talus and boulder rolls. However, for smaller failure volumes (typically less than 100 m³) the boulders runout significantly further than the talus.

The main problem with using the fahrboeschung method to predict runout is that it does not take into account the ramping effect caused by the shape of the slope below the source area, which can have a significant effect on debris runout. However, they are useful as comparison tools to compare how credible the RAMMS runout modelling results are.

From the assessment of the debris that fell from the three main cliffs (Redcliffs, Shag Rock Reserve and Wakefield Avenue/Richmond Hill), during the 2010/11 Canterbury earthquakes, no debris passed the 31° fahrboeschung angle line (Massey et al., 2012a).

Numerical method – RAMMS

The RAMMS software (RAMMS, 2011) takes into account the site slope geometry when modelling debris runout. The physical model of RAMMS Debris Flow uses the Voellmy friction law. This model divides the frictional resistance into two parts: 1) a dry-Coulomb type friction (coefficient μ) that scales with the normal stress; and 2) a velocity-squared drag or viscous-turbulent friction (coefficient ξ). The RAMMS model parameters were calculated from the back-analysis of 23 debris avalanches (ranging in volume from 200 to 35,000 m³) that fell from the slopes at Richmond Hill Road, Shag Rock Reserve and Redcliffs during the 22 February and 13 June 2011 earthquakes. The modelled parameters μ (μ) and ξ were optimised to obtain a good correlation between the modelled versus actual runout and deposited debris heights (Figure 33).

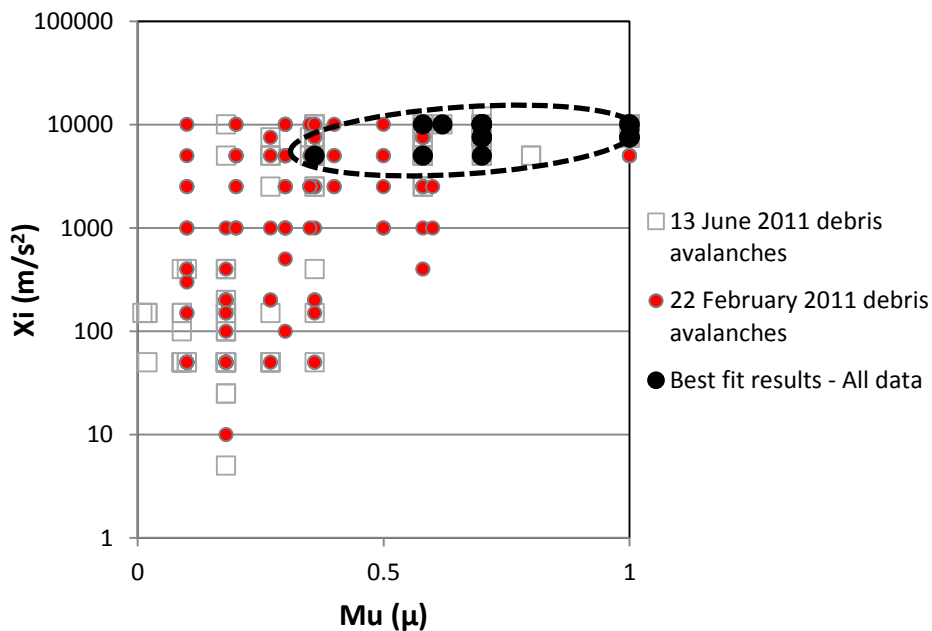


Figure 33 Range of parameters used to back-analyse the runout of debris avalanches in the Port Hills triggered by the recent earthquakes using the RAMMS software (RAMMS, 2011).

The model parameters that gave the “best fits” between modelled and actual runout distances and heights when: $\mu = 0.7$ and $\xi = 7,500 \text{ m/s}^2$. The ξ values are comparable to results from other assessments compiled by Andres (2010) for rockfalls (debris avalanches), but the μ values are larger than those shown by Andres (2010), possibly because the Port Hills debris avalanches are more clast-dominated (Figure 34).

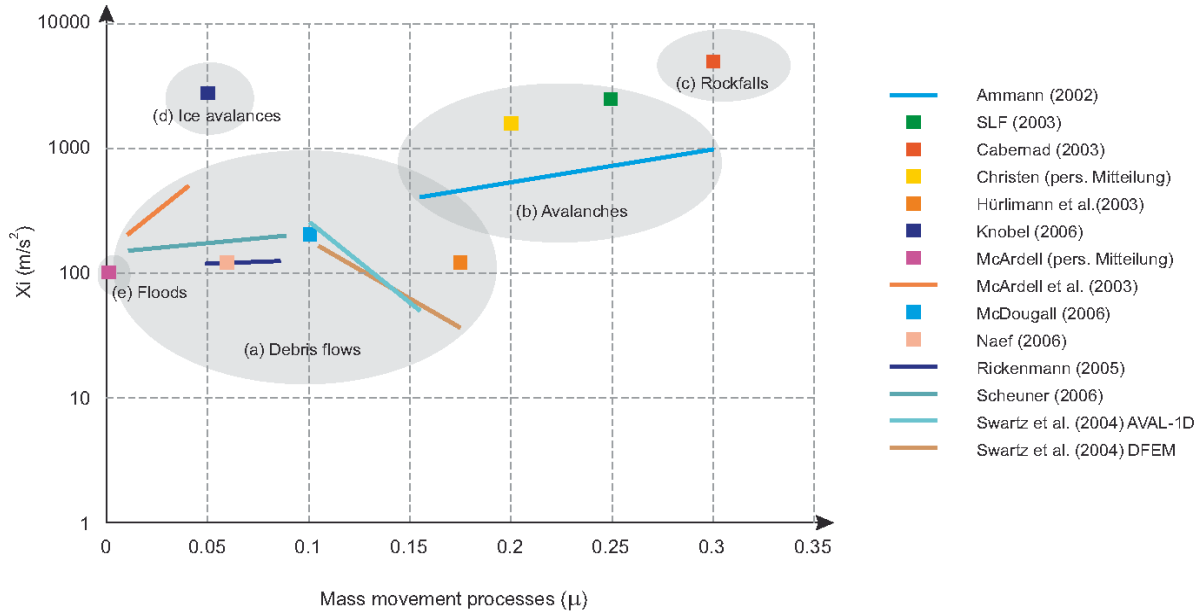


Figure 34 Range of parameters for different mass movement processes: a) debris flows, b) snow avalanches, c) snow avalanches, d) ice avalanches, e) debris floods. Modified from Andres (2010).

For each back-analysed debris avalanche, the modelled final debris thicknesses were compared to the actual deposit thicknesses interpolated from difference models derived from the airborne LiDAR surveys using a 1 m grid. For debris avalanches triggered by the 22 February 2011 earthquakes the deposit thicknesses were estimated from differences between the 2011a (March 2011) LiDAR survey and the 2003 LiDAR survey. For debris avalanches triggered by the 13 June 2011 earthquakes the 2011c (July 2011) and 2011a LiDAR surveys were used. Statistics from the comparison give a mean difference of $0.5 (\pm 0.4) m^3$, with a mode of $0.2 m^3$ (Figure 35) for the $1 m^2$ grid cells.

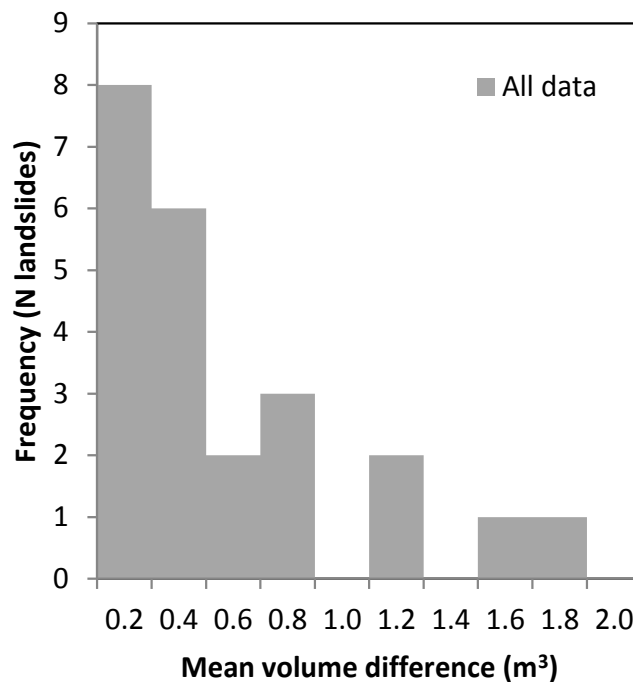


Figure 35 Mean volume difference between the RAMMS modelled volumes and the actual recorded volumes per $1 m^2$ grid cell. N = 23 debris avalanches triggered by 22 February and 13 June 2011 earthquakes.

For the 23 debris avalanches, the performance of the RAMMS and fahrboeschung models (based on the compiled 45 sections shown in Figure 32) were assessed against the actual field mapped runout distances. The RAMMS model performed well with a gradient of 1.01 (± 0.04) at one standard deviation and coefficient of determination (R^2) of 0.3 indicating the data are scattered. The empirical fahrboeschung model performed about the same as the RAMMS model, where the gradient was 1.06 (± 0.05) at one standard deviation but the coefficient of determination (R^2) of 0.5 indicates less scatter (Figure 36).

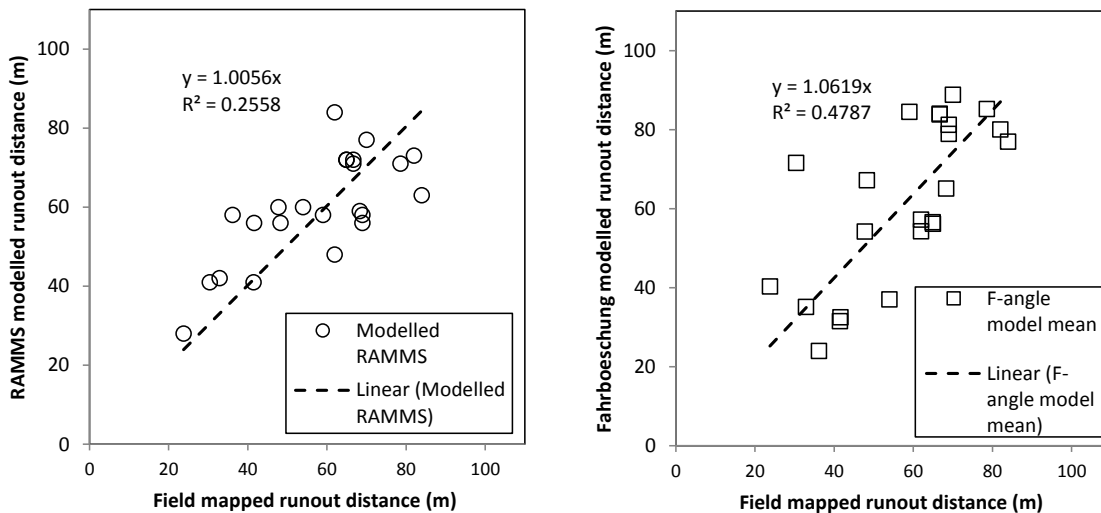


Figure 36 Comparison between the RAMMS modelled and the empirical modelled debris runout (Figure 32, and the actual recorded runout for debris avalanches triggered by the 22 February and 13 June 2011 earthquakes. N = 23 debris avalanches.

Numerical method – RocFall

In order to better define the debris velocities and to check the RAMMS runout distances in the distal runout zone, the two-dimensional rockfall modelling software RocFall, developed by RocScience has been used, as RocFall treats the debris as individual particles, while RAMMS treats the debris as an aggregated flow. The results of Rockfall run out simulations for Redcliffs cross-sections 2, 4 and 6 are shown in Appendix 9 with the corresponding “end-points” histograms indicating the farthest point reached by the simulation. Cross-sections 2, 4 and 6 have been modelled, adopting the parameters detailed in Massey et al. (2012b). Results are shown in Appendix 9.

The RocFall software program was used by Massey et al. (2012a) to analyse the runout limits of individual boulders that fell during the 2010/2011 Canterbury earthquakes. This was done to derive material parameters by back-analysis of the observed rockfall runouts, which were then subsequently used for forecasting rockfall runout in areas where little rockfall data were available.

Results for cross-sections 2, 4 and 6 show that boulders could reach fahrboeschung angles of 32°, 34° and 30° respectively. The fahrboeschung angle of 30° for cross-section 6, is slightly less than the lowest fahrboeschung angle recorded at Redcliffs (and other similar cliffs in the Port Hills), which was 31°, based on back analysis of the debris that fell from these cliffs during the 2010/11 earthquakes. In general the results from the methods used are similar (within the uncertainties of the methods).

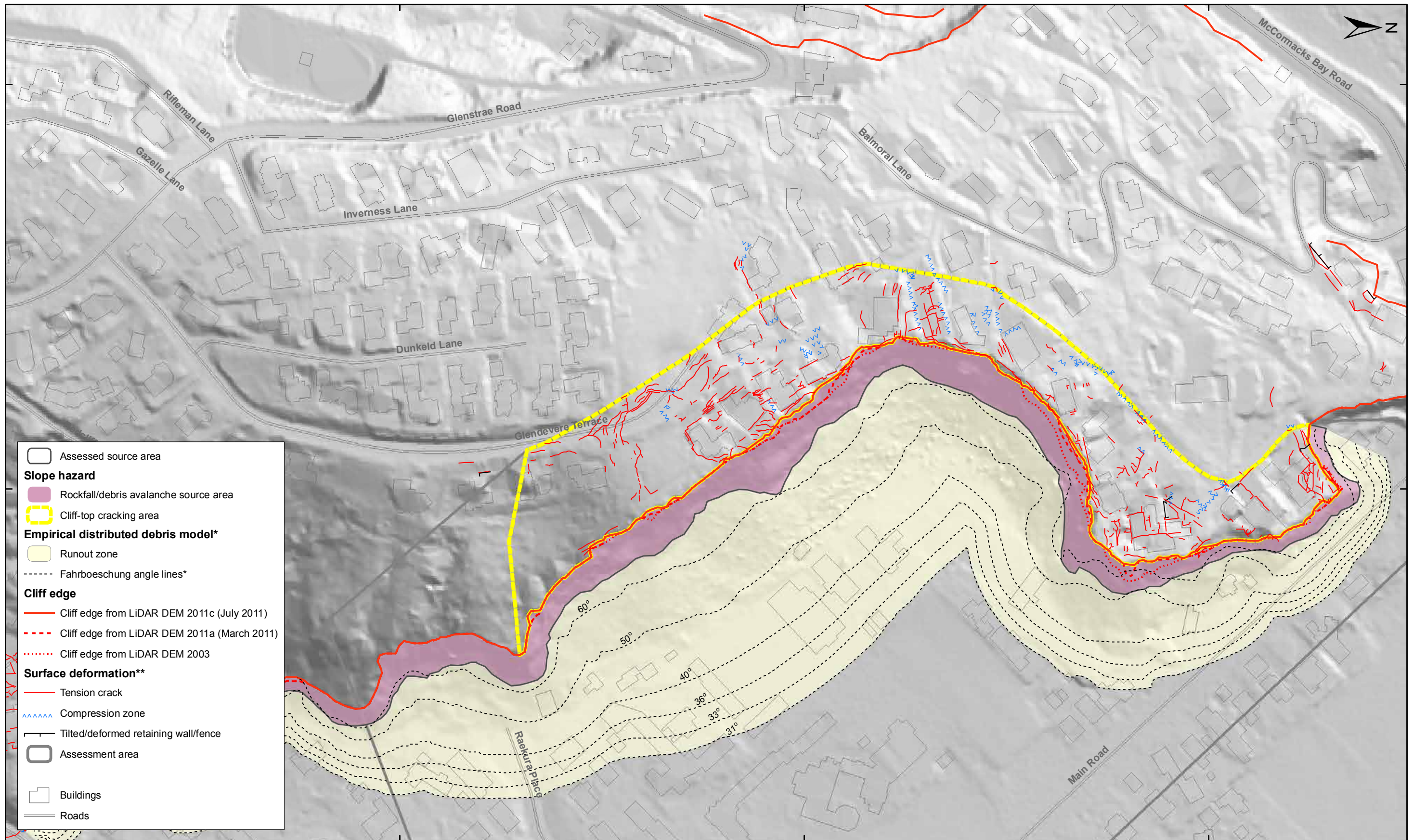
4.2.2.3 Forecast runout modelling

A hazard map (Figure 37) presents the empirical and numerical runout limits from the modelling. Figure 37, Map 1, shows the cliff collapse hazard map for the randomly distributed source areas, and the fahrboeschung angles from 60° to 31°. The 31° fahrboeschung angle is the runout limit of rocks from debris avalanches triggered by the 2010/11 earthquakes from the assessed cliffs (Redcliffs, Shag Rock Reserve, and Richmond Hill/Wakefield Avenue) in Massey et al. (2012a).

Figure 37, Map 2, shows the cliff collapse hazard map for the localised source areas 1–3 for the upper volume estimates (Scenario A). The mean and mean minus one standard deviation fahrboeschung angles for each source area assuming the upper volume estimates, are also shown. The estimated runout distances from the RAMMS modelling for the same source areas are also shown for the upper volume estimates. These show the likely runout limits of the debris from the assessed debris avalanche source areas.

RAMMS runout models are contained in Appendix 6 (debris height) and Appendix 7 (debris velocity), for source areas 1–3 (upper, middle and lower source volume estimates), along with the corresponding mean and mean minus one standard deviation fahrboeschung angles.

In general, there is a good correlation between the fahrboeschung angles and RAMMS runout limits for the assessed source areas.



SCALE BAR: 0 50 100 m

EXPLANATION:

* Modified from report CR2012/57
 ** Taken from report CR2012/317

Background shade model derived from NZAM post earthquake 2011c (July 2011) LiDAR survey resampled to a 1 m ground resolution.
 Roads and building footprints provided by Christchurch City Council (20/02/2012).
 PROJECTION: New Zealand Transverse Mercator 2000

DRW:
BL
 CHK:
CM, FDP



**CLIFF COLLAPSE HAZARD MAP
 (Randomly distributed debris)**

**Redcliffs
 Christchurch**

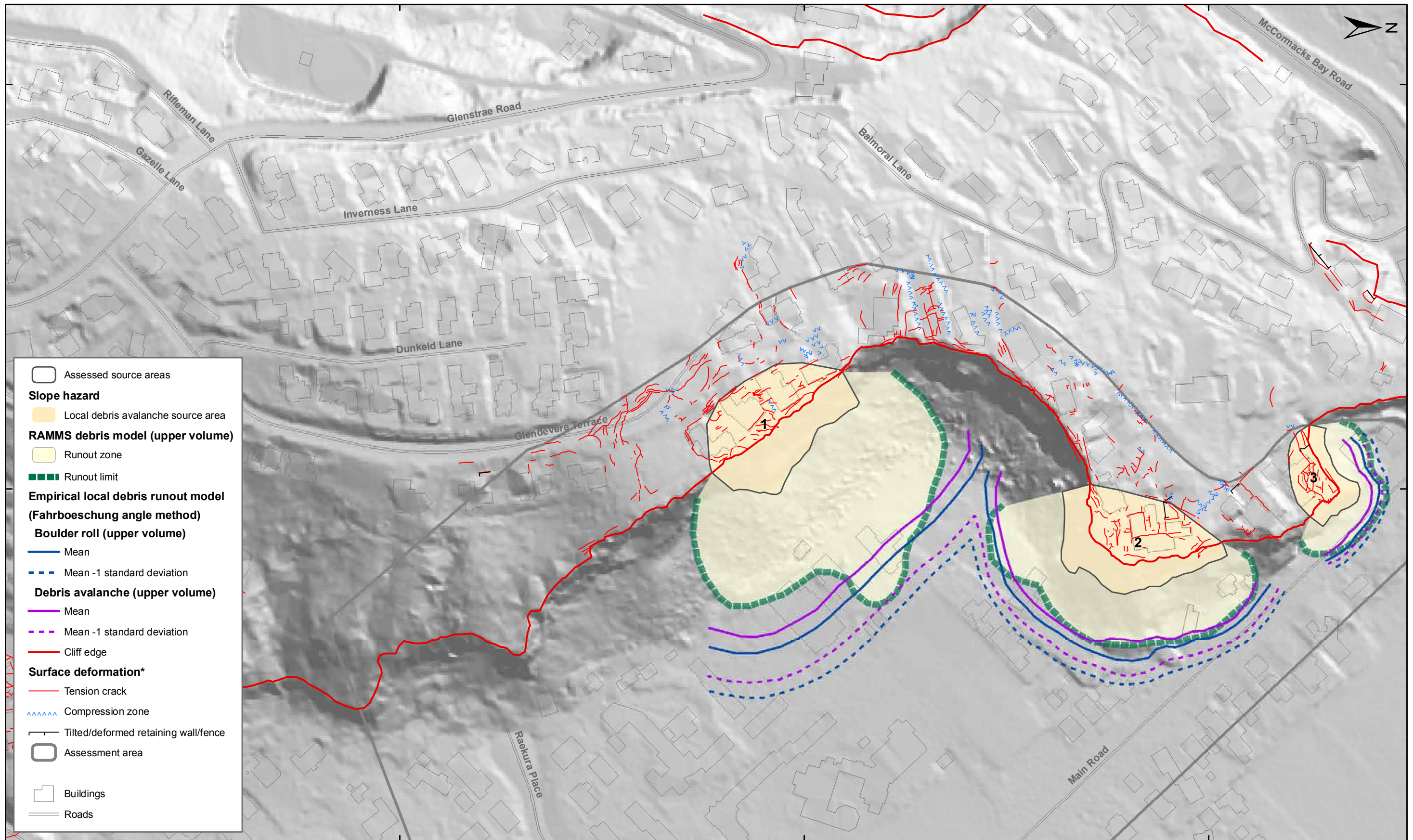
FIGURE 37

Map 1

FINAL

REPORT:
CR2014/78

DATE:
August 2014



SCALE BAR: 0 50 100 m

EXPLANATION:

* Taken from report CR2012/317

Background shade model derived from NZAM post earthquake 2011c (July 2011) LiDAR survey resampled to a 1 m ground resolution.
 Roads and building footprints provided by Christchurch City Council (20/02/2012).
 PROJECTION: New Zealand Transverse Mercator 2000

DRW:
BL

CHK:
CM, FDP



DEBRIS AVALANCHE HAZARD MAP
(Source areas 1, 2 and 3)

Redcliffs
Christchurch

FIGURE 37

Map 2

FINAL

REPORT:
CR2014/78

DATE:
August 2014

5.0 RISK ASSESSMENT RESULTS

5.1 TRIGGERING EVENT FREQUENCIES

Failure of the assessed sources could be triggered by earthquakes (dynamic conditions) or by water ingress (static conditions).

5.1.1 Frequency of earthquake triggers

For earthquake triggers, the frequency of a given free-field peak ground acceleration (A_{FF}) occurring is obtained from the New Zealand National Seismic Hazard Model (Table 25) (Stirling et al., 2012). The increased level of seismicity in the Christchurch region is incorporated in a modified form of the 2010 version of the National Seismic Hazard Model (Gerstenberger et al., 2011).

For these assessments, peak ground acceleration is used to represent earthquake-shaking intensity, as peak ground acceleration is the ground-motion parameter considered to be most directly related to coseismic landslide initiation (Wartman et al., 2013).

Table 25 The annual frequency of a given peak ground acceleration (PGA) band occurring on rock (Site Class B) for different years from the 2012 seismic hazard model for Christchurch (G. McVerry, personal communication 2014). Note: these are free field rock outcrop peak ground accelerations.

PGA Band (g)	0.1–0.3	0.3–0.5	0.5–0.8	0.8–1.2	1.2–1.6	1.6–2.0	2.0–3
Year 2012 annual frequency	0.3405	0.0874	0.0329	0.0084	0.0016	0.0004	0.0001
Year 2016 annual frequency	0.1381	0.0322	0.0119	0.0030	0.0006	0.0001	0.00005
Next 50-year average annual frequency	0.0729	0.0148	0.0054	0.0014	0.0003	0.0001	0.00002

To take into account the possibility of larger local failures of the slope the total volume of debris generated in each band was partitioned between: 1) random uniformly distributed failures of the cliff face comprising 40% of the total volume, that may fall from anywhere on the slope; and 2) local (non-random) larger failures comprising 60% of the total volume, corresponding to assessed source areas 1–3 (Table 26). Volumes were estimated based on the upper, middle and lower total volume estimates of debris generated in each band.

Table 26 Proportion of the total debris volume per peak ground acceleration band allocated to distributed and local failures, for upper, central and lower estimates of volume (rounded to the nearest 100 m³).

Estimated debris avalanche volumes ¹ (m ³)	Peak ground acceleration band (g)						
	0.1–0.3	0.3–0.5	0.5–0.8	0.8–1.2	1.2–1.6	1.6–2.0	2.0–3
Distributed debris: Upper volume	8,700	7,700	13,500	22,200	32,600	49,000	98,800
Localised debris: Upper volume	0	11,600	20,300	33,200	48,900	59,700	59,700
Distributed debris: Middle volume	3,900	3,500	6,000	9,900	14,500	19,400	36,300
Localised debris: Middle volume	0	5,200	9,000	14,800	21,800	29,100	34,300
Distributed debris: Lower volume	1,800	1,500	2,700	4,400	6,500	8,600	12,600
Localised debris: Lower volume	0	2,300	4,00	6,600	9,700	13,000	18,900

¹ Only the first digit in the number is significant.

5.1.1.1 Peak ground acceleration and permanent slope displacement

The probability of each local source area (1–3) being triggered in a given earthquake was based on the calculated permanent displacement, estimated from the decoupled results.

It is difficult to estimate the probability of triggering failure, leading to catastrophic slope collapse, where the debris runs out down slope forming a debris avalanche. It is also possible that permanent slope displacements could cause catastrophic damage to dwellings located at the cliff crest, even if the debris does not leave the source. The level of displacement chosen to differentiate between safe and unsafe behaviour (Abramson et al., 2002) differs between authors. Some examples are:

- a. Hynes-Griffin and Franklin (1984) suggest that up to 0.1 m displacements may be acceptable for well-constructed earth dams.
- b. Wieczorek et al. (1985) used 0.05 m as the critical parameter for a landslide hazard map of San Mateo County, California.
- c. Keefer and Wilson (1989) used 0.1 m for coherent slides in southern California
- d. Jibson and Keefer (1993) used a 0.05–0.1 m range for landslides in the Mississippi Valley.
- e. The State of California (1997) finds slopes acceptable if the Newmark displacement is less than 0.15 m. A slope with a Newmark displacement greater than 0.3 m is considered unsafe. For displacements in the “grey” area between 0.15 and 0.3 m, engineering judgement is required for assessment.

The estimated magnitude of permanent slope displacement of the assessed sources in a future earthquake was based on the decoupled assessment results. The permanent displacement of each source at a given level of free-field peak ground acceleration (A_{FF}) was estimated from the relationship between the yield acceleration (K_y) and the maximum average acceleration of the mass (K_{MAX}) (Figure 27). Different levels of peak ground acceleration were adopted based on the seven earthquake event bands, and each multiplied by the site-specific ratio of K_{MAX} to A_{FF} (assuming the mean plus one standard deviation) to estimate the equivalent maximum average acceleration of the mass (K_{MAX}) for the given value of A_{FF} . For example, an A_{FF} of 0.4 g would have an equivalent K_{MAX} of 0.9 g, assuming a ratio of 2.5 (Table 27).

5.1.1.2 Permanent slope displacement and likelihood of catastrophic slope failure

The probability of occurrence of each local source area (1–3) was based on the estimated permanent displacement, estimated from the decoupled results (Figure 27), as follows:

- If the estimated displacement of the source area is ≤ 0.1 m then the probability of catastrophic failure = 0.
- If the estimated permanent displacement of the source area is ≥ 1.0 m then the probability of catastrophic failure = 1.
- If the estimated permanent displacements are between 0.1 m and 1 m then the probability of failure (P) is calculated based on a linear interpolation between $P=0$ at displacements of 0.1 m, and $P = 1$, at displacements of 1 m.

It should be noted that the displacements at different ratios of K_y/K_{MAX} , were calculated using the synthetic earthquake acceleration time histories for the 22 February and 13 June 2011 earthquakes. Both of these events were near-field earthquakes of short duration, but had high amplitude. The calculated displacements in Figure 27 represent displacements in response to these earthquakes (adopting material parameters for model 3). Earthquakes of longer duration may affect the site in different ways. For example, the response of the loess and volcanic colluvium (at higher water contents representative of winter conditions) may be non-linear, and could lead to larger permanent displacements. Conversely, the peak amplitudes relating to longer duration earthquakes from more distant sources are likely to be lower and may not trigger displacement of the slope.

Table 27 Forecast modelling results from the dynamic slope stability assessment for cross-sections 2, 4 and 6, adopting model 3 material parameters, and no water in tension cracks. Estimated displacements are rounded to the nearest 0.1 m.

		Earthquake event band	1	2	3	4	5	6	7	
		Peak ground acceleration range of band (g)	0.1–0.3	0.3–0.5	0.5–0.8	0.8–1.2	1.2–1.6	1.6–2.0	2.0–3	
		Free field peak ground acceleration (A_{FF}) for representative event in band (g)	0.2	0.4	0.65	1.0	1.4	1.8	2.5	
		Year 2016 annual frequency of representative event in band	0.1381	0.0322	0.0119	0.0030	0.0006	0.0001	0.00005	
		Adopted K_{MAX} to A_{FF}¹ ratio	2.5 (mean plus 1 standard deviation)							
Cross-section	Adopted yield² acceleration (K_y) (g)	Representative equivalent maximum average acceleration (K_{MAX}) of each band (g)³	0.4	0.9	1.4	2.2	3.1	4.0	5.5	
2 (source area 2)	(0.3)	Estimated permanent displacement (m)	0.0	0.2	0.8	1.7	2.7	3.5	4.5	
		Probability of failure	0.0	0.1	0.7	1.0	1.0	1.0	1.0	
4 (source area 1)	0.2	Estimated permanent displacement (m)	0.0	0.3	1.2	2.3	3.3	4.1	5.0	
		Probability of failure	0.0	0.3	1.0	1.0	1.0	1.0	1.0	
6 (source area 3)	(0.5)	Estimated permanent displacement (m)	0.0	0.0	0.1	0.6	1.2	1.9	2.9	
		Probability of failure	0.0	0.0	0.0	0.5	1.0	1.0	1.0	

¹ A_{FF} represents the peak horizontal ground acceleration of the free field input motion, rounded to the nearest 0.1 g.

² Where shown in brackets, the yield acceleration was calculated using the pseudo-static slope stability method.

³ Rounded to the nearest 0.1 g.

5.1.1.3 Deaggregation of the National Seismic Hazard Model

The seismic performance of the slope in future earthquakes was inferred from assessing its performance in past earthquakes, mainly the 22 February, 16 April, 13 June and 23 December 2011 earthquakes, using the relationship established between peak ground acceleration and the amount of permanent slope displacement. These earthquakes varied in magnitude between M5.2 and M6.3, and were “near-field” i.e., their epicentres were very close, within 10 km, of the Redcliffs site.

The annual frequencies of a given level of peak ground acceleration occurring in the area are given by the National Seismic Hazard Model of New Zealand (Stirling et al., 2012). The National Seismic Hazard Model combines all of the various earthquake sources that could contribute to the seismic hazard at a given location. The National Seismic Hazard Model estimates for the Port Hills are based on a combination of different earthquake sources: 1) subduction zone; 2) mapped active faults; and 3) unknown or “background” earthquakes. For the risk assessment it is important to deaggregate the National Seismic Hazard Model to assess which earthquake sources contribute the most to it.

Buxton and McVerry (personal communications, 2014) suggest that it is magnitude M5.3–6.3 earthquakes on unknown active faults, within 20 km of the site that contribute most to the National Seismic Hazard Model. These earthquakes are similar to the 22 February, 16 April 13 June and 23 December 2011 earthquakes.

5.1.2 Frequency of rainfall triggers

As discussed in Section 4.1, it is possible that local source areas (1–3) could be triggered under non-seismic (static or natural) conditions, as strength degradation caused by future earthquakes and/or periodic wetting and drying of the slope face could lead to larger static failures in the future.

However, it is unlikely that a rainstorm will trigger a comparable number and volume of cliff collapses over an area similar to a large magnitude earthquake (typically $>M_w$ 6). This is because earthquake loading can greatly exceed the rock mass strength resulting in slope factors of safety of $\ll 1.0$, while intense rain can only reduce rock mass strength until it becomes unstable (factor of safety = 1.0).

Debris avalanche rates triggered by non-seismic events were taken from Massey et al. (2012a). The results from Massey et al. (2012a) for Redcliffs are shown in Table 28.

Table 28 Representative annual event frequency of debris avalanches occurring, and the representative volume of the avalanche, for each time-period band. These represent the estimated volumes of the material leaving the cliffs per site with a given frequency, for non-seismic triggers. Taken from Massey et al. (2012a) for Redcliffs, using historical data.

Location	Return period (years)	Number of events in band	Annual frequency of events	Mean event volume (m ³)	Annual accumulation rate (m ³ /year)
Redcliffs	1–15	5.5	0.37	5	1.8
	15–100	1.3	0.0133	170	2.3
	100–1,000	0.7	0.0007	1,500	1.0
	1,000–10,000	0.3	0.00003	10,000	0.3

Given the historical rates of rainfall triggered rockfall for the slope of about 5–6 m³/year (estimated from historical data in Massey et al., 2012a), the current rates of rockfall triggered by rainfall are considerably higher (480 m³ per year for 2012 and 90 m³/year for 2013). To take the increased non-seismic rockfall rates into account a factor of two has been applied to the annual rate in Table 28, based on the measured rates of rockfall from the terrestrial laser scan surveys.

At present the non-seismic rockfall rates derived from terrestrial laser scan surveys are considerably higher than 10–12 m³/year (historical rate multiplied by a factor of two), but these rates are expected to reduce with time as the more unstable boulders are removed from the slope. The rates recorded from the terrestrial laser scan surveys represent cumulative volumes of debris for a single year. Historically, a maximum yearly rate of up to 50 m³ has been recorded, but this reduces once divided over a longer time period.

If the site were to be affected in the near future by another large earthquake, it is probable that these currently high rates would continue to persist for much longer.

5.2 DWELLING OCCUPANT RISK

The results from the risk assessment are shown in Figure 38 (Maps 1–3) as the annual individual fatality risk for scenarios A, B and C (Table 2), adopting the input parameters as shown in Table 2. Map 1 shows the annual individual fatality risk estimated for cliff collapses (debris avalanches and cliff-top recession) adopting the upper debris volume and runout estimates. Map 2 shows the estimated annual individual fatality risk for cliff collapses adopting the middle debris volume and runout estimates. Map 3 shows the annual individual fatality risk adopting the lower debris volume and runout estimates.

5.2.1 Variables adopted for the risk assessment

Other variables used in the risk assessment were discussed at a workshop with Christchurch City Council on 18 March 2014. Based on the results from the workshop the risk estimates presented in Figure 38 adopt the following main variables:

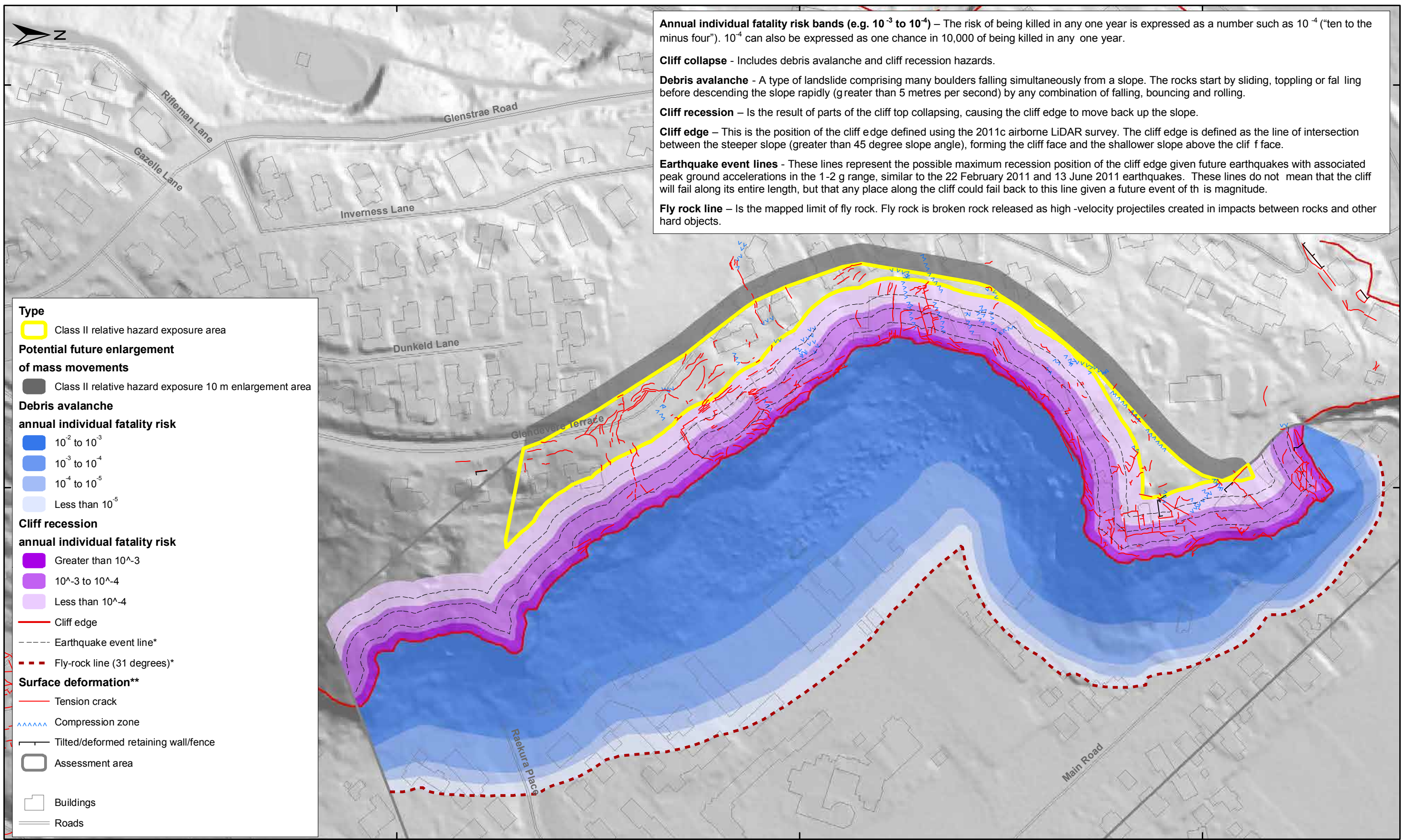
- $P_{(H)}$ for earthquake triggers the annual frequency of the triggering event adopt the 2016 seismic hazard model results, which include aftershocks.
- $P_{(S:H)}$ the probability that a person, if present, is in the path of the debris is based on variable (lower, middle and upper) estimates of the debris volume that could be triggered in an event.
- $P_{(T:S)}$ the probability that a person is present at a particular location, as the debris moves through it, of 67%. Assuming an “average” person spends 16 hours a day at home. For this assessment, GNS Science has assumed the same “average” occupancy rate value adopted by the Canterbury Earthquake Recovery Authority.
- $V_{(D:T)}$ the vulnerability of a person, if present and inundated by debris, is a constant vulnerability factor of 70% has been adopted for this risk assessment as it was the factor adopted by the Canterbury Earthquake Recovery Authority (CERA) for the previous risk assessments.

5.2.2 Debris avalanche

For comparison purposes only, the effect of including the three assessed source areas in the risk assessment are shown by including an estimation of the risk without these three source areas, where all of the debris generated in the peak ground acceleration bands is uniformly distributed across the slope (Figure 39). There is little difference between the two maps, indicating that for scenario B (Figure 38, Map 2) the presence of localised sources has little impact on the risk.

Other parameters such as the probability of a person being present ($P_{(T,S)}$) and the vulnerability of a person if present and hit are held constant across all scenarios where $P_{(T,S)} = 0.67$ and $V_{(D,T)} = 0.7$.

Graphs showing the results for each scenario with/without local seismic sources are shown in Figure 40 and 41. The number of 2 m by 2 m cells shown in the graphs indicates the spread of the risk at different levels of annual individual fatality risk between the scenarios.



Annual individual fatality risk bands (e.g. 10^{-3} to 10^{-4}) – The risk of being killed in any one year is expressed as a number such as 10^{-4} (“ten to the minus four”). 10^{-4} can also be expressed as one chance in 10,000 of being killed in any one year.

Cliff collapse - Includes debris avalanche and cliff recession hazards.

Debris avalanche - A type of landslide comprising many boulders falling simultaneously from a slope. The rocks start by sliding, toppling or falling before descending the slope rapidly (greater than 5 metres per second) by any combination of falling, bouncing and rolling.

Cliff recession – Is the result of parts of the cliff top collapsing, causing the cliff edge to move back up the slope.

Cliff edge – This is the position of the cliff edge defined using the 2011c airborne LiDAR survey. The cliff edge is defined as the line of intersection between the steeper slope (greater than 45 degree slope angle), forming the cliff face and the shallower slope above the cliff face.

Earthquake event lines - These lines represent the possible maximum recession position of the cliff edge given future earthquakes with associated peak ground accelerations in the 1-2 g range, similar to the 22 February 2011 and 13 June 2011 earthquakes. These lines do not mean that the cliff will fail along its entire length, but that any place along the cliff could fail back to this line given a future event of this magnitude.

Fly rock line – Is the mapped limit of fly rock. Fly rock is broken rock released as high-velocity projectiles created in impacts between rocks and other hard objects.

- Type**
- Class II relative hazard exposure area
- Potential future enlargement of mass movements**
- Class II relative hazard exposure 10 m enlargement area
- Debris avalanche annual individual fatality risk**
- 10^{-2} to 10^{-3}
 - 10^{-3} to 10^{-4}
 - 10^{-4} to 10^{-5}
 - Less than 10^{-5}
- Cliff recession annual individual fatality risk**
- Greater than 10^{-3}
 - 10^{-3} to 10^{-4}
 - Less than 10^{-4}
- Cliff edge
 - Earthquake event line*
 - Fly-rock line (31 degrees)*
- Surface deformation****
- Tension crack
 - Compression zone
 - Tilted/deformed retaining wall/fence
- Assessment area
 - Buildings
 - Roads



EXPLANATION:
 * Modified from report CR2012/57
 ** Taken from report CR2012/317
 Background shade model derived from NZAM post earthquake 2011c (July 2011) LiDAR survey resampled to a 1 m ground resolution.
 Roads and building footprints provided by Christchurch City Council (20/02/2012).
 PROJECTION: New Zealand Transverse Mercator 2000

DRW:
BL
 CHK:
CM, FDP



**CLIFF COLLAPSE
 ANNUAL INDIVIDUAL FATALITY RISK
 (Scenario B, 100% distributed)**

**Redcliffs
 Christchurch**

FIGURE 39

FINAL

REPORT: CR2014/78 DATE: August 2014

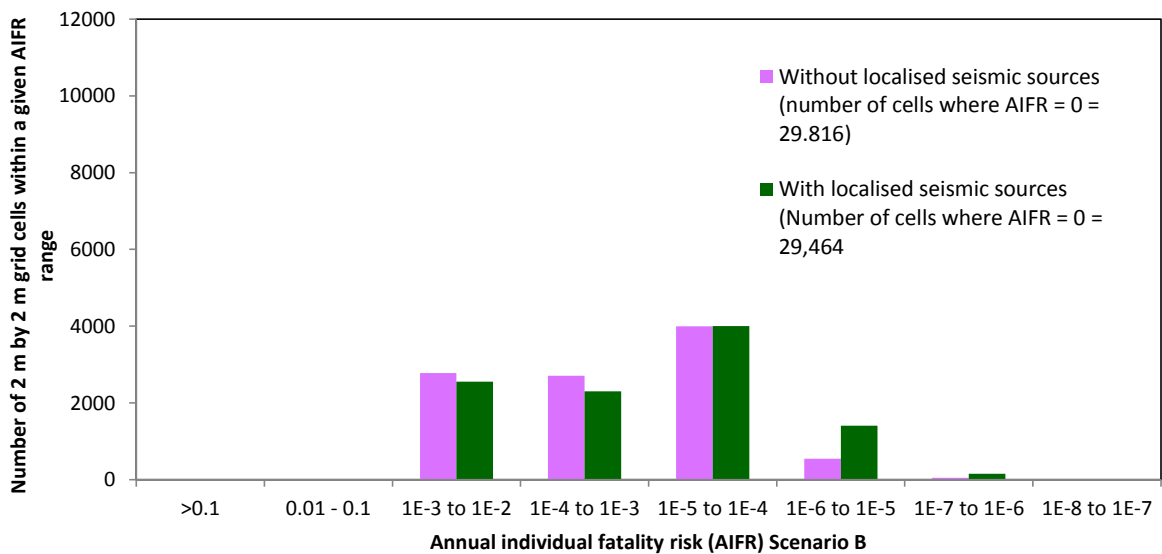
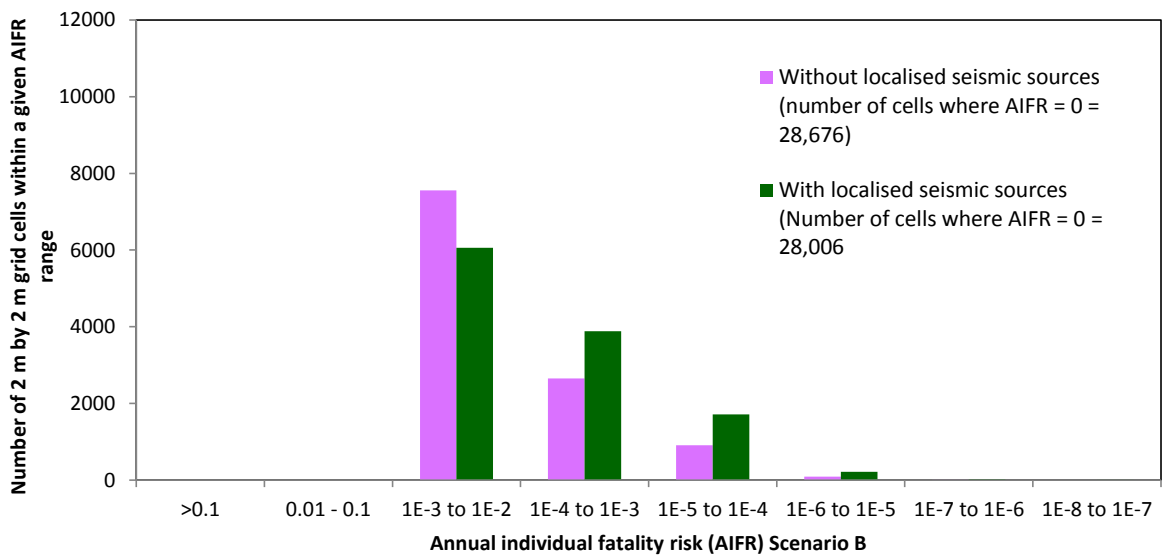
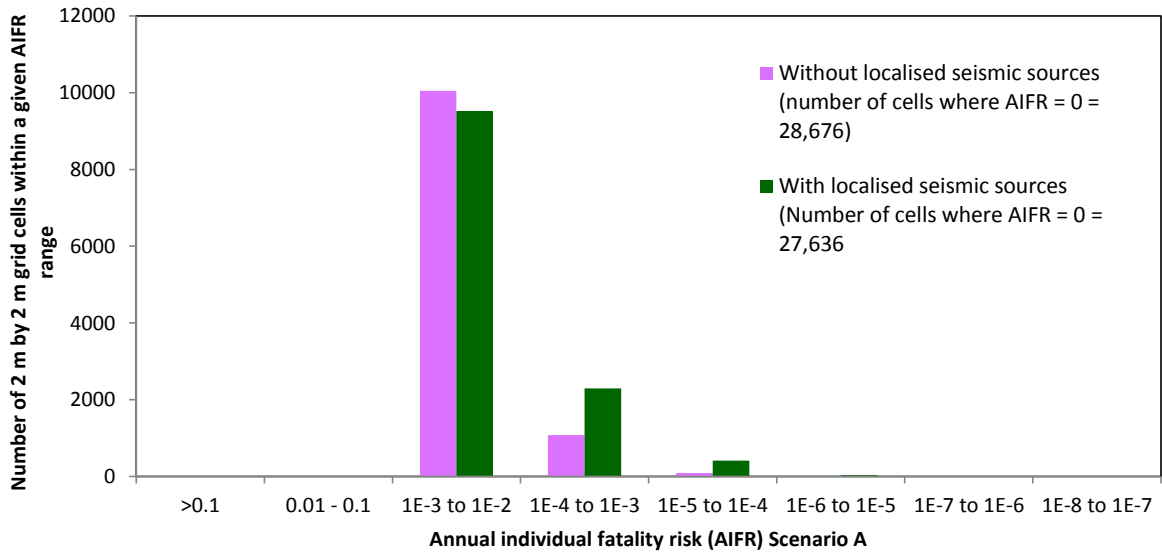


Figure 40 Results from the debris avalanche risk assessment per scenarios A, B and C (dwelling occupant).

5.2.3 Cliff-top recession

The area of cliff top lost per event was estimated using a 0.019 ratio of area lost to volume leaving the cliff face (from Massey et al., 2012a) (Tables 29 and 30).

Table 29 Area of cliff top lost per peak ground acceleration (PGA) band for upper, middle and lower volume estimates. Note only the first digit in the estimated area lost is significant, areas have been rounded to the nearest 10 m².

Area of cliff top lost (m ²)	PGA Band (g)						
	0.1–0.3	0.3–0.5	0.5–0.8	0.8–1.2	1.2–1.6	1.6–2.0	2.0–3
Distributed upper volume	170	150	260	420	620	930	1,880
Localised upper volume	0	220	390	630	930	1,130	1,130
Distributed middle volume	80	70	130	210	310	480	960
Localised middle volume	0	110	190	310	460	560	560
Distributed lower volume	30	30	50	90	130	170	250
Localised lower volume	0	40	80	130	190	260	380

Table 30 Volume of debris and area of cliff top lost per non-seismic band (based on historical rockfall rates in Massey et al., 2012a).

Time period (years)	Number of events in band	Annual frequency of events	Mean event volume (m ³)	Area lost (m ²)
1–15	5.5	0.37	5	0.1
15–100	1.3	0.0133	170	3
100–1,000	0.7	0.0007	1,500	30
1,000–10,000	0.3	0.00003	10,000	200

For distributed sources the proportion of land area lost at a given distance back from the cliff edge was estimated from the LiDAR change models. The method and results are detailed in Appendix 1 and in Massey et al. (2012a).

For local source areas 1–3 the land area lost at given distance back from the edge was estimated from the geometry of the potential source areas. To do this, the cliff top was considered as a series of 1 m by 1 m cells arranged parallel to the cliff edge. The numbers of 1 m cells within each source area – at 1 m intervals back from the current cliff edge – were counted, ensuring that for areas where different potential sources overlapped, the cells were only counted once. The annual individual fatality risk at given distances back from the cliff edge, for scenarios A–C, are shown in Figure 41. The position behind the cliff crest of the 10⁻⁴ risk contour changes between scenarios. As expected, the 10⁻⁴ contour for scenario A is the furthest back from the cliff edge (about 28 m) as this scenario comprises the upper volume estimates per assessed source, compared to scenario C (about 8 m).

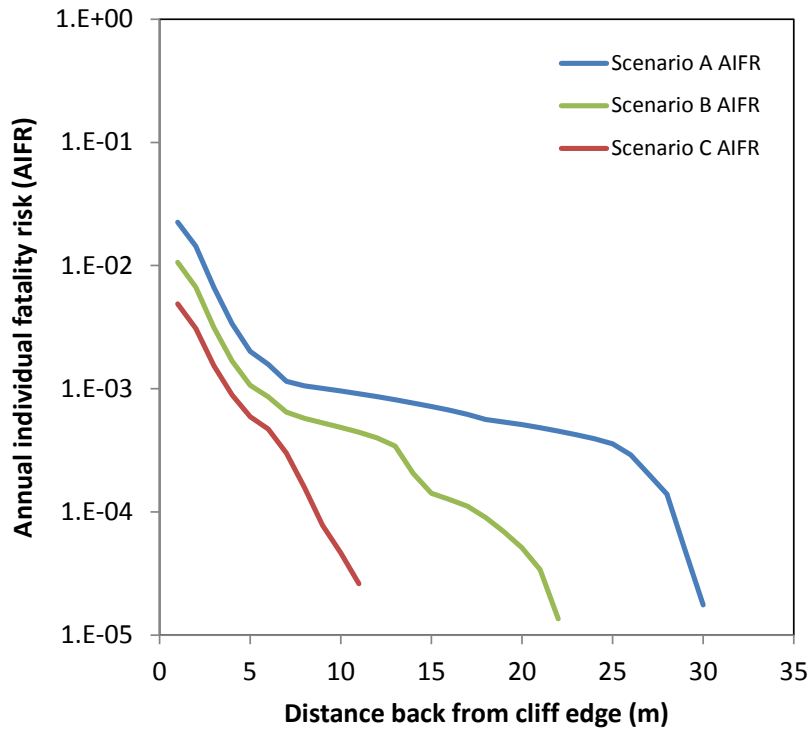


Figure 41 Results from the cliff top recession risk assessment, per scenarios A, B and C (dwelling occupant).

5.2.3.1 Slumping and cracking

The area of slope between the cliff-top recession risk zone and the mapped extent of cracking that was highlighted in the Stage 1 report as a Class I area, has now been re-assessed as being in a Class II area. A Class II area is defined in the Stage 1 report (Massey et al., 2013) as:

- Coherent slides and slumps of predominantly loess with associated cumulative inferred displacement of the mass of greater than 0.3 m, where dwellings and critical infrastructure is present within the moving mass. It is possible that renewed movement may severely impact critical infrastructure and dwellings. The level of disruption to critical infrastructure and dwellings is likely to be a function of where they are within the feature. The most hazardous places are the mainly extensional and compressional areas. Given the magnitudes of displacement it is unlikely that damage to dwellings would pose an immediate life risk to their occupants.

A 10 m wide area has been added to the inferred boundary of the Class II hazard exposure area, where the area of slumping and cracking could potentially in the future enlarge in an up-slope or lateral direction beyond the currently recognised boundary. This has been termed a “Class II relative hazard exposure 10 m enlargement area”.

5.3 ROAD USER RISK

The section of Main Road assessed for this report (Figure 42) is broadly similar in terms of traffic and usage to that below Quarry Road which was assessed by GNS Science in (Massey et al., 2014), although the length of road assessed in this report is shorter (81 m).

Individual road user risks per journey and per year are assessed using the same cellular grid as that used for dwellings. Previous assessments have found that the hazard of driving into or swerving to avoid debris contributes very little risk in comparison with that of being directly impacted by or inundated with debris. This assessment therefore considers only the “impacted/inundated by debris” hazard, and not the “drive into/swerve avoiding debris” hazard.

Risk assessments were carried adopting the scenarios A, B and C input parameters (as for the dwellings assessment), for the following road users:

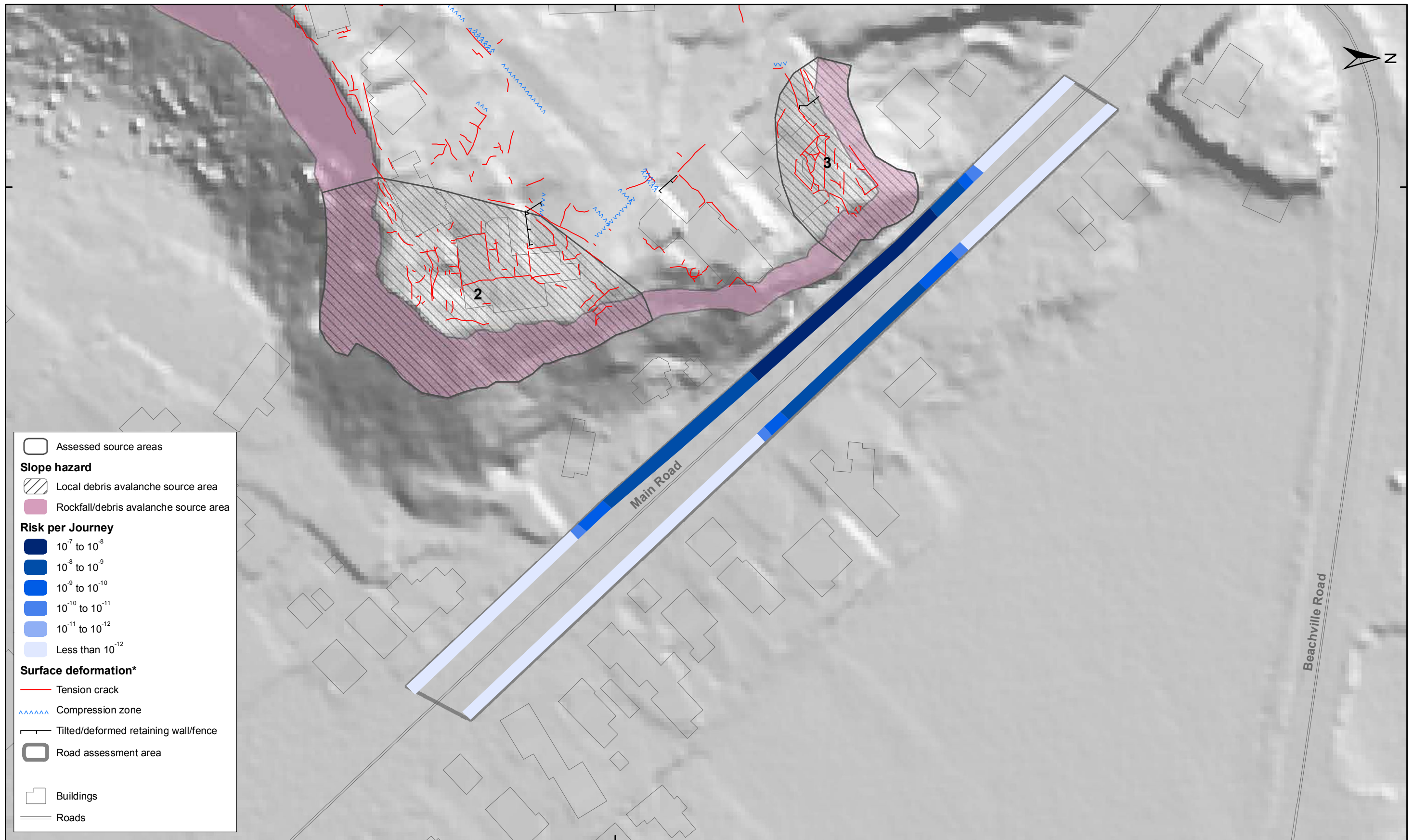
- Motor vehicle users (car, bus and truck occupants), and
- Vulnerable road users (motorcyclists, pedal cyclists and pedestrians).

The risk assessment methodology is described in Appendix 1.

Figure 42, Maps 1 and 2 show the risk per trip for a pedestrian along the outer and inner edge of Main Road from debris avalanches, for the upper and lower volume estimates respectively. Figure 43 and Figure 44 show the results in terms of risk per journey and risk per year for the middle debris volume estimate, in comparison with the average motor vehicle crash risk for an urban New Zealand road of the same length. Results show that:

1. The slope collapse risk on the NEAR (slope) side of the road is very much greater than the motor vehicle crash risk over the same length of road for all road users except motorcyclist, for whom it is comparable;
2. The slope collapse risk on the far (seaward, downhill) side of the road is virtually zero; and
3. The risk is greatest for the slowest moving road users (pedestrians), as it is they who spend most time at risk. However, it should be noted that this section of Main Road is currently closed to pedestrians.

Figure 45 and Figure 46 show the risk per journey for the lower and upper estimates of debris volume generated in seismic events (scenarios C and A respectively). The risk is acutely sensitive to debris volume on the low side, but less sensitive on the high side, because for several road cells the ‘middle’ debris volume estimates were already large enough to virtually assure death to someone present, so further rockfall makes little difference as a person can only be killed once. For the lower debris volume estimate (scenario C) there is virtually no risk contribution from rockfall, and motor vehicle crash risk outweighs rockfall risk for all road users except bus occupants – whose crash risk is relatively low.



5177200

SCALE BAR: 0 50 m

EXPLANATION:

* Taken from report CR2012/317

Background shade model derived from NZAM post earthquake 2011c (July 2011) LiDAR survey resampled to a 1 m ground resolution. Roads and building footprints provided by Christchurch City Council (20/02/2012). PROJECTION: New Zealand Transverse Mercator 2000

DRW:
DH, BL

CHK:
CM, FDP



ROAD USER RISK : PEDESTRIAN
Higher estimate

Redcliffs
Christchurch

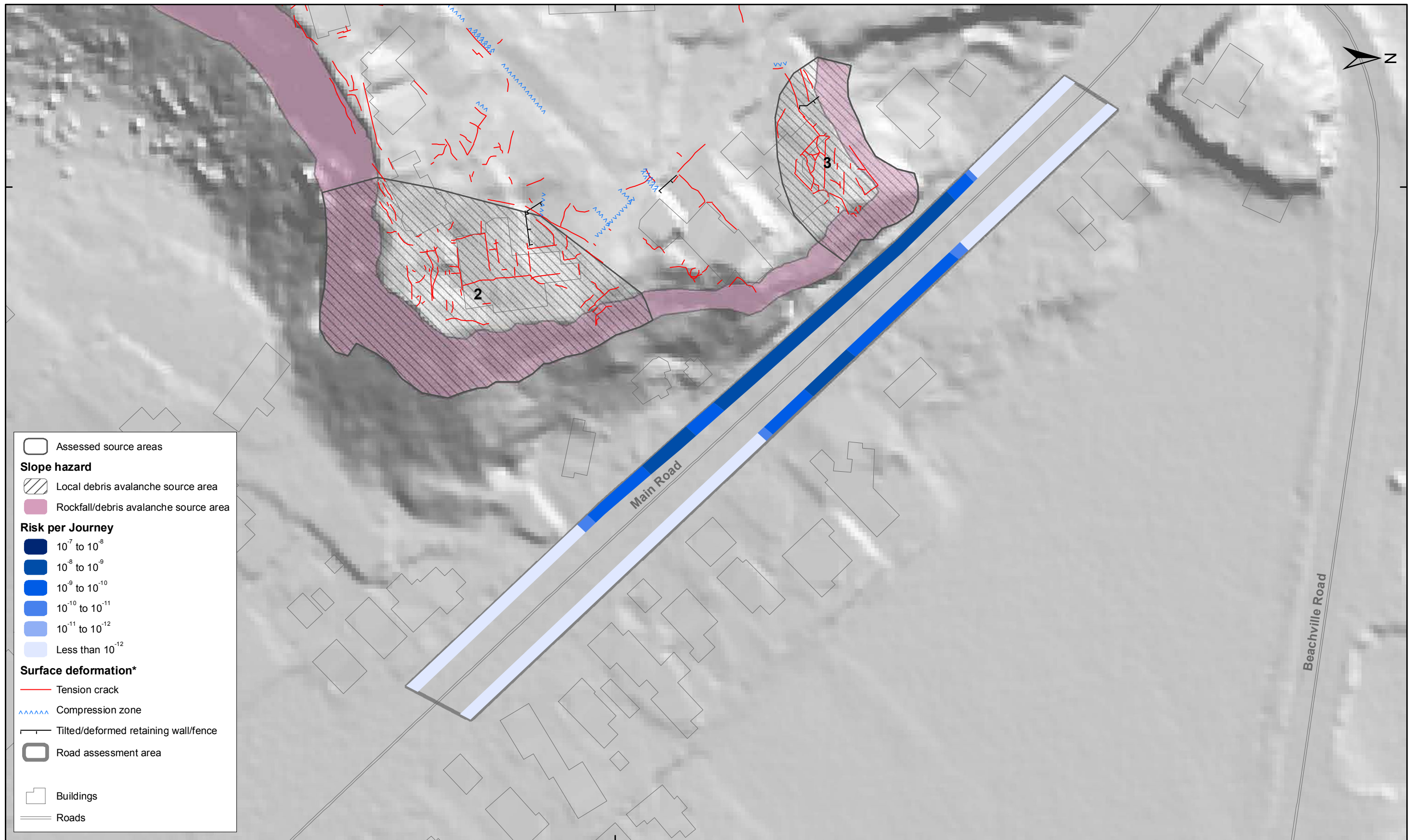
FIGURE 42

Map 1

FINAL

REPORT:
CR2014/78

DATE:
August 2014



5177200

SCALE BAR: 0 50 m

EXPLANATION:

* Taken from report CR2012/317

Background shade model derived from NZAM post earthquake 2011c (July 2011) LiDAR survey resampled to a 1 m ground resolution. Roads and building footprints provided by Christchurch City Council (20/02/2012). PROJECTION: New Zealand Transverse Mercator 2000

DRW:
DH, BL
CHK:
CM, FDP



ROAD USER RISK : PEDESTRIAN
Lower estimate

Redcliffs
Christchurch

FIGURE 42

Map 2

FINAL

REPORT: CR2014/78 DATE: August 2014

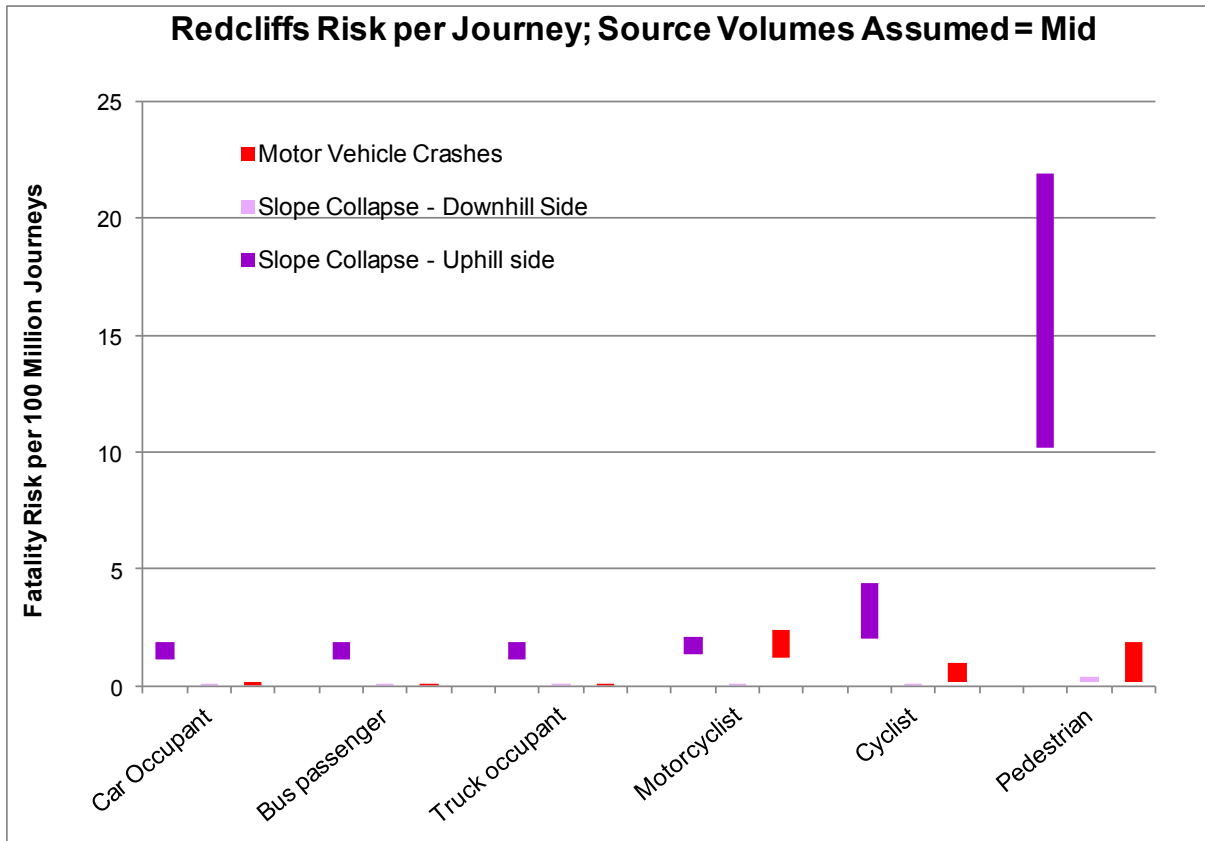


Figure 43 Road user risk per journey, central source volume estimates.

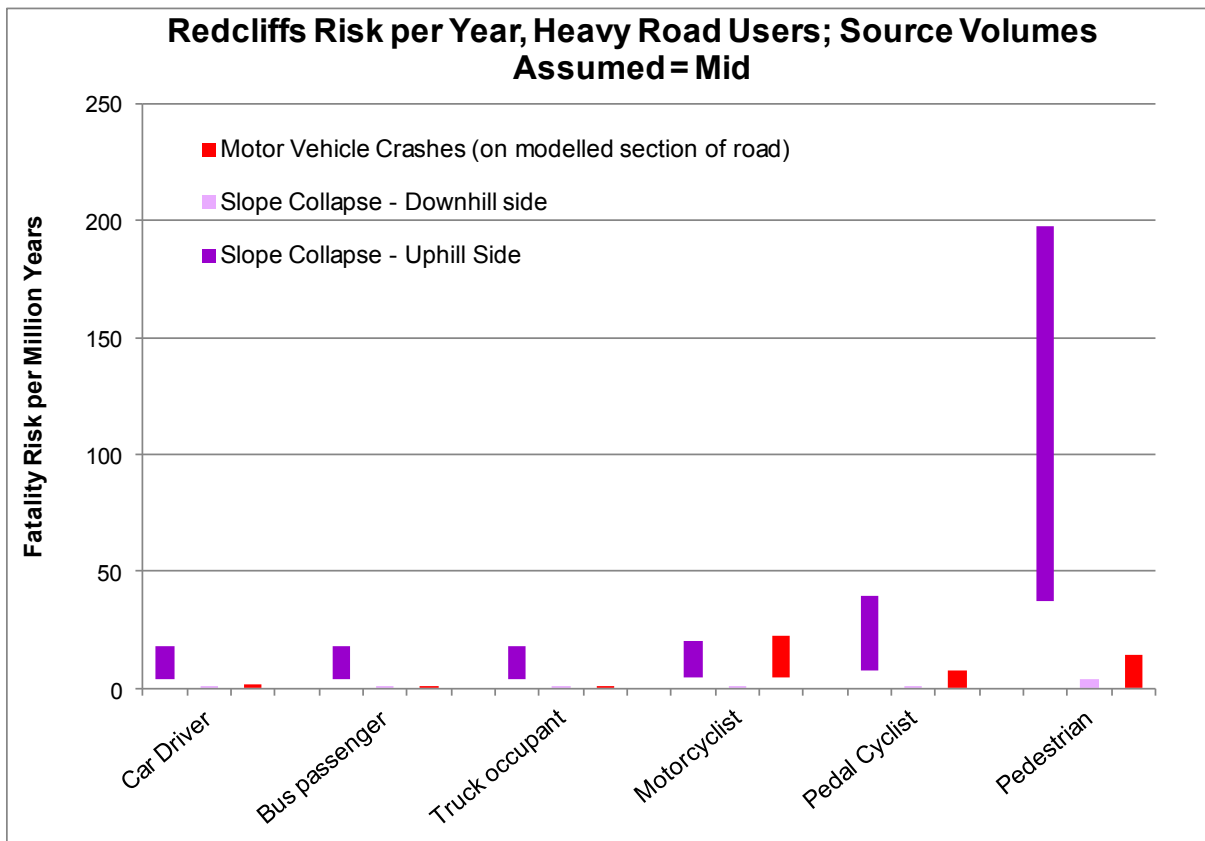


Figure 44 Road user annual fatality risk, central source volume estimates.

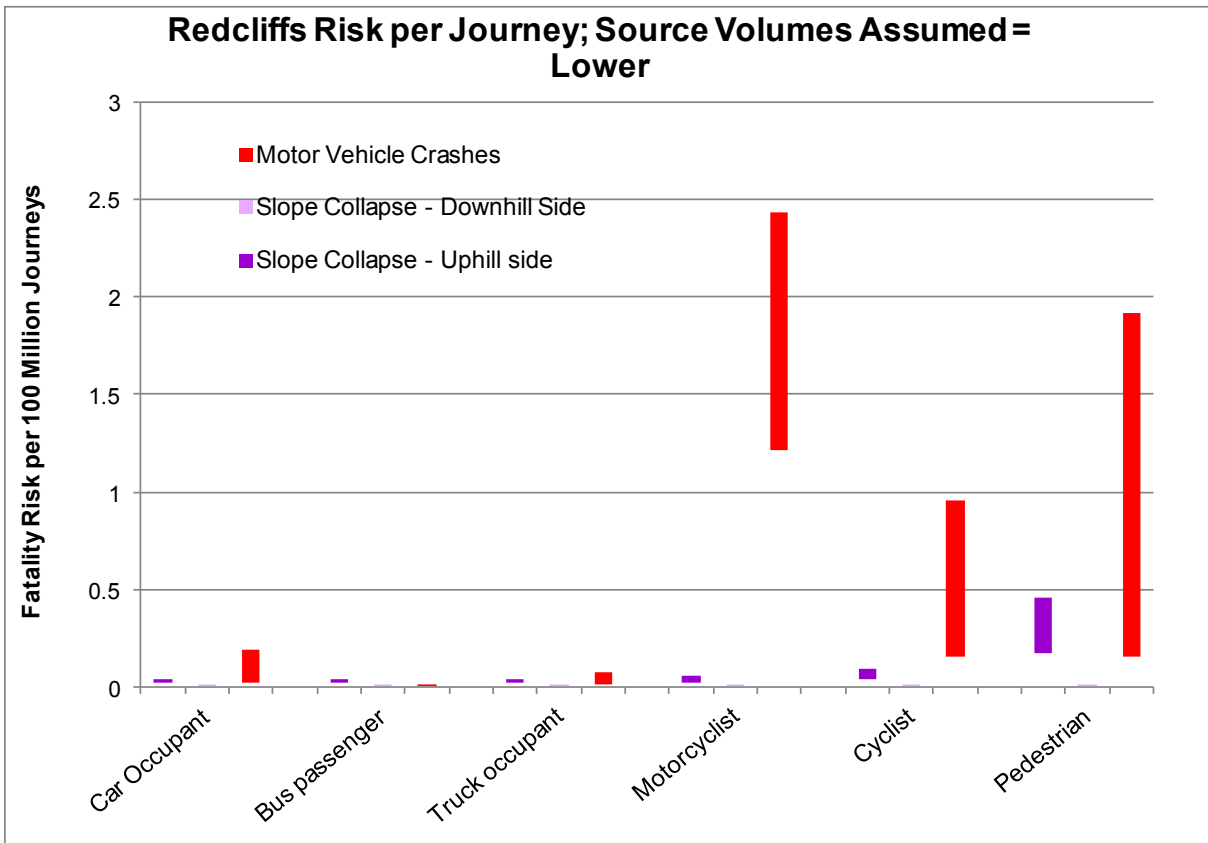


Figure 45 Risk per journey; lower assumed debris source volumes.

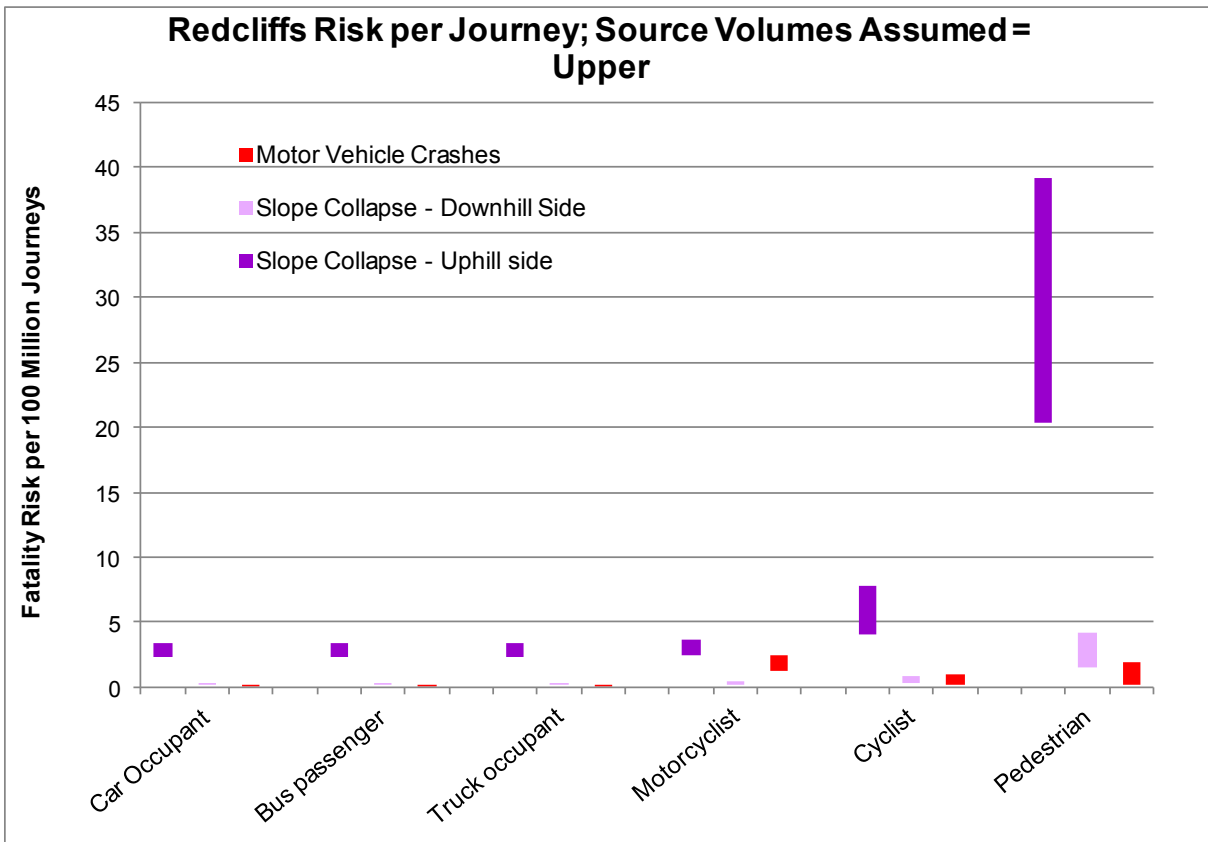


Figure 46 Risk per journey; upper assumed debris source volumes.

6.0 DISCUSSION

6.1 DWELLING OCCUPANT RISK

Important points of note from the results of the hazard and risk assessment undertaken in this study include:

1. Earthquake-triggered debris avalanches contribute most to the risk.
2. The inclusion of the assessed source areas 1–3 in the risk assessment increases the runout and hence the risk farther out from the toe of the slope, compared with the risk estimated assuming that the debris is randomly distributed across the slope. This can be seen in the risk estimates adopting scenario C input parameters (Figure 38, Map 3), which give the risk contours a more irregular shape.
3. For scenarios A and B (upper and middle volume and runout estimates), there is little difference between the risk estimates including the local source areas 1–3 (Figure 38, Map 2), and those without source areas 1–3 where the entire debris is distributed randomly across the slope (Figure 39). This is because the volume of debris and therefore risk is already high in these areas from distributed failures alone, and so the inclusion of additional debris from source areas 1–3 does not significantly increase the risk.
4. There is also little difference between the debris avalanche risk maps presented by Massey et al. (2012a) and the revised risk maps presented in this report. This indicates that the rapid, mainly empirically-based risk assessment, carried out soon after the 22 February and 13 June 2011 earthquakes, provided robust estimates of the risk that were “fit for purpose”.
5. The largest difference between the original risk estimates (Massey et al., 2012a) and those presented in this report is at the cliff crest. The inclusion of earthquake triggered source areas 1–3, increases the width of the cliff top recession risk zone.
6. The effects of source areas 1–3 on the cliff-top recession risk have been distributed across the entire cliff top and not just in the assessed source area locations; although this is the most likely location they could occur.

6.2 RISK TO THE ROAD USER

Important points of note from the risk assessment results for road users along Main Road at Redcliffs include:

1. The rockfall risk is greatest for the slowest road users (pedestrians, then cyclists), because their slower travel exposes them to risk for longer on each journey;
2. The rockfall risk is significantly higher on the portion of road closer to the slope (west) than on the opposite (east) side of the road; and
3. Within the range of estimated debris volumes (upper, middle and lower), the risk from debris avalanches ranges from being comparable with or smaller than the risk of “ordinary” road accidents, for the lower debris volume estimates, to substantially larger than the risk of “ordinary” road accidents for most road users.

Based on middle debris volume estimates, individual risk to road users of Main Road at Redcliffs, for the section of road assessed, is among the highest per journey assessed for Port Hills roads and comparable to the road risks assessed for the Deans Head mass movement. This is because of the potential for even a relatively frequent event, such as a Band 1 (0.1–0.3 g; Table 27) earthquake, to generate sufficient rockfall volume to cause a high risk of death for any road user present on the near side of the road at the time of the event. This high risk is because this part of the road is at the very bottom of the steep rock slope, within a fahrboeschung angle of about 60°.

The rockfall risk is about zero on the far side of the road, and nearly zero using the lower debris volume estimates modelled in this assessment.

Inclusion or exclusion of localised debris specific sources makes little difference to the results for road users. The risk is dominated by the contribution from earthquakes in Bands 1 and 2 (Table 27). Even the smallest earthquake band considered generates sufficient rockfall volume reaching the near side of the road (under the middle debris volume scenario) to give a high risk of death to any road user present in this section of road when such an event occurs.

6.3 RISK ASSESSMENT SENSITIVITY TO UNCERTAINTIES

In this section the sensitivity of the risk model to key uncertainties and reliability of the assessments are identified. The three sets of assumptions (used for scenarios A–C) are discussed, along with other variations in the input parameters not included in scenarios A–C.

The sensitivity of the estimated risk has been assessed to changes in the following:

6.3.1 Debris volumes

Volumes of debris triggered by the representative events for both seismic and non-seismic triggers:

- a. For seismically-triggered debris avalanches three volume ranges have been used to account for any uncertainty in the relationship between peak ground acceleration and volume leaving the slope.
- b. For non-seismically-triggered debris avalanche volumes a scale factor of two has been used to allow for a possible increased “long-term” rate of debris avalanches due to the now-dilated and highly disturbed nature of the cliffs.

6.3.2 Area of cliff-top lost

Area of cliff top lost as a result of the occurrence of the representative event for both earthquake and non-seismic triggers:

- a. For earthquake triggered recession, the variable debris volume estimates take into account the uncertainty in the relationship between peak ground acceleration and volume leaving the slope and the ratio of volume to cliff top area lost.
- b. For non-seismically triggered recession the scale factor (of two on the annual debris production rate) considers the likely “long-term” increased rates of cliff collapse due to the now dilated and highly disturbed nature of the cliffs.

- c. The relationship between the volume leaving the cliffs and the area of cliff top lost is varied from a ratio of 0.019 to a ratio of 0.025, i.e., for 100 m³ of debris leaving the cliff face the area lost would increase from 1.9 to 2.5 m².

6.3.3 Debris runout

Volume of debris passing a given distance down the slope:

- a. For randomly distributed failures the variation in the relationship between the volume passing a given fahrboeschung angle has been used.
- b. For earthquake triggered local debris avalanches the volume of material passing a given distance – estimated using the RAMMS model – has been assessed using different source volumes in the model (upper, middle and lower volume estimates).

The results (Figure 38) show that the largest impact on the risk is from the uncertainty in the volumes of material that could be generated at different bands of peak ground acceleration.

There are approximately two orders of magnitude difference (a factor of 100 times) in the risk between scenarios A and C, for the same location in the more distal areas of the debris runout zone (Figure 38, Maps 1 and 3). The risk in the zones closest to the slope toe does not change much between the scenarios.

Based on the results of the two-dimensional rockfall modelling (Appendix 9), it is possible that individual boulders (rockfalls) could exceed the runout limits of the empirical and numerical RAMMS models used to estimate the risk from debris avalanches in the study area. However, it is not possible to quantify the risk in these distal areas as there is no precedent on which to base them, indicating that although boulders could runout to fahrboeschung angles of 30° (cross-section 6), the likelihood of them doing so is relatively low (as demonstrated by the past runout of debris at the site).

6.3.4 Other sensitivities and uncertainties

Another impact on the risk is from the National Seismic Hazard Model. The annual frequency of a debris avalanche-triggering earthquake occurring is much higher in the next few years, and will decrease over the next decade. The time-varying nature of the seismic hazard has been considered by comparing the differences in risk associated with the year 2016- and 50-year seismic hazard model results (50-years being consistent with the design life used in typical seismic hazard analysis for residential building construction).

The risk estimates reduce by a factor of between two and three – for the same location in the more distal ends of the debris runout zone – when adopting the 50-year average annual frequencies compared to the year 2016 annual frequencies. There is little difference to the risk closer towards the slope toe.

6.3.5 How reliable are the results?

Potentially significant uncertainties noted and their likely implications for risk are summarised in Table 31.

Table 31 Uncertainties and their implications for risk.

Issue	Direction and scale of uncertainty	Implications for risk
a. Under-prediction of annual frequency for a given peak ground acceleration by the composite seismic hazard model.	Increasing, potentially considerable – but geomorphological evidence in the Port Hills suggests there is a sensible cap that can be placed on the upward uncertainty, which is about an order of magnitude.	Risk due to earthquakes could be systematically under- or over-estimated.
b. Choice of whether to use average earthquake annual frequencies for next 50-years, or higher frequencies (year 2016).	Moderate uncertainty between the use of the year 2016 and 50-year average annual frequencies. Refer to Massey et al. (2012a) for details. The magnitude of uncertainty depends on the location of the dwelling within the risk zones. The distal ends are more uncertain than the zones closer to the toe of the slope.	Longer term risk is potentially 5 times lower in the distal runout zone.
c. Volume of debris produced in each peak ground acceleration band, upper, middle and lower debris volume estimates.	Largest uncertainty in either direction, especially between the lower (scenario C) and upper (scenario A) debris volume estimates.	There are two orders of magnitude uncertainty (factor of 100) between the risk estimates from the lower and upper debris volumes
d. Volume of debris produced by other (non-seismic) events.	Large uncertainty either way in the annual frequency, but constrained by the geomorphology suggesting such extreme events (that dominate the risk) are at the medium and low frequency end. However, current frequency of debris production is higher due to the disturbed nature of the rock masses. It may take many years for the frequency to drop back to pre-earthquake rates.	Factor of 2 to 5 uncertainty in the upward direction between current rates of rockfall and the assumed longer term historical rates.
e. Ratio between the volume leaving the face and area of cliff top recessing.	Moderate uncertainty either way. However, ratios may increase as the rock mass become more disturbed as the earthquakes continue.	Factor of about 1.2 uncertainty in the upward direction, but lower in the downward direction.
f. Volume of debris travelling downslope and the number of boulders per m ³ of debris.	Quite well constrained and could be considerable but linked to the total volume of material leaving the slope.	Factor of about 1.4 uncertainty in the upward direction, but lower in the downward direction.
g. Occupancy (proportion of time people are at home)	Assumption of 100% occupancy instead of 67% would modestly increase the estimated risk.	Would increase by a factor of about 1.4.
h. Probability person killed if struck by debris.	Uncertainty potentially reducible but unlikely to make large difference – will always be fairly large given the volumes of debris involved or height of fall.	A change in the vulnerability from 70 to 100% would increase the risk by a factor of about 1.8.

7.0 CONCLUSIONS

With reference to the assessment area boundary as shown in Figure 2, the conclusions of this report are:

7.1 HAZARD

1. The strength of the rock mass forming the slope at Redcliffs has been reduced by earthquake-induced fractures and movement and it will continue to weaken over time due to factors such as physical and chemical weathering, wetting and drying and further ground movement. Failures, of volumes of rock greater than those that failed during the 2010/11 Canterbury earthquakes, from the cliff are now more likely to be triggered by future earthquakes or by non-earthquake triggers such as rain. Failure volumes triggered by earthquakes may now be larger than any that fell during the 2010/11 Canterbury earthquakes; they could be more similar in size to past failures (from the same slope) identified from pre-1940 aerial photographs and pre-2010/11 earthquakes slope geometry.
2. Revised debris-avalanche dwelling risk maps (revised from those by Massey et al., 2012a) – incorporating local larger source volumes, and both physically and empirically based debris runout models – have little effect on the original risk estimates.

7.2 Risk

7.2.1 Dwelling occupant

1. There are very few additional dwellings in the debris avalanche or cliff recession zones that do not already have “red zone” offers made by the Canterbury Earthquake Recovery Authority and based on the previously assessed cliff-collapse risk.
2. Earthquake-triggered cliff collapses contribute most to the risk.
3. The results show that the most critical uncertainty in the risk assessment is the volumes of material that could be generated at different bands of peak ground acceleration. There is approximately two orders of magnitude difference (a factor of 100 times) in the risk estimates between the upper and lower failure volume estimates (scenarios A and C respectively).
4. The inclusion of the assessed source areas 1–3 in the risk assessment increases the runout and hence the risk further out from the toe of the slope. However, there is little difference between the risk estimates including the local source areas 1–3 and those where the entire debris is distributed randomly across the slope. This is because the volume of debris and therefore risk is already high in these areas from distributed failures alone, and so the inclusion of additional debris from source areas 1–3 does not significantly increase the area where people are exposed to high levels of risk.
5. The largest difference between the original risk estimates (Massey et al., 2012a) and those presented in this report is at the cliff crest. The inclusion of earthquake triggered source areas 1-3, increases the width of the cliff top recession risk zone because the annual individual fatality risk bands have widened.

7.2.2 Road user

1. The rockfall risk is greatest for the slowest road users (pedestrians, then cyclists), because their slower travel exposes them to risk for longer on each journey.
 - a. The rockfall risk is significantly higher on the side nearest the slope than on the opposite side of the road.
 - b. Based on middle debris volume estimates, individual risk to road users of Main Road at Redcliffs, for the section of road assessed, is among the highest per journey assessed for Port Hills roads, and comparable to the road risks assessed for the Deans Head mass movement.
 - c. The rockfall risk falls to virtually zero on the far side of the road, and to virtually zero using the lower debris volume estimates modelled in this assessment.
2. The most pressing issue appears to relate to the section of Main Road within the risk zone. This section of Main Road currently has containers placed along the inside of the road, nearest the slope, to protect road users from falling debris. These measures are temporary. The footpath along this section of road is also closed.

8.0 RECOMMENDATIONS

GNS Science recommends that based on the results of this study, Christchurch City Council:

8.1 POLICY AND PLANNING

1. Decide what levels of life risk to dwelling occupants and road users will be regarded as tolerable.
2. Decide how Council will manage risk on land where life risk is assessed to be at the defined threshold of intolerable risk and where the level of risk is greater than the threshold.
3. Prepare policies and other planning provisions to address risk lesser than the intolerable threshold in the higher risk range of tolerable risk.

8.2 SHORT-TERM ACTIONS

8.2.1 Hazard monitoring strategy

1. Include the report findings in a slope stability monitoring strategy with clearly stated aims and objectives, and list how these would be achieved, aligning with the procedures described by McSaveney et al. (2014). In the meantime, extend the current survey network (by increasing the number of slope monitoring marks) further up the slope (particularly into source area 1), so as to maintain awareness of the behaviour of the slope.
2. Ensure that the emergency management response plan for the area identifies the dwellings that could be affected by movement and runout, and outlines a process to manage a response.

8.2.2 Monitoring alerts and early warning

Recognise the fact that monitoring alerts for slope deformation and groundwater changes cannot be relied upon to provide adequate early warning as experience from Port Hills and elsewhere shows that deformation and groundwater changes can occur rapidly, with little warning.

8.2.3 Surface/subsurface water control

Reduce water ingress into the slopes, where safe and practicable to do so, by:

- a. Identifying and relocating all water-reticulation services (water mains, sewer pipes and storm water) inside the identified mass-movement boundaries (at the slope crest) to locations outside the boundary, in order to control water infiltration into the slope. In particular, a storm water main currently traverses the crest of source area 1; and
- b. Filling the accessible cracks on the slope and providing an impermeable surface cover to minimise water ingress.
- c. Control surface water flow and direct away from mass movement area and into the appropriate storm water system.

8.2.4 Pavement closure

1. Maintain the closure of the pavement on the slope-side of the road, and continue to divert pedestrians onto the footpath on the seaward side of the road.
2. It is not known how effective the current temporary containers would be if impacted by a sizable debris avalanche (as per those discussed in this report). The effectiveness of such temporary risk management measures should be reassessed to ensure they are “fit-for-purpose”.

8.3 LONG-TERM ACTIONS

8.3.1 Engineering measures

1. There appears to be reasonable scope to realign the at-risk section of Main Road further away from the bottom of the slope, outside the debris avalanche risk zone.
2. For the section of Main Road within the risk zone, liaise with whoever is responsible for roading in this area to ensure that the debris avalanche risk is fully taken into account in any road design (or in the design of modifications to the road).

8.3.2 Reassessment

Reassess the risk and revise and update the findings of this report in a timely fashion, for example:

- a. in the event of any changes in ground conditions; or
- b. in anticipation of further development or land use decisions.

9.0 REFERENCES

- Abramson, L.W., Thomas, L.S., Sharma, S., Glenn, M.B. 2002. Slope stability and stabilisation methods. 2nd Edition. John Wiley and Sons Inc.
- Andres, N. 2010. Unsicherheiten von Digitalen Geländemodellen und deren Auswirkungen auf die Berechnung von Gletscherseeausbrüchen mit RAMMS (Dr. R. Purves, D. Schneider, Dr. C. Huggel).
- Ashford, S.A., Sitar, N. 2002. Simplified method for evaluating seismic stability of steep slopes. *Journal of Geotechnical and Geoenvironmental Engineering* 128: 119–128.
- Australian Geomechanics Society 2007. Practice note guidelines for landslide risk management. *Journal and news of the Australian Geomechanics Society* 42(1): 63–114.
- Barlow B., Niemirska M., Gandhi, R.P. 1983. Ten years of experience with falls from a height in children. *Journal of Paediatric Surgery* 18: 509–511.
- Bell, D. 1992. Rockfall protection measures for 44 Raekura Place. University of Canterbury, Canterbury Report. 1st November 2011.
- Bell, D.H., Glassey, P.J., Yetton, M.D. 1986. Chemical stabilisation of dispersive loessical soils, Banks Peninsula, Canterbury, New Zealand. *Proceedings of the 5th International Congress of the International Engineering Geological Society* 1: 2193–2208
- Bell, D.H., Trangmar, B.B. 1987. Regolith materials and erosion processes on the Port Hills, Christchurch, New Zealand. *Fifth International Symposium and Field Workshop on Landslides. Lausanne, A.A. Balkema. Volume 1: 77–83.*
- Bray, J.D., Rathje, E.M. 1998. Earthquake-induced displacements of solid-waste landfills. *Journal of Geotechnical and Geoenvironmental Engineering* 124: 242–253.
- Bray, J. D., Travasarou, T. 2007. Simplified procedure for estimating earthquake-induced deviatoric slope displacements. *Journal of Geotechnical Engineering and Environmental Engineering*. DOI: 10.1061/(ASCE)1090-0241(2007)133:4(381).
- California, State of, 1977. "Analysis and Mitigation of Earthquake-Induced Landslide Hazards," Guidelines for Evaluation and Mitigation of Seismic Hazards in California, Division of Mines and Geology, California Department of Conservation Special Publication 117, Chapter 5, 15 pp.
- Carey, J., Misra, S., Bruce, Z., Barker, P. 2014. Canterbury Earthquakes 2010/11 Port Hills Slope Stability: Laboratory testing factual report. GNS Science Consultancy Report CR2014/53.
- Choi, W.K. 2008. Dynamic properties of Ash-Flow Tuffs. PhD Thesis, The University of Texas at Austin.
- Chopra, A.K. 1966. Earthquake effects on dams. PhD Thesis, University of California, Berkeley.
- Clarke, M. 2012. Seismic refraction survey in the Port Hills of Christchurch, New Zealand. Victoria University post-graduate thesis.
- Codd, J., Revell, T. 2013. Project: Deans Head ground investigation report. Aurecon New Zealand Ltd. 2 September 2013. Document ID: 218782-011-05-01.
- Corominas J. 1996. The angle of reach as a mobility index for small and large landslides. *Canadian Geotechnical Journal* 33: 260–271.

- Corominas, J., Copons, R., Moya, J., Vilaplana, J. M., Altimir, J., Amigo, J. 2005. Quantitative assessment of the residual risk in a rockfall protected area. *Landslides* 2: 343–357. DOI:10.1007/s10346-005-0022-z.
- Craig, R.F. 1997. *Craig's Soil Mechanics*, 6th Edition, Spon Press, London.
- Cruden, D.M., Varnes, D.J. 1996. Landslide types and processes. *Landslide: investigation and mitigation*. Turner, K.A.; Schuster, R.L. (eds.). Special report, Transportation Research Board, National Research Council 247, Chapter 3, pp. 36–75.
- Dawson, E.M., Roth, W.H., Drescher, A. 1999. Slope stability analysis of by strength reduction. *Geotechnique* 122(6): 835–840.
- Du, J., Yin, K., Nadim, F., Lacaqsse, S. 2013. Quantitative vulnerability estimation for individual landslides. *Proceedings of the 18th International Conference on Soil Mechanics and Geotechnical Engineering, Paris 2013*. pp. 2181–2184.
- Eurocode 8. EN1998-5. 2004. Design of structures for earthquake resistance Part 5: Foundations, retaining structures and geotechnical aspects.
- Finlay, P.J., Mostyn, G.R., Fell, R. 1999. Landslides: Prediction of Travel Distance and Guidelines for Vulnerability of Persons. *Proceedings of the 8th Australia New Zealand Conference on Geomechanics, Hobart*. Australian Geomechanics Society, ISBN 1 86445 0029, Vol 1, pp.105–113.
- Geotechnics Ltd. 2014. GNS Science, Port Hills Inclinometers, Christchurch. Job No. 720085.001/REP.
- Gerstenberger, M., Cubrinovski, M., McVerry, G., Stirling, M., Rhoades, D., Bradley, B., Langridge, R., Webb, T., Peng, B., Pettinga, J., Berryman, K., Brackley, H. 2011. Probabilistic assessment of liquefaction potential for Christchurch in the next 50 years. *GNS Science Report 2011/15*.
- Goldwater, S. 1990. Slope Failure in Loess. A detailed Investigation, Allendale, Banks Peninsula. MSc Thesis, University of Canterbury.
- Griffiths, G., Pearson, C., McKerchar, A.I. 2009. Review of the frequency of high intensity rainfalls in Christchurch. NIWA Client Report: CHC2009-139 for Christchurch City Council. 26 pp.
- Hoek, E. 1999. Putting Numbers to Geology – an Engineer's Viewpoint. The Second Glossop Lecture, *Quarterly Journal of Engineering Geology* 32(1): 1–19.
- Holden, C., Kaiser, A., Massey, C. I. 2014. Broadband ground motion modelling of the largest M5.9+ aftershocks of the Canterbury 2010-2011 earthquake sequence for seismic slope response studies. *GNS Science Report 2014/13*.
- Hynes-Griffin, M.E., Franklin, A.G. 1984. Rationalizing the seismic coefficient method. *Miscellaneous Paper No. G.L. 84-13*, U.S. Army Engineer Waterways Experiment Station, Vicksburg, Mississippi.
- Ishibashi, I., Zhang, X. 1993. Unified dynamic shear moduli and damping ratios of sand and clay. *Soils and Foundations* 3(1): 182–191.
- Jibson, R.W. 2007. Regression models for estimating coseismic landslide displacement. *Engineering Geology* 91: 209–218.
- Jibson, R.W., Keefer, D.K. 1993. Analysis of the seismic origin of landslides: Examples from the New Madrid Seismic Zone. *Geological Society of America Bulletin* 21: 521–536.
- Keefer, D.K., Wilson, R.C. 1989. Predicting earthquake-induced landslides, with emphasis on arid and semi-arid environments. *Proceedings of Landslides in a Semi-Arid Environment, Vol. 2*, Inland Geological Society, Riverside, California, pp. 118–149.

- Keylock, D., Domaas, U. 1999. Evaluation of topographic models of rockfall travel distance for use in hazard applications. *Antarctic and Alpine Research* 31(3): 312–320.
- Kramer, S.L. 1996. *Geotechnical earthquake engineering*. Prentice Hall, Upper Saddle River, New Jersey.
- Makdisi, F.I., Seed, H.B. 1978. Simplified procedure for evaluating embankment response. *Journal of Geotechnical Engineering Division*. American Society of Civil Engineers 105(GT12): 1427–1434.
- Massey, C., Della Pasqua, F. 2013. Canterbury Earthquakes 2010/11 Port Hills Slope Stability: Working Note 2013/06 on the interim findings from investigations into the Redcliffs mass movement. GNS Science Letter Report 2013/304LR.
- Massey, C.I., McSaveney, M.J., Yetton, M.D., Heron, D., Lukovic, B., Bruce, Z.R.V. 2012a. Canterbury Earthquakes 2010/11 Port Hills Slope Stability: Pilot study for assessing life-safety risk from cliff collapse. GNS Science Consultancy Report 2012/57.
- Massey, C.I., Gerstenberger, M., McVerry, G., Litchfield, N. 2012b. Canterbury Earthquakes 2010/11 Port Hills Slope Stability: Additional assessment of the life-safety risk from rockfalls (boulder rolls). GNS Science Consultancy Report 2012/214.
- Massey, C.I., Yetton, M.J., Carey, J., Lukovic, B., Litchfield, N., Ries, W., McVerry, G. 2013. Canterbury Earthquakes 2010/11 Port Hills Slope Stability: Stage 1 report on the findings from investigations into areas of significant ground damage (assessed source areas). GNS Science Consultancy Report 2012/317.
- Massey, C.I., Della Pasqua, F., Taig, T., Lukovic, B., Ries, W., Heron, D. 2014. Canterbury Earthquakes 2010/11 Port Hills Slope Stability: Debris avalanche risk assessment for Deans Head. GNS Science Consultancy Report 2014/77.
- McDowell, B.J. 1989. Site investigations for residential development on the Port Hills, Christchurch. MSc Thesis, University of Canterbury.
- McFadgen, B.G., Goff, J.R. 2005. An earth systems approach to understanding the tectonic and cultural landscapes of linked marine embayments: Avon-Heathcote Estuary (Ihutai) and Lake Ellesmere (Waihora), New Zealand. *Journal of Quaternary Science* 20(3): 227–237.
- McSaveney, M.J., Litchfield, N., Macfarlane, D. 2014. Canterbury Earthquakes 2010/11 Port Hills Slope Stability: Criteria and procedures for responding to landslides in the Port Hills. GNS Science Consultancy Report 2013/171.
- Moon, A.T., Wilson, R.A., Flentje, P. 2005. Developing and using landslide size frequency models. <http://ro.uow.edu.au/engpapers/384>.
- Morgenstern, N.R., Price, V.E. 1965. The analysis of the stability of general slip surface. *Geotechnique* XV(1): 79-93.
- Newmark, N. 1965. Effects of earthquakes on dams and embankments. *Geotechnique* 15: 139–160.
- New Zealand Geotechnical Society 2005. Field description of soil and rock. Guideline for the field classification and description of soil and rock for engineering purposes.
- New Zealand Ministry of Transport (NZ MoT), 2012. Motor Vehicle Crashes in New Zealand 2012, NZ Ministry of Transport (and counterpart reports for 2011 and 2010).
- New Zealand Transport Agency (NZTA), 2013. Bridge manual (SP/M/022). 3rd edition. July 2013.
- Pletz, Z., Revell, T. 2013. Project: Moa Bone Point, ground investigation report. Aurecon New Zealand Ltd. Revision 2. 10 September 2013. Document ID: 218782-011-06-01.

- RAMMS 2011. A modelling system for debris flows in research and practice. User manual v1.4 Debris Flow. WSL Institute for Snow and Avalanche research SLF.
- Schanbel, P.B., Lysmer, J. Seed, H.B. 1972. SHAKE; a computer program for earthquake response analysis of horizontally layered sites. Report No. EERC 72-12, University of California, Berkeley.
- Slope Indicator 2005. Digitilt inclinometer probe. Data sheet. Geo Slope Indicator. <http://www.slopeindicator.com/pdf/digitilt-vertical-inclinometer-probe-datasheet.pdf>
- Slope/W 2012. Stability modelling with Slope/W. An engineering methodology. November 2012 Edition. GEO-SLOPE International Ltd.
- Southern Geophysical Ltd., 2013. Geophysical investigation: Borehole shear-wave testing, Port Hills, Christchurch. Southern Geophysical Ltd. Report for GNS Science.
- Stirling, M., McVerry, G., Gerstenberger, M., Litchfield, N., Van Dissen, R., Berryman, K., Barnes, P., Wallace, L., Bradley, B., Villamor, P., Langridge, R., Lamarche, G., Nodder, S., Reyners, M., Rhoades, D., Smith, W., Nicol, A., Pettinga, J., Clark, K., Jacobs, K. 2012. National Seismic Hazard Model for New Zealand: 2010 Update. Bulletin of the Seismological Society of America 102: 1514–1542.
- Tonkin and Taylor 2012a. Christchurch Earthquake Recovery Geotechnical Factual Report Balmoral / Glendevore. Report prepared for the Earthquake Commission. Ref 52010.0400
- Tonkin and Taylor 2012b. Christchurch Earthquake Recovery Geotechnical Factual Report Kinsey / Clifton. Report prepared for the Earthquake Commission. Ref 52010.0400.
- Trotter, M.M. 1975. Archeological investigations at Redcliffs, Canterbury, New Zealand. Records of the Canterbury Museum 9: 189–220.
- Wartman, J., Dunham, L., Tiwari, B., Pardel, D. 2013. Landslides in eastern Honshu induced by the 2011 Tohoku Earthquake. Bulletin of the Seismological Society of America 103: 1503–1521, doi: 10.1785/0120120128.
- Wieczorek, G.F., Wilson, R.C., Harp, E.L. 1985. Map showing slope stability during earthquakes in San Mateo County, California. Miscellaneous Investigations Map I-1257-E, U.S. Geological Survey.
- Woelz, S. 2012. Refraction seismic survey, Christchurch, January 2012. Preliminary results. Victoria University of Wellington.
- Yetton, M.D. 1992. Engineering Geological and geotechnical factors affecting development on Banks Peninsula and surrounding areas – Field guide. Bell, D.H. (ed.): Landslides - Proceedings of the Sixth International Symposium, Christchurch, 10-14 February 1992, Rotterdam, A.A. Balkema, Vol. 2(3).

10.0 ACKNOWLEDGEMENTS

GNS Science acknowledges: Mark Yetton (Geotech Consulting Ltd.) for advice during the assessment and Jon Carey (GNS Science) for carrying out some of the field mapping of the site. The authors also thank Nicola Litchfield, Jon Carey, Danielle Mieler, and Rob Buxton (GNS Science) for reviewing this report; and Dr Laurie Richards and Dr Joseph Wartman for their independent reviews.

APPENDICES

A1 APPENDIX 1: METHODS OF ASSESSMENT

A1.1 HAZARD ASSESSMENT METHOD

A1.1.1 Slope stability modelling

The purpose of the stability assessment was to determine the likelihood of cliff collapse of assessed source areas 1–3, under both static (non-earthquake) and dynamic (earthquake) conditions.

The key output from the static stability assessment is a factor of safety of the given source area and associated volume, while the key output from the dynamic assessment is the magnitude of permanent slope displacement of the given source area expected at given levels of earthquake-induced ground acceleration. These two assessments are then used to determine: 1) the likely local source volumes of material that could be generated under the different conditions; and 2) probability that they will be generated in an earthquake event.

A1.1.1.1 Static slope stability

If a slope has a static factor of safety of 1.0 or less, the slope is assessed as being unstable. Slopes with structures designed for civil engineering purposes are typically designed to achieve a long-term factor of safety of at least 1.5 under drained conditions, as set out in the New Zealand Transport Agency (NZTA) 3rd edition of the bridge manual (NZTA, 2013).

Static assessment of the slope was carried out by limit equilibrium method using the Rocscience SLIDE[®] software and the general limit equilibrium method (Morgenstern and Price, 1965). The failure surfaces were defined using the path search feature in the SLIDE[®] software, and a zone of tension cracks was modelled corresponding to mapped crack locations on the surface and in exposures. For the assessment, tension cracks depths were defined: 1) based on the relationship of Craig (1997), where the depth of tensions cracks was determined by the software in order to satisfy the thrust line verification method in the numerical model; and 2) based on field observations of cracks, where the tension cracks were thought to extend from the surface, downwards through the upper basalt lava breccia and into the underlying basalt lava.

Models were run based on geological cross-sections 2, 4 and 6, representing assessed source areas 2, 1 and 3 respectively. The critical slide surface was determined based on the lowest calculated factor of safety. Sensitivity of the slope factor of safety to different geotechnical material strength parameters (models 1–3), was carried out. These strength parameters were derived from in-house laboratory testing on samples of materials taken from the site, and samples of similar materials taken from other sites in the Port Hills and published information on similar materials. Strength parameters were also assessed by back analysis in the limit equilibrium and dynamic analyses.

The finite element modelling adopts the shear strength reduction technique for determining the stress reduction factor or slope factor of safety (e.g., Dawson et al., 1999). Finite element modelling was undertaken on the same cross-sections adopted for the limit equilibrium modelling assessment, using the Rocscience Phase² finite element modelling software. This was done to check the outputs from the limit equilibrium modelling, because the finite element models do not need to have the slide-surface geometries defined.

A1.1.1.2 Dynamic stability assessment (decoupled method)

In civil engineering, the serviceability state of a slope is that beyond which unacceptably large permanent displacements of the ground mass take place (Eurocode 8, EN-1998-5, 2004). Since the serviceability of a slope after an earthquake is controlled by the permanent deformation of the slope; analyses that predict coseismic slope displacements (permanent slope displacements under earthquake loading) provide a more useful indication of seismic slope performance than static stability assessment alone (Kramer, 1996).

The dynamic (earthquake) stability of the slope was assessed with reference to procedures outlined in Eurocode 8 (EN-1998-5, 2004) Part 5. For the Redcliffs assessed source areas, the magnitude of earthquake-induced permanent displacements was assessed for selected cross-sections adopting the decoupled method and using different synthetic earthquake time-acceleration histories as inputs.

The decoupled seismic slope deformation method (Makdisi and Seed, 1978) is a modified version of the classic Newmark (1965) sliding block method that accounts for the dynamic response of the sliding mass. The “decoupled” assessment is conducted in two steps:

1. A dynamic response assessment to compute the “average” accelerations experienced at the base by the slide mass (Chopra, 1966); and
2. A displacement assessment using the Newmark (1965) double-integration procedure using the average acceleration history as the input motion.

The average acceleration time history is sometimes expressed as the horizontal equivalent acceleration time history (e.g., Bray and Rathje, 1998), but they are both the same thing. The average acceleration time history represents the shear stress at the base of the potential sliding mass, as it captures the cumulative effect of the non-uniform acceleration profile in the potential sliding mass. The method assumes that the displacing mass is a rigid-plastic body, and no internal plastic deformation of the mass is accounted for.

The two steps above are described below in more detail.

1. Dynamic response assessment:
 - a. Two-dimensional dynamic site response assessment using Quake/W was carried out adopting synthetic time acceleration histories for the four main earthquakes known to have triggered debris avalanches, cliff-top deformation and cracking in the Port Hills. The modelled versus actual displacements inferred from survey results and crack apertures were compared to calibrate the models.
 - b. Synthetic out-of-phase vertical and horizontal free-field rock-outcrop horizontal and vertical time acceleration histories for the site – at 0.02 second intervals for the 22 February, 16 April, 13 June and 23 December 2011 earthquakes – were used as inputs for the assessment (refer to Holden et al. (2014) for details).
 - c. The equivalent linear soil behaviour model was used for the assessment, using drained conditions. Strain-dependent shear-modulus reduction and damping functions for the rock materials were based on data from Schanbel et al. (1972) and Choi (2008). For the loess shear modulus and damping ratio functions from Ishibashi and Zhang (1993) were adopted assuming a plasticity index of 5 (Carey et al., 2014) and variable confining (overburden) stress, based on the overburden thickness of the loess at each cross-section assessed.

- d. Shear wave velocity surveys were carried out by Southern Geophysical Ltd. for GNS Science (Southern Geophysical Ltd., 2013). These works comprised the surveying of a surface-generated shear wave signal at 2 m intervals between the surface and the maximum reachable depth inside drillholes BH-MB-01 and BH-MB-02.
2. Displacement assessment steps:
- a. The dynamic stress response computed with Quake/W – from each input synthetic earthquake time history – were assessed using Slope/W Newmark function to examine the stability and permanent deformation of the slope subjected to earthquake shaking using a procedure similar to the Newmark (1965) method (detailed by Slope/W, 2012).
 - b. For the Slope/W assessment, a range of material strength parameters was adopted (models 1–3) for the rock, colluvium and loess as per those used in the static stability assessment. This was done to assess the sensitivity of the modelled permanent deformation of the slope to changing material strength.
 - c. For each trial slide surface, Slope/W uses: 1) the initial lithostatic stress condition to establish the static strength of the slope (i.e., the static factor of safety); and 2) the dynamic stress (from Quake/W) at each time step to compute the dynamic shear stress of the slope and the factor of safety at each time step during the modelled earthquake. Slope/W determines the total mobilised shear force arising from the dynamic inertial forces. This dynamically driven mobilised shear force is divided by the total slide mass to obtain an average acceleration for a given slide surface at a given time step. This average acceleration response for the entire potential sliding mass represents one acceleration value that affects the stability at a given time step during the modelled earthquake.
 - d. For a given trial slide surface Slope/W:
 - i. Computes the average acceleration corresponding to a factor of safety of 1.0. This is referred to as the yield acceleration. The critical yield acceleration of a given slide mass is the minimum acceleration required to produce movement of the block along a given slide surface (Kramer, 1996). The average acceleration of the given slide mass, at each time step, is then calculated along the slide surface (base of the slide mass).
 - ii. Integrates the area of the average acceleration (of the trial slide mass) versus time graph when the average acceleration is at or above the yield acceleration. From this it then calculates the velocity of the slide mass at each time interval during the modelled earthquake.
 - iii. Estimates the permanent displacement, by integrating the area under the velocity versus time graph when there is a positive velocity.
 - e. To calibrate the results, the permanent displacement of the slide mass for a given trial slide surface geometry (for a given cross-section) was compared with crack apertures and survey mark displacements, and also with the geometry and inferred mechanisms of failure that occurred during the 2010/11 Canterbury earthquakes. Those soil strength parameters that resulted in modelled displacements of similar magnitude to the recorded or inferred slope displacements were then used for forecasting future permanent slope displacements under similar earthquakes.

Forecasting permanent slope displacements

To forecast likely slope displacements in future earthquakes, the relationship between the yield acceleration (K_y) and the maximum (peak) acceleration (K_{MAX}) of the average acceleration of a given slide mass, was used. Using the results from the decoupled (Slope/W) assessment, the maximum average acceleration (K_{MAX}) was calculated for each selected slide surface (failure mass), from the average acceleration versus time plot – where the average acceleration versus time plot is the response of the given slide mass to the input acceleration history. The decoupled assessment uses the 22 February and 13 June 2011 synthetic earthquake acceleration histories, as inputs (Holden at al., 2014), and the calibrated material strength parameters derived from back analysis (bullet 2. e. above).

The K_y/K_{MAX} relationship was used to determine the likely magnitude of permanent displacement of a given failure mass – with an associated yield acceleration (K_y) – at a given level of average acceleration within the failure mass (K_{MAX}).

Permanent coseismic displacements were estimated for a range of selected trial slide surfaces from each cross-section. These results were then used in the risk assessment to assess the probability of failure of a given range of slide surfaces.

Forecasting probability of failure

The probability that the source areas 1–3 would fail during a given earthquake event was based on the estimated amount of permanent displacement of the failure mass, estimated from the decoupled results. For this assessment, the term “fail” refers to a state where the magnitude of permanent displacement causes the given failure mass to break down, forming a mobile debris avalanche.

For this assessment the following assumptions were adopted:

- If the estimated displacement of the source is ≤ 0.1 m then the probability of catastrophic failure = 0, assuming that the source area is unlikely to fail catastrophically if permanent displacements are ≤ 0.1 m. This was based on measurements of slopes that underwent permanent displacement (i.e., cracking) but where the displacement magnitudes were < 0.1 m and where catastrophic failure did not occur.
- If the estimated permanent displacement of the source ≥ 1.0 m then the probability of catastrophic failure = 1. Meaning that the source area is likely to fail catastrophically if displacements are ≥ 1 m. This was based on the magnitudes of displacement inferred from crack apertures at the cliff crests in the Port Hills. Cumulative displacements at the cliff edge, inferred from crack apertures and survey displacements, tended not to exceed 1 m when measured up to the cliff edge. However, in these locations the cliff edge had fallen away, indicating failure at cumulative displacements of greater than 1 m.
- If the estimated permanent displacements are between 0.1 m and 1 m then the probability of failure (P) is calculated based on a linear interpolation between $P=0$ at displacements of 0.1 m, and $P=1$, at displacements of 1 m.

A1.1.1.3 Estimation of slope failure volumes

The most likely locations and volumes of potential failures were estimated based on the numerical analyses, current surveyed displacement magnitudes, material exposures, crack distributions and slope morphology.

Three failure volumes (upper, middle and lower) were estimated for each potential source area to represent a range of source volumes. The credibility of these potential failure volumes was evaluated by comparing them against: 1) the volumes of relict failures recognised in the geomorphology near the site and elsewhere in the Port Hills; 2) historically recorded failures; and 3) the volumes of material lost from the Redcliffs slope and other similar slopes, during the 2010/11 Canterbury earthquakes.

There are four main sources of information on historical non-seismic failures for the Port Hills:

1. Archived newspaper reports (paperspast.natlib.govt.nz). Papers Past contains more than three million pages of digitised New Zealand newspapers and periodicals. The collection covers the years 1839–1945 and includes 84 publications from all regions of New Zealand;
2. The GNS Science landslide database, which is “complete” only since 1996;
3. Insurance claims made to the Earthquake Commission for landslips which are “complete” only since 1996; and
4. Information from local consultants (M. Yetton, Geotechnical Consulting Ltd. and D. Bell, University of Canterbury) which incompletely covers the period from 1968 to present (McSaveney et al., 2014).

A1.1.1.4 Debris runout modelling

The potential runout of debris from the local assessed source areas 1–3 was assessed empirically by the fahrboeschung method and also by numerical modelling. The potential runout of debris from the distributed sources was assessed empirically by the fahrboeschung methods.

1. Empirical fahrboeschung method:
 - a. The fahrboeschung model is based on a relationship between topographical factors and the measured lengths of runout of debris (Corominas, 1996). The fahrboeschung¹ (often referred to as the “travel angle”) method (Keylock and Domaas, 1999) uses the slope of a straight line between the top of the source area (the crown) and the furthest point of travel of the debris. The analysis assumes the slope crest to be the crown of each potential source area.
 - b. For distributed source areas, the volume of debris passing a given location within the study area is based on the volumes of material that fell and passed a given fahrboeschung angle, at Redcliffs, during the 22 February and 13 June 2011 earthquakes.
 - c. For local assessed source areas 1–3, an empirical relationship established from a compilation of 45 slope sections through discrete debris avalanches that were triggered by the 22 February and 13 June 2011 earthquakes, was used to check the limits of debris runout estimated by the numerical model. This relationship was not used to proportion debris down the slope, as the numerical RAMMS model was used for this.

¹ Fahrboeschung is a German word meaning “travel angle” adopted in 1884 by a pioneer in landslide runout studies, Albert Heim. It is still used in its original definition.

2. Numerical methods – RAMMS:

- a. Numerical modelling of landslide runout was carried out using the RAMMS® debris-flow software. This software, developed by the Snow and Avalanche Research Institute based in Davos, Switzerland, simulates the runout of debris flows and snow and rock avalanches across complex terrain. The module is used worldwide for landslide runout analysis and uses a two-parameter Voellmy rheological model to describe the frictional behaviour of the debris (RAMMS, 2011). The physical model of RAMMS Debris Flow uses the Voellmy friction law. This model divides the frictional resistance into two parts: a dry-Coulomb type friction (coefficient μ) that scales with the normal stress and a velocity-squared drag or viscous-turbulent friction (coefficient ξ).
- b. RAMMS software takes into account the slope geometry of the site when modelling debris runout. The RAMMS model parameters were calculated from the back-analysis of 23 debris avalanches (ranging in volume from 200 to 35,000 m³) that fell from the slopes at Richmond Hill Road, Shag Rock Reserve and Redcliffs during the 22 February and 13 June 2011 earthquakes.
- c. The modelling results give likely debris runout, area affected, volume, velocity and the maximum and final height of debris in a given location at any moment in the runout.
- d. The RAMMS modelling uses a “bare earth” topographic model, and so the runout impedance of buildings and larger trees is not considered (other than incidentally in back analysis).

A1.1.2 Risk assessment

The risk metric assessed is the annual individual fatality risk from cliff collapse and this is assessed for dwelling occupants and users of Main Road within the assessment area. The quantitative risk assessment uses risk-estimation methods that follow appropriate parts of the Australian Geomechanics Society framework for landslide risk management (Australian Geomechanics Society, 2007). It provides risk estimates suitable for use under SA/SNZ ISO1000: 2009.

A1.1.2.1 Fatality risk to dwelling occupants

The risk is based on the annual individual fatality risk and is assessed for dwelling occupants. The risk includes the assessment of the fatality risk to an individual in a residential home from: 1) debris avalanches (derived from the cliffs); and 2) cliff-top recession. The risk method was similar to the one detailed in Massey et al. (2012a), but now includes the possibility of larger debris avalanches occurring from local assessed source areas 1–3 on the cliff, which because they are larger, could travel further down slope were they to occur.

Annual individual fatality risk is the probability (likelihood) that a particular individual will be killed by a cliff collapse in spending one year at their place of residence. For most localities this probability is a small number. The report therefore makes extensive use of the scientific number format of expressing risk in terms of powers of ten. For example, the number 10^{-4} (“10 to the power of minus 4”) is the fraction 1/10,000, and the decimal number 0.0001; it may also be expressed as 0.01%. The units of risk are dimensionless probability per unit of time and the units of annual fatality risk are probability of death per year.

To investigate the influence of uncertainties in the input parameters used in the risk model, three risk-assessment scenarios were examined. These scenarios were based on: 1) an upper, central and lower estimate of the volumes of material that could fall from the slope; and 2) the volume of that debris passing a given distance down the slope. The other parameters represented GNS Science's "best" and "reasonable but more cautious" estimates based on the range of uncertainties identified in the available data at the time of writing. The results for each scenario were modelled using the ArcGIS programme to produce the contoured maps of risk.

For debris avalanches and cliff top recession the risk assessment comprised the following steps:

1. Divide the study area into a series of 2 m by 2 m grid cells.
2. Consider the possible range of triggering events (following the method of Moon et al., 2005) in terms of a set of earthquake triggers and a set of non-seismic (e.g., rain) triggers.
3. Choose a small set of representative events for each type of trigger spanning the range of event severity, from the lowest to the highest.
4. For each representative event, estimate:

For debris avalanches:

- a. the frequency of the event and the volume of material produced in that event ($P_{(H)}$)
- b. the proportion of debris reaching or passing a given grid cell and the probability of a person at that location being in the path of at least one of the boulders in the debris – the earthquake events include debris from both the randomly distributed sources and the local assessed source areas 1–3 ($P_{(S:H)}$)
- c. the probability that a person is present at a given location in their dwelling as the debris moves through it ($P_{(T:S)}$)
- d. the probability that a person is killed if present and in the path of one or more boulders within the debris ($V_{(D:T)}$)

For cliff-top recession:

- a. the frequency of the event and the area of cliff top lost ($P_{(H)}$)
 - b. the proportion of cliff top lost at a given distance back from the cliff edge and the probability that one of the N square metres of cliff top is lost at that location ($P_{(S:H)}$) factoring in both randomly distributed failures and the local assessed source areas 1–3
 - c. the probability that a person is present at a given location at the cliff top as the material falls ($P_{(T:S)}$)
 - d. the probability that a person if present on an area of cliff top that falls is killed ($V_{(D:T)}$)
5. Multiply 4(a)–(d) for debris avalanche and cliff-top recession to estimate the annual individual fatality risk to individuals at different locations below the cliff or at the cliff crest, contributed by each representative event.
 6. Sum the risks from all events 4(a)–(d) separately for debris avalanche and cliff-top recession to estimate the overall risk.

7. Enter the risk value for each grid cell (a 2 m by 2 m grid was used in this study) into a GIS programme and interpolate between the risks estimated in each grid cell to produce contours of equal risk across the GIS map.

A1.1.2.2 Non-seismic events

Rates of debris avalanches and rockfalls triggered without earthquakes, mainly rain, were taken from Massey et al. (2012a). These rates were used to estimate the contribution to total risk from non-seismic triggering events. Four representative event-trigger frequencies were used and the volumes of the debris triggered by events with these frequencies were estimated using a series of steps (frequency was expressed as its inverse, i.e. as return period):

Step 1 – Estimate the trigger frequency of events of a given size that have occurred over a given time period for all sites using the available data. Four event return-period bands were used: 1) 1–14 years; 2) 15–99 years; 3) 100–1,000 years; and 4) >1,000 (nominally 1,000–10,000 years).

Step 2 – Assume a conservative volume of $N \text{ m}^3$ per “typical” event in each band, assuming the same volumes per event for all cliffs.

Step 3 – Estimate the annual frequency of a given volume event occurring in each band.

A1.1.2.3 For seismic events

Debris avalanche volumes likely to be generated in an earthquake were determined from the relationship between the volumes of material leaving the cliffs during the 2010/11 Canterbury earthquakes (per square metre of cliff face), and the calculated free field rock outcrop peak ground acceleration at the Redcliffs site (Holden et al., 2014).

Step 1 – Estimate the volumes of material that could be generated at different levels of peak ground acceleration adopting seven event bands, that cover the range of peak ground accelerations from 0.01 to 3 g. For each band adopt a representative event, in terms of the volume generated, by taking the midpoint of each band, and the corresponding volume generated (adopting upper, middle and lower volume estimates based on the statistical range of the data).

Step 2 – for each representative event (volume of debris), calculate the annual frequency of the event occurring. The frequency of a given free field peak ground acceleration band occurring is obtained from the National Seismic Hazard Model. The increased level of seismicity in the Christchurch region is incorporated in a modified form of the 2010 version of the National Seismic Hazard Model (Stirling et al., 2012), which incorporates the now-increased probabilities of rupture for major faults in the region (Gerstenberger et al., 2011). The risk assessment adopts the year 2016 seismic hazard model results, assuming “aftershocks”.

This differs from the previous cliff collapse assessment in Massey et al. (2012a), which used the year 2012 model results (these were the available results at the time of that report). At the instruction of Christchurch City Council, for the risk assessment in this report the year 2016 model results have been adopted to take into account the currently elevated seismic hazard, which is elevated above the 50-year average due to the 2010/11 Canterbury earthquakes.

The model results used in this assessment also include the contributions from all earthquakes, including earthquakes that follow a main earthquake (aftershocks). This differs from the seismic hazard model results adopted by the Canterbury Earthquake Recovery Authority for land zoning purposes, where contributions from aftershocks were removed. Aftershocks were removed because the Canterbury Earthquake Recovery Authority policy makers assumed that people would be evacuated after a large earthquake, and therefore would not be present in their dwelling, and not exposed to cliff collapses triggered by subsequent aftershocks.

GNS Science has assumed the year 2016 seismic hazard model results including contributions from all earthquakes (including aftershocks), as it is not the role of GNS Science to recommend an evacuation policy after a large earthquake.

Step 3 – Take into account the possibility of larger local failure of assessed source areas 1–3. To do this the total volume of debris generated in each band was partitioned between: 1) Random uniformly distributed failures of the cliff face comprising 40% of the total volume, that fall from anywhere on the slope; and 2) Local (non-random) failures comprising 60% of the total volume, corresponding to assessed source areas 1–3.

Step 4 – Calculate the probability of each assessed source area occurring based on the results of the decoupled assessment and the estimated amount of permanent slope displacement (detailed in previous section A1.1.2.3).

Step 5 – Check that the total combined volume of assessed source areas 1–3 is not less than or greater than the 60% of the total volume attributed to these failures per band. At lower event bands the total volume of all the assessed source areas 1–3 significantly exceeds the estimated total debris avalanche volumes produced in the band. For the upper event bands, the total volume of the combined source areas 1–3 is less than the 60% of the total volume produced in the band and attributed to them. Therefore the probability (*P*) of each source occurring is calculated such that *P* x total volume of all assessed sources associated with earthquake events (*V*) = the expected total volume from the sources per given band (Figure A1.1). Thus, the summed volume of the assessed source areas per band cannot exceed 60% of the total volume produced in that band. However, if the total volume of all assessed source areas associated with a given band is less than the total expected volume in that band, the difference in volume is partitioned back to the distributed failures (Figure A1.1).

Expanded calculation of P(each localised source occurring)		
Prob of source i occurring given an earthquake =	P_i	
Relative probability of source i occurring =	<i>p_i</i>	based on estimated Newmark displacement
Total volume anticipated, all sources =	V	
Volume of source i	<i>V_i</i>	
The requirement is that	$V = \sum P_i \cdot V_i$	(summed over all sources)
But	$P_i = C \cdot p_i$	where C is a constant
So	$V = C \cdot \sum p_i \cdot V_i$	

Figure A1.1 Expanded calculation of the probability of each local source area “scoop” occurring.

A1.1.2.4 Impact from debris avalanches

$P_{F1(S:H)}$ is the probability of the debris reaching or passing a portion of slope as it travels downhill from the source area. The probability of one boulder hitting an object when passing through a particular portion of the slope, perpendicular to the boulder path, is expressed as:

$$P_{F1(S:H)} = \frac{(D + d)}{L} \quad \text{Equation 3A}$$

where D is the diameter of the design boulder (assumed to be 0.5 m) that travels along a path either side of d , within which the boulder cannot miss, d is the diameter of an object such as a person or width of a building, and L is the unit length of slope perpendicular to the runout path, in this case L is 2 m which corresponds to the 2 m by 2 m grid-cell width adopted for the risk assessment.

However, the debris leaving the cliffs during the 2010/11 Canterbury earthquakes predominantly consisted of a mass of boulder- and cobble-sized blocks that were not all equal in volume. The distribution of block sizes within the debris has been simply quantified by counting and measuring boulders within the debris at the toe of the cliff. Based on this assessment a volume of 0.07 m³ has been adopted, which is based on a 50th percentile boulder width of 0.5 m and assuming that boulders are spherical. This means that each cubic metre of debris comprises about eight boulders (taking into account the space between the boulders). For the assessment, a conservative estimate of 15 boulders per cubic metre of debris has been adopted. If it is assumed that each cubic metre of debris comprises about 15 boulders of 0.07 m³ in volume, then the probability of one cubic metre of debris hitting an object when passing through a particular portion of the slope is expressed as.

$$P_{F15(S:H)} = 1 - \left(1 - \frac{(D + d)}{L}\right)^{15} \quad \text{Equation 3B}$$

The probability of one cubic metre of debris formed of 15 boulders reaching/passing the same portion of slope increases as a function of the volume of debris travelling down the slope. The probability of one cubic metre of N cubic metres of debris hitting an object when passing through that same portion of slope is then given, by:

$$P_{FN(S:H)} = 1 - (1 - P_{F15(S:H)})^N \quad \text{Equation 3C}$$

For the purposes of risk estimation, it is necessary to have a quantitative measure of the size of a person. In this report, a “person” is assumed to be a cylinder of 1 m diameter and unspecified height (no specification of height was required in the model). The assumed value covers the order-of-magnitude range from about 0.3 m (vertical e.g., the person is standing) to about 3 m (horizontal, e.g., the person is lying down).

For randomly distributed sources, the volume of debris passing a given distance down the slope is taken from the empirical relationship. For the local assessed source areas 1–3 the debris is distributed using the numerical RAMMS model (refer to Section A1.1.2.5).

A1.1.2.5 Cliff-top recession

For cliff-top recession, the recession of the cliff edge is approximately proportional to the cube root of the volume lost from the cliff face. The relationship between the volume lost from the cliff face and the corresponding area of cliff top lost during the 2010/11 Canterbury

earthquakes is reported in Massey et al. (2012a) for Richmond Hill/Wakefield Avenue, Shag Rock Reserve and Redcliffs. From these data the ratio of area lost per unit of volume leaving the cliff face is about of $0.016 \pm 0.001\text{m}^2$ per m^3 (at one standard deviation). That is, for every 100 m^3 of cliff face lost, about 1.6 m^2 ($\pm 6\%$) of cliff top area is expected to be lost. For this assessment, however, a ratio of 0.019 was adopted, which is the ratio plus two standard deviations (95% error limit).

A1.1.2.6 Falling due to cliff-top recession

$P_{R(S:H)}$ is the probability of a particular location at the cliff top falling and a person falling with it should they be present in that location when the cliff top falls. The probability of a person if present at the cliff top falling, given one metre of cliff top recessing, perpendicular to cliff edge, is expressed as.

$$P_{R1(S:H)} = \frac{(2D)}{L} \tag{Equation 4A}$$

where D is the approximate area occupied by a person at the cliff edge, assumed to be 1 m^2 , and L is the unit length of cliff parallel to the cliff edge.

The probability of a person falling is dependent upon the total area of cliff edge that collapses during a given event, and how close the person is to the outer edge, as the proportion of cliff top that collapses in any event decreases away from the cliff edge. Therefore the probability of a person falling if one square metre of N square metres of cliff top were to fall is given by:

$$P_{RN(S:H)} = 1 - (1 - P_{R1(S:H)})^N \tag{Equation 4B}$$

For randomly distributed failures triggered by earthquakes and for non-seismic failures (both are assumed to be randomly distributed along the cliff), the proportion of cliff top lost per metre back from the cliff edge is based on what happened to the cliff edge at Redcliffs during the 2010/11 Canterbury earthquakes (Massey et al., 2012a). For assessed source areas 1–3 the proportion of cliff top lost per metre back from the cliff edge is calculated from the geometry of the source areas, adopting the lower, middle and upper area estimates.

Although the most likely locations of source areas 1–3 have been determined, it is possible that such failures could occur from elsewhere along the steep cliff face, especially as the rock mass, forming the slope, is now open and dilated. Therefore the risk estimates including the local source areas 1–3 have been distributed across the cliff top in the assessment area and not just in the locations of the assessed source areas 1–3.

A1.1.2.7 Probability of a person being present

$P_{(T:S)}$ is the probability an individual is present in the portion of the slope when a boulder moves through it. It is a function of the proportion of time spent by a person at a particular location each day and can range from 0% if the person is not present, to 100% if the person is present all of the time.

For planning and regulatory purposes it is established practice to consider individual risk to a “critical group” of more highly-exposed-to-risk people. For example, there are clearly identifiable groups of people (with significant numbers in the groups) who do spend the vast majority of their time in their homes – the very old, the very young, the disabled and the sick.

The assumption used in the risk assessment (contained in Massey et al., 2012a) for judging whether risk controls should be applied to individual homes was thus that most-exposed individuals at risk would be those who spend 100% of their time at home.

In other international rockfall risk assessments (e.g., Corominas et al., 2005), values ranging from 58% (for a person spending 14 hours a day at home) to 83% (for a person spending 20 hours a day at home), have been used to represent the “average” person and the “most exposed” person, respectively. However, in reality the most exposed person is still likely to be present 100% of their time.

For the land zoning assessments carried out by the Canterbury Earthquake Recovery Authority – with regards to rockfall and debris avalanche risk – their policy adopted an “average” occupancy rate, to assess the average annual individual fatality risk from rockfall across the exposed population in order to estimate the risk to the average person.

For this assessment, GNS Science has assessed the sensitivity of the risk assessment results to a range of values representing the most exposed and average person. It has been assumed that the most exposed person spends 100% of their time at home, and that an average person spends on average 16 hours a day at home ($16/24 = 0.67$ or 67%).

When a person is at home they tend to spend more time in their home than in their garden. Whilst in their home they cannot occupy every part of it at the same time. To proportion the person across their home, GNS Science has assumed that Port Hills homes have a footprint area (assuming a single story dwelling) of $A_F = 100 \text{ m}^2$. The probability that a person will be occupying a given area within their home at any one time can be expressed as:

$$P_{(T:S)} = \frac{(0.67)}{(A_F / P_A)} \tag{Equation 5}$$

Where 0.67 (67%) is the proportion of time an average person spends in their home and P_A is the area of home occupied by a person at any one time. For this assessment, GNS Science has adopted the area of the grid used for the risk assessment, in this case a 2 m by 2 m (4 m^2) grid-cell to represent P_A . Therefore the probability of person being present in a given grid cell within their home is assumed to be 0.03 (3%) for the average person.

A1.1.2.8 Probability of the person being killed if hit or falling

This is the probability of a person being killed if present and either in the path of one or more boulders or on an area of cliff top that falls. Vulnerability (V) depends on the landslide intensity, the characteristics of the elements at risk, and the impact of the landslide (Du et al., 2013).

This probability is expressed as vulnerability, the term used to describe the amount of damage that results from a particular degree of hazard. Vulnerability ranges between 0 and 1 and for fatality risk represents the likelihood of an injury sustained by the individual being fatal (1) and the possibility of getting out of the way to avoid being struck.

Studies from Hong Kong (e.g., Finlay et al., 1999) summarised the vulnerability ranges and recommended likelihood of death “if struck by rockfall”. The vulnerability of an individual in open space if struck by a rockfall is given as 0.1–0.7, with a recommended value of 0.5, assuming that it may be possible to get out of the way. For people in homes, it would be unlikely that a person would be able to take evasive action as they would not see the boulder

coming. However, this argument is counterbalanced by the level of protection a house may provide by stopping a boulder from entering it, but conversely, flying debris (shrapnel) inside a house may contribute to injury.

Data on homes damaged in the cliff-collapse areas of the Port Hills indicate they were struck by many boulders, and in some cases the building collapsed. Finlay et al. (1999) recommend using a vulnerability of 1.0 if a person is in a building and if the building is hit by debris and collapses, or is inundated with debris. However, Du et al. (2013) propose vulnerability ranges from 0.24 for timber buildings to 0.45 for masonry buildings indicating that somebody is more likely to survive in a timber building that has collapsed.

At Redcliffs one person was killed in their home when it was struck by many hundreds of boulders, which caused it to collapse and another person was hit by boulders and killed whilst in their garden. In other parts of the Port Hills, a further three people died when they were buried by many boulders while outside.

The “landslide intensity” related to a debris avalanche is a function of the numbers of boulders passing through a given location and their velocity. In this risk assessment the probability of being in the path of one or more of N boulders within the debris (should a person be present) has been calculated separately as $P_{(S:H)}$.

Debris velocities derived from RAMMS model outputs are typically >5 m/s for most of the runout areas assessed. However, the velocity rapidly drops to <0.05 m/s in the distal limits of runout over a relatively short distance of several metres. These calculations are similar to field observations made from video footage although, some boulders within the distal debris fringe (mainly individual boulders) travelled at higher velocities, i.e., “fly rock”. Fly-rock may occur when moving blocks impact and fracture resulting in high velocity rock fragments being released.

The two-dimensional rockfall modelling (Appendix 9) suggests that boulder velocities in the distal runout zone are still in the range of about 3 to 5 m/s and not < 0.5 m/s as suggested by RAMMS. Such velocities are more consistent with field observations. At these boulder velocities, of about 5 m/s (18 km/hr), it is unlikely that a person could get out of the way of a boulder (Australian Geomechanics Society, 2007).

Based on these results, a constant vulnerability factor of 70% has been adopted for this risk assessment as it was the factor adopted by the Canterbury Earthquake Recovery Authority for the previous risk assessments. A constant vulnerability value is thought reasonable as the velocity of the boulders, even in the distal runout zone are still relatively high with people unlikely to be able to get out of the way. The protective effects of buildings have not been taken into account, this is because most people killed by falling boulders during the 22 February 2011 earthquake were outside and therefore not protected by buildings. However, it is noted that buildings do have a sheltering effect as only 45% of buildings hit by boulders were penetrated (Massey et al., 2012b).

For a person falling from a cliff, the severity of injury increases with the height of fall, but it also depends on the age of the person, nature of the impact surface and how the body hits the surface. The chance of surviving increases if landing on a surface that can deform, such as snow or water. In a study by Barlow et al. (1983), the height at which 50% of children die from a fall is between 12 and 15 m. The cliffs in this study range from 40 to 70 m in height and the nature of the surface onto which a person would fall is boulder size debris formed of

rock. Taking all these considerations into account, for this study, $V_{(D:T)}$, the probability of being killed if a person is on an area of cliff that falls, is assumed to be 0.7 as there might be a chance that a person could get away from the edge of the cliff before it falls.

A1.2 ROAD-USER RISK ASSESSMENT

This assessment uses a simplified version of the method used for Deans Head (Massey et al., 2014). This appendix describes:

- The background and context in terms of the road, its users and the slope collapse hazards they face (A1.1.1);
- The general modelling approach adopted (A1.1.2);
- Main Road traffic parameters for this road section, including the effect of the road being blocked at the time of a slope collapse event (A1.1.3);
- The estimation of individual road user risk per journey due to impact or inundation by slope collapse debris (A1.1.4); and
- Calculation of aggregate risk per journey and other risk metrics derived from it (A1.1.5).

It should be emphasised from the outset that the risk estimates for road users throughout this report use simple models which in many cases cannot be and have not been directly validated against hard evidence. There is a good deal of approximation, informed by the authors' knowledge of the area and of transport accidents more generally. Risk estimates per journey are presented as approximate ranges of possible values; presenting "point values" might provide a spurious sense of the accuracy of the assessment results.

A1.2.1 Background and Context

The section of Main Road modelled is shown in Figure A1.2 (and Figure 2 of the main report), and a Google Street View image, looking northwest along the road section modelled is shown in Figure A1.3.



Figure A1.2 Main Road section modelled (opposite Redcliffs Park).



Figure A1.3 View northwest along the Main Road section assessed for Redcliffs (image taken from Google Earth).

There are no turnings along this short (81 m) section of road except for Puriwhero Lane which has been closed since the 22 February 2011 earthquakes. There are no particular hazards such as steep drops or water into which a road user might fall when swerving from the road in the event of an accident.

Therefore, the hazard assessed for this section of Main Road is the direct impact of debris from cliff collapses (debris avalanches) falling onto road users or their vehicles.

Road user risk is assessed for:

- a. Car occupants;
- b. Bus occupants;
- c. Truck occupants;
- d. Motorcyclists;
- e. Pedal Cyclists; and
- f. Pedestrians.

The modelling approach is explained in Section A1.2.2.

A1.2.2 Risk Modelling Approach

Risk is assessed in terms of the risk per journey to the assessed road users. The risk per journey is calculated for each grid adopting the same grid used in the dwelling risk assessment. To streamline the calculation, risk is calculated for cells running along the near (slope side) and far (seaward) sides of the road, rather than for all cells within the road area. The basic equation used to estimate risk per journey (with dimensions of each term in brackets) is given as:

$$\text{Risk (probability of death per journey)} = SC_{\text{event}} \times P_{\text{death}} \times T_{\text{journey}} \quad \text{Equation 6}$$

Where: SC_{event} is the debris avalanche event frequency (in units of events/yr), P_{death} is the probability of death per event, if present and $T_{journey}$ is the time a road user is present per journey (in units of years per journey).

Risk contributions are calculated for each cell, each road user and each representative event per earthquake and non-earthquake band (adopting the inputs parameters for scenarios A–C), which are then summed to provide overall estimates of risk per journey for each side of the road.

The risk per journey outputs are then used to estimate risk per year to heavy users of this section of road, and to estimate the average expected total annual fatalities due to cliff collapse. The risks per journey are compared with the background motor vehicle crash risk that would be expected for this length of an average New Zealand urban road.

There is limited potential for multiple vehicles/road users to be involved in a single cliff collapse event at this site (the modelled road section is only 81 m long), so no “societal risk” calculation has been carried out.

The risk calculations rely on being able to estimate how many road users travel over the road section in question and how fast they travel. These issues are discussed in Section A1.2.3.

A1.2.3 Traffic Parameters on Main Road at Redcliffs

For an individual road user’s trip, their travel speed determines the time they are at risk. Traffic does generally keep moving along this stretch of road, but at peak times becomes congested meaning vehicles are closer together (hence more are at risk) and travelling somewhat more slowly (hence at risk for longer periods) than at other times.

Average speeds and traffic densities (in terms of spacing between vehicles) taking into account periods of slow or static traffic are worked out using the traffic count data collected by Christchurch City Council on an hour-by-hour basis. There are no direct data available in recent years any closer to Redcliffs than the Sumner West Surf Club site to the east and the Causeway to the west. Traffic counts have therefore been taken as the averages of those used for Dean’s Head to the east and Quarry Road to the west of the Redcliffs road section modelled. The resulting most recent available traffic counts for each hour of the week are shown in Table A1.1. Note that these are counts of motor vehicle traffic; “vulnerable road users” (motorcyclists, pedal cyclists and pedestrians) are not included.

While there is considerable use of this road section by pedal cyclists and a moderate level of motorcycle traffic, there is relatively light pedestrian usage as the footpath along the slope side of the road is currently closed, and blocked by containers, while pedestrians have been rerouted to the seaward side of the road adjacent to Redcliffs Park. More comprehensive counts of different road users are available for Main Road considerably further to the west (at the junction with Ferrymead Terrace), and these have been used to inform rough estimates of the split of motor vehicles between cars and trucks. Rough estimates based on the authors’ own observations are made of cyclist, motorcyclist and pedestrian numbers of road users. Buses are considered separately (see below).

Table A1.1(a) Estimated westbound traffic on Main Road at Redcliffs.

Period Ending	Mon	Tues	Wed	Thur	Fri	Sat	Sun	Averages	
								4Day	7Day
01:00	5	4	5	7	10	18	24	5	10
02:00	3	4	4	4	7	15	20	4	8
03:00	3	3	3	10	5	16	18	5	9
04:00	6	7	5	10	10	14	18	7	10
05:00	18	13	15	24	22	17	20	18	18
06:00	65	65	56	61	69	35	26	62	54
07:00	255	243	281	250	258	107	65	257	208
08:00	993	1001	967	921	886	220	141	970	733
09:00	984	1028	969	1030	955	423	302	1003	813
10:00	705	708	696	753	762	669	570	715	695
11:00	622	588	541	639	639	814	757	598	657
12:00	585	586	526	618	670	839	853	579	668
13:00	488	476	461	510	555	655	758	484	558
14:00	457	441	418	470	518	634	774	447	530
15:00	454	427	420	509	531	562	754	452	523
16:00	490	478	475	543	552	520	727	497	541
17:00	479	471	484	509	522	484	563	486	502
18:00	380	384	404	397	388	288	317	391	365
19:00	345	362	380	391	399	288	289	369	350
20:00	244	242	265	292	304	264	181	261	256
21:00	116	126	143	144	143	101	109	132	126
22:00	78	94	89	99	105	84	63	90	87
23:00	43	45	51	46	72	68	31	46	51
00:00	11	13	14	22	39	44	11	15	22

Table A1.1(b) Estimated eastbound traffic on Main Road at Redcliffs.

Period Ending	Mon	Tues	Wed	Thur	Fri	Sat	Sun	Averages	
								4Day	7Day
01:00	27	21	28	40	54	99	137	29	58
02:00	10	12	11	11	20	45	62	11	24
03:00	6	5	7	20	10	32	36	9	17
04:00	6	7	5	10	10	14	18	7	10
05:00	5	3	4	6	6	4	5	5	5
06:00	17	17	15	16	19	9	7	16	14
07:00	68	65	75	67	69	29	17	69	56
08:00	247	249	241	229	221	55	35	242	183
09:00	350	366	345	366	340	150	107	357	289
10:00	268	269	265	286	290	254	217	272	264
11:00	298	281	259	306	306	390	362	286	315
12:00	343	343	308	362	392	491	499	339	391
13:00	500	488	472	523	568	670	776	496	571
14:00	560	540	511	575	634	775	947	546	649
15:00	611	574	565	685	714	757	1015	609	703
16:00	709	691	688	785	798	752	1052	718	782
17:00	789	776	798	840	860	798	928	801	827
18:00	930	939	988	972	949	703	775	957	894
19:00	562	589	618	638	649	469	470	602	571
20:00	317	314	345	380	396	343	236	339	333
21:00	227	247	280	282	279	198	214	259	247
22:00	205	246	234	260	274	220	164	236	229
23:00	155	163	182	164	257	243	111	166	182
00:00	56	65	70	107	193	217	52	75	109

There is a clear inverse correlation between traffic density and speed. Table A1.2 has been developed by the authors to provide a rough representation of the way in which vehicles speeds vary with traffic levels; it has been tailored so that, when coupled with the traffic counts here and in our Quarry Road and Deans Head reports (Massey et al., 2014a,b), the predicted average traffic speeds at different times of day are broadly consistent with our own (considerable) experience of using this road over the past 2–3 years. The average separations shown are those resulting from uniform distribution of the average number of vehicles in each category, assuming all travel exactly at the average speed.

Table A1.2 Correlation between traffic levels and average speeds/separations.

1-way vehicles/hr	Speed range (kph)		Average separation (m)	
	lower speed	upper speed	lower speed	upper speed
<400	40	50	>95	>120
400-600	38	48	95	120
600-800	36	45	60	75
800-900	32	40	40	50
900-1000	22	30	24	33
1000-1100	15	20	15	20
>1100	10	15	9	14

Table A1.2 can be used in combination with the traffic levels in Table A1.1 to provide estimates of the average traffic speeds for each hour of the day and day of the week, in both directions along the road. Average traffic speeds for the purpose of estimating average times at risk from cliff collapse hazards are then estimated simply by averaging over 24 x 7 hours, to produce the following estimates at Redcliffs:

- Average speed (both directions, lower) = 34.9 km/hr
- Average speed (both directions, upper) = 44.0 km/hr

Note that the lower travel speed corresponds to higher risk estimates as it takes longer to travel through the at-risk area. A summary of assumed numbers of road users, average speeds, and numbers of journeys per day for heavy road users (used as the basis for estimating annualised individual fatality risk for heavy road users) is provided in Table A1.3.

Table A1.3 Summary of road user numbers and average speeds.

Road user	Trips/day, heavy user		Trips/year, all users		Average speed, kph	
	lower	upper	vehicles	people	lower risk	higher risk
Cars	1	2	5478385	8695720	44.0	34.9
Buses	1	2	39244	598660	44.0	34.9
Heavy goods	1	2	188834	299732	44.0	34.9
Motorcycles	1	2	292200	292200	44.0	34.9
Cyclists	1	2	29220	29220	25	15
Pedestrians	1	2	14610	14610	5	3

(cars/trucks split as per Main Rd/Ferrymead Rd junction; cycles/pedestrians estimated by authors)

A1.2.4 Individual Risk per Journey – Hazard 1 (Impacted/Inundated by Debris)

In reviewing the model developed for assessing the impact of debris inundation, from earth/debris flows, on road users, the “rockfall” impact model has been updated in order to improve the calculation of the probability that a random boulder passing through a cell will strike a road user whose centre is also within that cell. Vulnerabilities (probabilities of death if in the path of a boulder) have also been reviewed to take into account the different circumstances.

The impact of cliff collapse, in terms of the numbers of boulders passing through a given section of road (grid cell) is assessed by analogy with the model used to assess the risk to dwelling occupants. However, for the road users, the vulnerabilities have been reduced to take into account that road users, in contrast with people in dwellings, are all outdoors and facing their direction of travel at all times.

A1.2.4.1 Cliff collapse modelling

A road user located within a 1 m by 1 m grid cell could be hit by a boulder, within the debris, passing through that cell or through the cells either side, as illustrated in Figure A1.4 for cell width (*W*), boulder diameter (*d*) and person diameter (*D*).

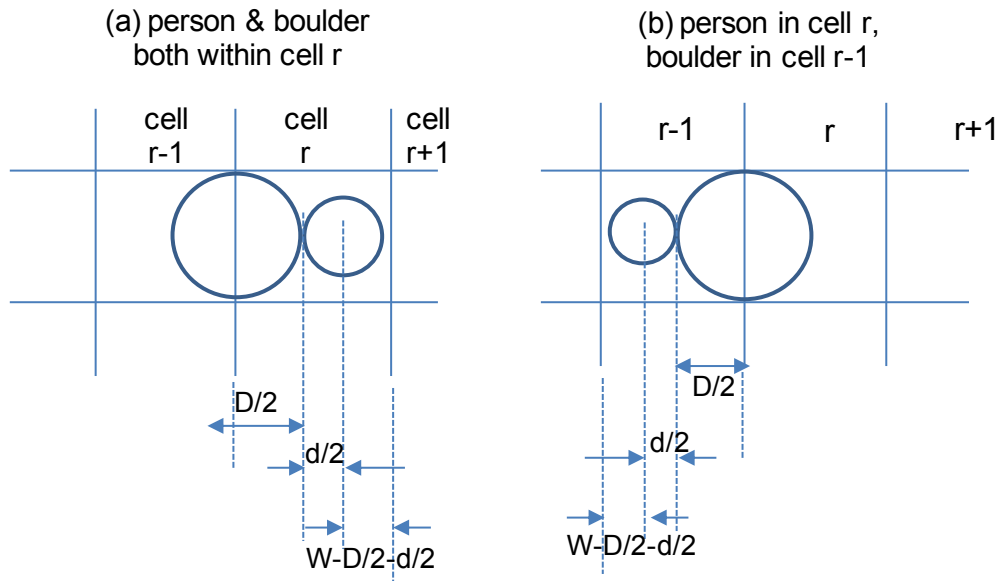


Figure A1.4 Possible boulder/road user collision configurations.

In the first situation, if $(D+d)/2 > W$ then collision is inevitable. But in this assessment that is not the case; we have $D = 1$ m, $d = 0.5$ m and $W = 1$ m. Therefore, with the person located with their centre on the left edge of the cell as in Figure A1.4(a), there is a gap of width $W - D/2 - d/2$ within which the centre of the boulder can pass without striking the person. As the person shifts to the right this gap decreases, reaching zero when the person's centre is $D/2 + d/2$ from the right hand edge of the cell ($W - D/2 - d/2$ from the left edge). There is thus an average gap of width $0.5(W - D/2 - d/2)$ pertaining over a distance $(W - D/2 - d/2)$ from the left hand edge of the cell, and the same again on the right. The proportion of the cell within which the boulder can pass without striking the person is thus:

$$\begin{aligned}
 & 2 \text{ (right and left side)} \times (0.5/W) \cdot (W-D/2-d/2) \text{ average gap as proportion of cell width} \\
 & \times (2/W) \cdot (W-D/2-d/2) \text{ proportion of cell width over which gap present.} \\
 & = (W-D/2-d/2)^2 / W^2
 \end{aligned}$$

The probability $P_{1,r}$ of the person in cell r being struck by a boulder passing randomly through cell r is thus $1 - (W-D/2-d/2)^2 / W^2$. **Equation 7**

We now consider a boulder passing randomly through cell r-1 to the left of the cell containing the person situated on the extreme left edge of cell r. If the boulder centre is within $(D/2 + d/2)$ of the right edge of cell r-1 then it will strike the person. The width of the space within cell r-1 within which the boulder must pass to strike the person in cell r decreases linearly as the person shifts to the right, reaching 0 when the person centre is $D/2 + d/2$ from the left edge of the cell. There is thus an average width of:

$$\begin{aligned}
 & 0.5 (D/2+d/2)/W \text{ as a proportion of the width of the cell, applying over a distance} \\
 & (D/2+d/2)/W \text{ proportion of cell r from the left edge of the cell,}
 \end{aligned}$$

for which the boulder will strike the person. The same probability of the person in cell r being struck applies to a boulder passing randomly through cell r+1 to the right of cell r. Denoting these probabilities $P_{1,r-1}$ and $P_{1,r+1}$ respectively we then have:

$$P_{1,r-1} = P_{1,r+1} = 0.5 (D/2+d/2)^2 / W^2 \quad \text{Equation 8}$$

For a single boulder passing randomly through each of these three cells, the probability P_1 of the person being in the path of 1 or more boulders is given by:

$$P_1 = 1 - (1 - P_{1,r-1}) \times (1 - P_{1,r}) \times (1 - P_{1,r+1}) \quad \text{Equation 9}$$

The probability of death for road user j per single boulder passing through each of these cells is now calculated as:

$$P_{\text{death},1,j} = P_{1,j} \times V_{1,j,\text{rockfall}} \quad \text{Equation 10}$$

A significant complication now is that the number of boulders passing through each cell may be different. This might be possible to model if the cells formed a continuous straight line along an axis of the model grid, but in this case they do not. We therefore introduce the approximation for the purposes of calculating the probability of being killed by N boulders passing through the cell that THE SAME number of boulders passes through the cells either side. The probability of death for N boulders passing through the cell is then:

$$P_{\text{death},N,j} = 1 - (1 - P_{\text{death},1,j})^N \quad \text{Equation 11}$$

This is then multiplied by the proportion of a year for which the user is present in the cell (based on the average travel speeds in Table A1.3 above) and the frequency of the triggering event which gave rise to the N boulders per cell (as per Equation 6 above) to calculate the contribution of this cell and this slope collapse scenario to the road user's individual risk per journey.

The values of the parameters used in this assessment are as follows:

No. of boulders passing through cell – taken directly from dwelling model output

Years present in cell per journey – as shown in Table A1.4 (based on average road user speeds as in Table A1.3 above).

Table A1.4 Road user speeds and times per journey within 2 m cell.

Road user	Average speed, kph		Time (yrs/jny) spent in cell	
	lower risk	higher risk	lower risk	higher risk
Car occupant	44.0	34.9	5.18E-09	6.54E-09
Bus Occupant	44.0	34.9	5.18E-09	6.54E-09
Truck occupant	44.0	34.9	5.18E-09	6.54E-09
Motorcyclist	44.0	34.9	5.18E-09	6.54E-09
Pedal Cyclist	25	15	9.13E-09	1.52E-08
Pedestrian	5	3	4.56E-08	7.61E-08

Vulnerabilities – Values of 0.4 (lower) and 0.7 (higher) are used for motorcyclists, and of 0.3 (lower) and 0.5 (higher) for all other road users. Note that these are probabilities of death if in the path of a single boulder; each successive boulder confers the same probability of death again. This contrasts with some of our earlier assessments in which we applied the vulnerability to the “Probability of being in the path of one or more boulders”. This approach (treating vulnerability as independent of number of boulders) was based on the primary contribution to survival being the ability of the individual to get out of the way of boulders. With the lack of any obvious place of escape in the event of rockfall at the Redcliffs road

section modelled we consider it more appropriate here to assume that getting out of the way is unlikely. We recognise that motor vehicles will provide some modest protection against boulders relative to the vulnerable road users (cyclists and pedestrians), but consider that for pedestrians and pedal cyclists this is offset by their greater ability to hear what is going on off the road and to take evasive action before boulders fall. Motorcyclists are considered to have the worst of both worlds (vulnerability if struck, and inability to hear environmental noises), hence their higher assumed vulnerability.

A1.2.5 Road user risk per journey and risk parameters derived from it

The parameters shown in the above tables are uncertain. As in our previous work on road user risk from rockfall, inputs and outputs are presented as ranges from “reasonable lower” to “reasonable upper” values. No statistical significance is attached to these ranges; the results are regarded as providing a sensible range, given the associated uncertainties, within which to assume the actual risk might lie. Perhaps the single largest uncertainty is in the volume of material which flows from the debris sources; as for the dwelling risk assessments this has been explicitly considered by carrying out all assessments three times, for upper, central and lower estimates of debris source volumes.

The risk equation is evaluated for each cell in the grid for each cliff-collapse scenario considered, as described in Section A1.2.4. The grid used was simplified relative to that used in modelling dwelling risk by excluding cells that did not form part of the roadway in order to streamline the calculation process; in all other respects the rockfall modelling used to estimate individual road-user risk was identical to that used to estimate individual dwelling occupant risk.

As in the dwelling occupant assessment, the set of scenarios modelled covers:

- Seven seismic trigger scenarios ranging from 0.1–0.3 g up to 2–3 g peak ground acceleration, with an increasing probability as shaking increases that cliff collapse will be triggered;
- Four non-seismically triggered cliff collapse scenarios (corresponding to different severities of weather-induced rockfall); and
- Source areas 1, 2 and 3, with probabilities of triggering in each seismic scenario taken exactly as for the dwelling assessment (note – only source area 3 generates debris sufficient to reach the road).

The risk per journey in a given cell is then calculated by summing over all source areas.

The overall risks per journey were calculated by summing over all cells making up the NEAR (landward) side of Main Road and the FAR (seaward) side of Main Road, allowing the risks on either side of the road to be compared with each other and with the existing motor vehicle crash risk (based on average statistics for New Zealand urban roads, from Ministry of Transport publications on road crashes and casualties and on number of journeys and distance travelled by different road user groups; NZ MoT, 2012).

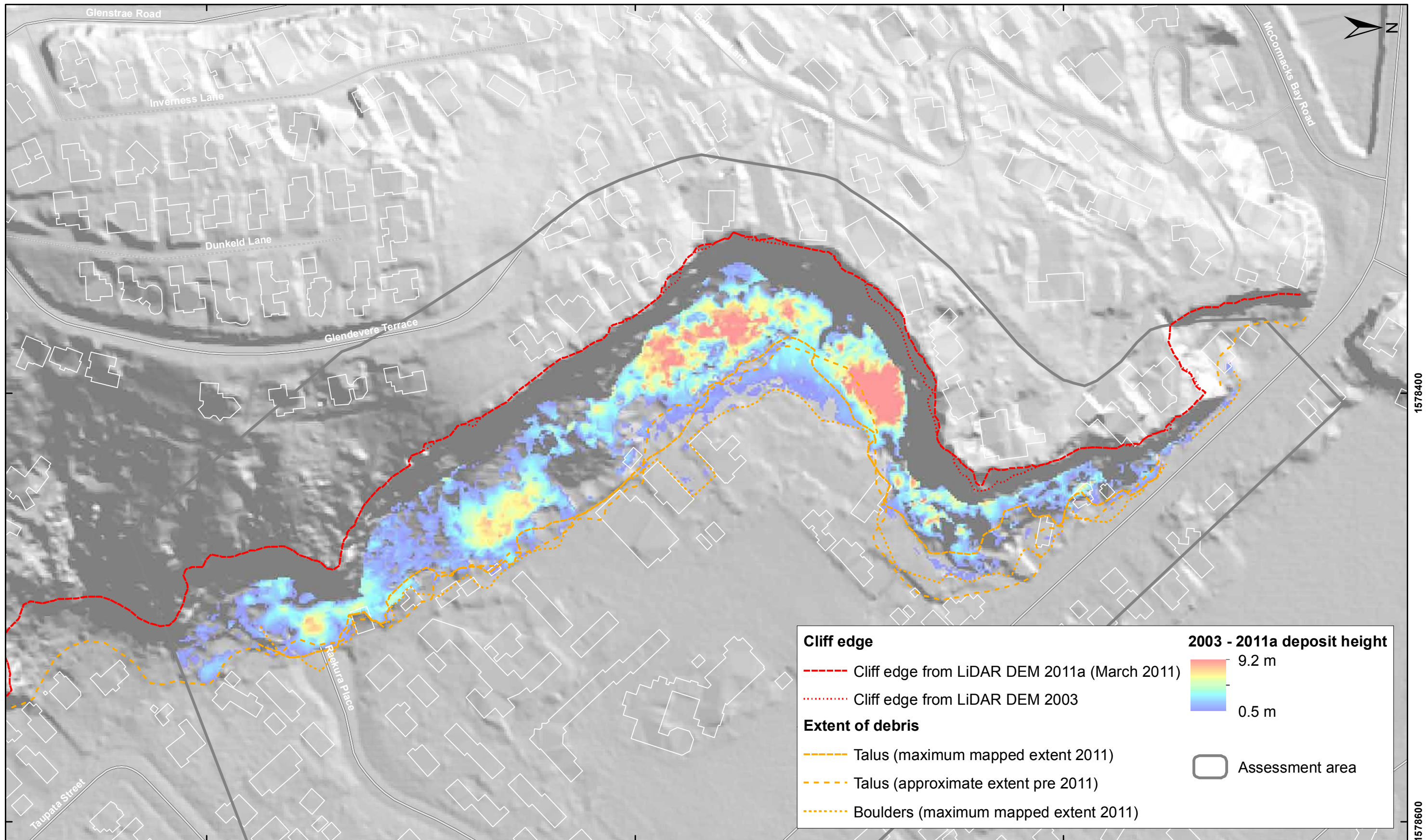
The individual risk per journey is then used to calculate individual risk per year for heavy users of the road, the average expected fatalities per year, and the average time expected between fatal accidents as shown in Table A1.5.

Current New Zealand road traffic accident statistics were used to provide comparison information on the risk road users would face in their ordinary travel along this section of Main Road for a journey of the same length (81 m) as that covered in the risk assessment model.

Table A1.5 Calculation of risk parameters of interest from single cell risk per journey.

Aggregation of Risk Parameters for Cells			
(a) Risk per journey			
Risk R_{ij} for road user j within cell i =	$R1_{ij} + R2_{ij}$		
Risk R_j per journey to road user j =	sum of R_{ij} for all relevant i (all cells on uphill side or downhill side of road, as appropriate)		
(b) Other key risk parameters			
Annual Individual Fatality Risk for user j	$= R_j \times M_{j,ind}$	$M_{j,ind} =$ Journeys/year by individual heavy road user of type j	
Average expected fatalities per year, user j	$= R_j \times M_{j,tot}$	$M_{j,tot} =$ Journeys/year by ALL road users of type j	
Probability of 1 or more fatal accidents/year (road user type j)	$= P_j = 1 - (1-R_j)^{M_{j,tot}}$		
Probability of 1 or more fatal accidents/year (among ALL road users)	$= 1 - (1-P_{car}) \times (1-P_{motorcycle}) \times (1-P_{cycle}) \times (1-P_{pedestrian})$		

A2 APPENDIX 2: RESULTS FROM AIRBORNE LIDAR SURVEYS



Cliff edge

- Cliff edge from LiDAR DEM 2011a (March 2011)
- Cliff edge from LiDAR DEM 2003

Extent of debris

- - - Talus (maximum mapped extent 2011)
- - - Talus (approximate extent pre 2011)
- Boulders (maximum mapped extent 2011)

2003 - 2011a deposit height

9.2 m

0.5 m

□ Assessment area



EXPLANATION:

Background shade model derived from NZAM post earthquake 2011a (March 2011) LiDAR survey resampled to a 1 m ground resolution.
 Roads and building footprints provided by Christchurch City Council (20/02/2012).
 PROJECTION: New Zealand Transverse Mercator 2000

DRW:
DH, BL

CHK:
CM



**RESULTS FROM AIRBORNE LiDAR SURVEYS
 ESTIMATED TALUS DEPOSITS
 2003 - March 2011**

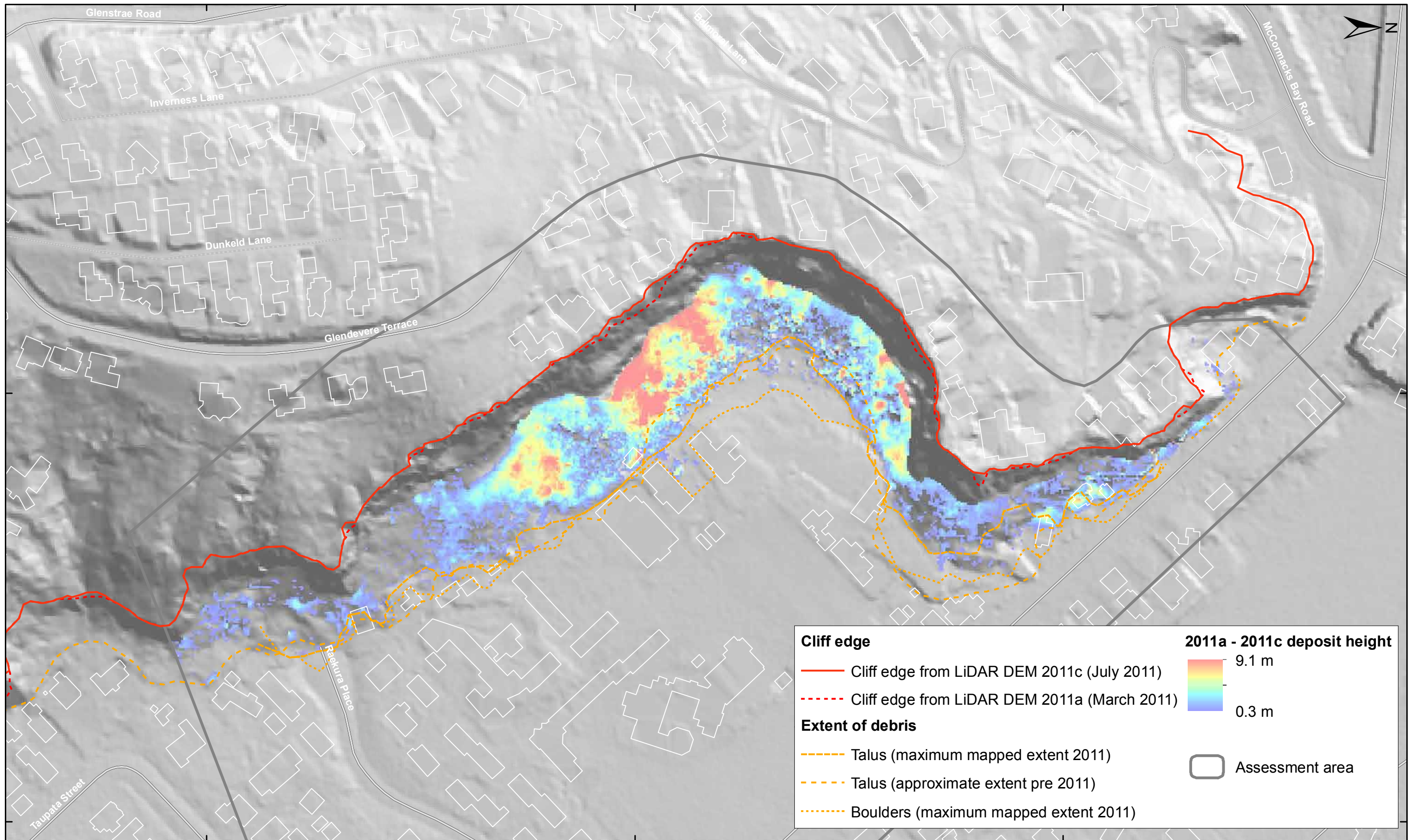
**Redcliffs
 Christchurch**

APPENDIX 2

Map 2

FINAL

REPORT: CR2014/78 DATE: August 2014



Cliff edge

- Cliff edge from LiDAR DEM 2011c (July 2011)
- - - Cliff edge from LiDAR DEM 2011a (March 2011)

Extent of debris

- - - Talus (maximum mapped extent 2011)
- - - Talus (approximate extent pre 2011)
- Boulders (maximum mapped extent 2011)

2011a - 2011c deposit height

9.1 m

0.3 m

□ Assessment area



EXPLANATION:

Background shade model derived from NZAM post earthquake 2011c (July 2011) LiDAR survey resampled to a 1 m ground resolution.
 Roads and building footprints provided by Christchurch City Council (20/02/2012).
 PROJECTION: New Zealand Transverse Mercator 2000

DRW:
DH, BL

CHK:
CM



**RESULTS FROM AIRBORNE LiDAR SURVEYS
 ESTIMATED TALUS DEPOSITS
 March 2011 - July 2011**

**Redcliffs
 Christchurch**

APPENDIX 2

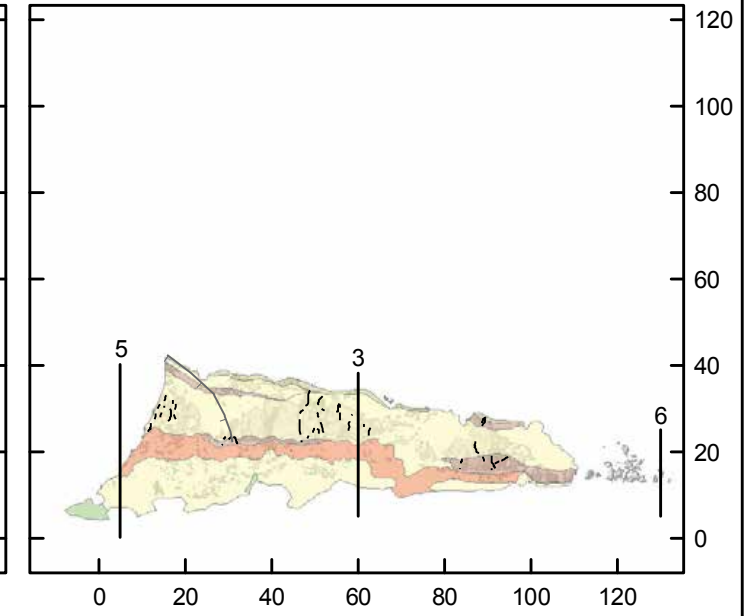
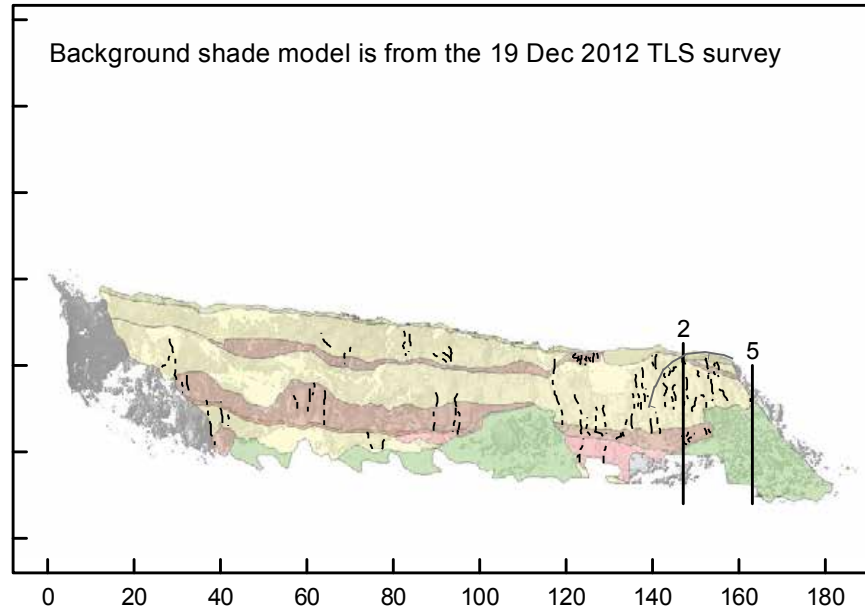
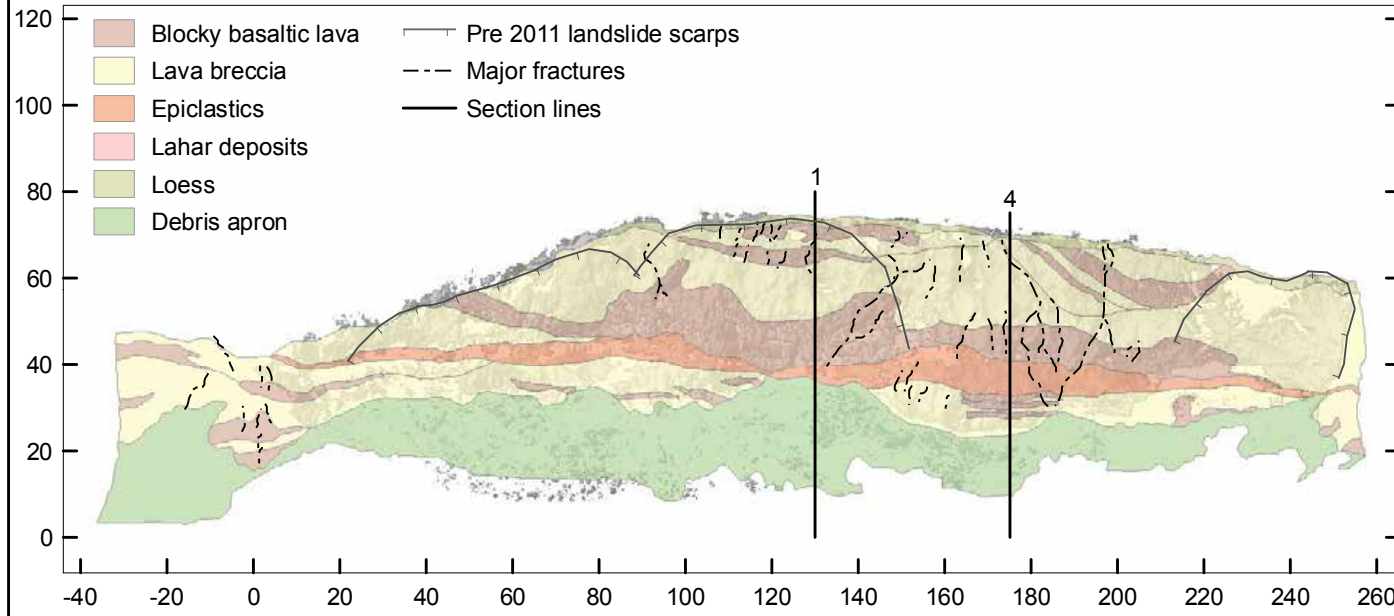
Map 3

FINAL

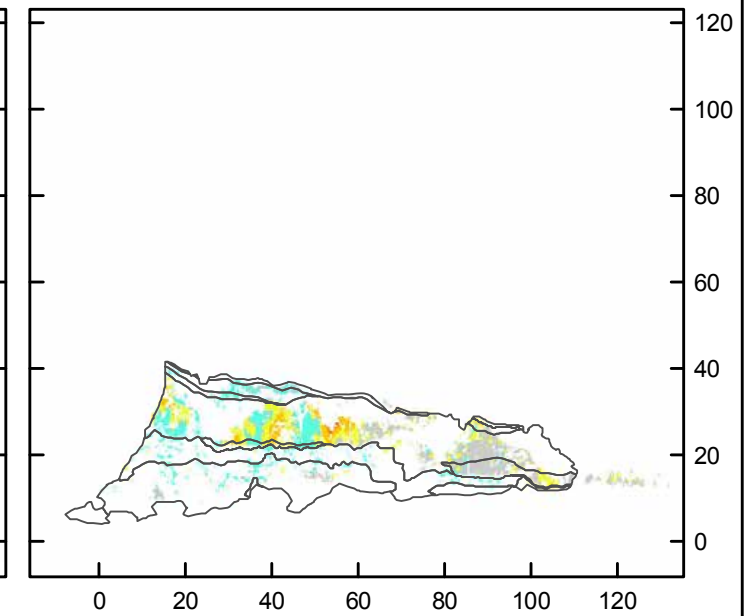
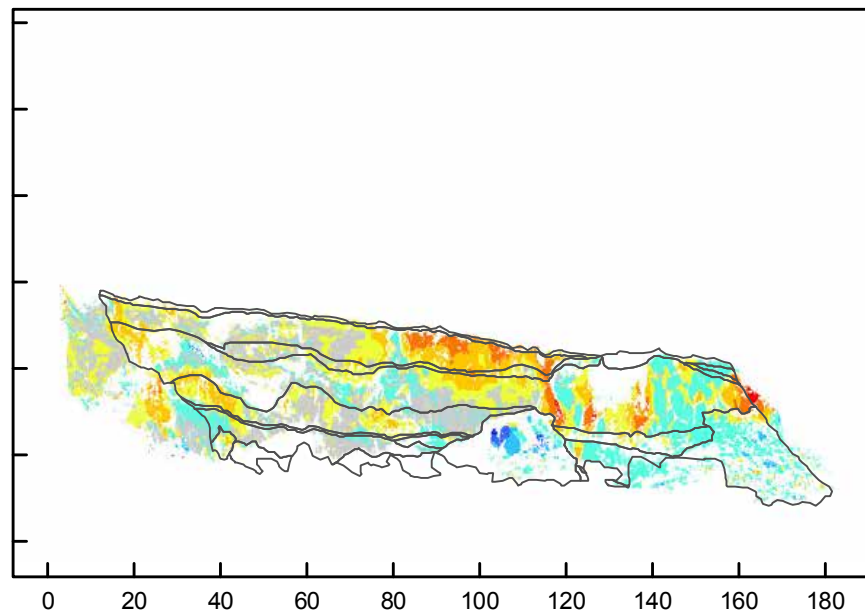
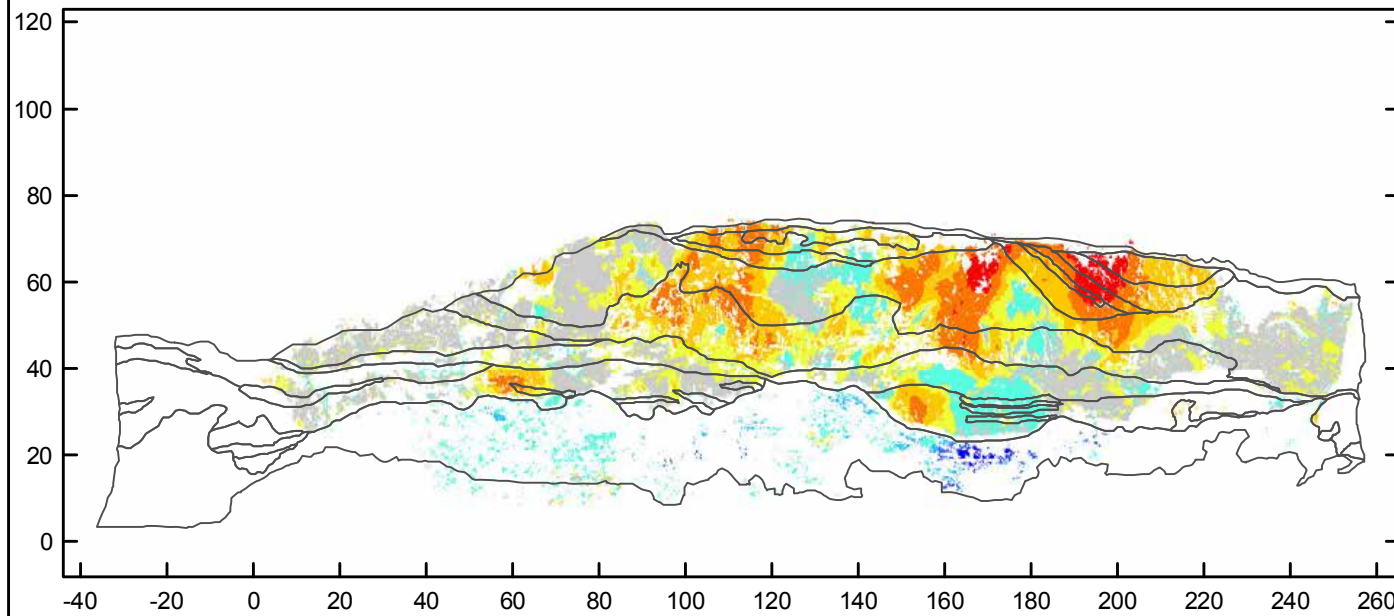
REPORT: CR2014/78 DATE: August 2014

A3 APPENDIX 3: RESULTS FROM TERRESTRIAL LASER SCAN SURVEYS

Geology



Surface change model 2 March 2011 - 19 December 2012

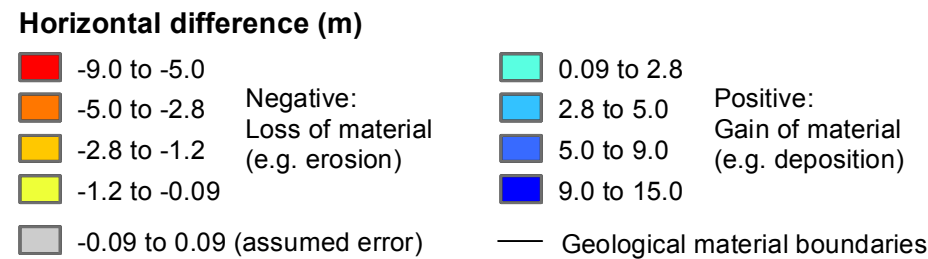


**Surface change model
3 March 2011 - 19 December 2012**

Redcliffs Southwest

Redcliffs Northwest

Redcliffs Road



EXPLANATION:
Surface change models show horizontal changes of the cliff-face surface between given survey dates. Changes in the order of +/- 0.09 m are assumed to be error. The surveys were carried out using RIEGL LMSZ420i terrestrial laser scanner (TLS) in 2011 and 2012. The views are all frontal elevation i.e. as if standing at the bottom of the cliff looking towards it, with the data projected onto the chainage.

DRW:
BL
CHK:
CM



**RESULTS FROM TERRESTRIAL LASER SCAN SURVEYS
CLIFF FRONTAL ELEVATION, GEOLOGY MAP
AND SURFACE CHANGE MODELS**

**Redcliffs
Christchurch**

APPENDIX 3

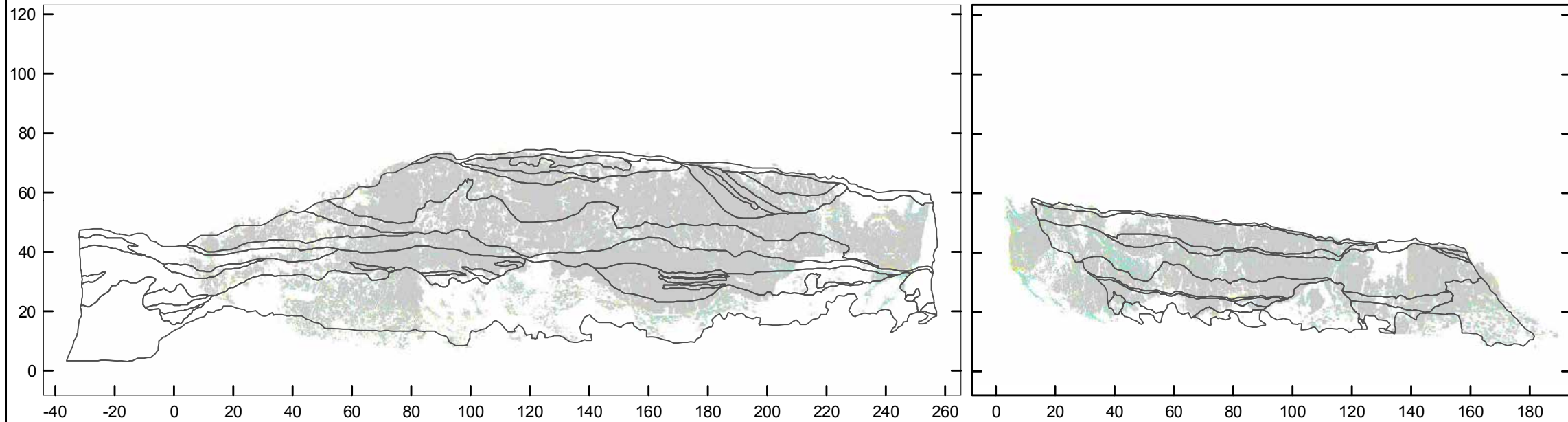
Map 1

FINAL

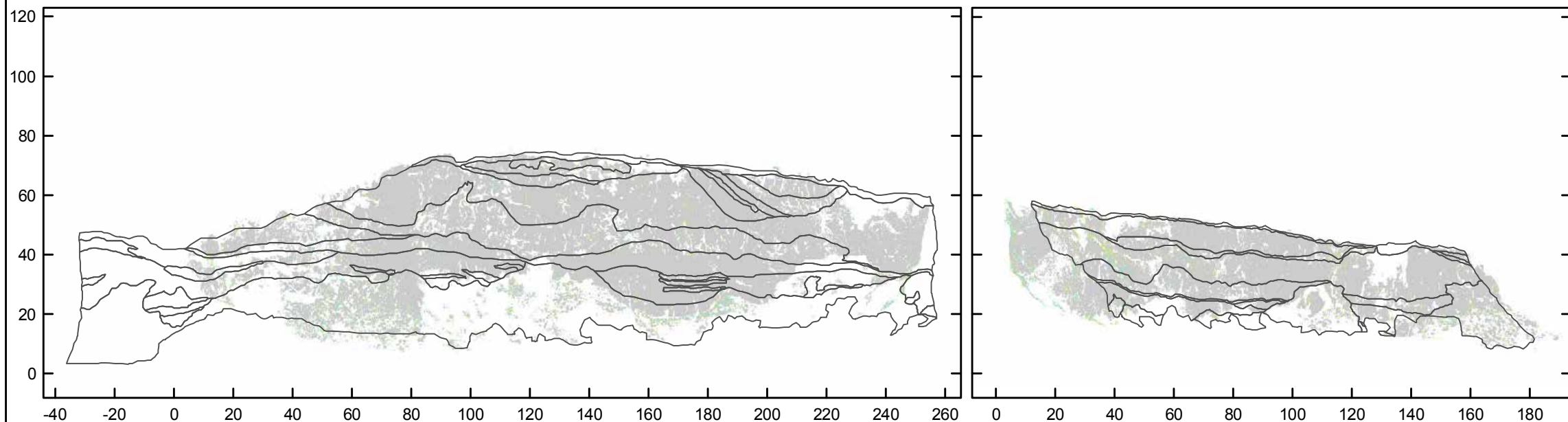
REPORT:
CR2014/78

DATE:
August 2014

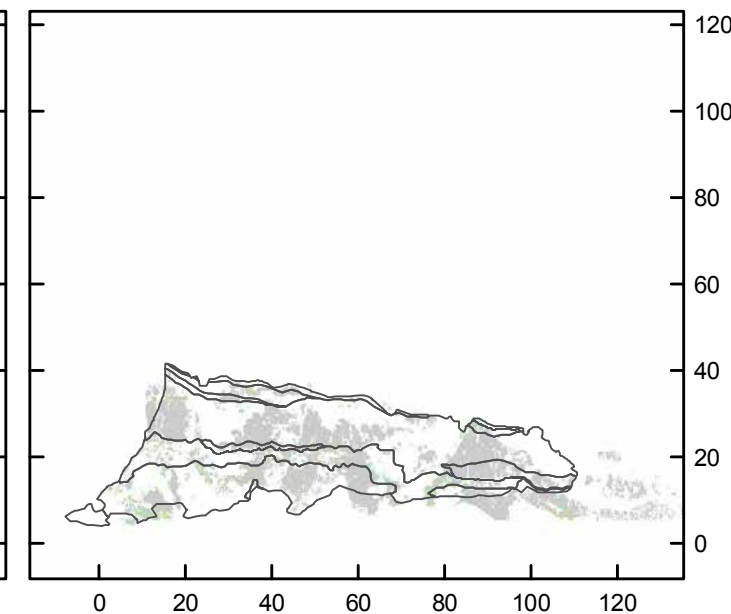
Surface change model 2 March 2011 - 3 March 2011



Surface change model 3 March 2011 - 6 March 2011



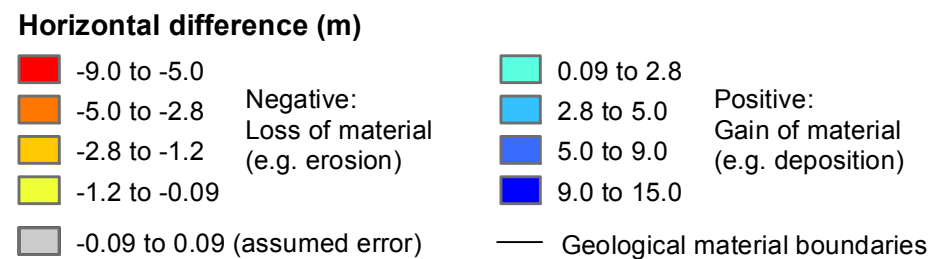
Surface change model
2 March 2011 - 8 March 2011



Redcliffs Southwest

Redcliffs Northwest

Redcliffs Road



EXPLANATION:

Surface change models show horizontal changes of the cliff-face surface between given survey dates. Changes in the order of +/- 0.09 m are assumed to be error. The surveys were carried out using RIEGL LMSZ420i terrestrial laser scanner (TLS) in 2011 and 2012. The views are all frontal elevation i.e. as if standing at the bottom of the cliff looking towards it, with the data projected onto the chainage.

DRW:
BL
CHK:
CM



**RESULTS FROM TERRESTRIAL LASER SCAN SURVEYS
CLIFF FRONTAL ELEVATION, GEOLOGY MAP
AND SURFACE CHANGE MODELS**

**Redcliffs
Christchurch**

APPENDIX 3

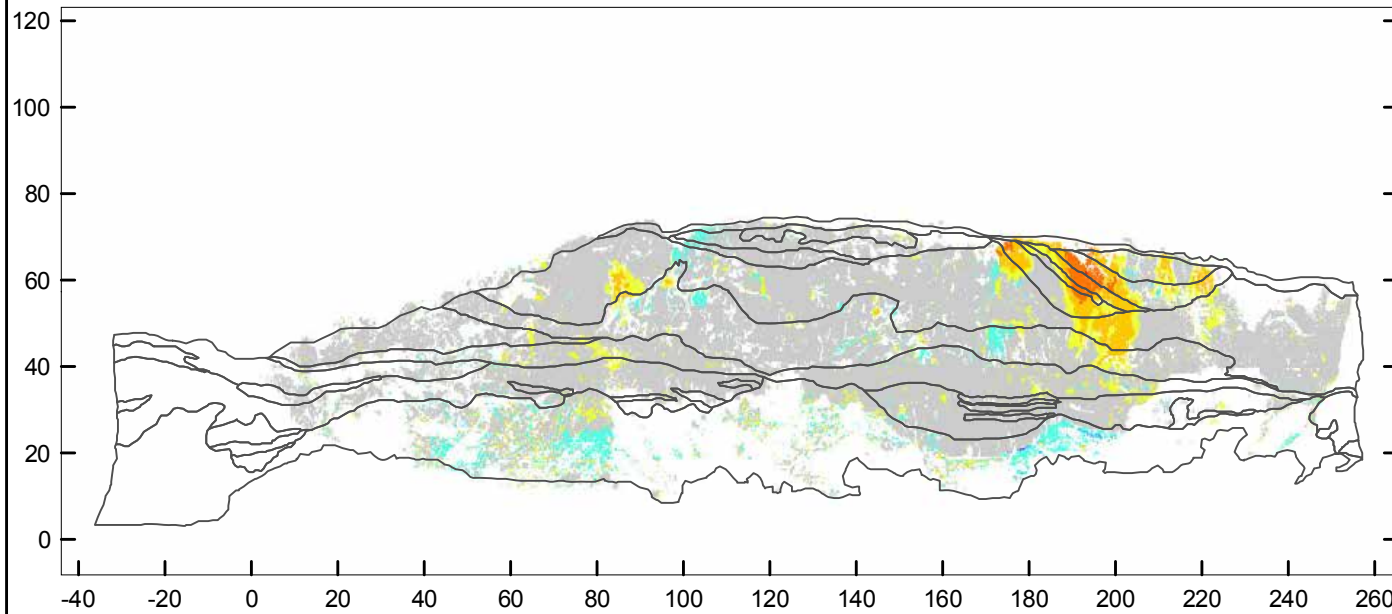
Map 2

FINAL

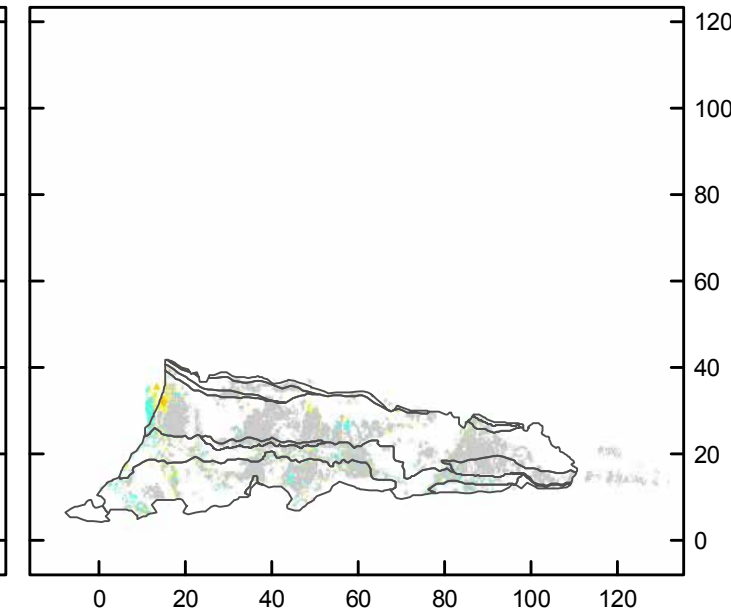
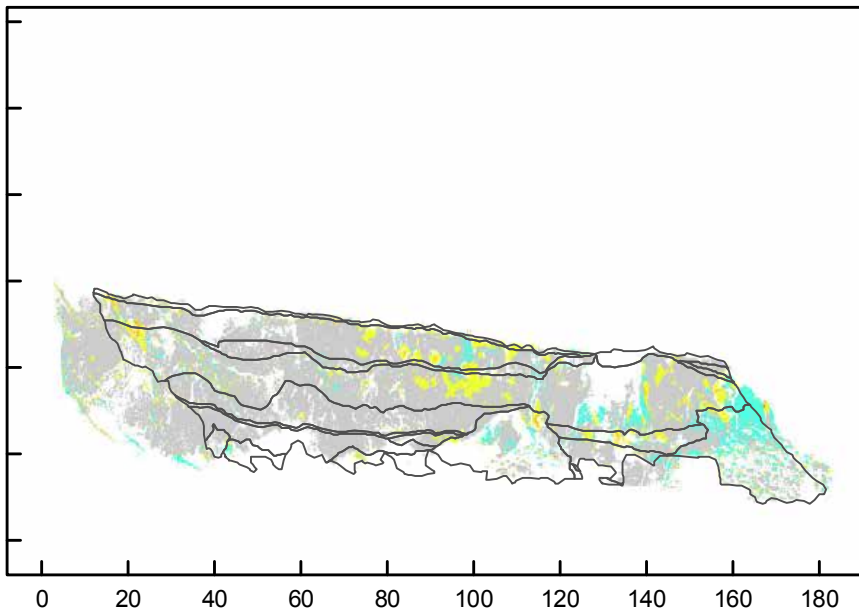
REPORT:
CR2014/78

DATE:
August 2014

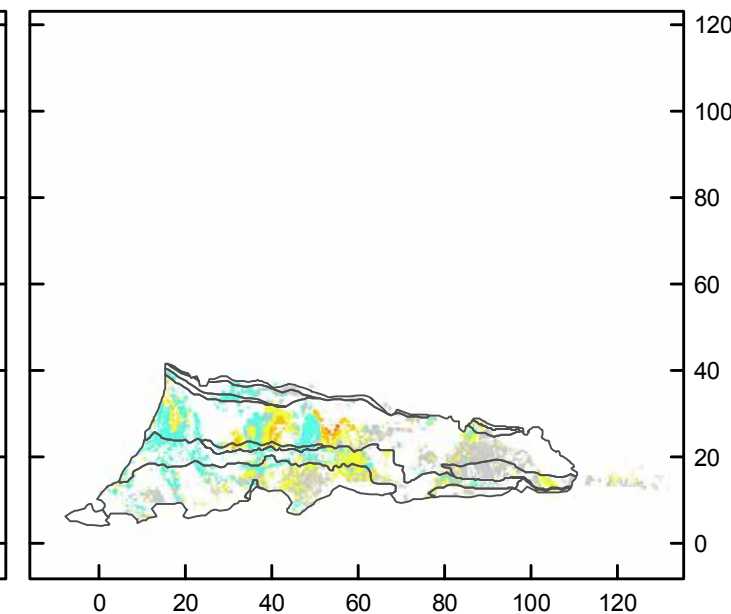
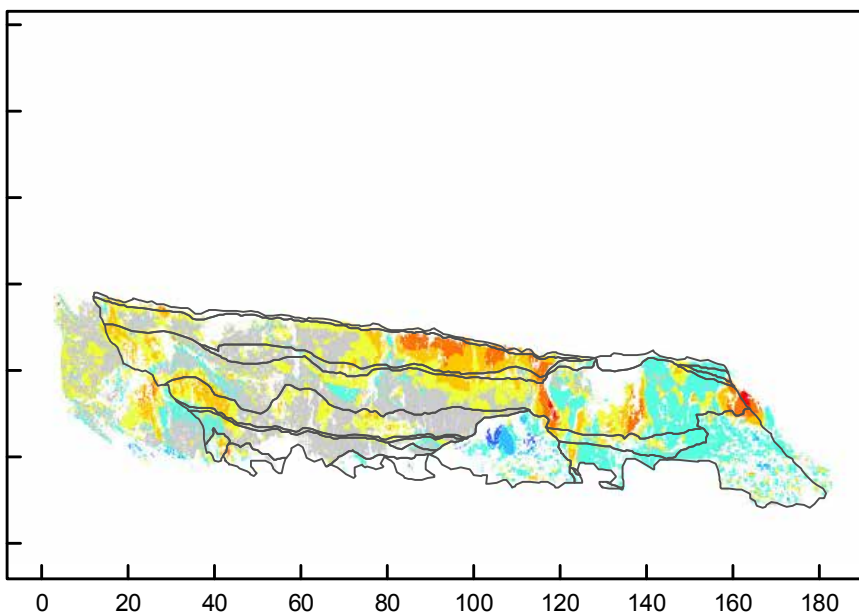
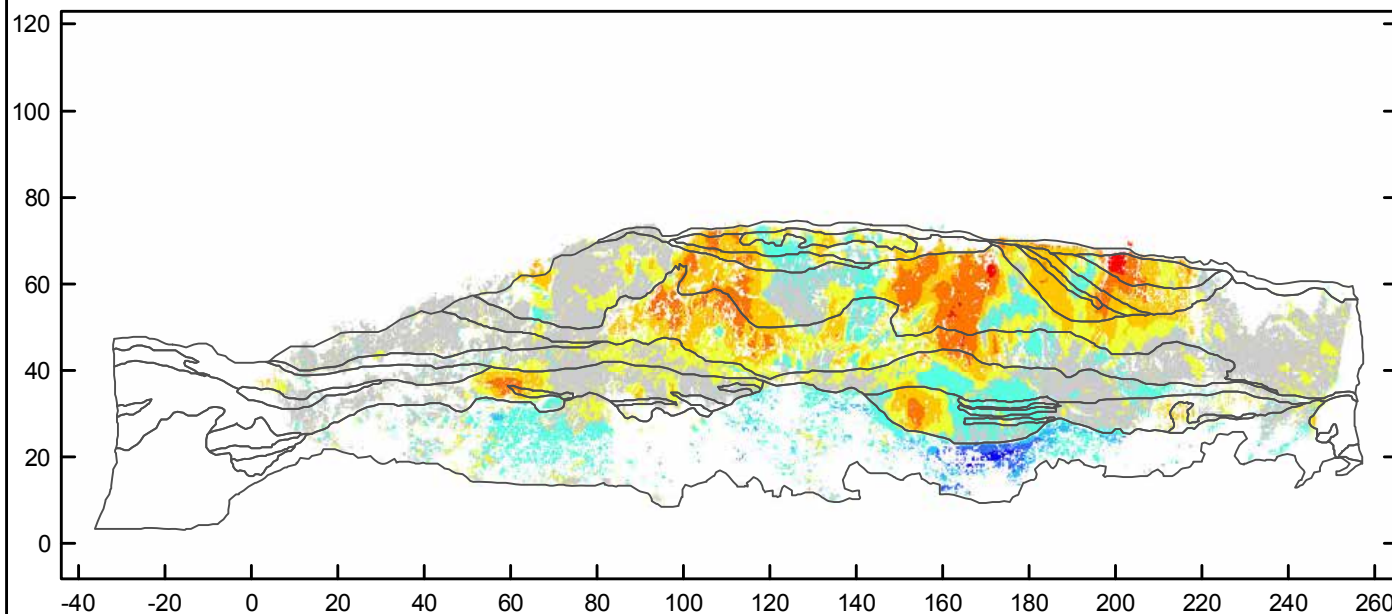
Surface change model 6 March 2011 - 3 May 2011



Surface change model 8 March 2011 - 3 May 2011



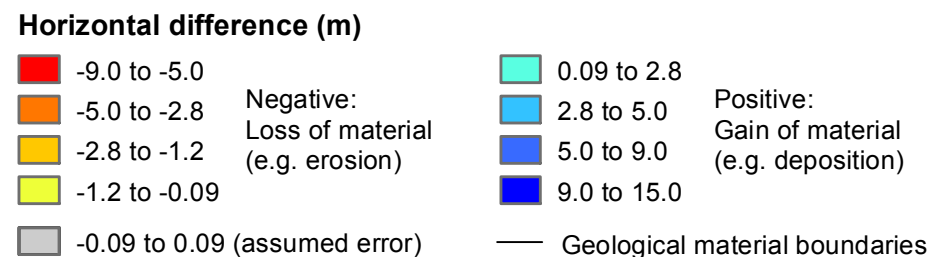
Surface change model 3 May 2011 - 15 June 2011



Redcliffs Southwest

Redcliffs Northwest

Redcliffs Road



EXPLANATION:

Surface change models show horizontal changes of the cliff-face surface between given survey dates. Changes in the order of +/- 0.09 m are assumed to be error. The surveys were carried out using RIEGL LMSZ420i terrestrial laser scanner (TLS) in 2011 and 2012. The views are all frontal elevation i.e. as if standing at the bottom of the cliff looking towards it, with the data projected onto the chainage.

DRW:
BL
CHK:
CM



**RESULTS FROM TERRESTRIAL LASER SCAN SURVEYS
CLIFF FRONTAL ELEVATION, GEOLOGY MAP
AND SURFACE CHANGE MODELS**

**Redcliffs
Christchurch**

APPENDIX 3

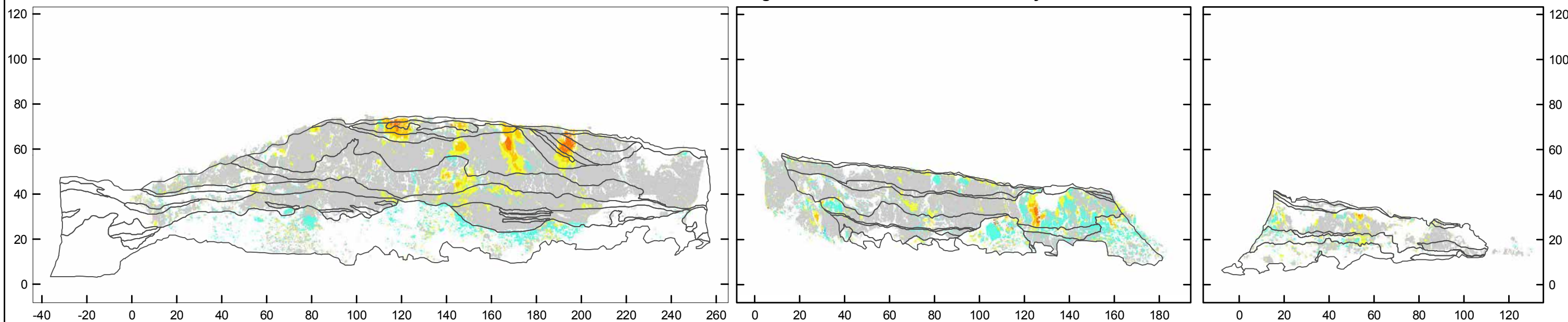
Map 3

FINAL

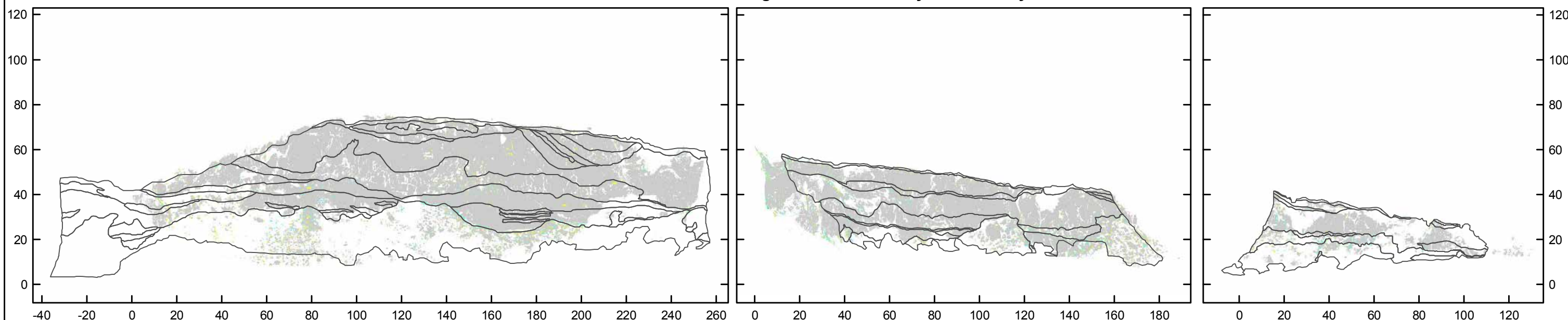
REPORT:
CR2014/78

DATE:
August 2014

Surface change model 15 June 2011 - 18 January 2012



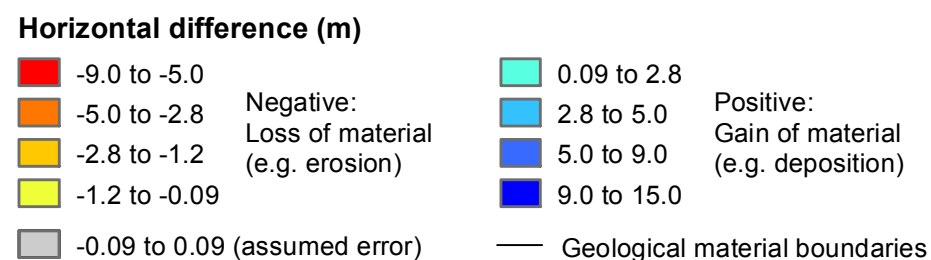
Surface change model 18 January 2012 - 1 May 2012



Redcliffs Southwest

Redcliffs Northwest

Redcliffs Road



EXPLANATION:

Surface change models show horizontal changes of the cliff-face surface between given survey dates. Changes in the order of +/- 0.09 m are assumed to be error. The surveys were carried out using RIEGL LMSZ420i terrestrial laser scanner (TLS) in 2011 and 2012. The views are all frontal elevation i.e. as if standing at the bottom of the cliff looking towards it, with the data projected onto the chainage.

DRW:
BL
CHK:
CM



**RESULTS FROM TERRESTRIAL LASER SCAN SURVEYS
CLIFF FRONTAL ELEVATION, GEOLOGY MAP
AND SURFACE CHANGE MODELS**

**Redcliffs
Christchurch**

APPENDIX 3

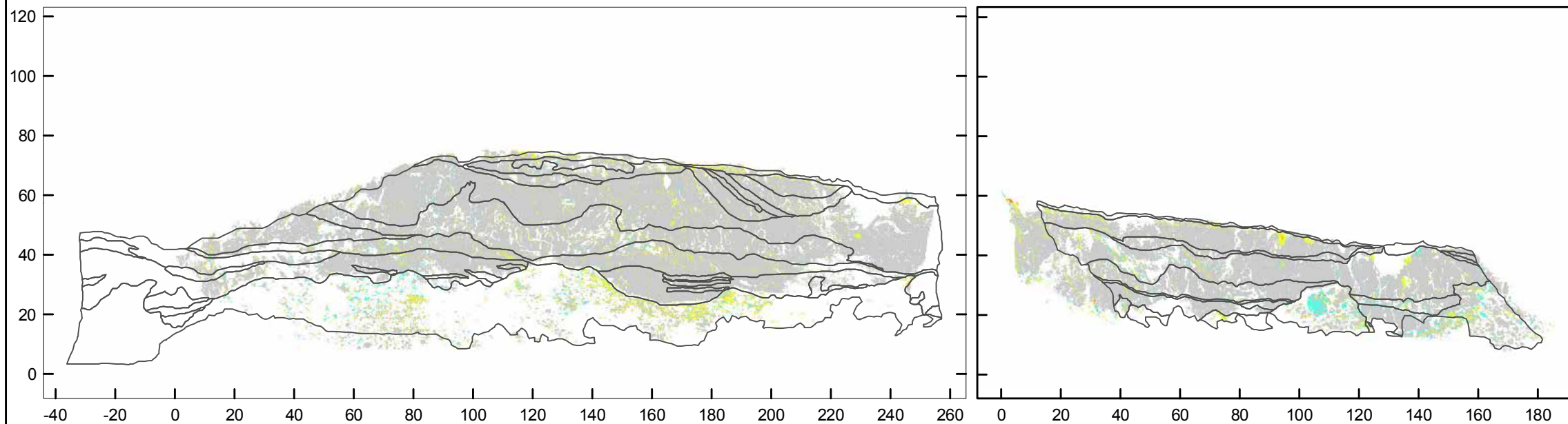
Map 4

FINAL

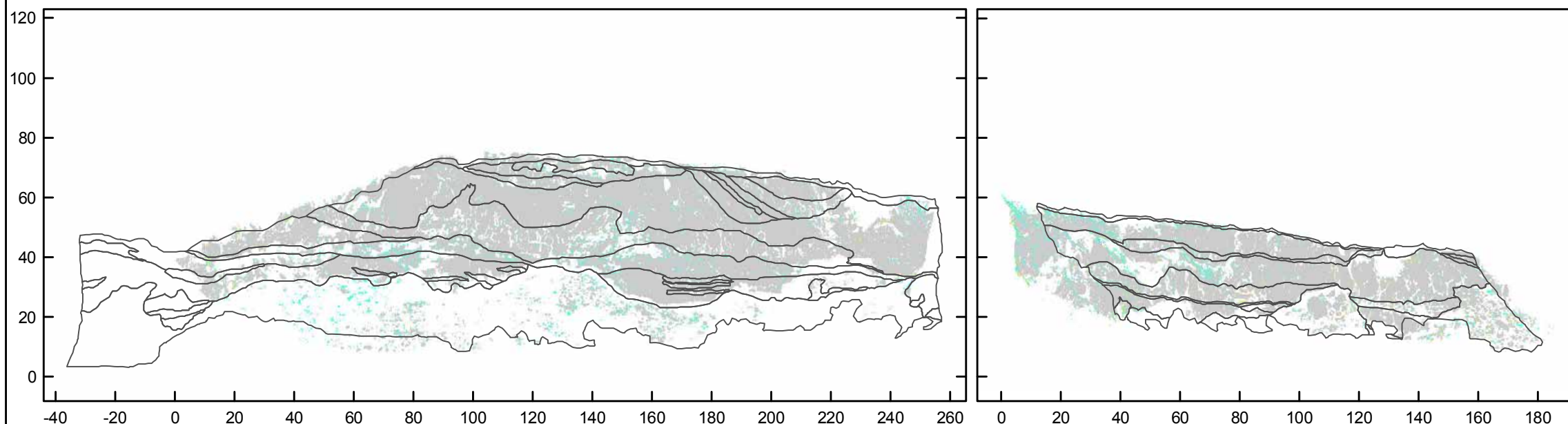
REPORT:
CR2014/78

DATE:
August 2014

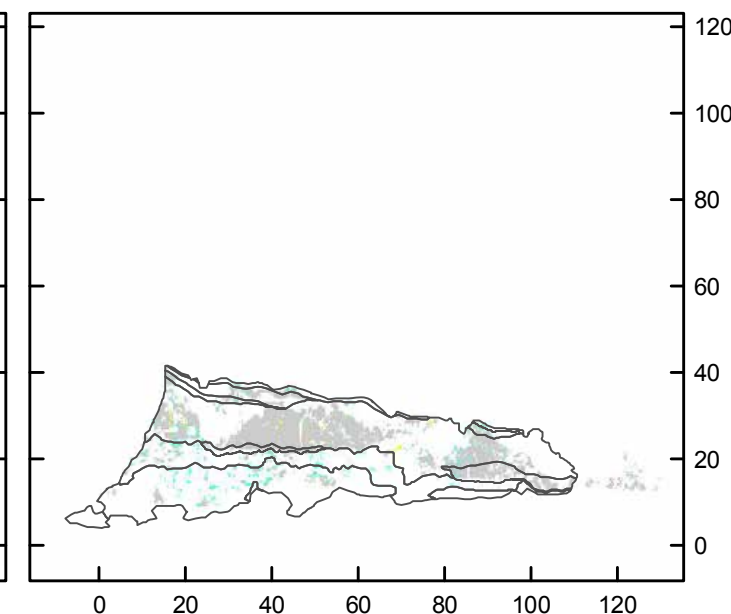
Surface change model 1 May 2012 - 11 September 2012



Surface change model 11 September 2012 - 19 December 2012



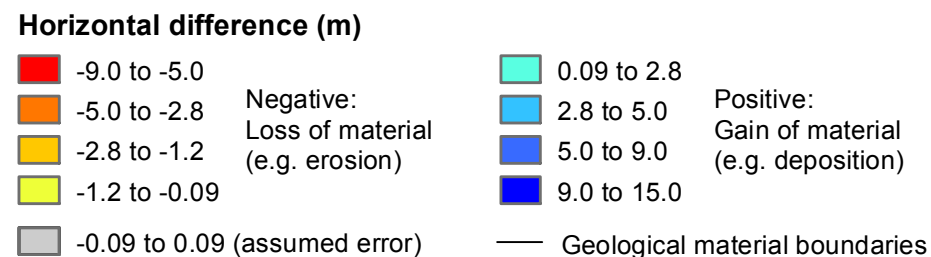
Surface change model 1 May 2012 - 19 December 2012



Redcliffs Southwest

Redcliffs Northwest

Redcliffs Road



EXPLANATION:

Surface change models show horizontal changes of the cliff-face surface between given survey dates. Changes in the order of +/- 0.09 m are assumed to be error. The surveys were carried out using RIEGL LMSZ420i terrestrial laser scanner (TLS) in 2011 and 2012. The views are all frontal elevation i.e. as if standing at the bottom of the cliff looking towards it, with the data projected onto the chainage.

DRW:
BL
CHK:
CM



**RESULTS FROM TERRESTRIAL LASER SCAN SURVEYS
CLIFF FRONTAL ELEVATION, GEOLOGY MAP
AND SURFACE CHANGE MODELS**

**Redcliffs
Christchurch**

APPENDIX 3

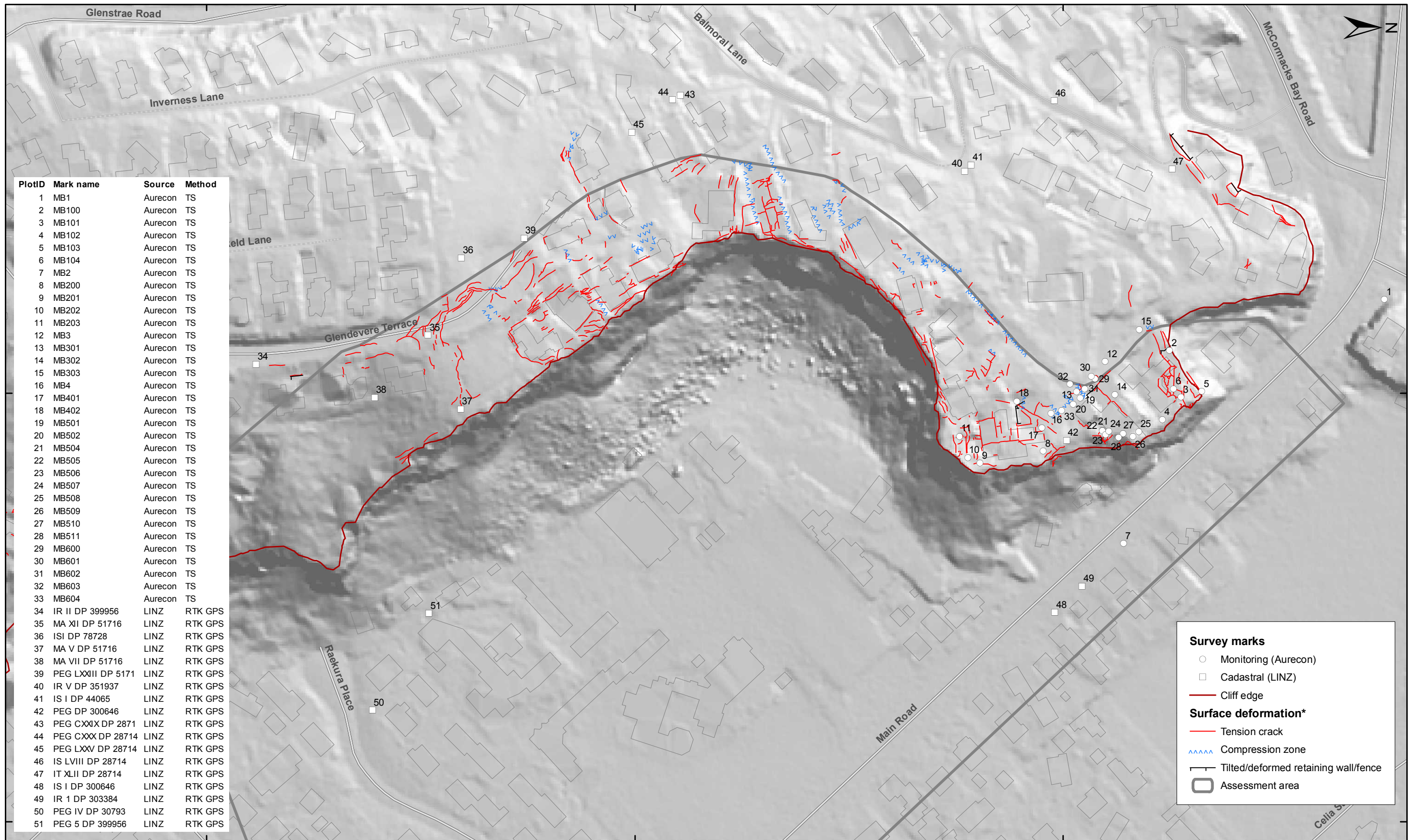
Map 5

FINAL

REPORT:
CR2014/78

DATE:
August 2014

**A4 APPENDIX 4: RESULTS FROM SURVEYS OF CADASTRAL AND
MONITORING SURVEY MARKS**



PlotID	Mark name	Source	Method
1	MB1	Aurecon	TS
2	MB100	Aurecon	TS
3	MB101	Aurecon	TS
4	MB102	Aurecon	TS
5	MB103	Aurecon	TS
6	MB104	Aurecon	TS
7	MB2	Aurecon	TS
8	MB200	Aurecon	TS
9	MB201	Aurecon	TS
10	MB202	Aurecon	TS
11	MB203	Aurecon	TS
12	MB3	Aurecon	TS
13	MB301	Aurecon	TS
14	MB302	Aurecon	TS
15	MB303	Aurecon	TS
16	MB4	Aurecon	TS
17	MB401	Aurecon	TS
18	MB402	Aurecon	TS
19	MB501	Aurecon	TS
20	MB502	Aurecon	TS
21	MB504	Aurecon	TS
22	MB505	Aurecon	TS
23	MB506	Aurecon	TS
24	MB507	Aurecon	TS
25	MB508	Aurecon	TS
26	MB509	Aurecon	TS
27	MB510	Aurecon	TS
28	MB511	Aurecon	TS
29	MB600	Aurecon	TS
30	MB601	Aurecon	TS
31	MB602	Aurecon	TS
32	MB603	Aurecon	TS
33	MB604	Aurecon	TS
34	IR II DP 399956	LINZ	RTK GPS
35	MA XII DP 51716	LINZ	RTK GPS
36	ISI DP 78728	LINZ	RTK GPS
37	MA V DP 51716	LINZ	RTK GPS
38	MA VII DP 51716	LINZ	RTK GPS
39	PEG LXIII DP 5171	LINZ	RTK GPS
40	IR V DP 351937	LINZ	RTK GPS
41	IS I DP 44065	LINZ	RTK GPS
42	PEG DP 300646	LINZ	RTK GPS
43	PEG CXXIX DP 2871	LINZ	RTK GPS
44	PEG CXXX DP 28714	LINZ	RTK GPS
45	PEG LXXV DP 28714	LINZ	RTK GPS
46	IS LVIII DP 28714	LINZ	RTK GPS
47	IT XLII DP 28714	LINZ	RTK GPS
48	IS I DP 300646	LINZ	RTK GPS
49	IR 1 DP 303384	LINZ	RTK GPS
50	PEG IV DP 30793	LINZ	RTK GPS
51	PEG 5 DP 399956	LINZ	RTK GPS

Survey marks

- Monitoring (Aurecon)
- Cadastral (LINZ)
- Cliff edge

Surface deformation*

- Tension crack
- ~~~~~ Compression zone
- Tilted/deformed retaining wall/fence
- Assessment area



EXPLANATION:
 * Taken from the report CR2012/317
 Background shade model derived from NZAM post earthquake 2011c (July 2011) LiDAR survey resampled to a 1 m ground resolution.
 Roads and building footprints provided by Christchurch City Council (20/02/2012).
 PROJECTION: New Zealand Transverse Mercator 2000

DRW:
BL
 CHK:
CM, GA, FDP



**SURVEY MARKS
Index Map**

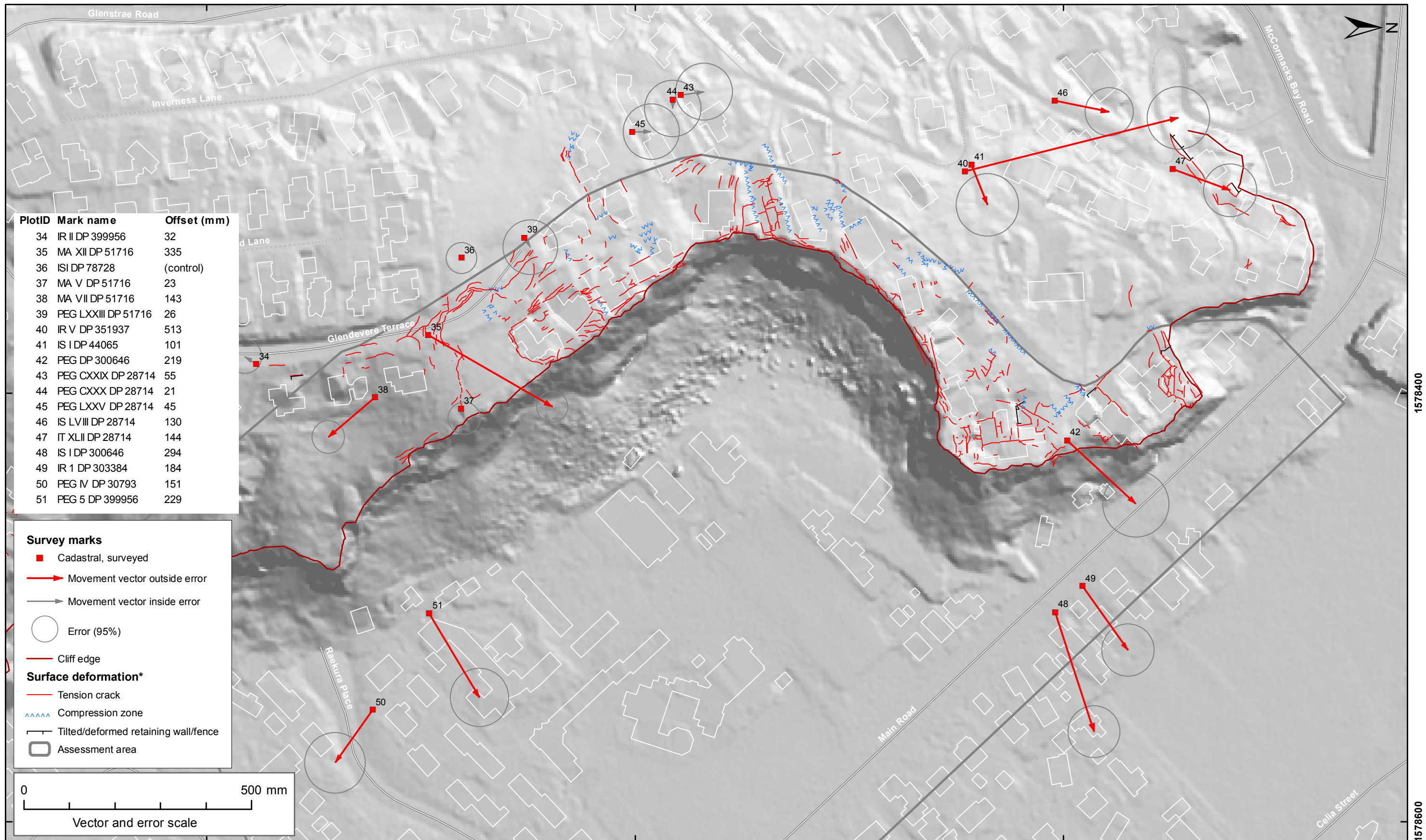
**Redcliffs
Christchurch**

APPENDIX 4

Map 1

FINAL

REPORT: CR2014/78 DATE: August 2014

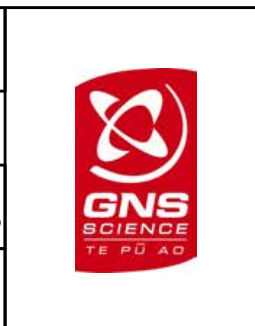


SCALE BAR: 0 50 100 m

EXPLANATION:
 * Taken from the report CR2012/317
 Background shade model derived from NZAM post earthquake 2011c (July 2011) LiDAR survey resampled to a 1 m ground resolution.
 Roads and building footprints provided by Christchurch City Council (20/02/2012).
 PROJECTION: New Zealand Transverse Mercator 2000

DRW:
BL

CHK:
CM, GA, FDP



MOVEMENT VECTORS
Cadastral Marks (Source: LINZ)
Total Movement - Pre 22-02-2011 to 11-02-2012

Redcliffs
Christchurch

APPENDIX 4

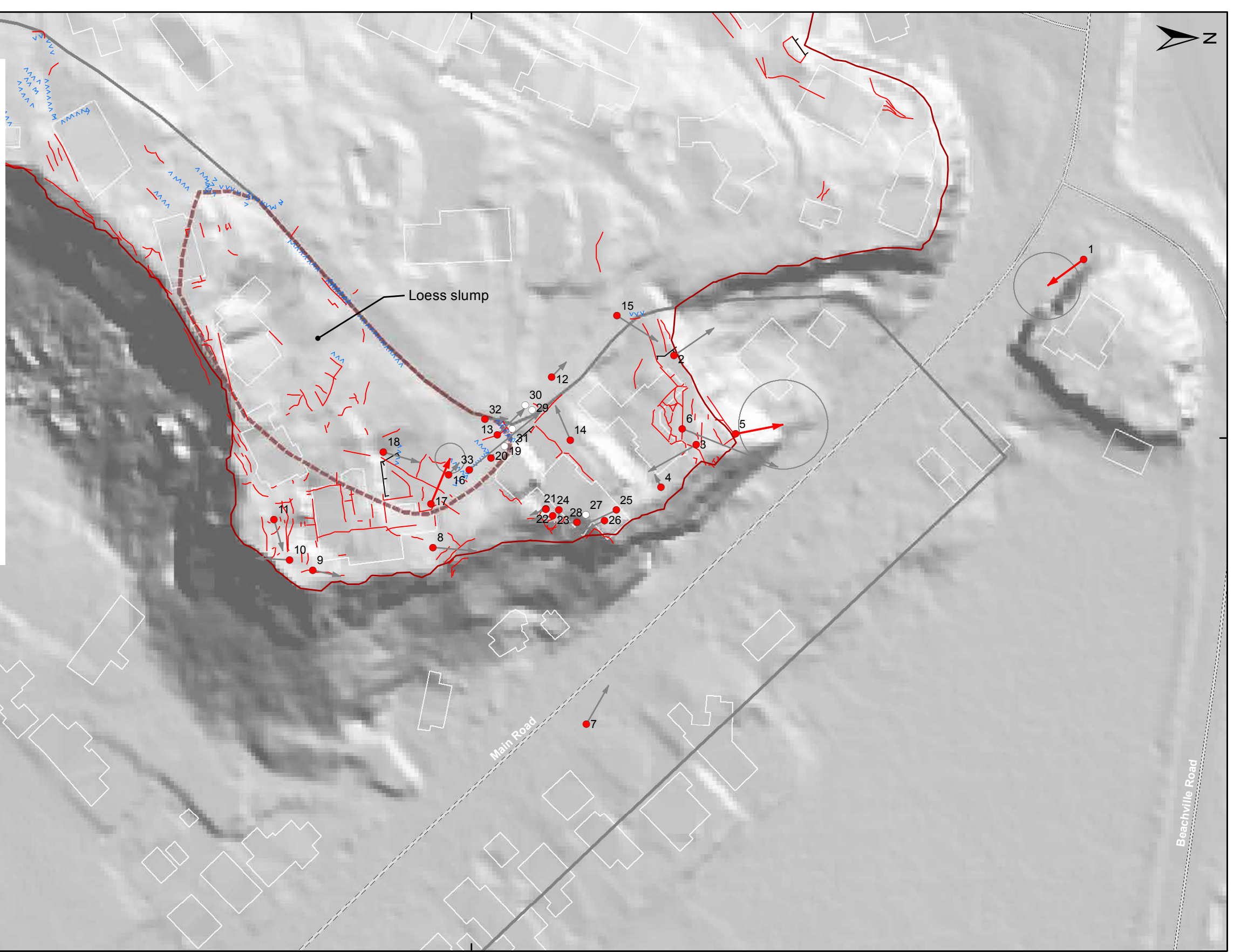
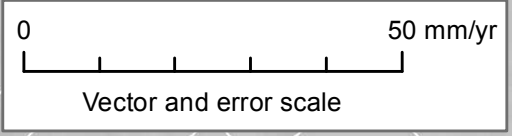
Map 2

FINAL

REPORT: CR2014/78 DATE: August 2014

PlotID	Mark name	Rate (mm/yr)	StartDate	EndDate
1	MB1	11	5/11/2012	5/04/2013
2	MB100	12	5/11/2012	5/04/2013
3	MB101	14	5/11/2012	5/04/2013
4	MB102	4	5/11/2012	5/04/2013
5	MB103	12	5/11/2012	5/04/2013
6	MB104	25	5/11/2012	5/04/2013
7	MB2	11	5/11/2012	5/04/2013
8	MB200	11	5/11/2012	5/04/2013
9	MB201	7	5/11/2012	5/04/2013
10	MB202	8	5/11/2012	5/04/2013
11	MB203	8	5/11/2012	5/04/2013
14	MB302	9	5/11/2012	5/04/2013
18	MB402	9	5/11/2012	5/04/2013
12	MB3	5	5/11/2012	21/05/2013
13	MB301	9	5/11/2012	28/06/2013
15	MB303	12	5/11/2012	28/06/2013
16	MB4	4	5/11/2012	28/06/2013
17	MB401	12	5/11/2012	28/06/2013
20	MB502	1	5/11/2012	28/06/2013
21	MB504	2	5/11/2012	28/06/2013
22	MB505	4	5/11/2012	28/06/2013
23	MB506	5	5/11/2012	28/06/2013
24	MB507	6	5/11/2012	28/06/2013
25	MB508	12	5/11/2012	28/06/2013
26	MB509	8	5/11/2012	28/06/2013
28	MB511	8	5/11/2012	28/06/2013
32	MB603	6	5/11/2012	28/06/2013
33	MB604	23	5/11/2012	28/06/2013

- Survey marks**
- Monitoring, surveyed
 - Monitoring, non-surveyed
 - ➔ Movement vector outside error
 - ➔ Movement vector inside error
 - Error (95%)
 - Cliff edge
- Surface deformation****
- Tension crack
 - AAAAA Compression zone
 - Tilted/deformed retaining wall/fence
 - Assessment area



EXPLANATION:
 * Movement with assumed earthquake induced landslide movement and tectonic (earthquake) movement removed. Movement estimated from least squares adjustment (assuming a linear trend).
 ** Taken from report CR2012/317
 Background shade model derived from NZAM post earthquake 2011c (July 2011) LiDAR survey resampled to a 1 m ground resolution.
 Roads and building footprints provided by Christchurch City Council (20/02/2012).
 PROJECTION: New Zealand Transverse Mercator 2000

DRW:
BL

CHK:
CM, GA, FDP



MOVEMENT VECTORS
Monitoring Marks (Source: Aurecon NZ Ltd)
Filtered Linear Movement*

Redcliffs
Christchurch

APPENDIX 4

Map 3

FINAL

REPORT: CR2014/78	DATE: August 2014
----------------------	----------------------

A5 APPENDIX 5: FIELD MAPPING OF CRACKS FOLLOWING THE MAIN EARTHQUAKES (CARRIED OUT BY M. YETTON, GEOTECH LTD)



SHEET 1






SHEET 2

LEGEND

Observed Cracks and Deformation
(ground, buildings, landscaping etc)
with crack widths and other features
noted as mapped:


-  25 RED - Mapped 05 March 2011
-  25 YELLOW - Mapped May 2011
(crack width changes and observations may also be noted on previously recorded cracks)
-  25 BLUE - Mapped June 2011
(crack width changes and observations may also be noted on previously recorded cracks)
-  25 GREEN - Mapped September 2011
(crack width changes and observations may also be noted on previously recorded cracks)

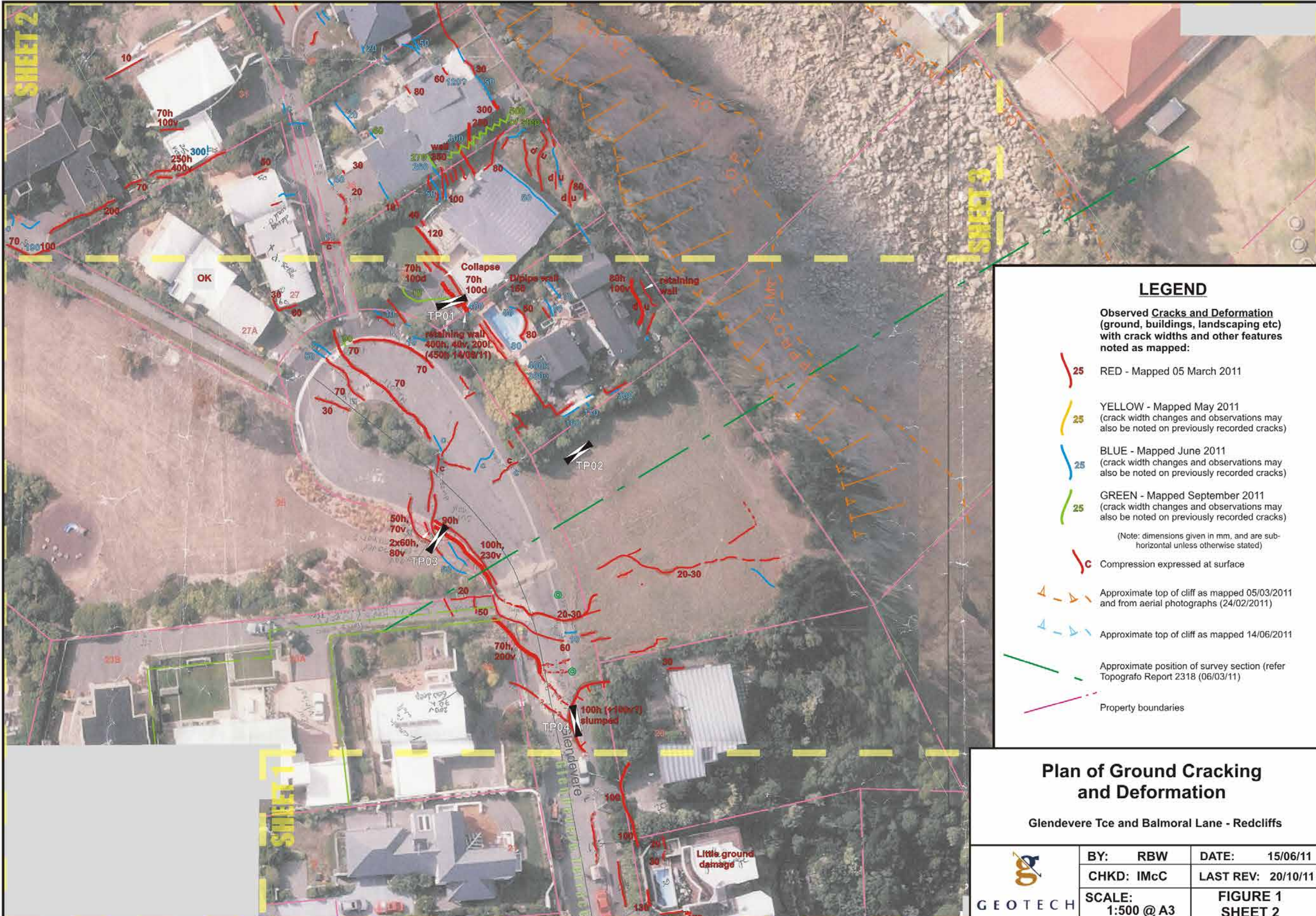
(Note: dimensions given in mm, and are sub-horizontal unless otherwise stated)

-  C Compression expressed at surface
-  Approximate top of cliff as mapped 05/03/2011 and from aerial photographs (24/02/2011)
-  Approximate top of cliff as mapped 14/06/2011
-  Approximate position of survey section (refer Topografo Report 2318 (06/03/11))
-  Property boundaries

Plan of Ground Cracking and Deformation

Glendevore Tce and Balmoral Lane - Redcliffs

 GEOTECH	BY: RBW	DATE: 15/06/11
	CHKD: IMcC	LAST REV: 20/10/11
	SCALE: 1:500 @ A3	FIGURE 1 SHEET 1



LEGEND

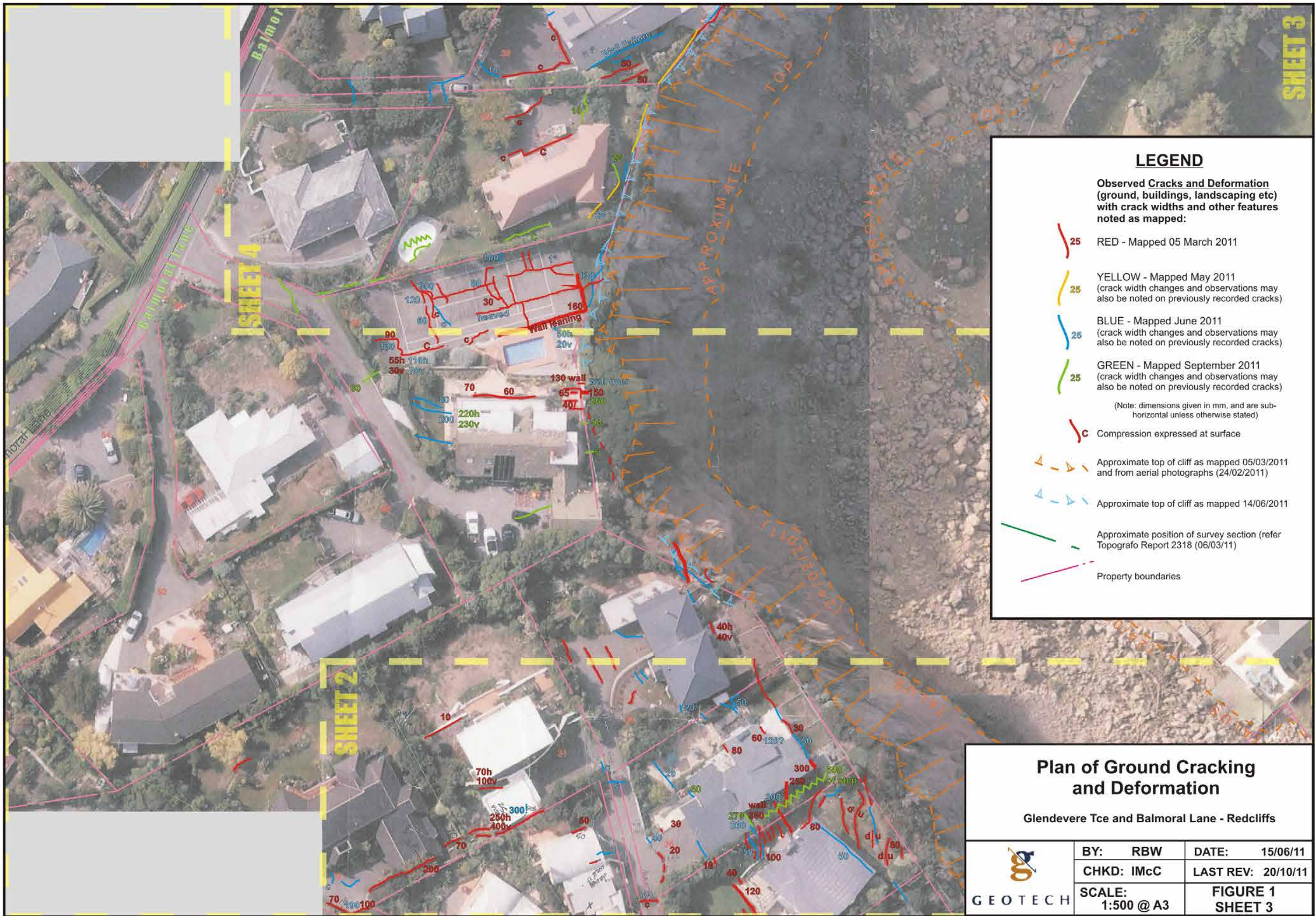
Observed Cracks and Deformation (ground, buildings, landscaping etc) with crack widths and other features noted as mapped:

- 25 RED - Mapped 05 March 2011
- 25 YELLOW - Mapped May 2011 (crack width changes and observations may also be noted on previously recorded cracks)
- 25 BLUE - Mapped June 2011 (crack width changes and observations may also be noted on previously recorded cracks)
- 25 GREEN - Mapped September 2011 (crack width changes and observations may also be noted on previously recorded cracks)
- (Note: dimensions given in mm, and are sub-horizontal unless otherwise stated)
- c Compression expressed at surface
- Approximate top of cliff as mapped 05/03/2011 and from aerial photographs (24/02/2011)
- Approximate top of cliff as mapped 14/06/2011
- Approximate position of survey section (refer Topografo Report 2318 (06/03/11))
- Property boundaries

Plan of Ground Cracking and Deformation

Glendever Tce and Balmoral Lane - Redcliffs

	BY: RBW	DATE: 15/06/11
	CHKD: IMcC	LAST REV: 20/10/11
	SCALE: 1:500 @ A3	FIGURE 1 SHEET 2



LEGEND

Observed Cracks and Deformation (ground, buildings, landscaping etc) with crack widths and other features noted as mapped:

- 25 RED - Mapped 05 March 2011
 - 25 YELLOW - Mapped May 2011 (crack width changes and observations may also be noted on previously recorded cracks)
 - 25 BLUE - Mapped June 2011 (crack width changes and observations may also be noted on previously recorded cracks)
 - 25 GREEN - Mapped September 2011 (crack width changes and observations may also be noted on previously recorded cracks)
- (Note: dimensions given in mm, and are sub-horizontal unless otherwise stated)
- C Compression expressed at surface
 - - - Approximate top of cliff as mapped 05/03/2011 and from aerial photographs (24/02/2011)
 - - - Approximate top of cliff as mapped 14/06/2011
 - - - Approximate position of survey section (refer Topografo Report 2318 (06/03/11))
 - - - Property boundaries









Plan of Ground Cracking and Deformation

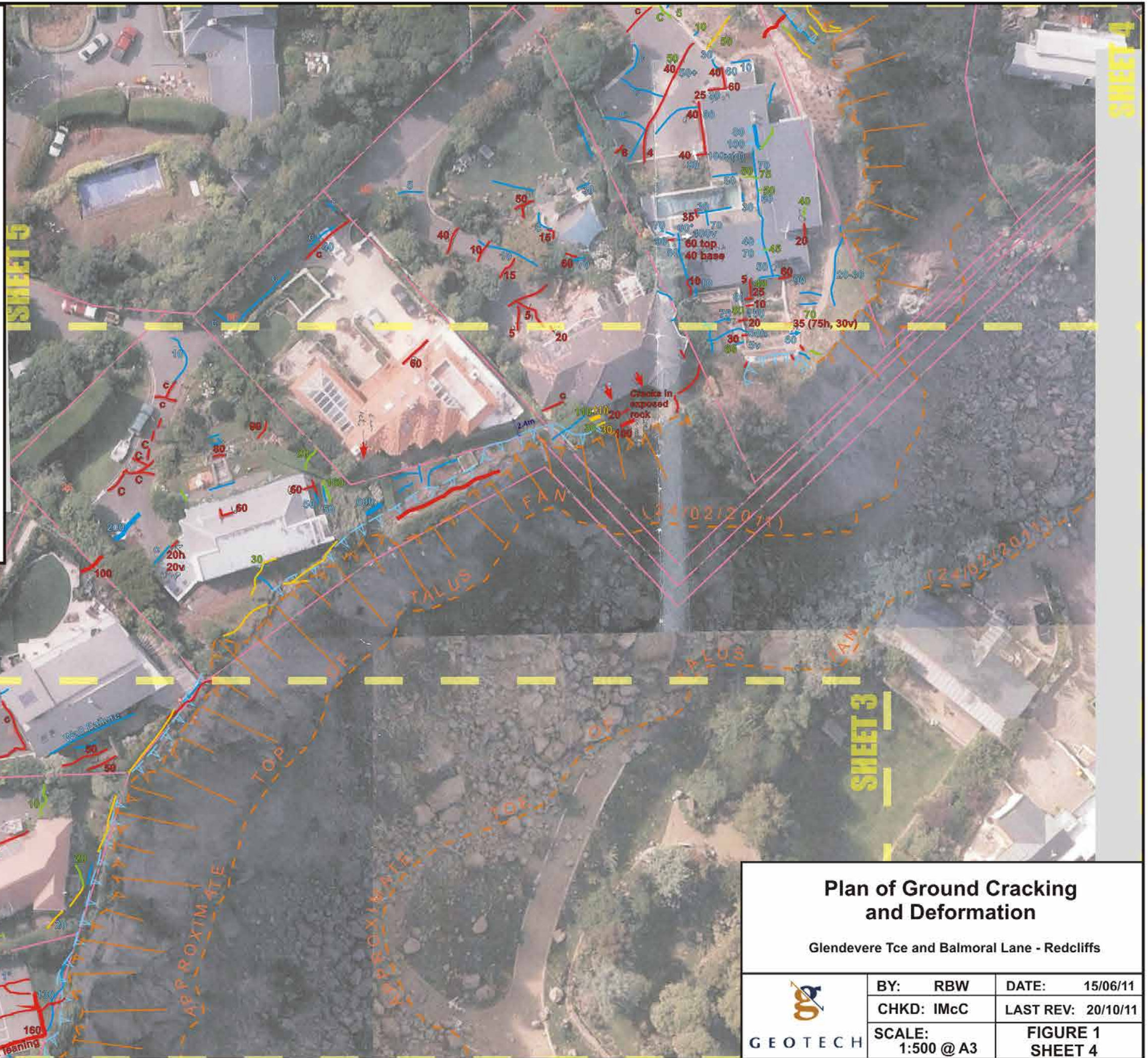
Glendevore Tce and Balmoral Lane - Redcliffs

 GEOTECH	BY: RBW	DATE: 15/06/11
	CHKD: IMcC	LAST REV: 20/10/11
	SCALE: 1:500 @ A3	FIGURE 1 SHEET 3

LEGEND


Observed Cracks and Deformation (ground, buildings, landscaping etc) with crack widths and other features noted as mapped:

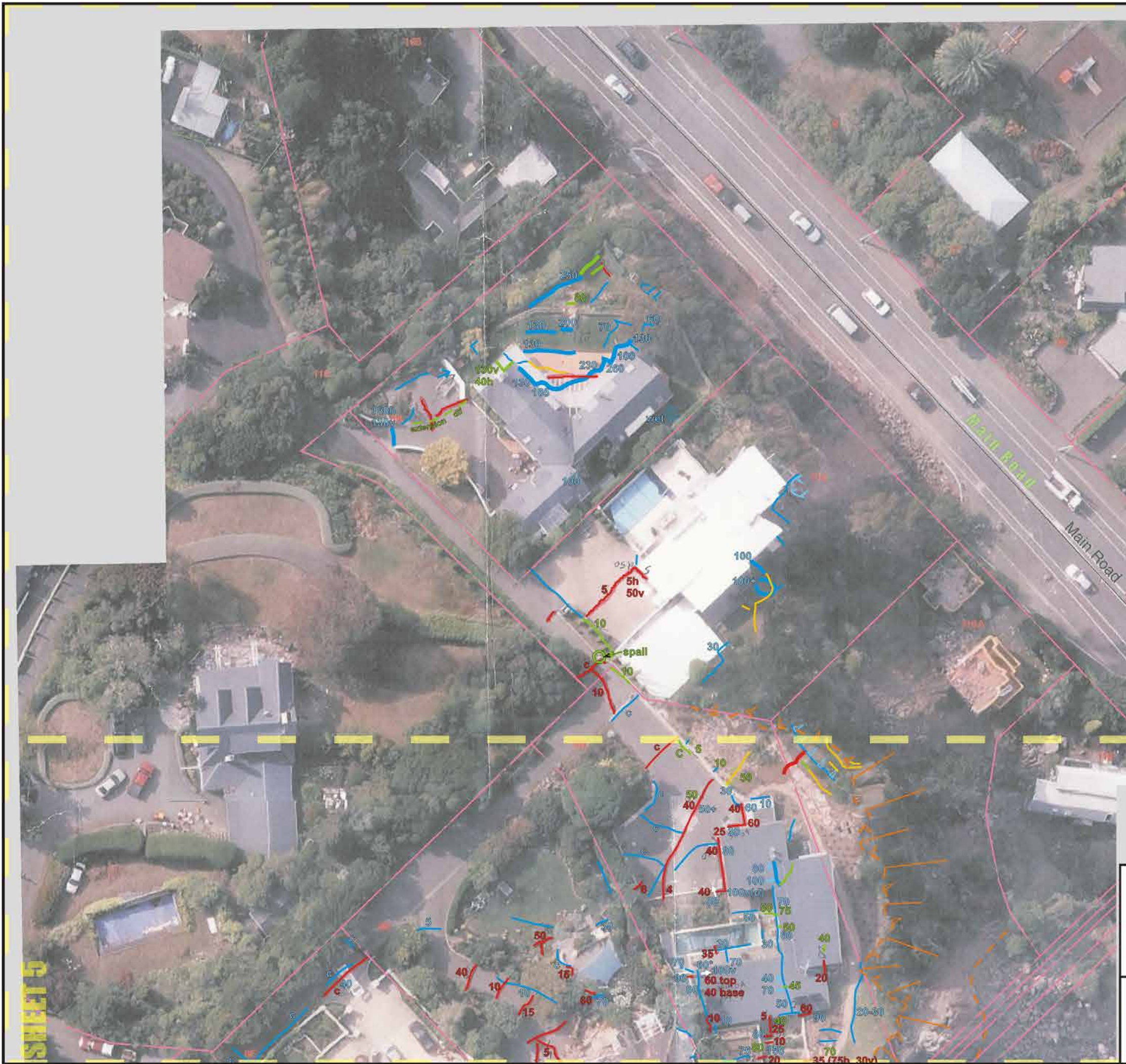
-  25 RED - Mapped 05 March 2011
 -  25 YELLOW - Mapped May 2011
(crack width changes and observations may also be noted on previously recorded cracks)
 -  25 BLUE - Mapped June 2011
(crack width changes and observations may also be noted on previously recorded cracks)
 -  25 GREEN - Mapped September 2011
(crack width changes and observations may also be noted on previously recorded cracks)
- (Note: dimensions given in mm, and are sub-horizontal unless otherwise stated)
-  c Compression expressed at surface
 -  Approximate top of cliff as mapped 05/03/2011 and from aerial photographs (24/02/2011)
 -  Approximate top of cliff as mapped 14/06/2011
 -  Approximate position of survey section (refer Topografo Report 2318 (06/03/11))
 -  Property boundaries



Plan of Ground Cracking and Deformation

Glendevera Tce and Balmoral Lane - Redcliffs

 GEOTECH	BY: RBW	DATE: 15/06/11
	CHKD: IMcC	LAST REV: 20/10/11
	SCALE: 1:500 @ A3	FIGURE 1 SHEET 4



LEGEND

Observed Cracks and Deformation (ground, buildings, landscaping etc) with crack widths and other features noted as mapped:

-  RED - Mapped 05 March 2011
 -  YELLOW - Mapped May 2011
(crack width changes and observations may also be noted on previously recorded cracks)
 -  BLUE - Mapped June 2011
(crack width changes and observations may also be noted on previously recorded cracks)
 -  GREEN - Mapped September 2011
(crack width changes and observations may also be noted on previously recorded cracks)
- (Note: dimensions given in mm, and are sub-horizontal unless otherwise stated)
-  C Compression expressed at surface
 -  Approximate top of cliff as mapped 05/03/2011 and from aerial photographs (24/02/2011)
 -  Approximate top of cliff as mapped 14/06/2011
 -  Approximate position of survey section (refer Topografo Report 2318 (06/03/11))
 -  Property boundaries

Plan of Ground Cracking and Deformation

Glendevere Tce and Balmoral Lane - Redcliffs

 GEOTECH	BY: RBW	DATE: 15/06/11
	CHKD: IMcC	LAST REV: 20/10/11
	SCALE: 1:500 @ A3	FIGURE 1 SHEET 5

A6 APPENDIX 6: RESULTS FROM THE TWO-DIMENSIONAL SITE RESPONSE ASSESSMENT FOR CROSS-SECTION 4

The results from the two-dimensional site response modelling are shown for cross-section 4. The maximum acceleration (A_{MAX}) at the slope crest derived from the modelling of each synthetic earthquake time history has been plotted in Figure A6.1. The slope crest is defined as the convex break in slope between the lower steeper slope and the upper less steep slope. Each point on the graph represents the response of this location to a given synthetic free field rock outcrop earthquake input motion (Table A6.1).

The highest modelled peak ground accelerations during the modelled earthquakes coincide with the convex break in slope (A_{MAX}) at the cliff crest.

The fundamental frequency of the slope varies from 1.8 to 2.3 Hz based on the equation in Bray and Travasarou (2007), where frequency = $1/(4 \times H/V_s)$, and H = slope height of 70 m, and V_s = average shear wave velocity for the main slope materials (basalt lava breccia) of 500–640 m/s. The dominant frequency of the input motions is between 3.6 Hz and 5.7 Hz. The “tuning ratio” defined as the ratio between the dominant frequency of the input motion and the fundamental frequency of the slope (Wartman et al., 2013), is about 2.0–3.2 for a shear wave velocity of 500 m/s, and 1.6–2.5 for a shear wave velocity of 640 m/s.

Results from the seismic response assessment suggest that the mean peak ground acceleration amplification factors (S_T) for cross-section 4 is about 2.6 (± 0.1) for horizontal motions, and 3.3 (± 0.3) for vertical motions – errors at one standard deviation, based on all the data in Table A5.1 (Figure A6.1).

Table A6.1 Results from the two-dimensional site response assessment for cross-section 4, using the out-of-phase synthetic free-field rock outcrop motions for the Redcliffs site by Holden et al. (2014) as inputs to the assessment. PGA is peak ground acceleration.

Earthquake (2011)	Free-field input PGA (horizontal) – A_{FF} (g)	Free-field input PGA (vertical) – A_{FF} (g)	Maximum PGA (horizontal) at convex break in slope – A_{MAX} (g)	Maximum PGA (vertical) at convex break in slope – A_{MAX} (g)
22 February	0.88	0.66	2.30	2.01
16 April	0.05	0.02	0.20	0.13
13 June	0.38	0.27	0.96	1.16
23 December	0.16	0.13	0.53	0.60

Results from the seismic response assessment suggest that the peak ground acceleration amplification factors (S_T) for Redcliffs vary between 2.5 and 4.3 times for horizontal motions, with a mean of 2.2, and 3.1 and 4.4 times for vertical motions (Figure A6.2).

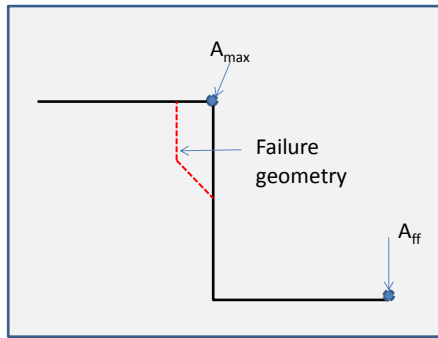
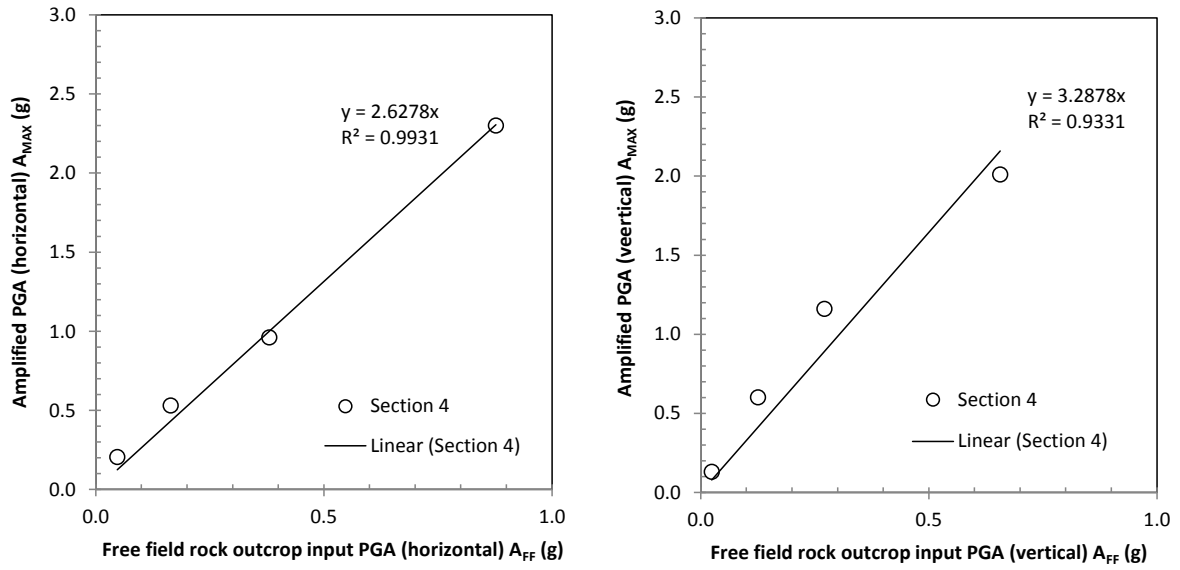


Figure A6.1 Amplification relationship between the synthetic free-field rock outcrop input motions (A_{FF}) and the modelled cliff crest maximum accelerations (A_{MAX}) for cross-section 4. A schematic diagram showing the locations of the various recorded accelerations is shown.

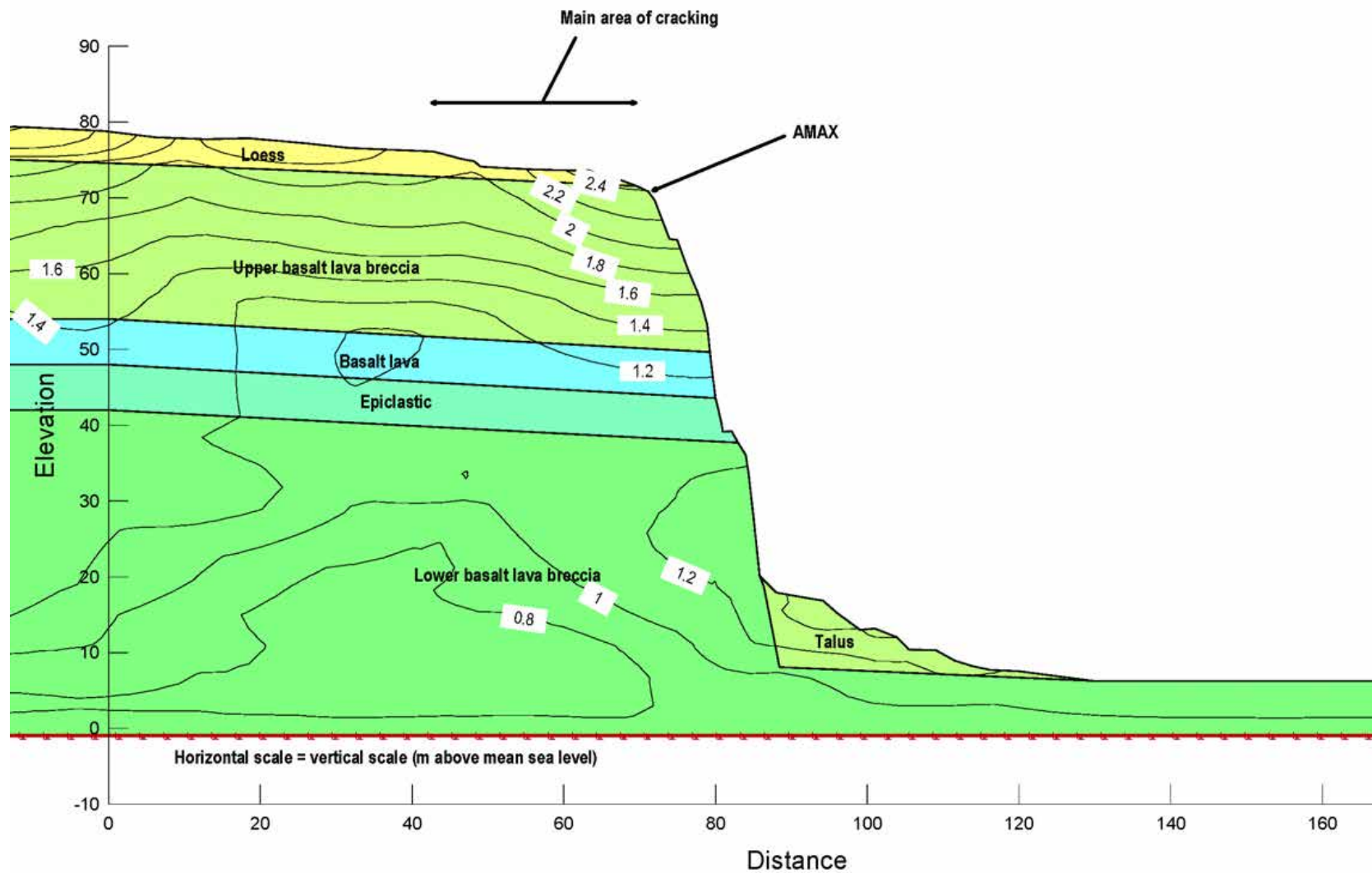


Figure A6.2 Modelled peak horizontal ground acceleration contours for the 22 February 2011 earthquake at Redcliffs, cross-section 4, adopting the 2003 airborne LiDAR slope surface geometry. Contours are peak horizontal ground accelerations (g).

The relationship between the modelled vertical and horizontal peak ground accelerations simulated at the slope crest (A_{MAX}) is shown in Figure A6.3. The gradient of a linear fit is 0.93 (± 0.1) – errors at one standard deviation. However, the relationship between horizontal and vertical peak ground accelerations appears non-linear, and better represented by a curve.

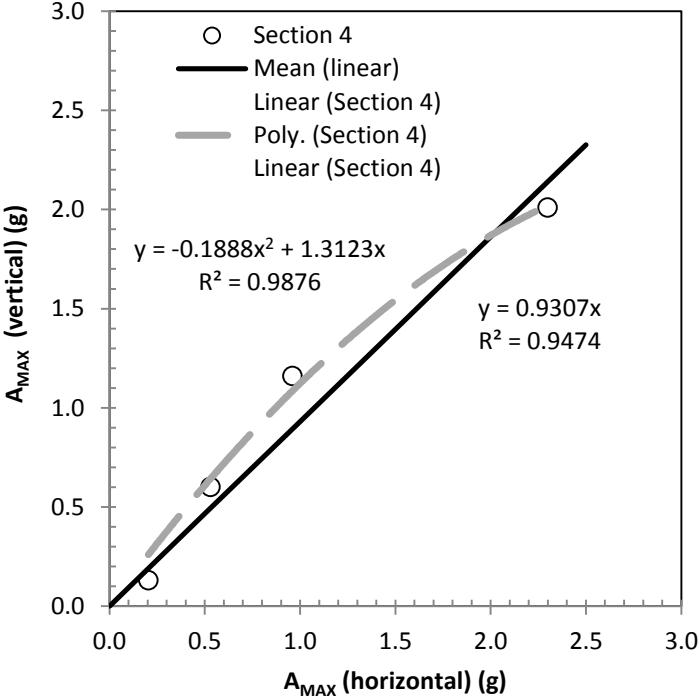


Figure A6.3 Relationship between the modelled horizontal and vertical maximum accelerations modelled at the convex break in slope (A_{MAX}) for cross-section 4, using the synthetic free-field rock outcrop motions for the Redcliffs site by Holden et al. (2014) as inputs to the assessment.

Results from this assessment have shown that the relationship between the peak ground acceleration of the free-field input motion and the corresponding modelled peak acceleration at the slope crest (A_{MAX}), although approximately linear for all horizontal motions assessed, is non-linear at lower peak input ground accelerations. Vertical motions are non-linear over the range of motions assessed. For the range of modelled peak horizontal accelerations, the horizontal amplification factor (S_T) is typically in the order of about 2.6 times the input free-field peak horizontal acceleration.

The results from this assessment show that the amplification of peak ground accelerations at the cliff crest are higher for the 16 April and 23 December 2011 earthquakes (between 3.2 and 4.3 times the peak acceleration of the free field input motions, Table A6.1) when compared to the 22 February and 13 June 2011 earthquakes (between 2.6 and 2.5 times the peak acceleration of the free field input motions, Table A6.1). These results are similar to those reported by others, e.g., Bray and Rathje (1998) and Kramer (1996), indicating that the choice of amplification factor used, should vary with the magnitude of the peak acceleration of the input motion.

Eurocode 8, Part 5, Annex A, gives some simplified amplification factors for the seismic action used in the verification of the stability of slopes. Such factors, denoted S_T , are to a first approximation considered independent of the fundamental period of vibration and, hence, multiply as a constant scaling factor.

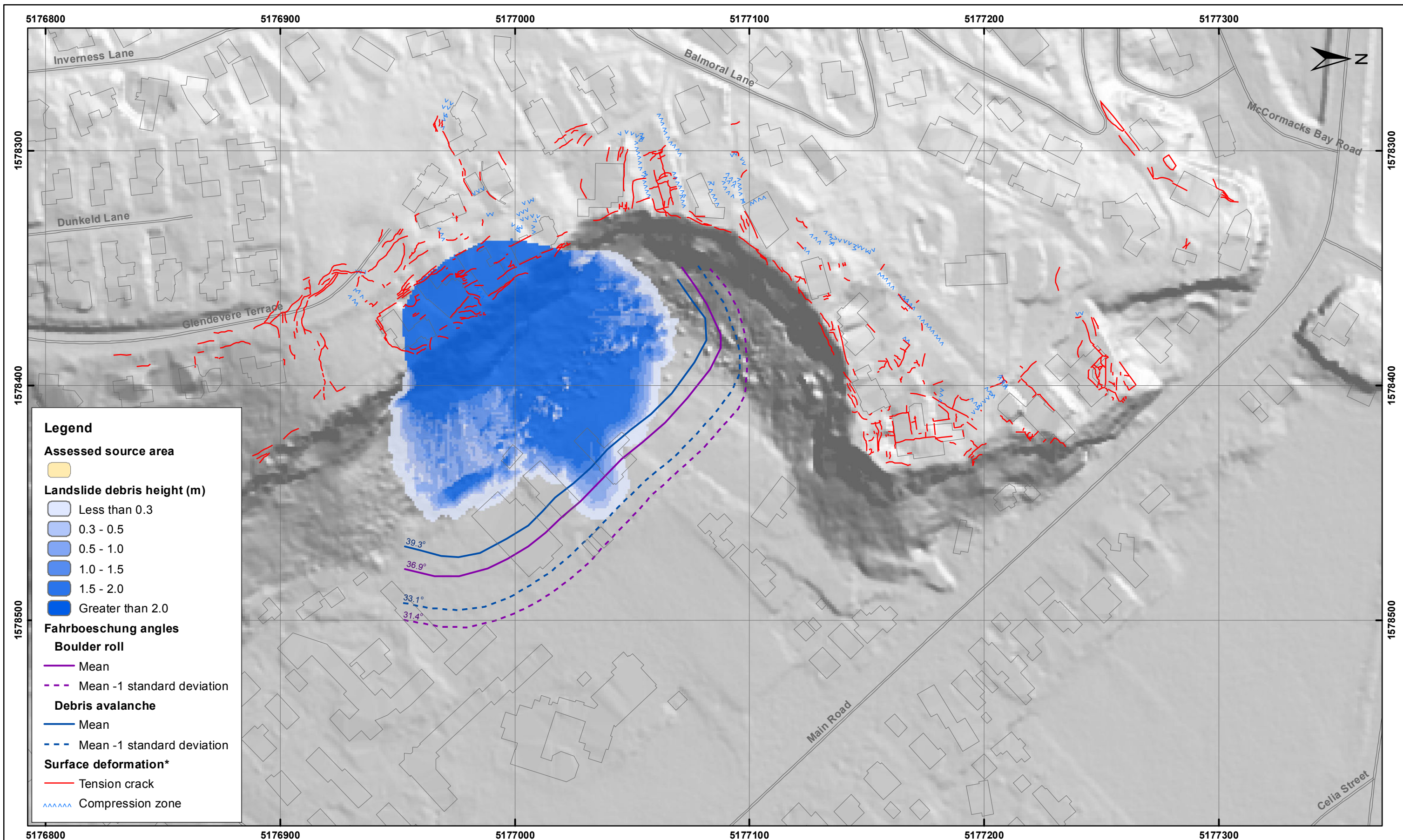
Eurocode 8, Part 5, Annex A recommends:

1. Isolated cliffs and slopes. A value $S_T \geq 1.2$ should be used for sites near the top edge;
2. Ridges with crest width significantly less than the base width. A value $S_T \geq 1.4$ should be used near the top of the slopes for average slope angles greater than 30° and a value $S_T > 1.2$ should be used for smaller slope angles;
3. Presence of a loose surface layer. In the presence of a loose surface layer, the smallest S_T value given in a) and b) should be increased by at least 20%;
4. Spatial variation of amplification factor. The value of S_T may be assumed to decrease as a linear function of the height above the base of the cliff or ridge, and to be unity at the base; and
5. These amplification factors should in preference be applied when the slopes belong to two-dimensional topographic irregularities, such as long ridges and cliffs of height greater than about 30 m.

Ashford and Sitar (2002) recommend an S_T of 1.5 be applied to the maximum free-field acceleration behind the crest based on their assessment of slopes in homogenous materials, typically $>60^\circ$ to near vertical and of heights (toe to crest) of typically >30 m. This factor is based on the assessment of slopes that failed during the 1989 Loma Prieta M_w 6.9 earthquake.

Results from the seismic response assessment suggest that the horizontal peak ground acceleration amplification factor (S_T) for Redcliffs range from 2.5 to 4.3 (mean of 2.6) (cross-section 4) times greater than the free field input motions, and that the relationship is non-linear. These are larger than those values reported by Ashford and Sitar (2002), and in part reflect the different materials forming the slopes at Redcliffs (rock rather than soil). These higher factors may also be a function of the site to earthquake source distances. In the case of Redcliffs, the site is within 10 km of the epicentres of the 22 February, 16 April, 13 June and 23 December 2011 earthquakes, making them all “near-field” earthquakes.

**A7 APPENDIX 7: RAMMS MODELLING RESULTS FOR SOURCE AREAS 1–
3. ESTIMATED LANDSLIDE RUNOUT HEIGHT**

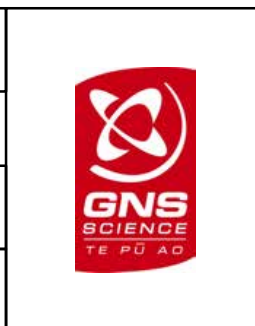


SCALE BAR: 0 50 100 m

EXPLANATION:
 * Taken from report CR2012/317
 Background shade model derived from NZAM post earthquake 2011c (July 2011) LiDAR survey resampled to a 1 m ground resolution. Roads and building footprints and types provided by Christchurch City Council (20/02/2012).
 PROJECTION: New Zealand Transverse Mercator 2000

DRW:
BL, WR

CHK:
CM, FDP



ESTIMATED LANDSLIDE RUNOUT HEIGHT
Source 1 - Upper Volume (32,000 m³)

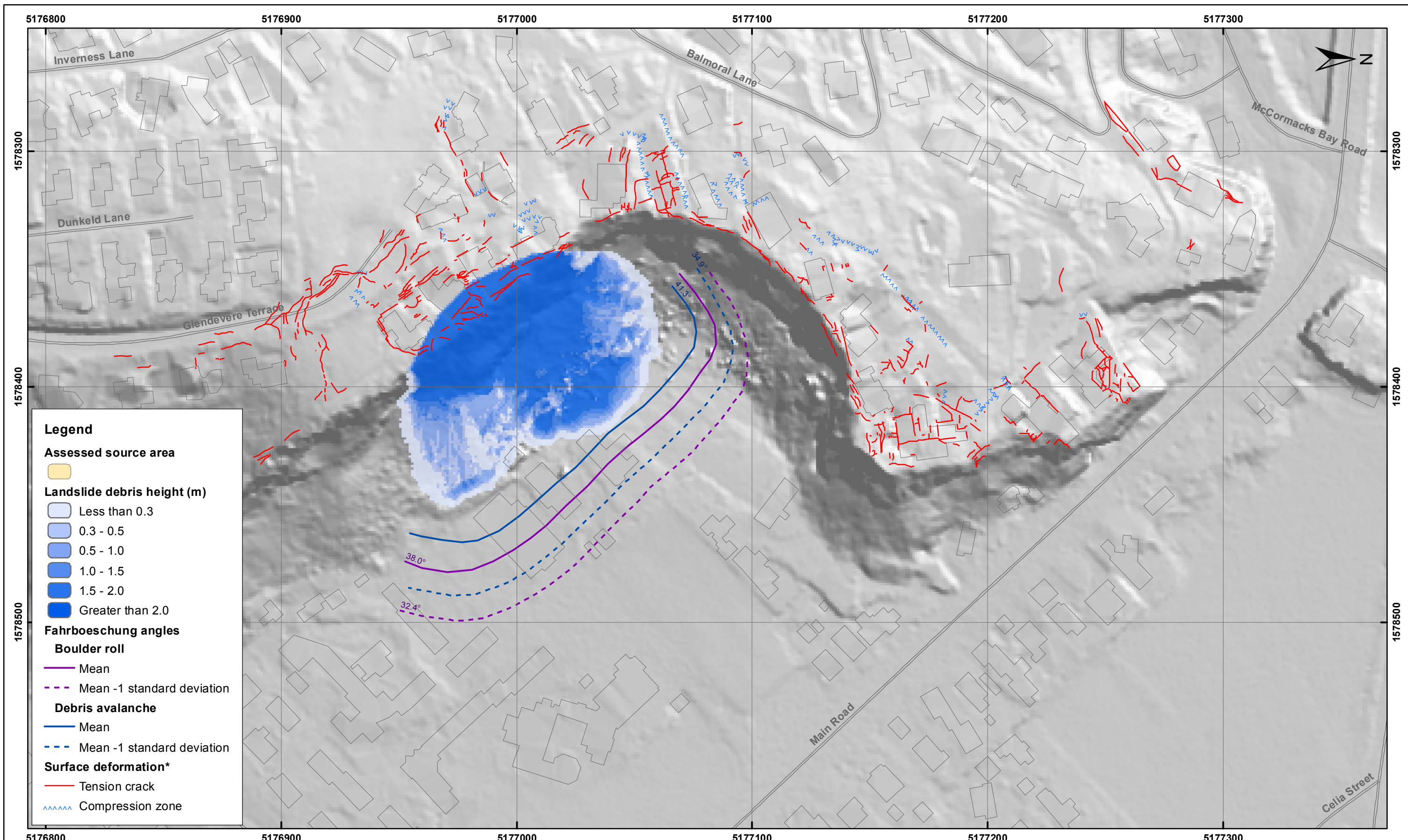
Redcliffs - Port Hills
Christchurch

APPENDIX 7

Map 1

FINAL

REPORT: CR2014/78 DATE: August 2014



SCALE BAR: 0 50 100 m

EXPLANATION:
 * Taken from report CR2012/317
 Background shade model derived from NZAM post earthquake 2011c (July 2011) LiDAR survey resampled to a 1 m ground resolution. Roads and building footprints and types provided by Christchurch City Council (20/02/2012).
 PROJECTION: New Zealand Transverse Mercator 2000

DRW:
BL, WR

CHK:
CM, FDP



ESTIMATED LANDSLIDE RUNOUT HEIGHT
Source 1 - Middle Volume (12,800 m³)

Redcliffs - Port Hills
Christchurch

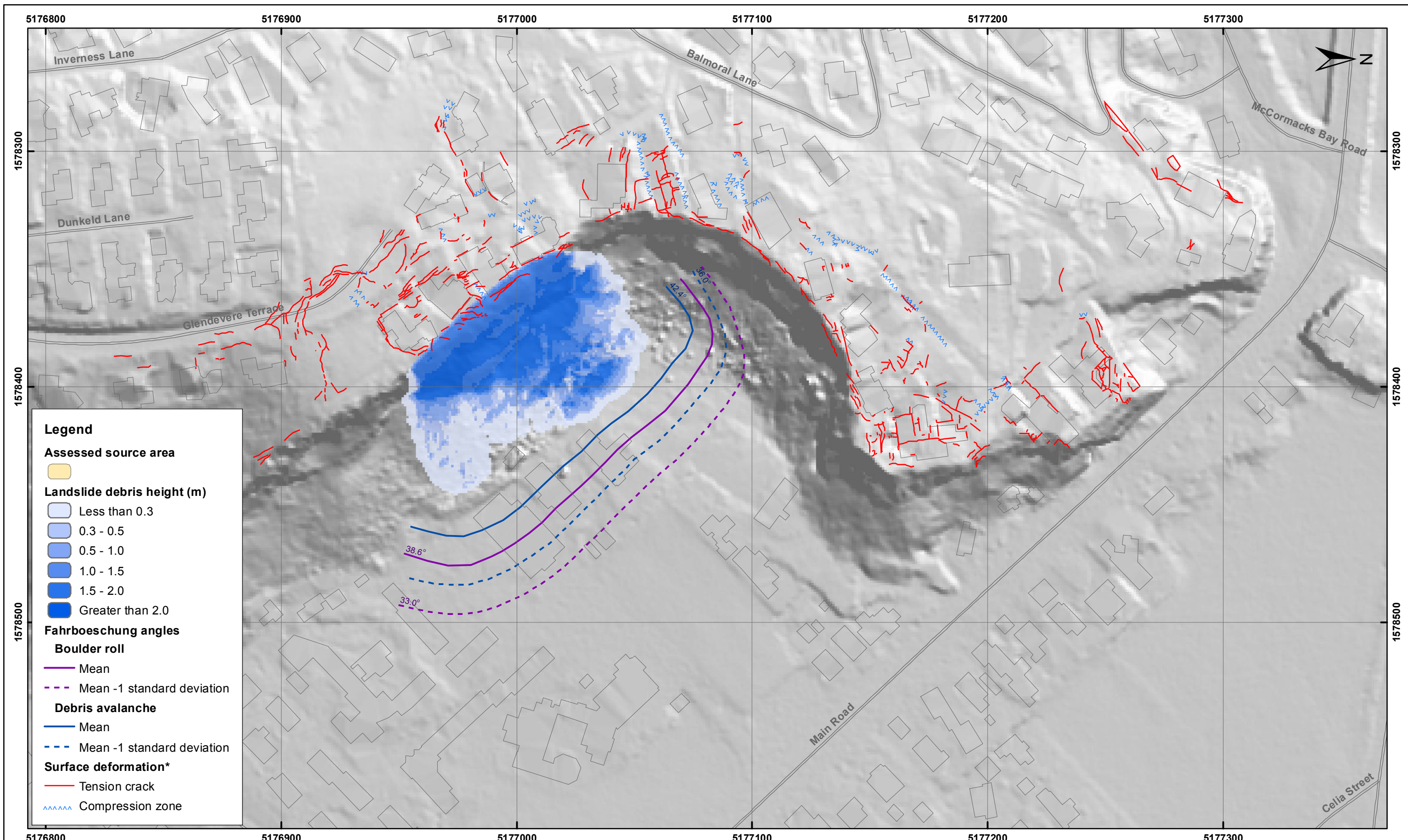
APPENDIX 7

Map 2

FINAL

REPORT:
CR2014/78

DATE:
August 2014



SCALE BAR: 0 50 100 m

EXPLANATION:
 * Taken from report CR2012/317
 Background shade model derived from NZAM post earthquake 2011c (July 2011) LiDAR survey resampled to a 1 m ground resolution. Roads and building footprints and types provided by Christchurch City Council (20/02/2012).
 PROJECTION: New Zealand Transverse Mercator 2000

DRW:
BL, WR

CHK:
CM, FDP



ESTIMATED LANDSLIDE RUNOUT HEIGHT
Source 1 - Lower Volume (7,700 m³)

Redcliffs - Port Hills
Christchurch

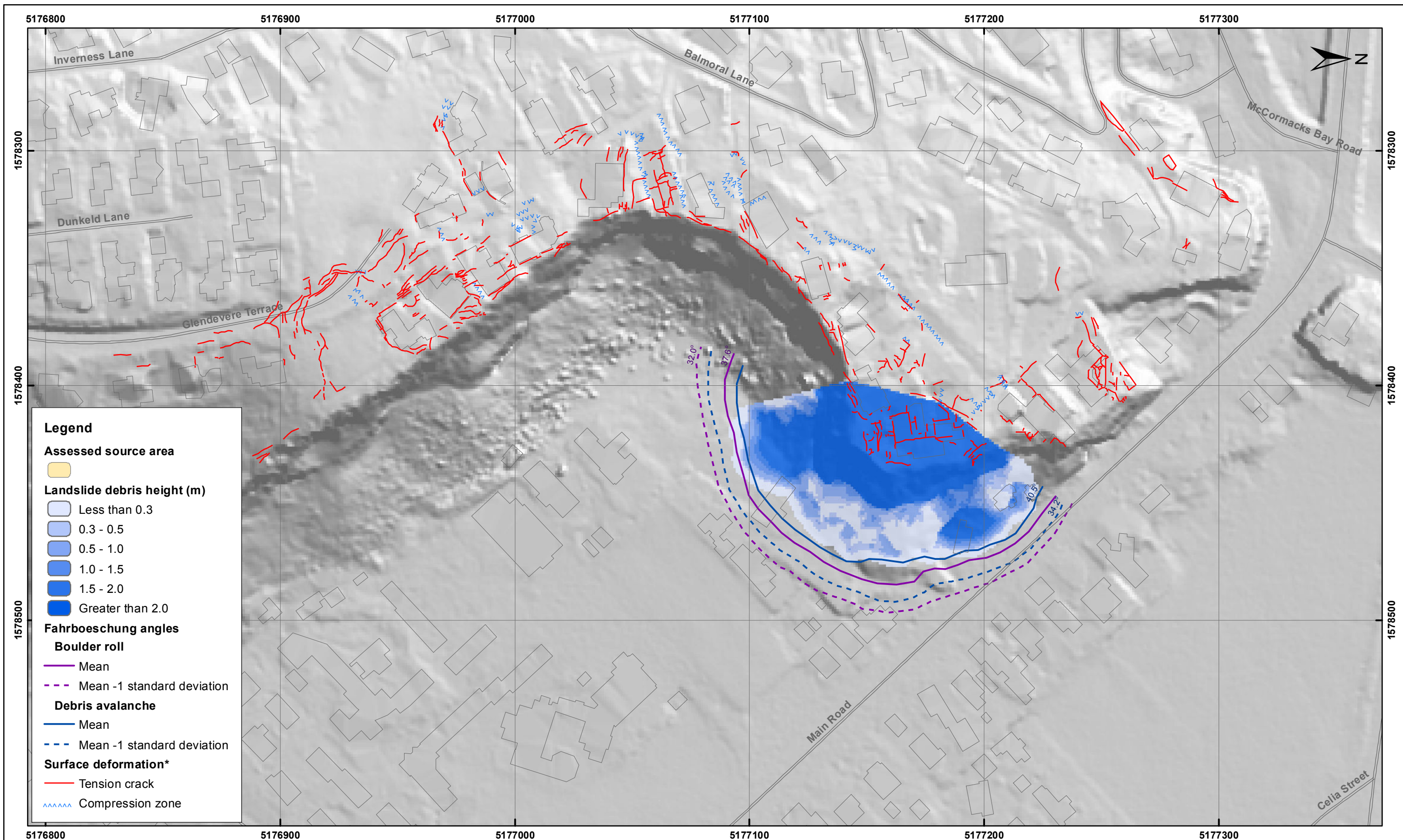
APPENDIX 7

Map 3

FINAL

REPORT:
CR2014/78

DATE:
August 2014



EXPLANATION:

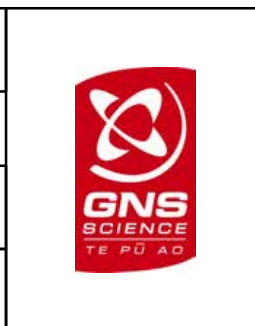
* Taken from report CR2012/317

Background shade model derived from NZAM post earthquake 2011c (July 2011) LiDAR survey resampled to a 1 m ground resolution. Roads and building footprints and types provided by Christchurch City Council (20/02/2012).

PROJECTION: New Zealand Transverse Mercator 2000

DRW:
BL, WR

CHK:
CM, FDP



ESTIMATED LANDSLIDE RUNOUT HEIGHT
Source 2 - Upper Volume (18,300 m³)

Redcliffs - Port Hills
Christchurch

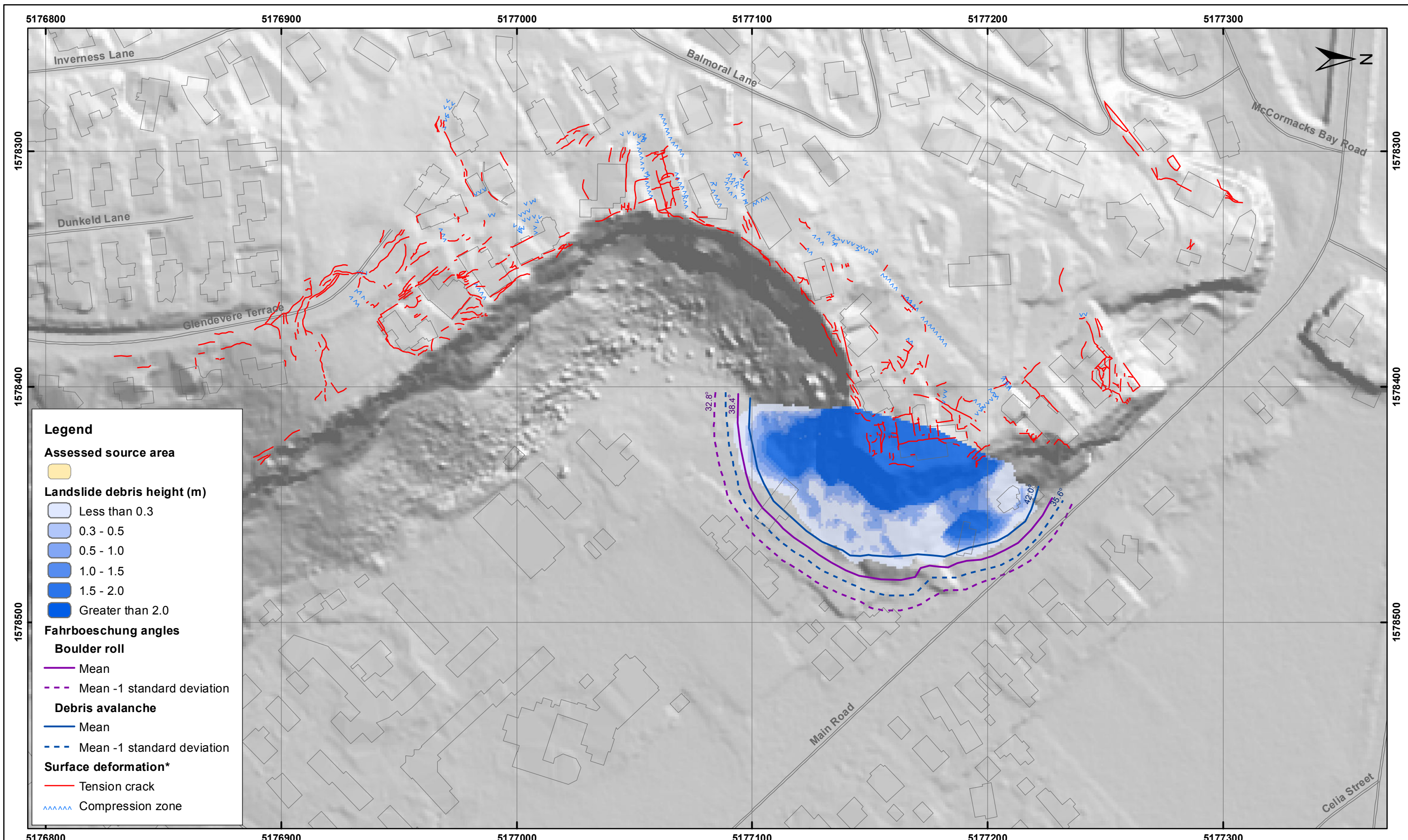
APPENDIX 7

Map 4

FINAL

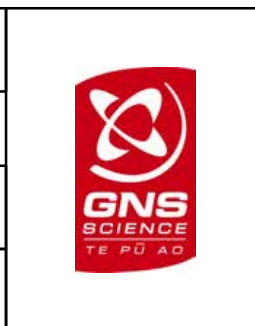
REPORT:
CR2014/78

DATE:
August 2014



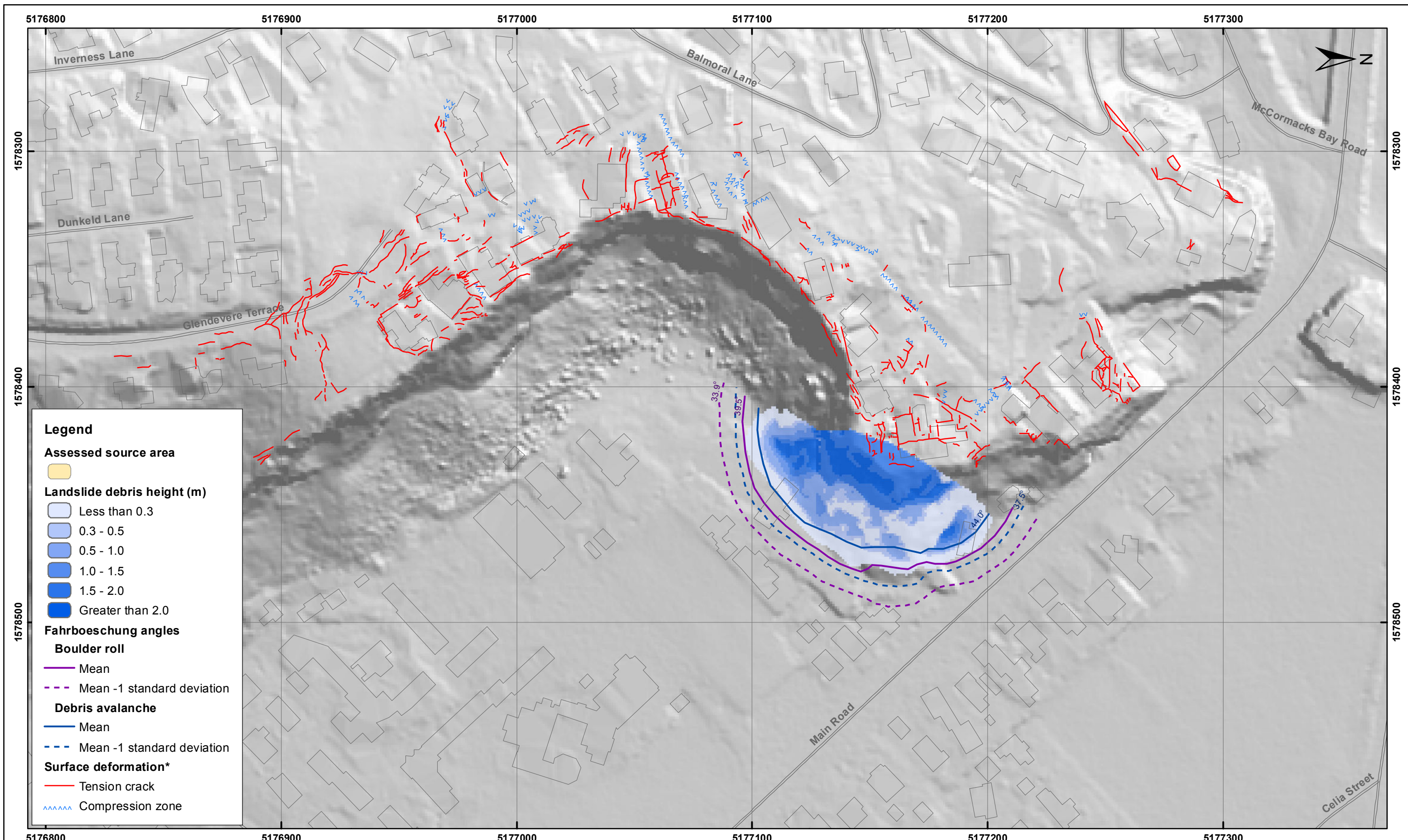
EXPLANATION:
 * Taken from report CR2012/317
 Background shade model derived from NZAM post earthquake 2011c (July 2011) LiDAR survey resampled to a 1 m ground resolution. Roads and building footprints and types provided by Christchurch City Council (20/02/2012).
 PROJECTION: New Zealand Transverse Mercator 2000

DRW:
BL, WR
 CHK:
CM, FDP



ESTIMATED LANDSLIDE RUNOUT HEIGHT
Source 2 - Middle Volume (9,400 m³)
Redcliffs - Port Hills
Christchurch

APPENDIX 7
 Map 5
FINAL
 REPORT: CR2014/78
 DATE: August 2014



SCALE BAR: 0 50 100 m

EXPLANATION:
 * Taken from report CR2012/317
 Background shade model derived from NZAM post earthquake 2011c (July 2011) LiDAR survey resampled to a 1 m ground resolution.
 Roads and building footprints and types provided by Christchurch City Council (20/02/2012).
 PROJECTION: New Zealand Transverse Mercator 2000

DRW:
BL, WR

CHK:
CM, FDP



ESTIMATED LANDSLIDE RUNOUT VELOCITY
Source 2 - Lower Volume (3,700 m³)

Redcliffs - Port Hills
Christchurch

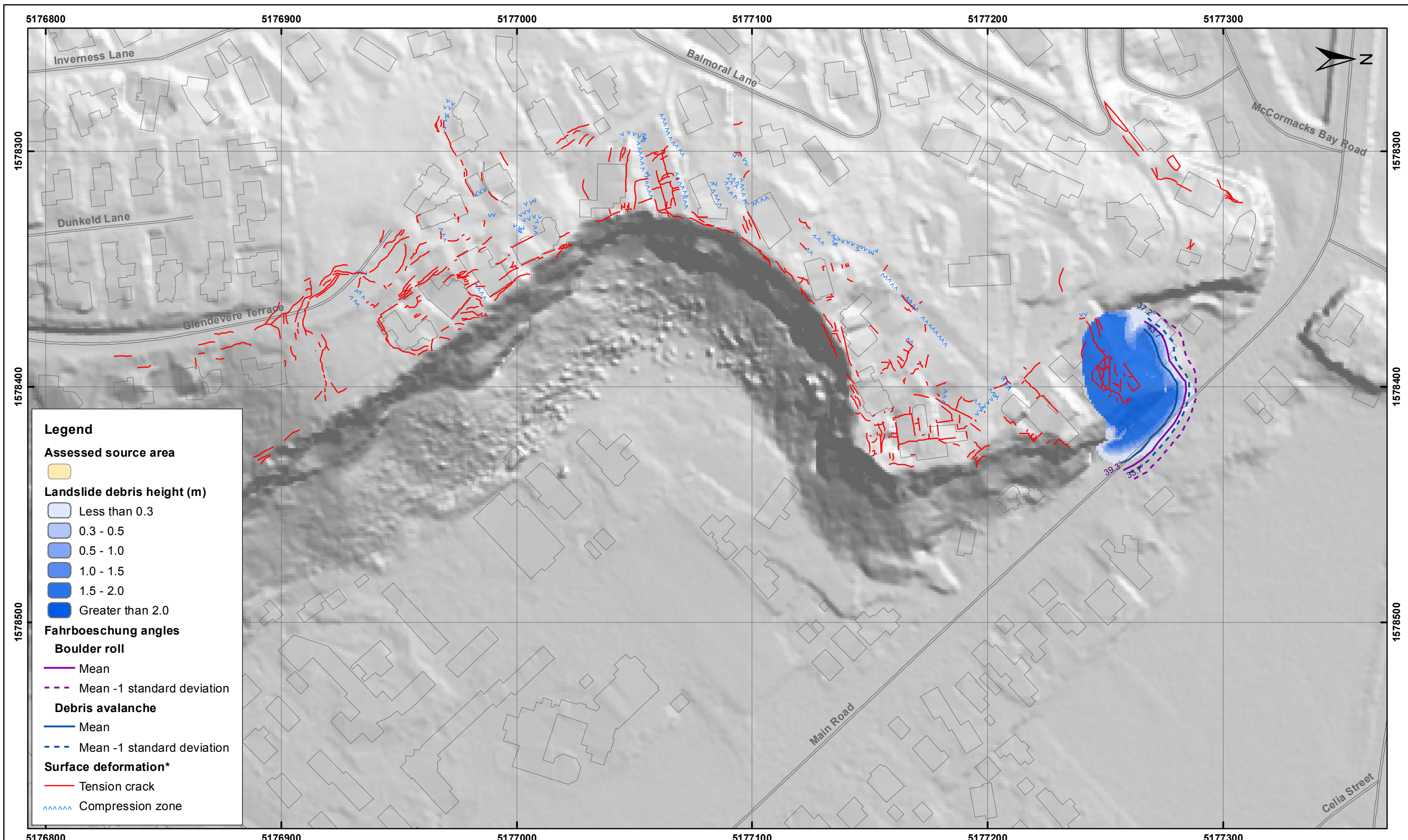
APPENDIX 7

Map 6

FINAL

REPORT:
CR2014/78

DATE:
August 2014



SCALE BAR: 0 50 100 m

EXPLANATION:
 * Taken from report CR2012/317
 Background shade model derived from NZAM post earthquake 2011c (July 2011) LiDAR survey resampled to a 1 m ground resolution.
 Roads and building footprints and types provided by Christchurch City Council (20/02/2012).
 PROJECTION: New Zealand Transverse Mercator 2000

DRW:
BL, WR

CHK:
CM, FDP



ESTIMATED LANDSLIDE RUNOUT HEIGHT
Source 3 - Upper Volume (4,300 m³)

Redcliffs - Port Hills
Christchurch

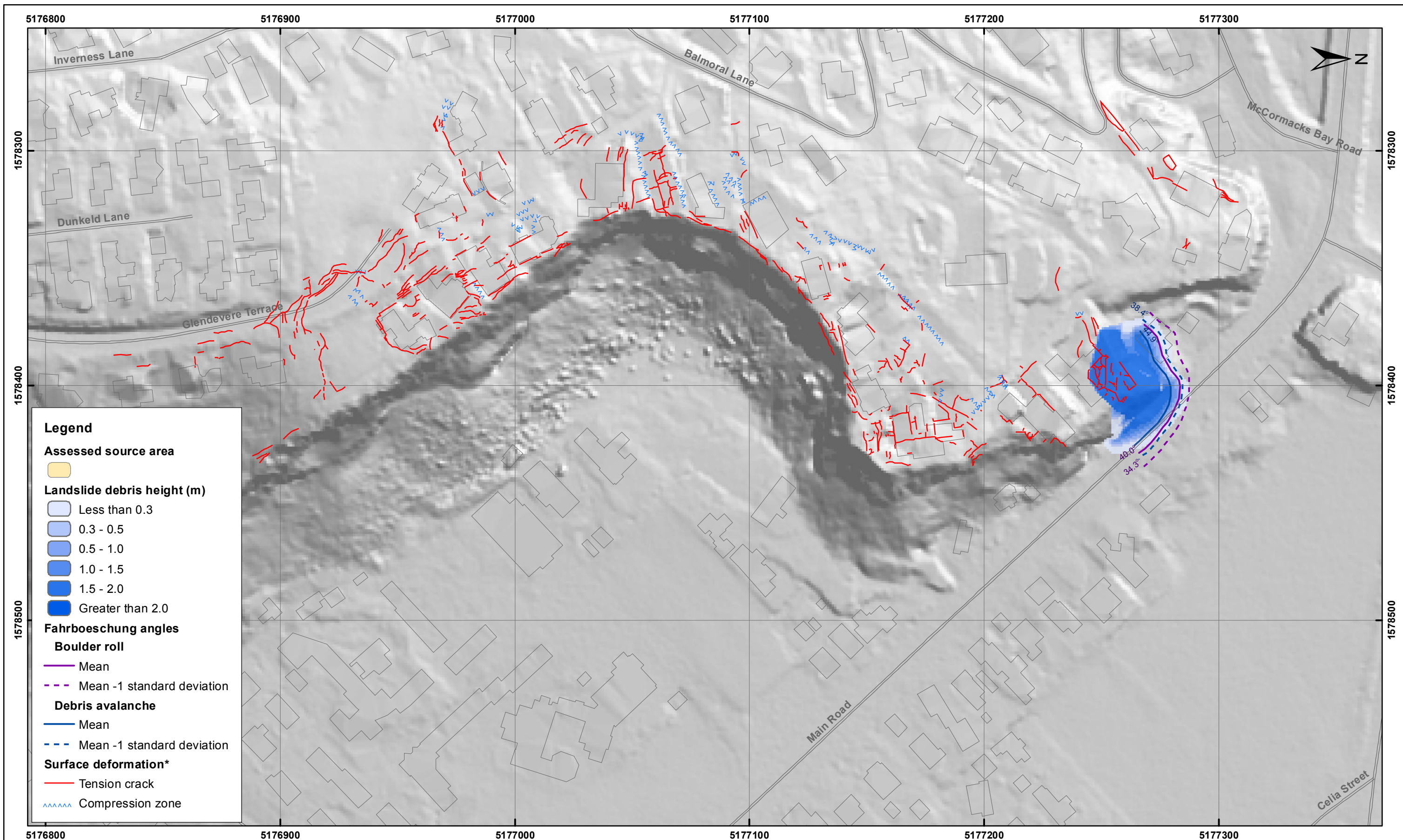
APPENDIX 7

Map 7

FINAL

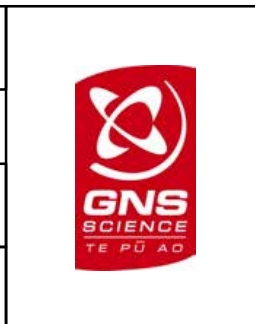
REPORT:
CR2014/78

DATE:
August 2014



EXPLANATION:
 * Taken from report CR2012/317
 Background shade model derived from NZAM post earthquake 2011c (July 2011) LiDAR survey resampled to a 1 m ground resolution.
 Roads and building footprints and types provided by Christchurch City Council (20/02/2012).
 PROJECTION: New Zealand Transverse Mercator 2000

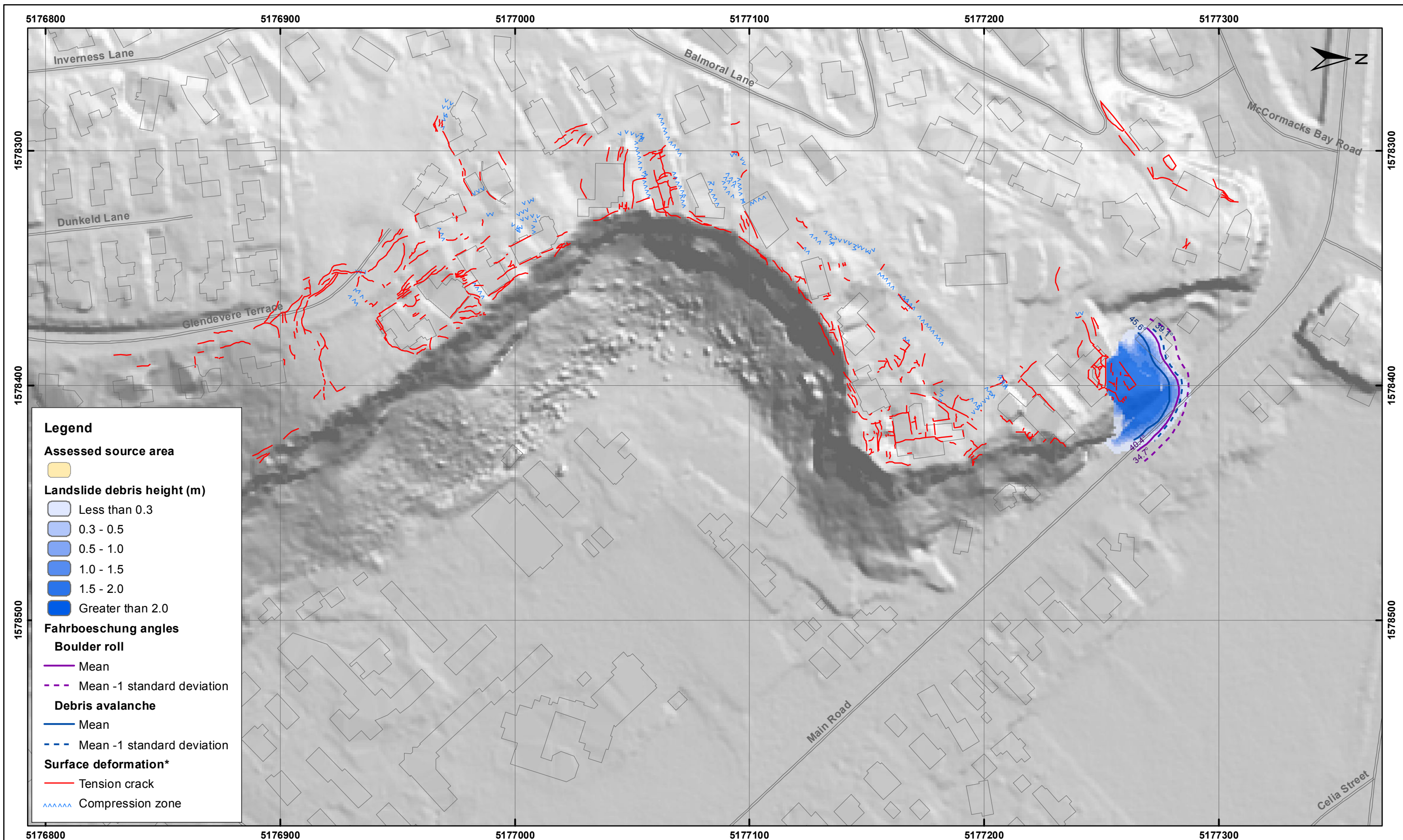
DRW:
BL, WR
 CHK:
CM, FDP



ESTIMATED LANDSLIDE RUNOUT HEIGHT
Source 3 - Middle Volume (2,500 m³)

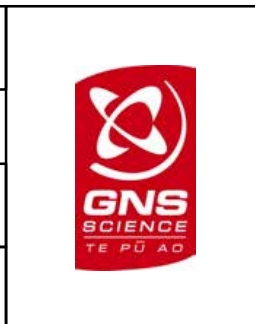
Redcliffs - Port Hills
Christchurch

APPENDIX 7
 Map 8
FINAL
 REPORT: CR2014/78
 DATE: August 2014



EXPLANATION:
 * Taken from report CR2012/317
 Background shade model derived from NZAM post earthquake 2011c (July 2011) LiDAR survey resampled to a 1 m ground resolution. Roads and building footprints and types provided by Christchurch City Council (20/02/2012).
 PROJECTION: New Zealand Transverse Mercator 2000

DRW:
BL, WR
 CHK:
CM, FDP

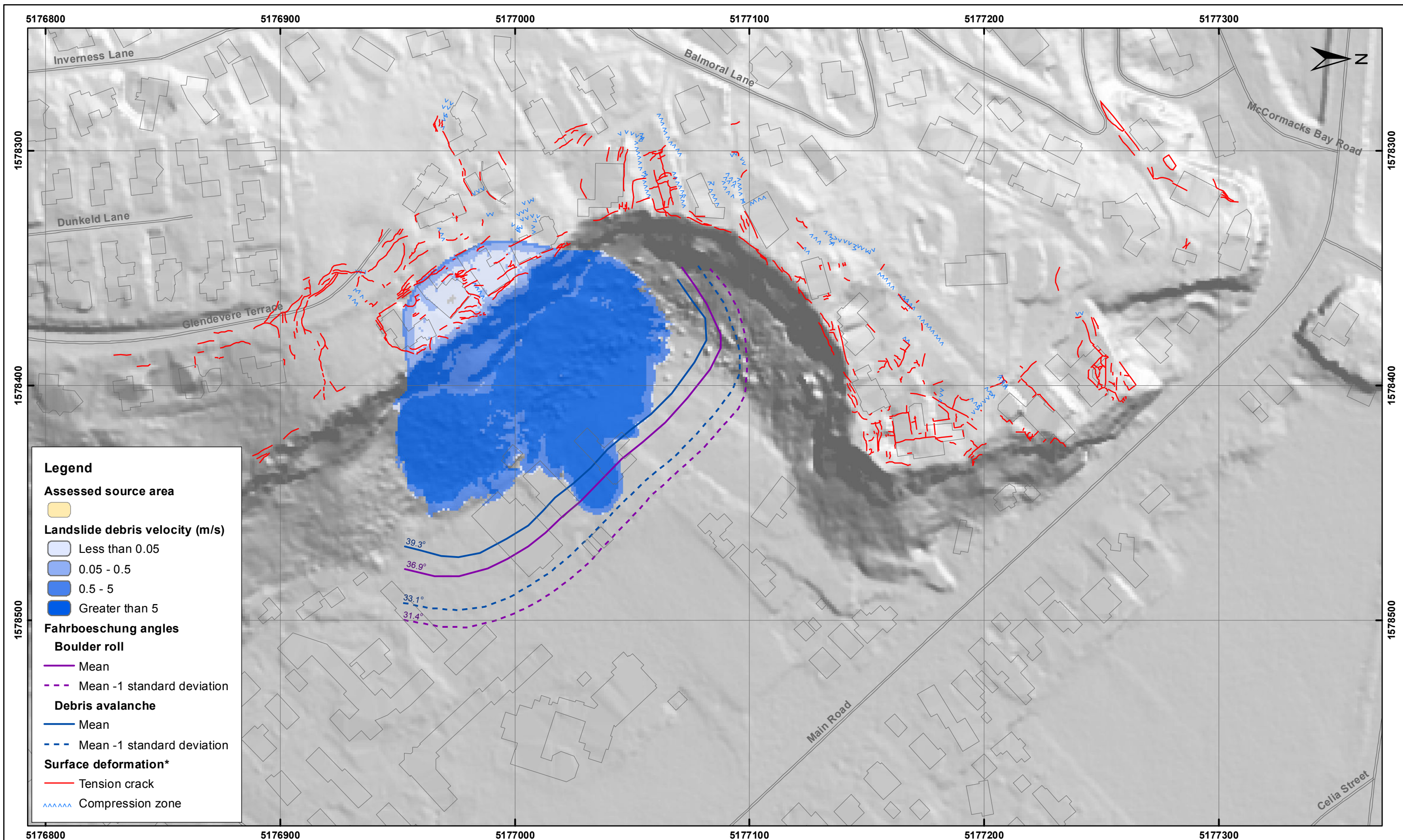


ESTIMATED LANDSLIDE RUNOUT HEIGHT
Source 3 - Lower Volume (1,800 m³)

Redcliffs - Port Hills
Christchurch

APPENDIX 7
 Map 9
FINAL
 REPORT: CR2014/78
 DATE: August 2014

A8 APPENDIX 8: RAMMS MODELLING RESULTS FOR SOURCE AREAS 1–3, ESTIMATED LANDSLIDE RUNOUT VELOCITY



SCALE BAR: 0 50 100 m

EXPLANATION:
 * Taken from report CR2012/317
 Background shade model derived from NZAM post earthquake 2011c (July 2011) LiDAR survey resampled to a 1 m ground resolution. Roads and building footprints and types provided by Christchurch City Council (20/02/2012).
 PROJECTION: New Zealand Transverse Mercator 2000

DRW:
BL, WR

CHK:
CM, FDP



ESTIMATED LANDSLIDE RUNOUT VELOCITY
Source 1 - Upper Volume (32,000 m³)

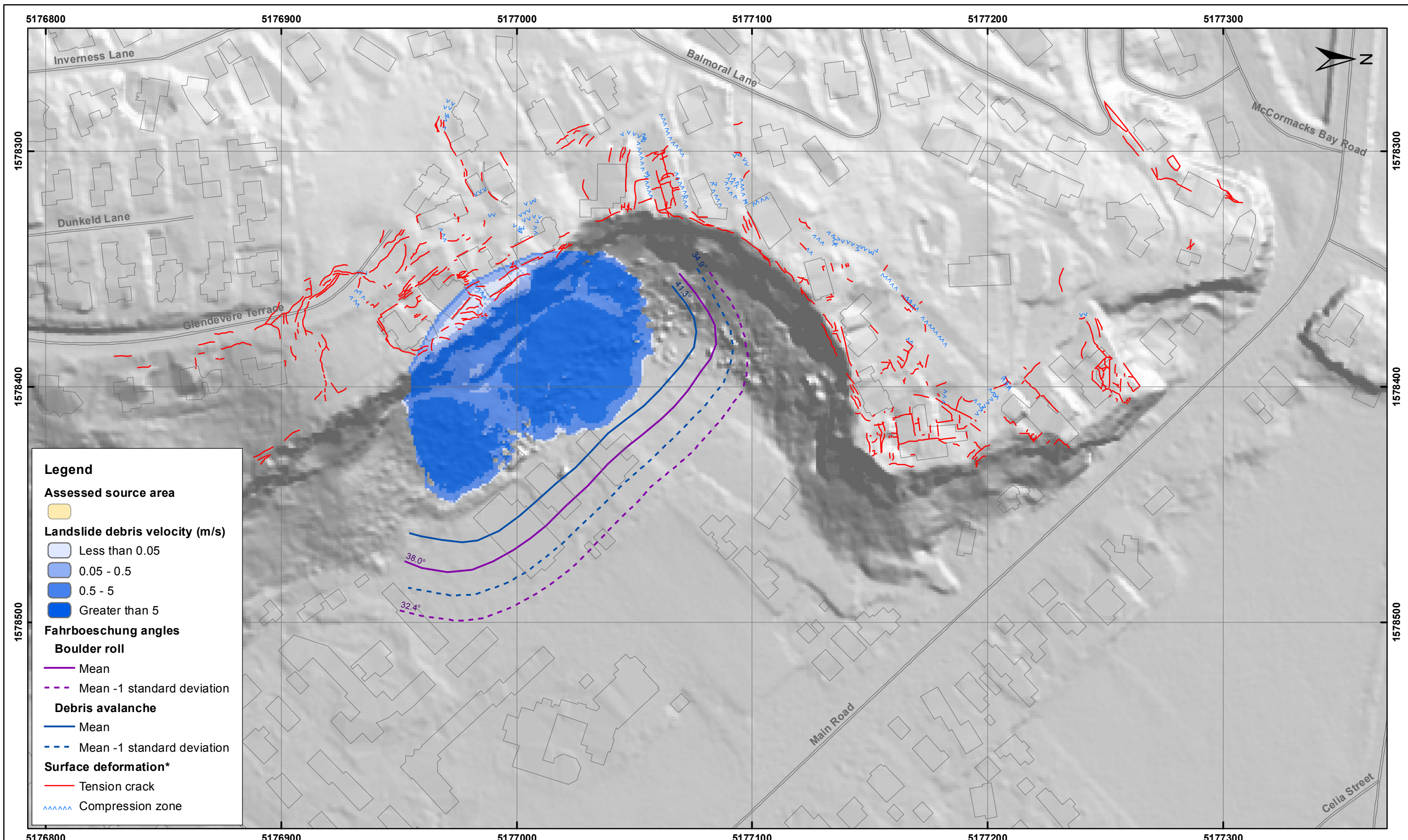
Redcliffs - Port Hills
Christchurch

APPENDIX 8

Map 1

FINAL

REPORT: CR2014/78 DATE: August 2014



SCALE BAR: 0 50 100 m

EXPLANATION:
 * Taken from report CR2012/317
 Background shade model derived from NZAM post earthquake 2011c (July 2011) LiDAR survey resampled to a 1 m ground resolution. Roads and building footprints and types provided by Christchurch City Council (20/02/2012).
 PROJECTION: New Zealand Transverse Mercator 2000

DRW:
BL, WR

CHK:
CM, FDP



ESTIMATED LANDSLIDE RUNOUT VELOCITY
Source 1 - Middle Volume (12,800 m³)

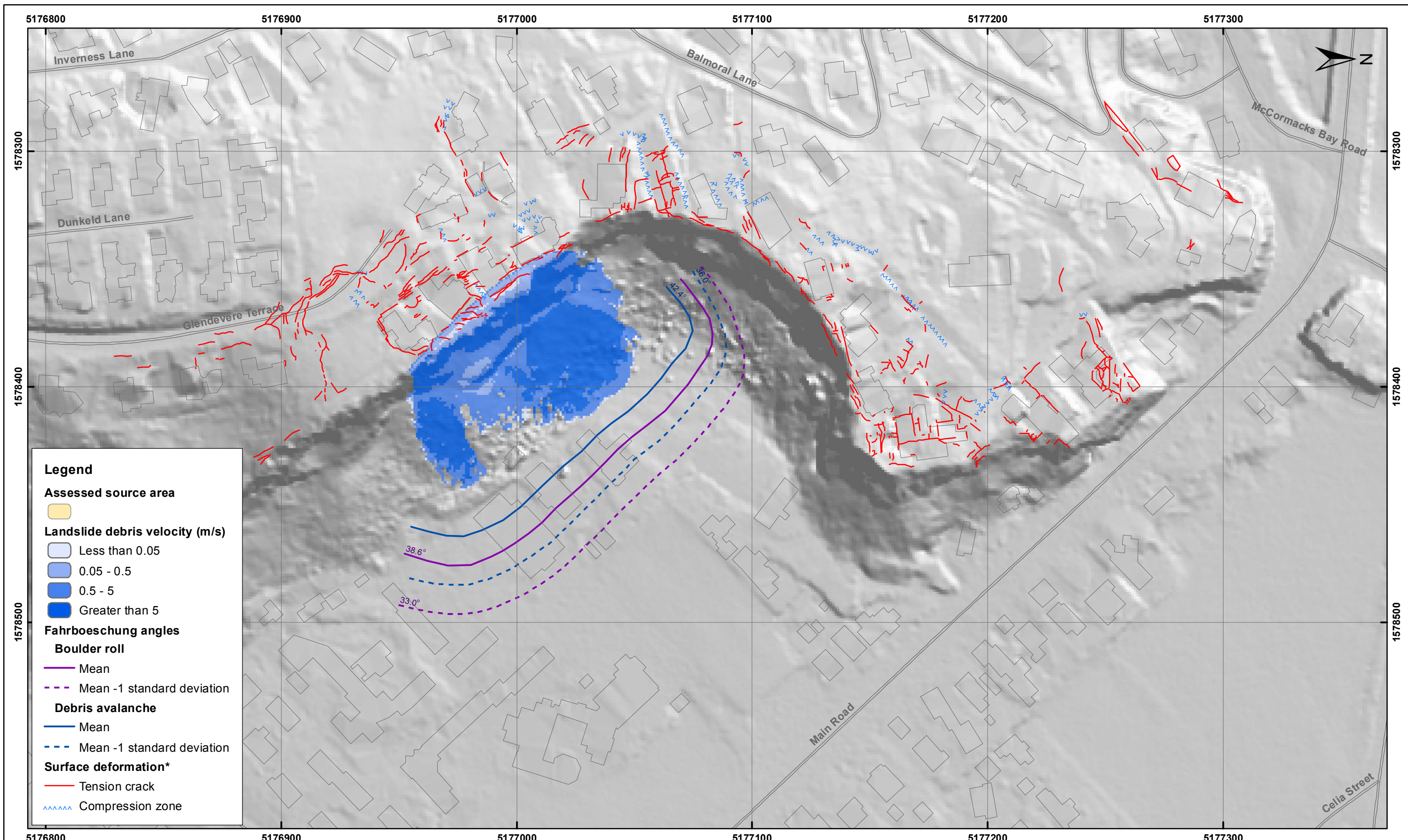
Redcliffs - Port Hills
Christchurch

APPENDIX 8

Map 2

FINAL

REPORT: CR2014/78 DATE: August 2014



SCALE BAR: 0 50 100 m

EXPLANATION:
 * Taken from report CR2012/317
 Background shade model derived from NZAM post earthquake 2011c (July 2011) LiDAR survey resampled to a 1 m ground resolution. Roads and building footprints and types provided by Christchurch City Council (20/02/2012).
 PROJECTION: New Zealand Transverse Mercator 2000

DRW:
BL, WR

CHK:
CM, FDP



ESTIMATED LANDSLIDE RUNOUT VELOCITY
Source 1 - Lower Volume (7,700 m³)

Redcliffs - Port Hills
Christchurch

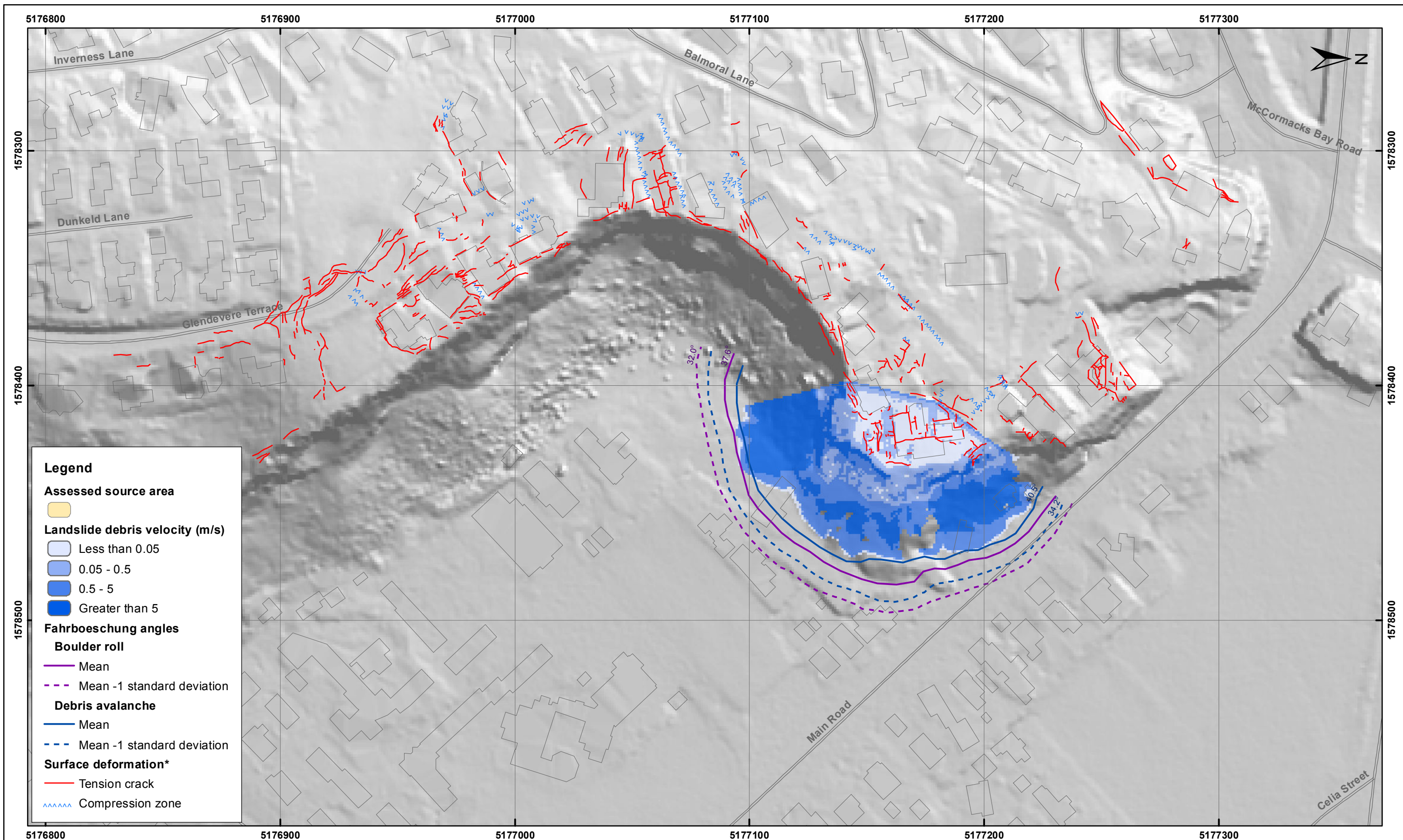
APPENDIX 8

Map 3

FINAL

REPORT:
CR2014/78

DATE:
August 2014



Legend

Assessed source area

Yellow box

Landslide debris velocity (m/s)

- Light blue box: Less than 0.05
- Medium blue box: 0.05 - 0.5
- Dark blue box: 0.5 - 5
- Blue box: Greater than 5

Fahrboeschung angles

Boulder roll

- Solid purple line: Mean
- Dashed purple line: Mean -1 standard deviation

Debris avalanche

- Solid blue line: Mean
- Dashed blue line: Mean -1 standard deviation

Surface deformation*

- Red line: Tension crack
- Blue wavy line: Compression zone



EXPLANATION:

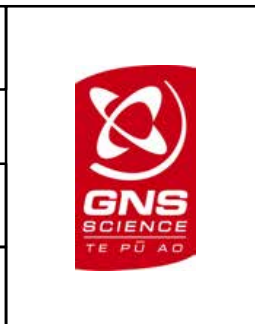
* Taken from report CR2012/317

Background shade model derived from NZAM post earthquake 2011c (July 2011) LiDAR survey resampled to a 1 m ground resolution. Roads and building footprints and types provided by Christchurch City Council (20/02/2012).

PROJECTION: New Zealand Transverse Mercator 2000

DRW:
BL, WR

CHK:
CM, FDP



ESTIMATED LANDSLIDE RUNOUT VELOCITY
Source 2 - Upper Volume (18,300 m³)

Redcliffs - Port Hills
Christchurch

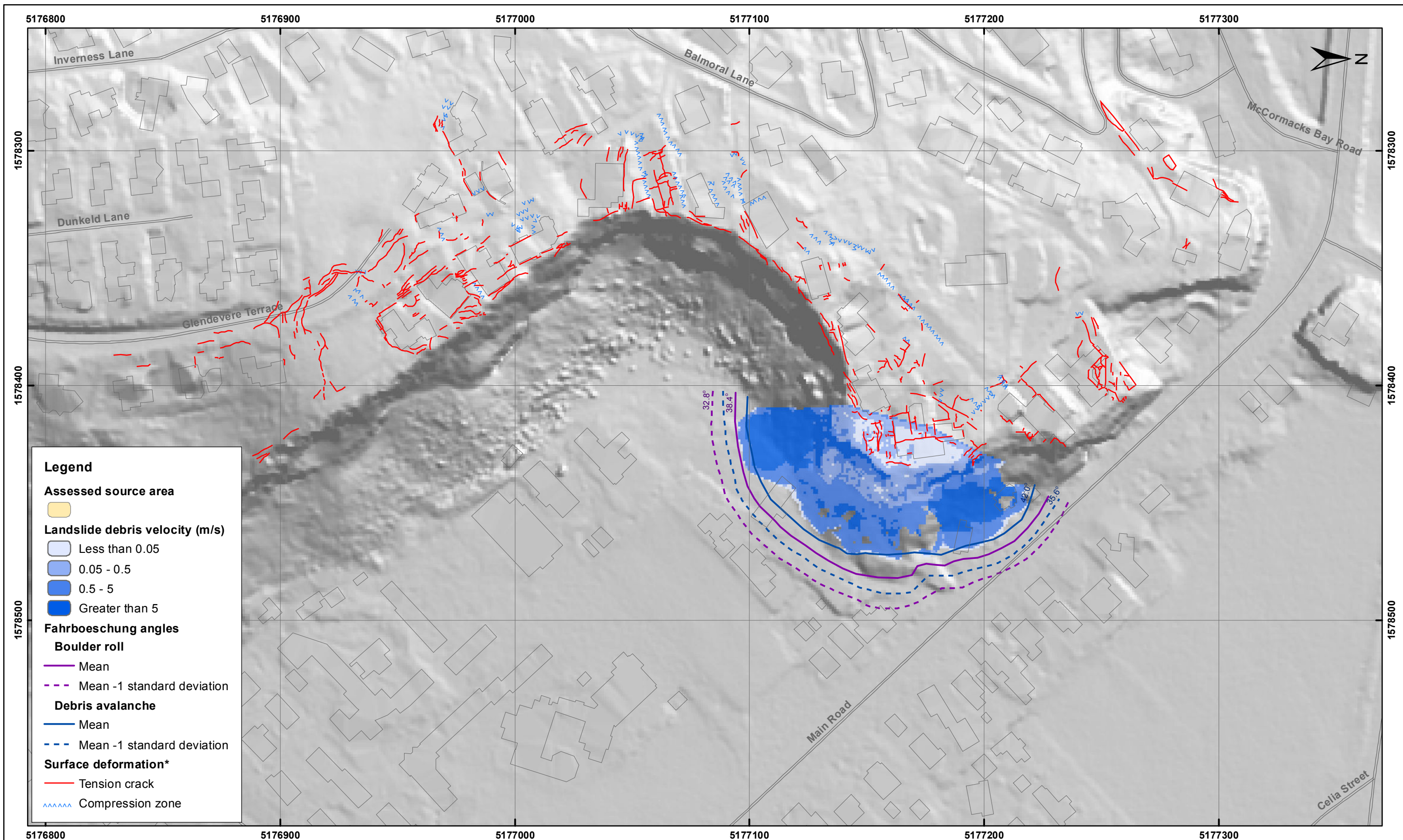
APPENDIX 8

Map 4

FINAL

REPORT:
CR2014/78

DATE:
August 2014



Legend

Assessed source area

Landslide debris velocity (m/s)
 Less than 0.05
 0.05 - 0.5
 0.5 - 5
 Greater than 5

Fahrboeschung angles
Boulder roll
 Mean
 Mean -1 standard deviation
Debris avalanche
 Mean
 Mean -1 standard deviation

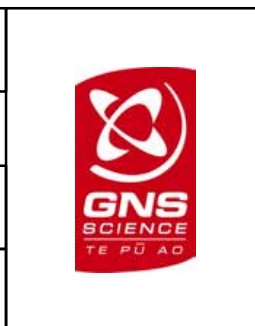
Surface deformation*
 Tension crack
 Compression zone



EXPLANATION:
 * Taken from report CR2012/317
 Background shade model derived from NZAM post earthquake 2011c (July 2011) LiDAR survey resampled to a 1 m ground resolution. Roads and building footprints and types provided by Christchurch City Council (20/02/2012).
 PROJECTION: New Zealand Transverse Mercator 2000

DRW:
BL, WR

CHK:
CM, FDP



ESTIMATED LANDSLIDE RUNOUT VELOCITY
Source 2 - Middle Volume (9,400 m³)

Redcliffs - Port Hills
Christchurch

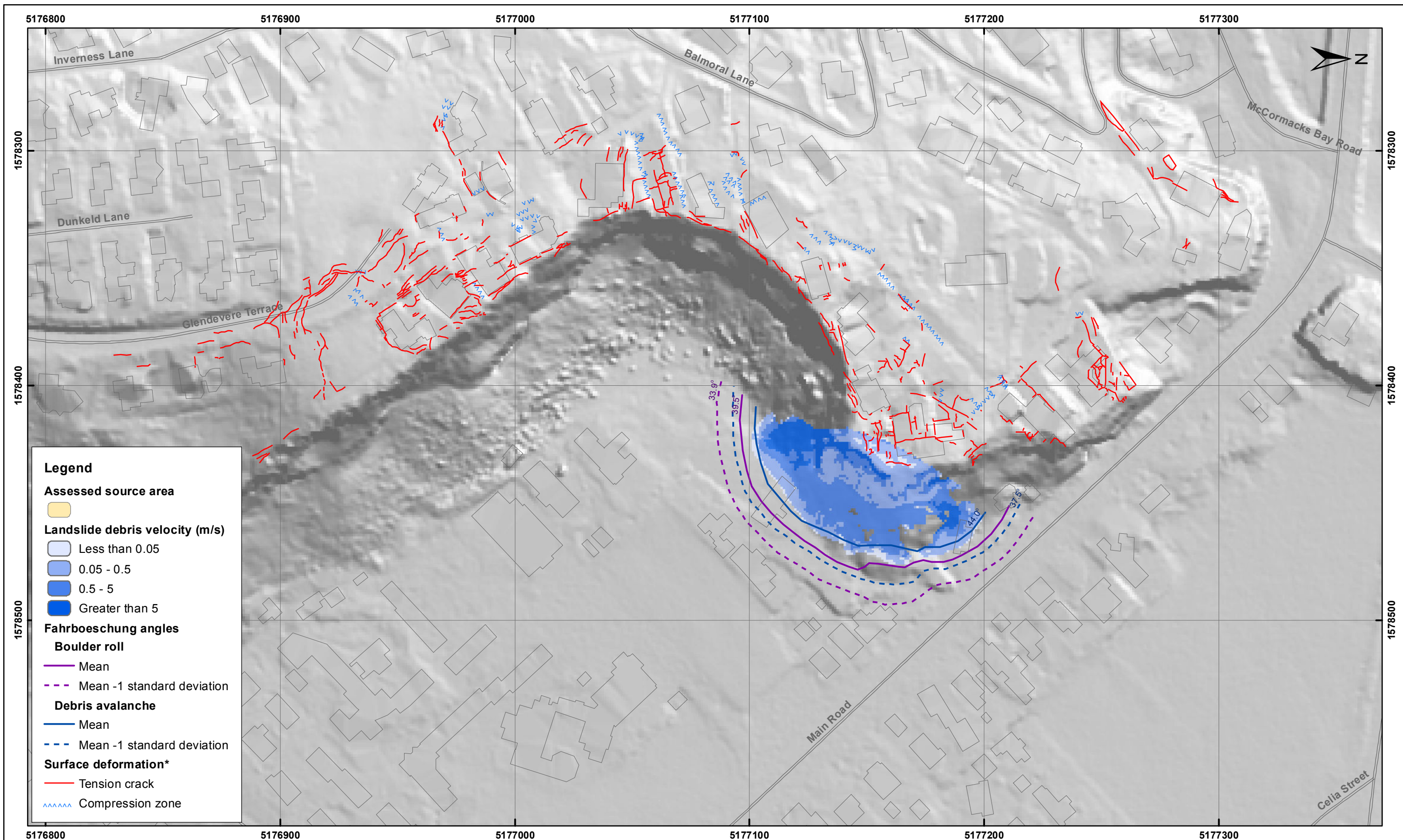
APPENDIX 8

Map 5

FINAL

REPORT:
CR2014/78

DATE:
August 2014



SCALE BAR: 0 50 100 m

EXPLANATION:
 * Taken from report CR2012/317
 Background shade model derived from NZAM post earthquake 2011c (July 2011) LiDAR survey resampled to a 1 m ground resolution. Roads and building footprints and types provided by Christchurch City Council (20/02/2012).
 PROJECTION: New Zealand Transverse Mercator 2000

DRW:
BL, WR

CHK:
CM, FDP



ESTIMATED LANDSLIDE RUNOUT VELOCITY
Source 2 - Lower Volume (3,700 m³)

Redcliffs - Port Hills
Christchurch

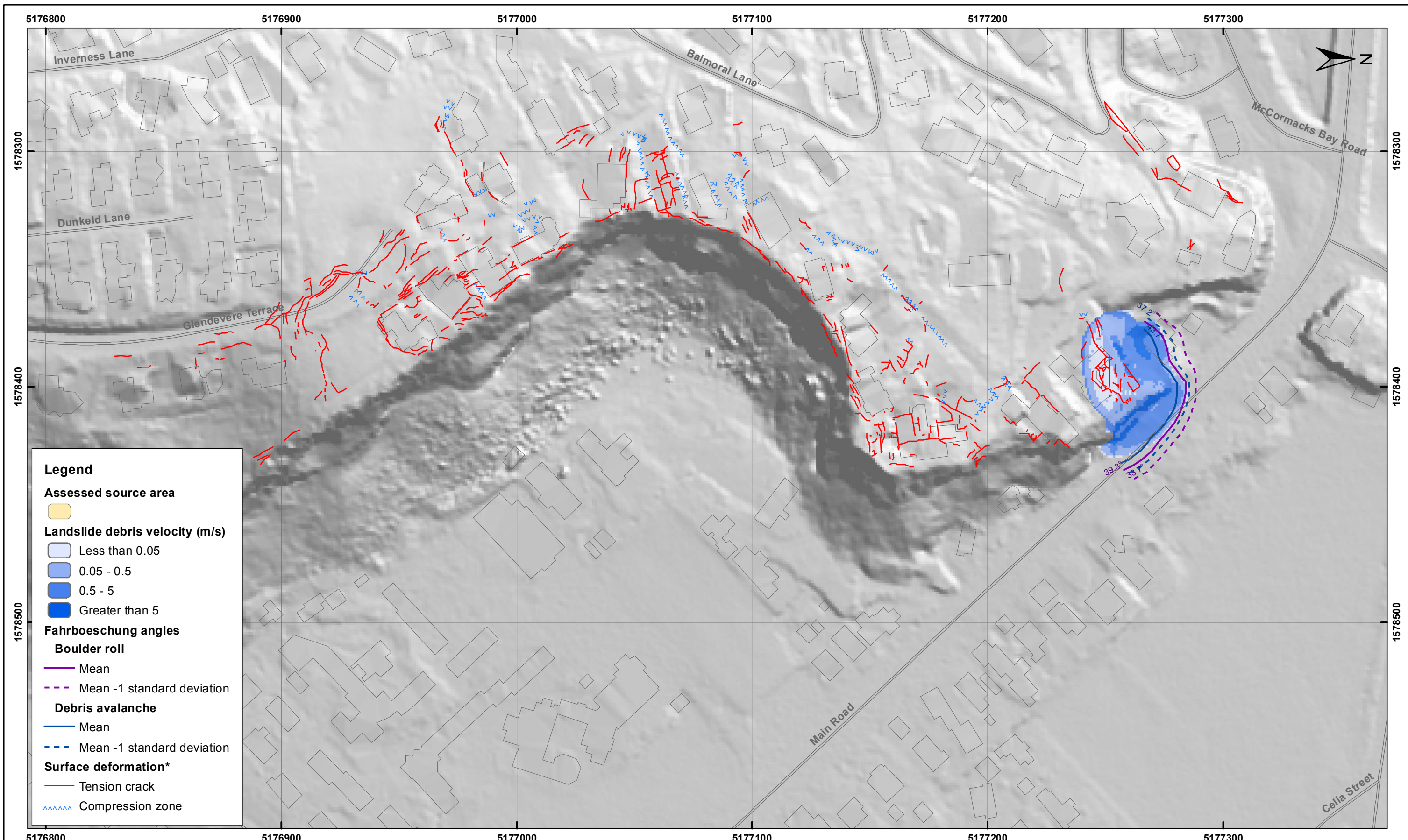
APPENDIX 8

Map 6

FINAL

REPORT:
CR2014/78

DATE:
August 2014



SCALE BAR: 0 50 100 m

EXPLANATION:
 * Taken from report CR2012/317
 Background shade model derived from NZAM post earthquake 2011c (July 2011) LiDAR survey resampled to a 1 m ground resolution. Roads and building footprints and types provided by Christchurch City Council (20/02/2012).
 PROJECTION: New Zealand Transverse Mercator 2000

DRW:
BL, WR

CHK:
CM, FDP



ESTIMATED LANDSLIDE RUNOUT VELOCITY
Source 3 - Upper Volume (4,300 m³)

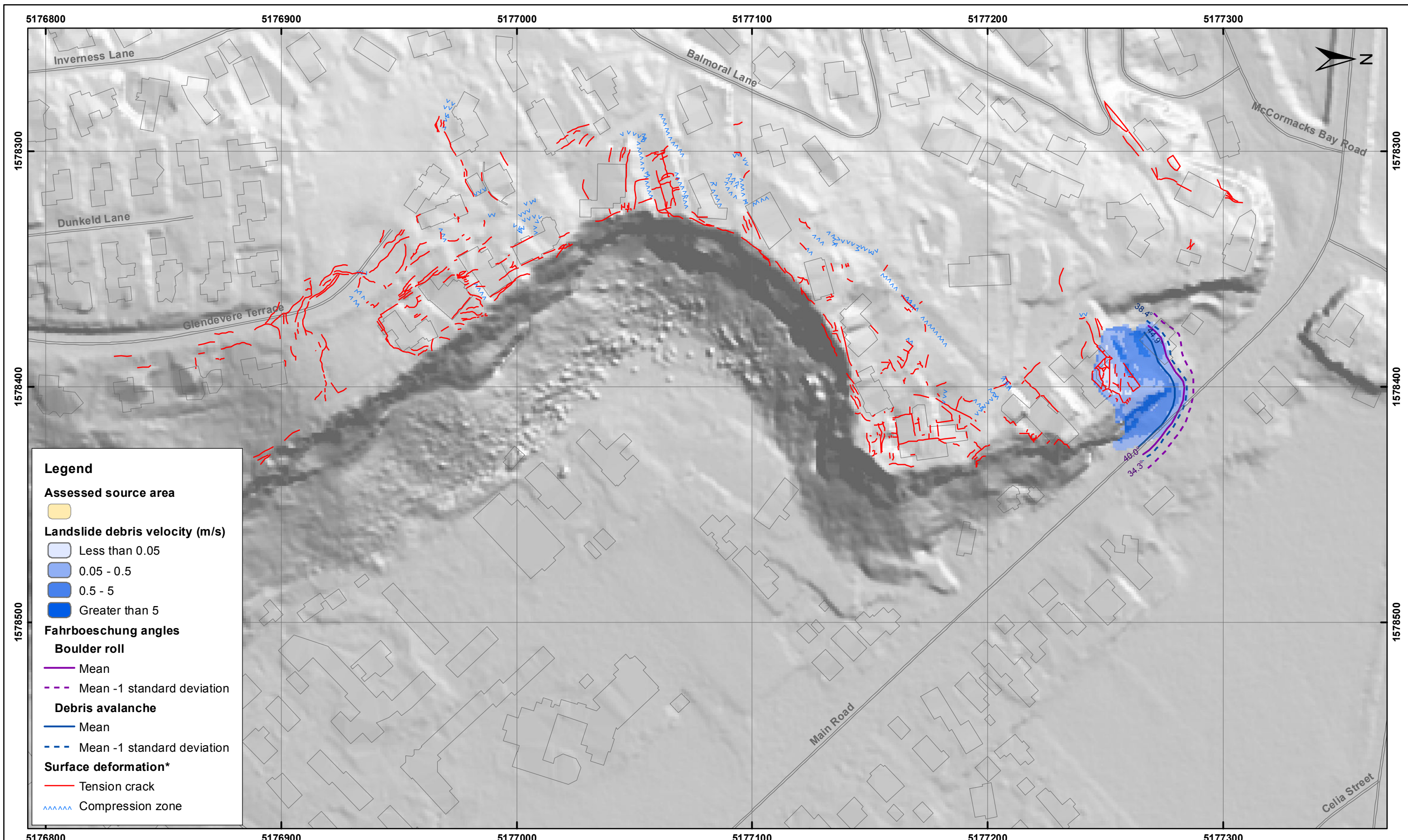
Redcliffs - Port Hills
Christchurch

APPENDIX 8

Map 7

FINAL

REPORT: CR2014/78 DATE: August 2014



SCALE BAR: 0 50 100 m

EXPLANATION:

* Taken from report CR2012/317

Background shade model derived from NZAM post earthquake 2011c (July 2011) LiDAR survey resampled to a 1 m ground resolution. Roads and building footprints and types provided by Christchurch City Council (20/02/2012).

PROJECTION: New Zealand Transverse Mercator 2000

DRW:
BL, WR

CHK:
CM, FDP



ESTIMATED LANDSLIDE RUNOUT VELOCITY
Source 3 - Middle Volume (2,500 m³)

Redcliffs - Port Hills
Christchurch

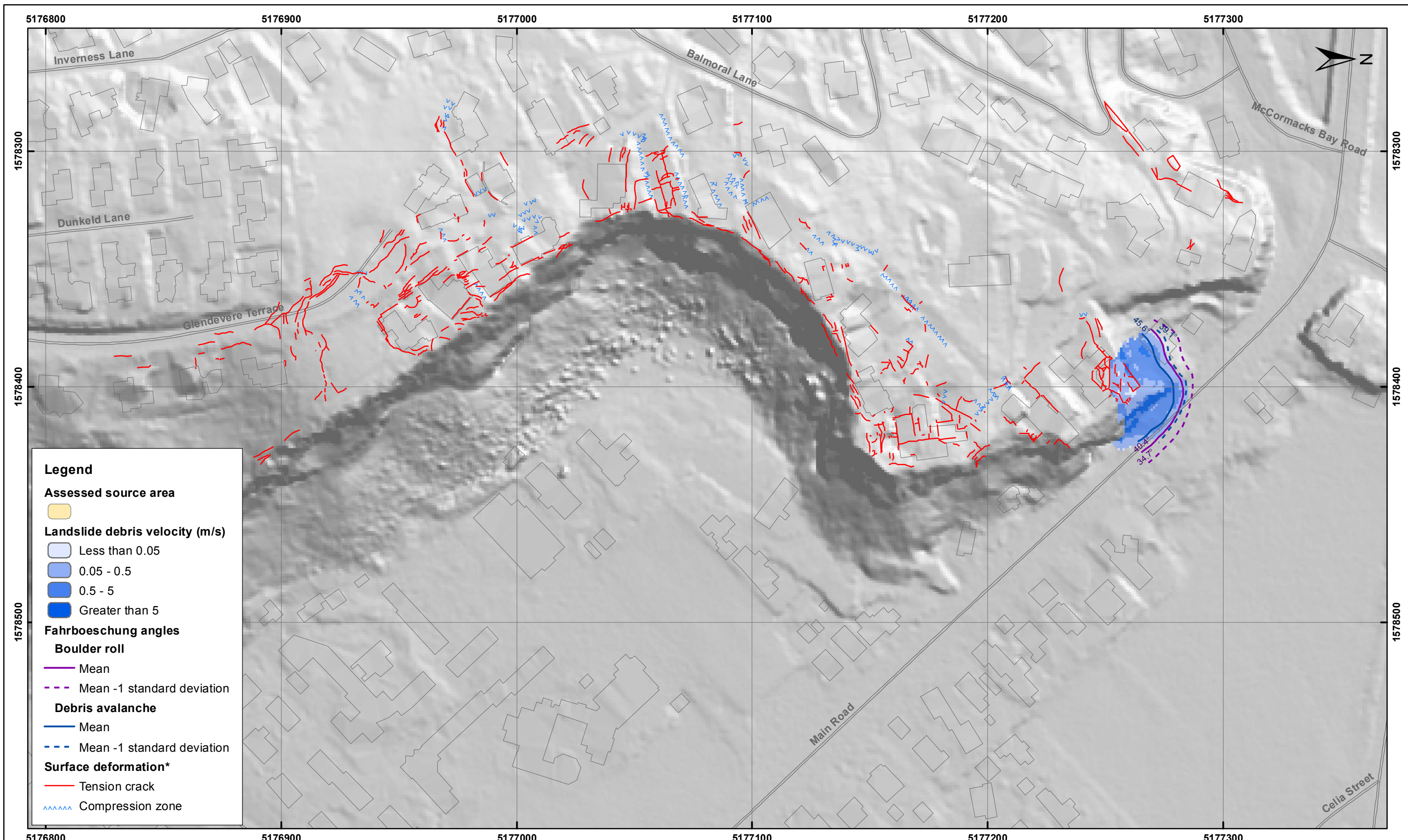
APPENDIX 8

Map 8

FINAL

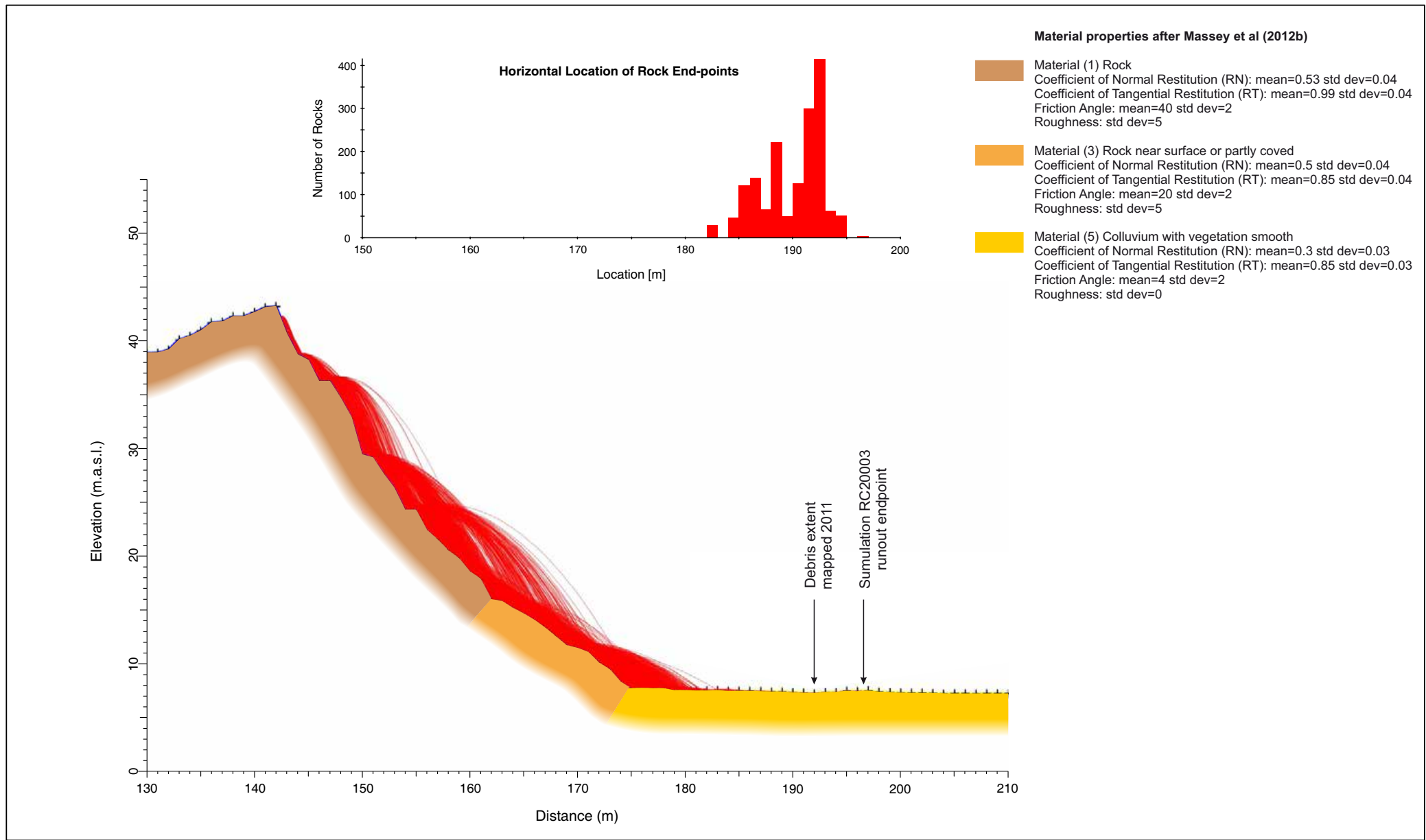
REPORT:
CR2014/78


DATE:
August 2014

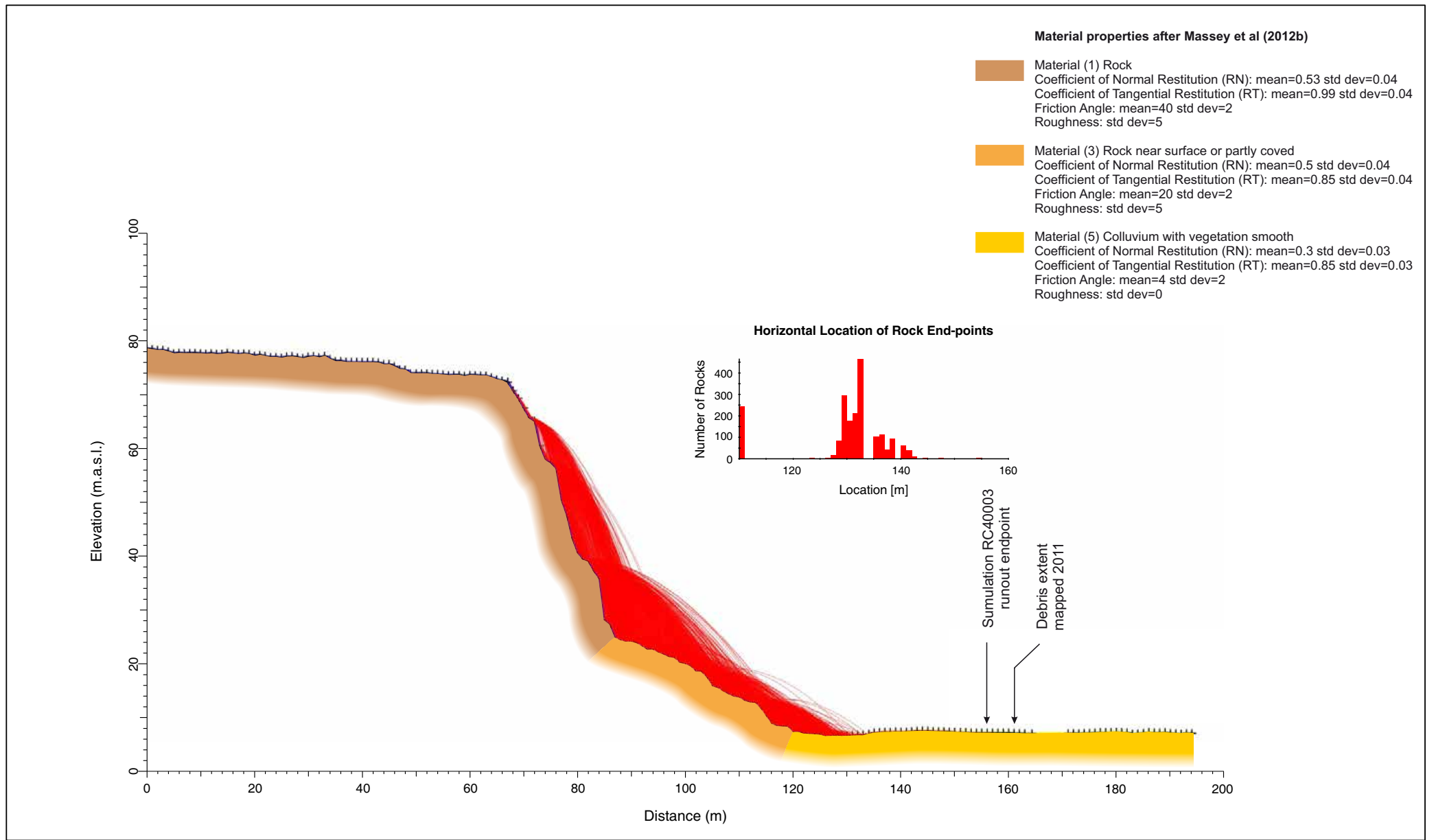



SCALE BAR: 0 50 100 m			ESTIMATED LANDSLIDE RUNOUT VELOCITY Source 3 - Lower Volume (1,800 m³)	APPENDIX 8	
EXPLANATION: * Taken from report CR2012/317 Background shade model derived from NZAM post earthquake 2011c (July 2011) LiDAR survey resampled to a 1 m ground resolution. Roads and building footprints and types provided by Christchurch City Council (20/02/2012). PROJECTION: New Zealand Transverse Mercator 2000	DRW: BL, WR CHK: CM, FDP			Redcliffs - Port Hills Christchurch	Map 9 FINAL REPORT: CR2014/78 DATE: August 2014

A9 APPENDIX 9: ROCFALL MODELLING RESULTS FOR CROSS-SECTIONS 2, 4 AND 6

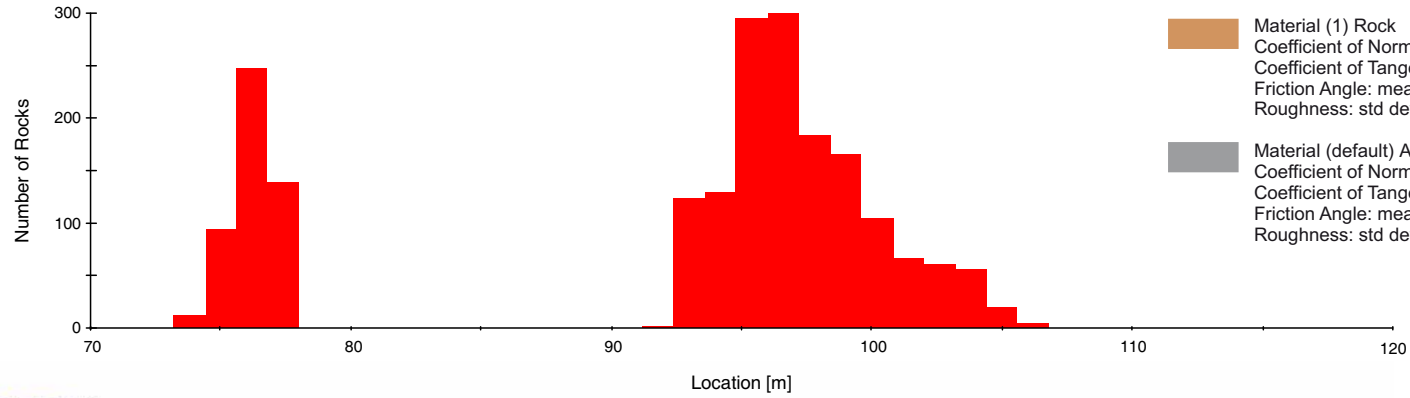


Input material parameters from Massey et al 2012b Number of rocks = 2000 Unit weight 27 KN/m ³ Cut of velocity 0.1m/sec Simulated rock mass 1,000kg (~0.3m ³)	DRW: PC		SECTION 2 RocFall® simulation RC20003		APPENDIX 9	
	CHK: CM/FDP		Redcliffs Christchurch		FINAL	
				REPORT: CR2014/78	DATE: August 2014	



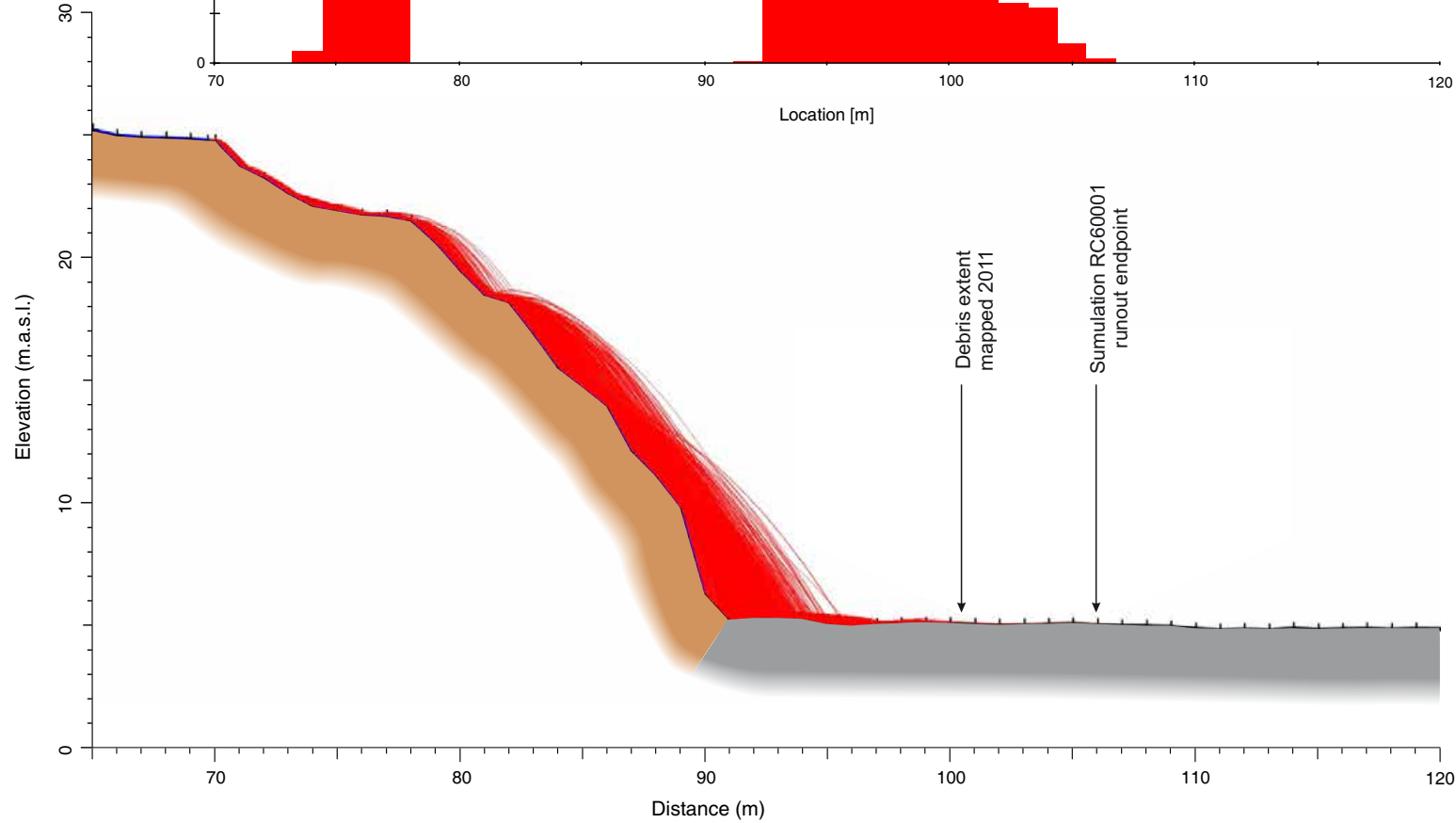
Input material parameters from Massey et al 2012b Number of rocks = 2000 Unit weight 27 KN/m ³ Cut of velocity 0.1m/sec Simulated rock mass 1,000kg (~0.3m ³)	DRW: PC		SECTION 4 RocFall® simulation RC40003		APPENDIX 9	
	CHK: CM/FDP		Redcliffs Christchurch		FINAL	
					REPORT: CR2014/78	DATE: August 2014

Horizontal Location of Rock End-points



Material properties after Massey et al (2012b)

- Material (1) Rock
 - Coefficient of Normal Restitution (RN): mean=0.53 std dev=0.04
 - Coefficient of Tangential Restitution (RT): mean=0.99 std dev=0.04
 - Friction Angle: mean=40 std dev=2
 - Roughness: std dev=5
- Material (default) Asphalt
 - Coefficient of Normal Restitution (RN): mean=0.5 std dev=0.04
 - Coefficient of Tangential Restitution (RT): mean=0.9 std dev=0.04
 - Friction Angle: mean=30 std dev=2
 - Roughness: std dev=0



Input material parameters from Massey et al 2012b
 Number of rocks = 2000
 Unit weight 27 KN/m³
 Cut of velocity 0.1m/sec
 Simulated rock mass 1,000kg (~0.3m³)

DRW:
PC
 CHK:
CM/FDP



SECTION 6
RocFall® simulation RC60001

Redcliffs
Christchurch

APPENDIX 9

FINAL

REPORT:
CR2014/78

DATE:
August 2014

A10 APPENDIX 10: STERONET KINEMATIC ANALYSIS OF REDCLIFFS DISCONTINUITY DATA

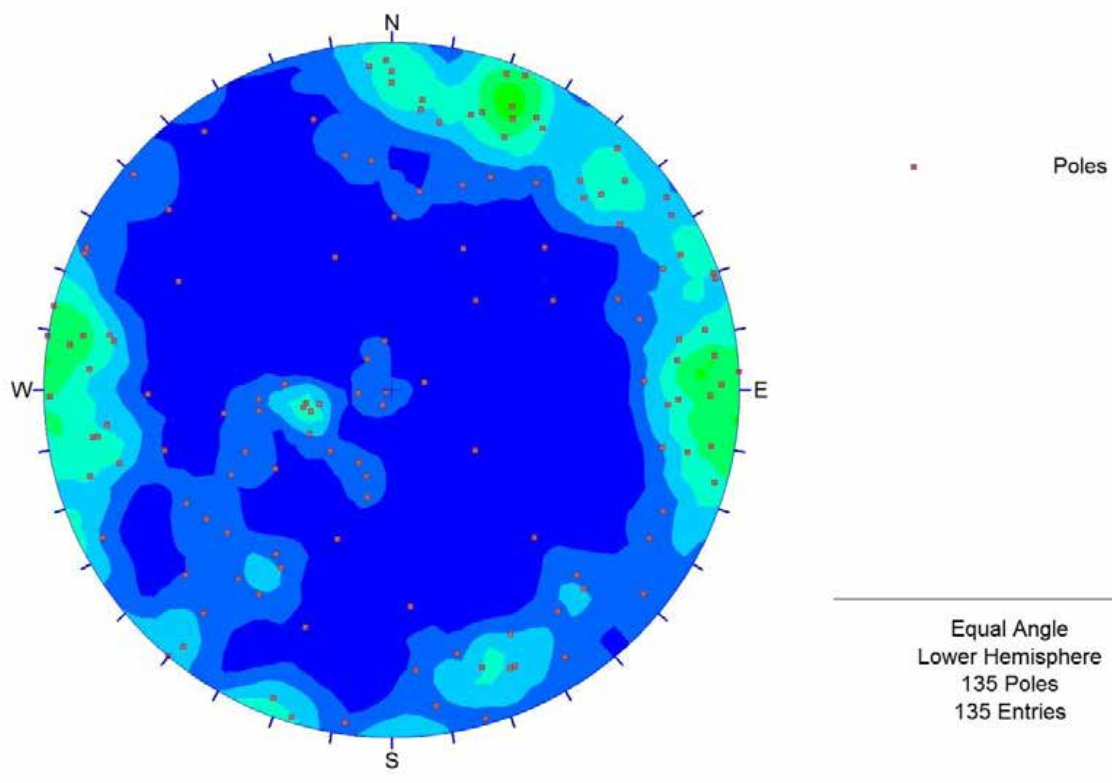
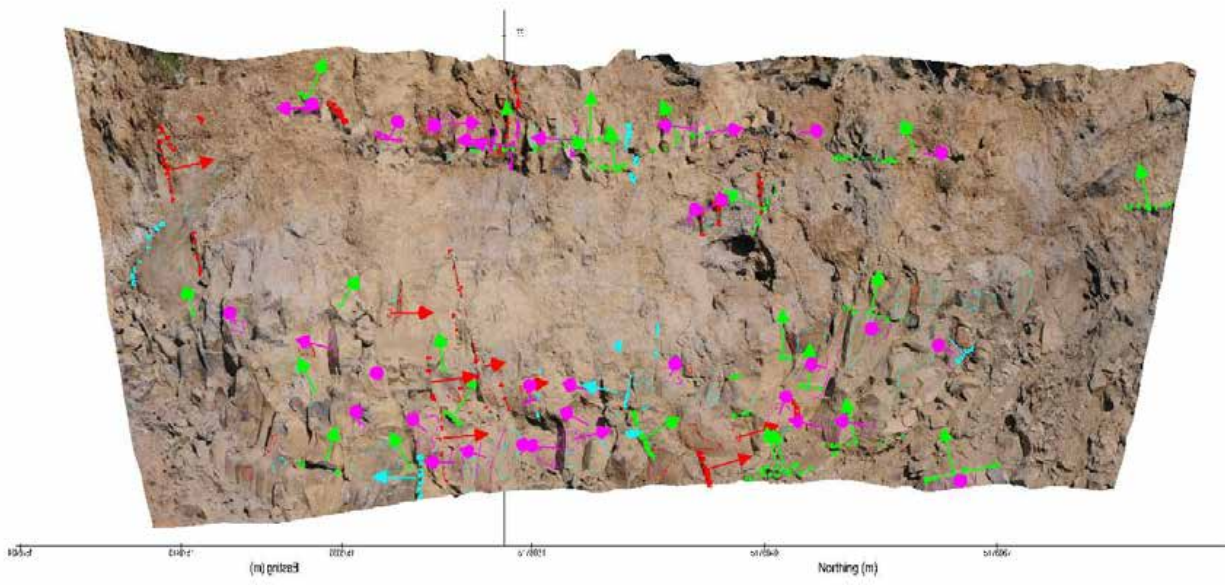
The methods adopted to derive the results in Appendix 10 are described in:

Brideau, M-A., Massey, C.I., Archibald, G.C., Jaboyedoff, M. 2012 Terrestrial photogrammetry and LiDAR investigation of the cliffs associated with the seismically triggered rockfalls during the February and June 2011 Christchurch earthquakes. p. 1179–1185 In: Eberhardt, E.B., Froese, C., Turner, K., Leroueil, S., Landslides and engineered slopes: protecting society through improved understanding: proceedings of the 11th International and 2nd North American Symposium on Landslides and Engineered Slopes, Banff, Canada, 3–8 June 2012. CRC Press.

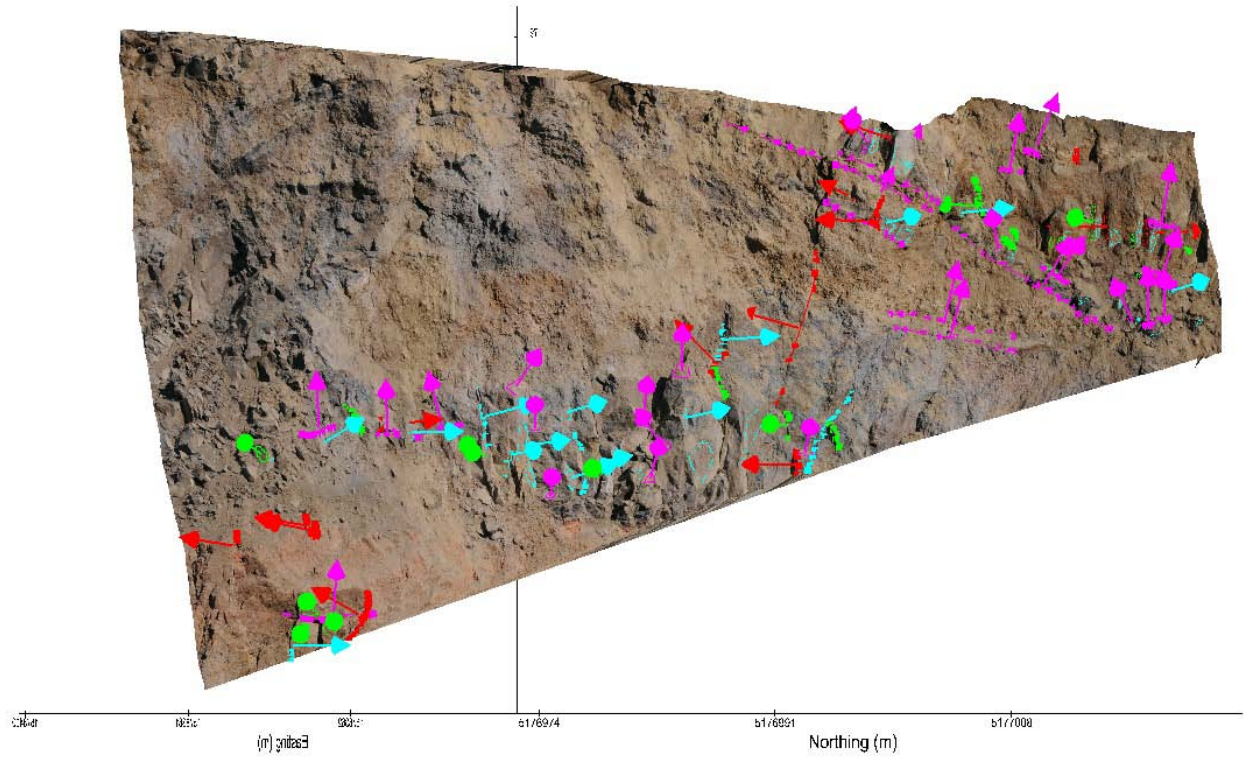


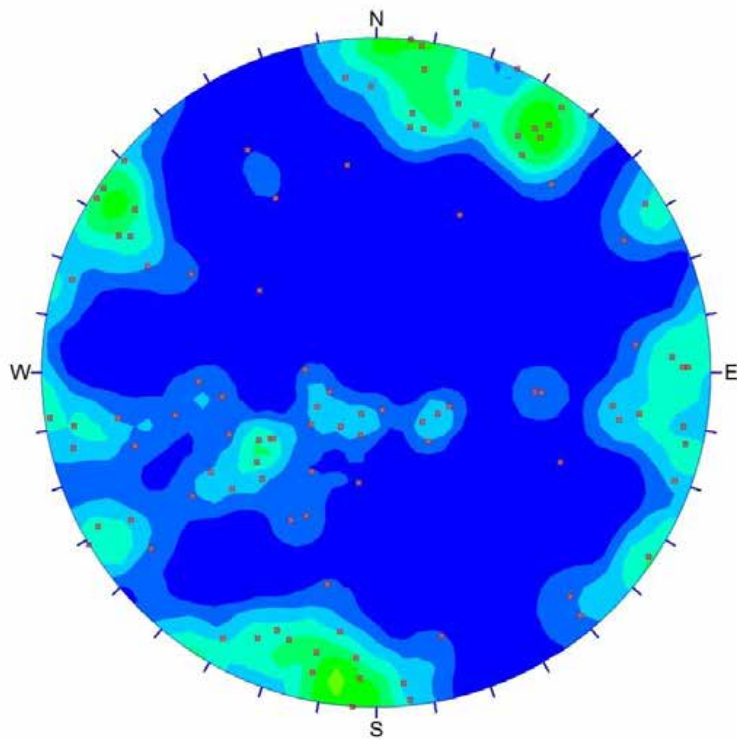
Redcliffs School image pair 1: Structural data – July 19 2011





Redcliffs School image pair 2: Structural data – July 19 2011



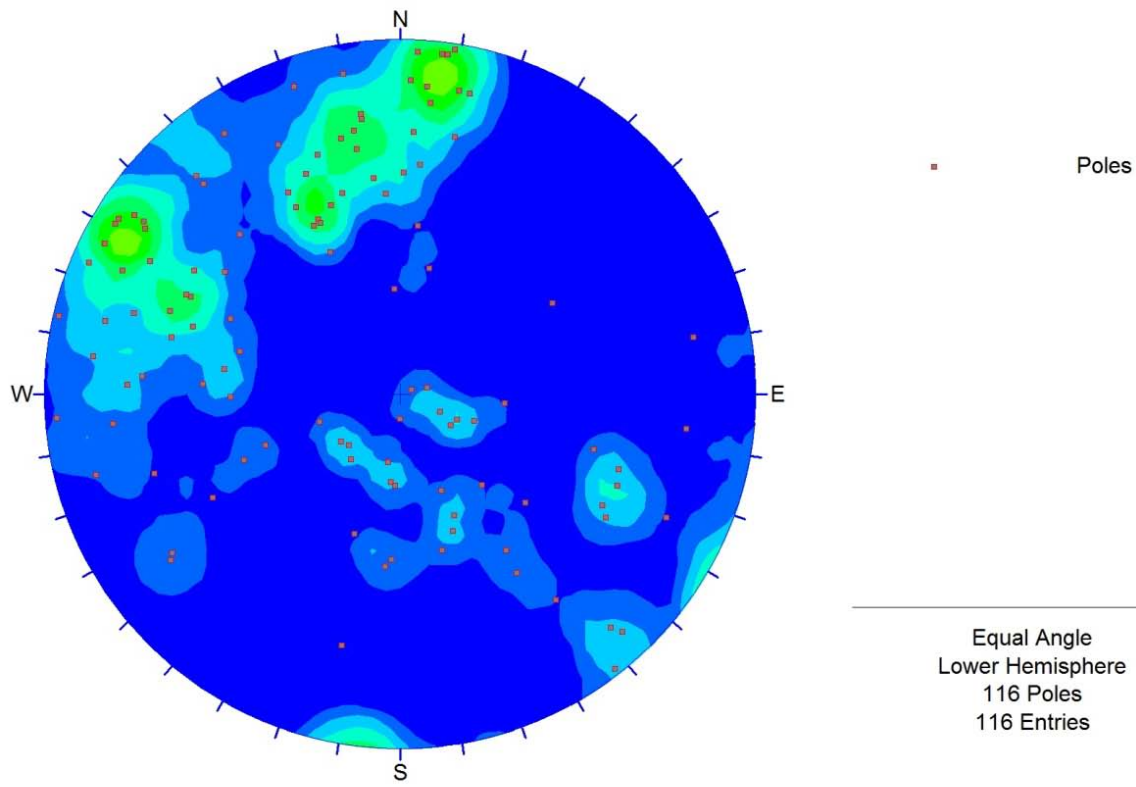
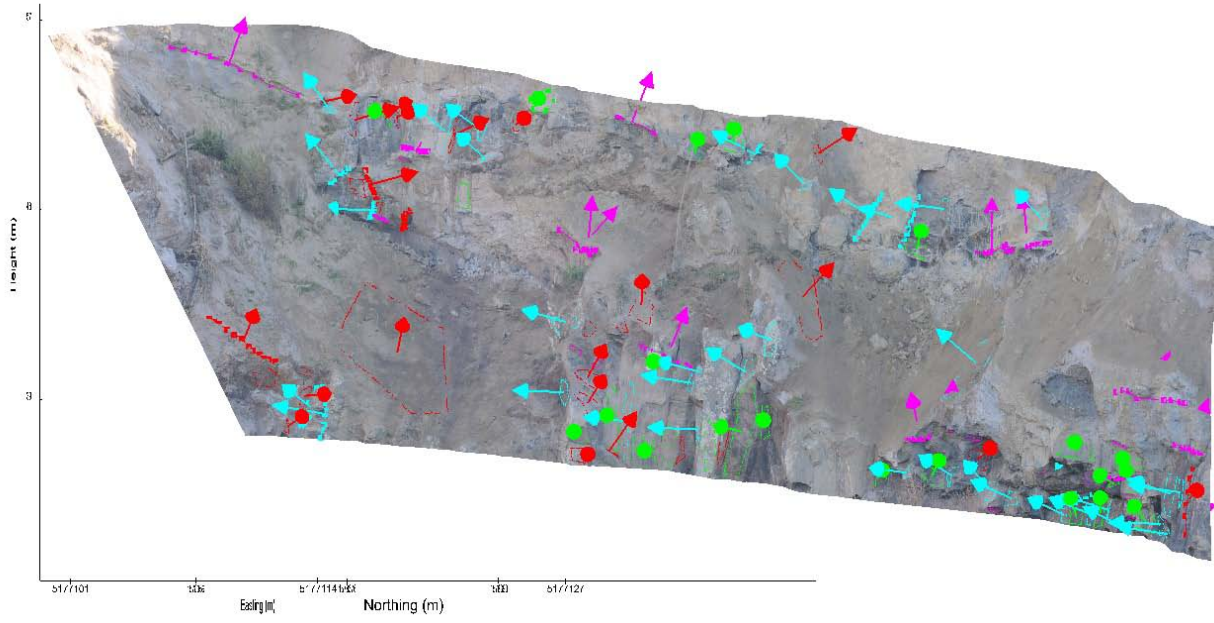


■ Poles

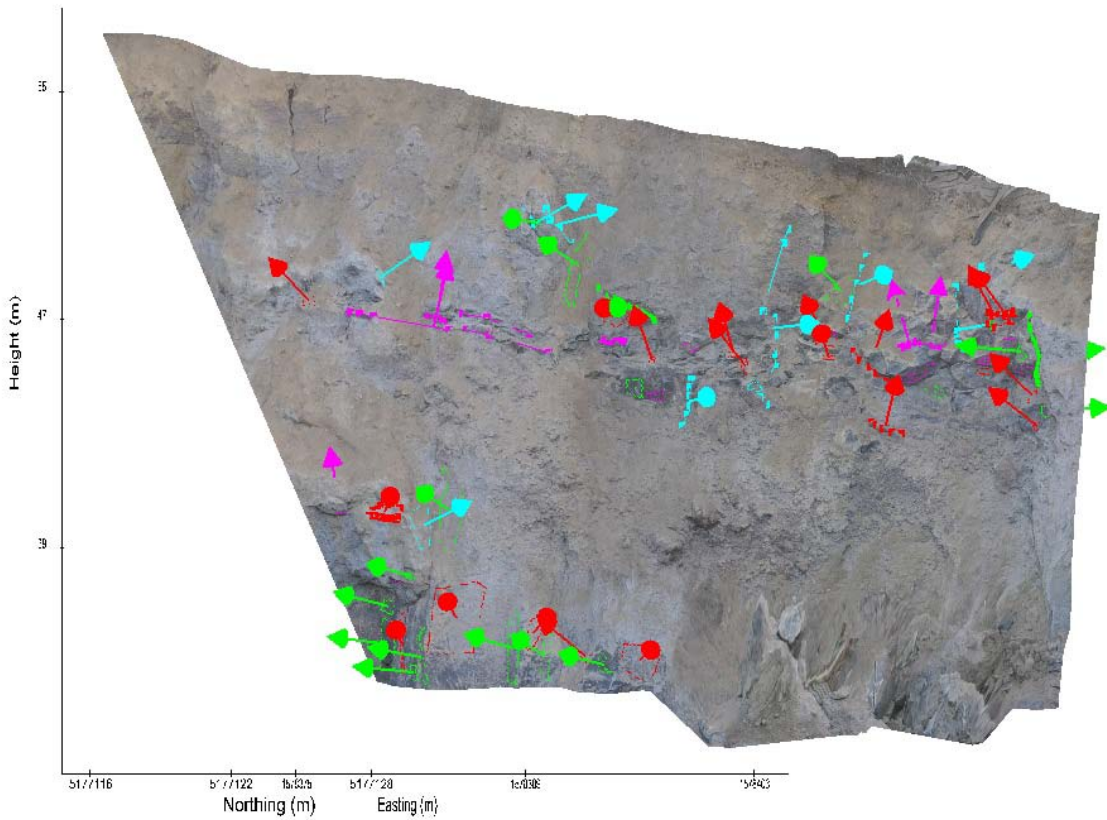
Equal Angle
Lower Hemisphere
103 Poles
103 Entries

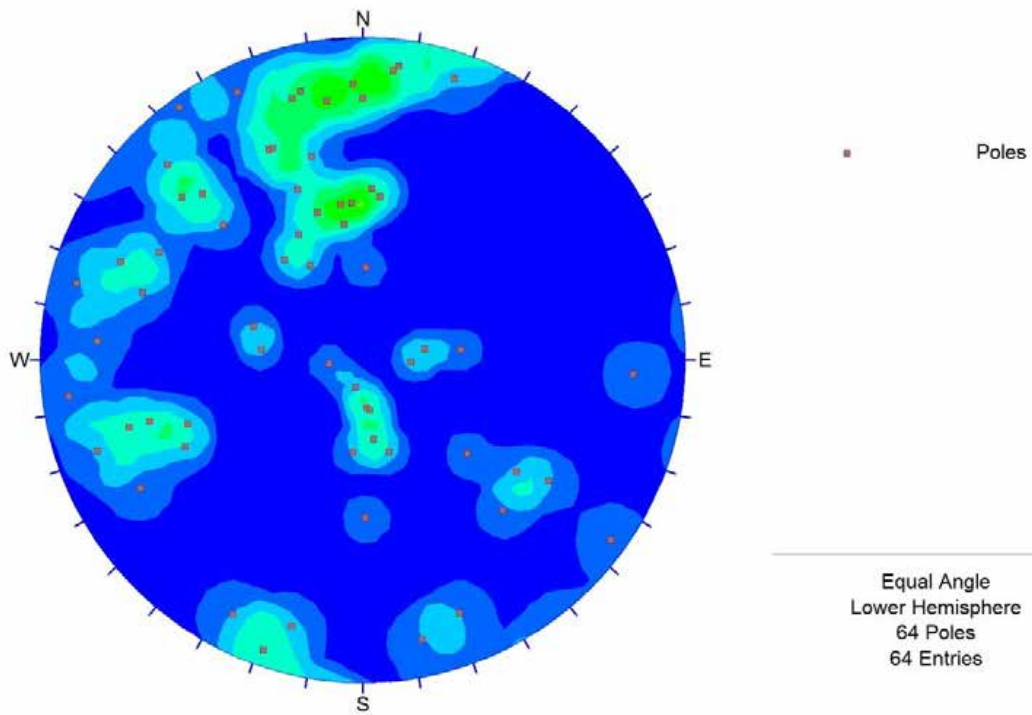
Redcliffs School image pair 3: Structural data – July 19 2011





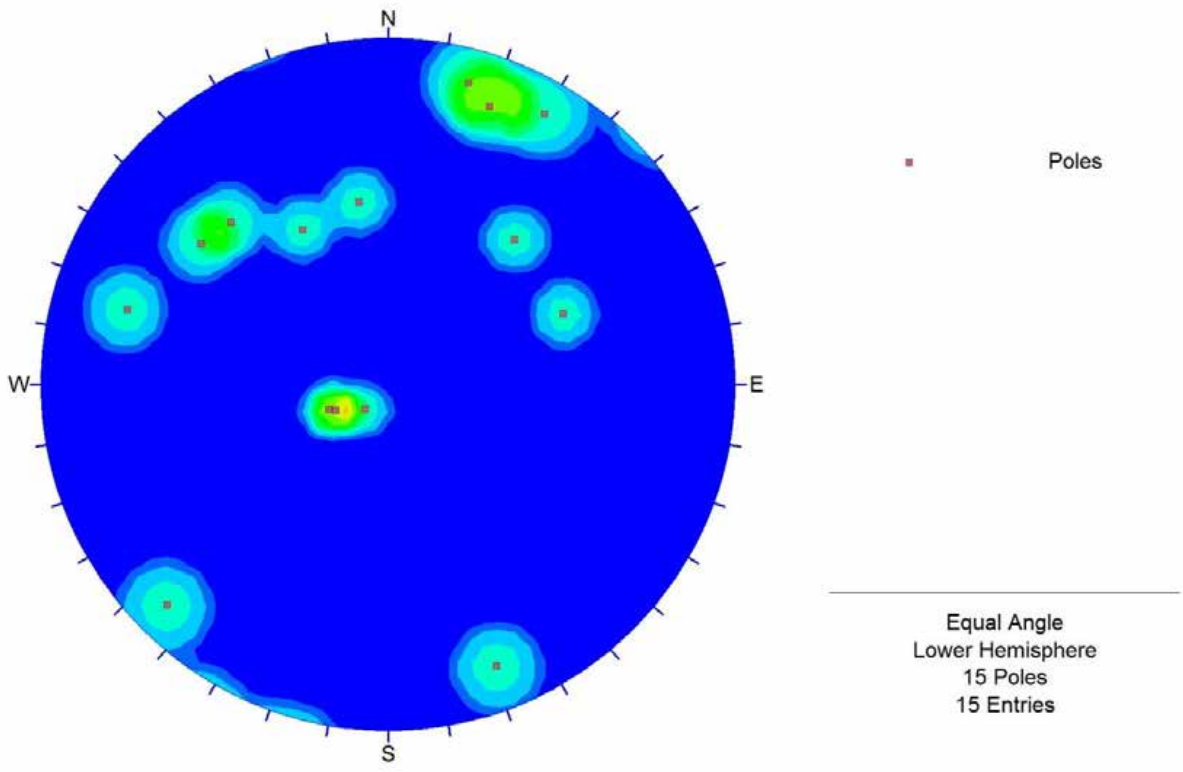
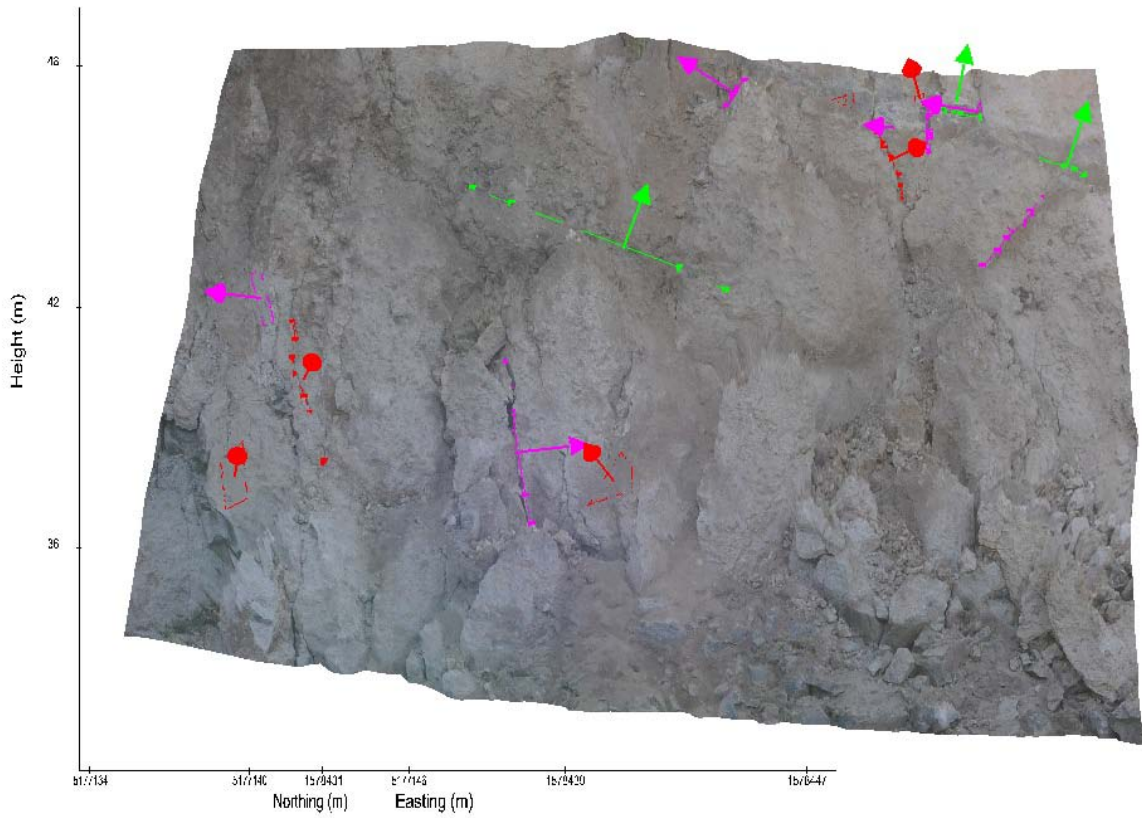
Redcliffs School image pair 4: Structural data – July 19 2011



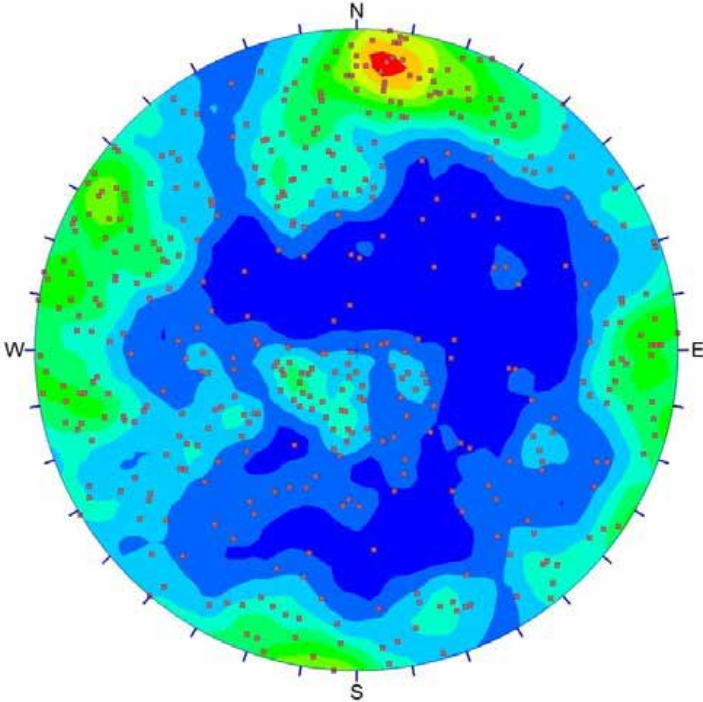


Redcliffs School image pair 5: Structural data – July 19 2011





Redcliffs School: All image pairs combined together, July 19 2011

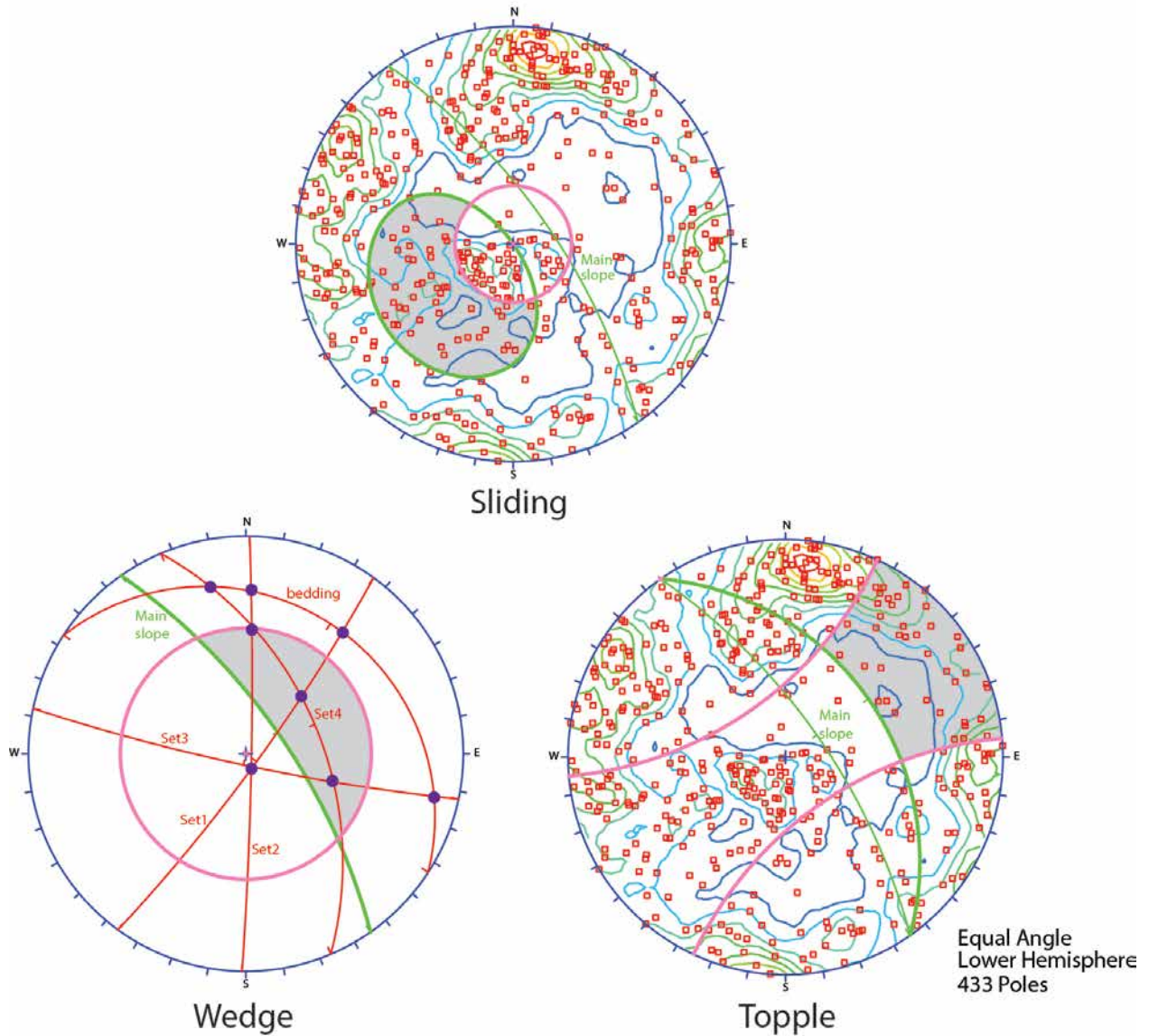


• Poles

Equal Angle
Lower Hemisphere
433 Poles
433 Entries

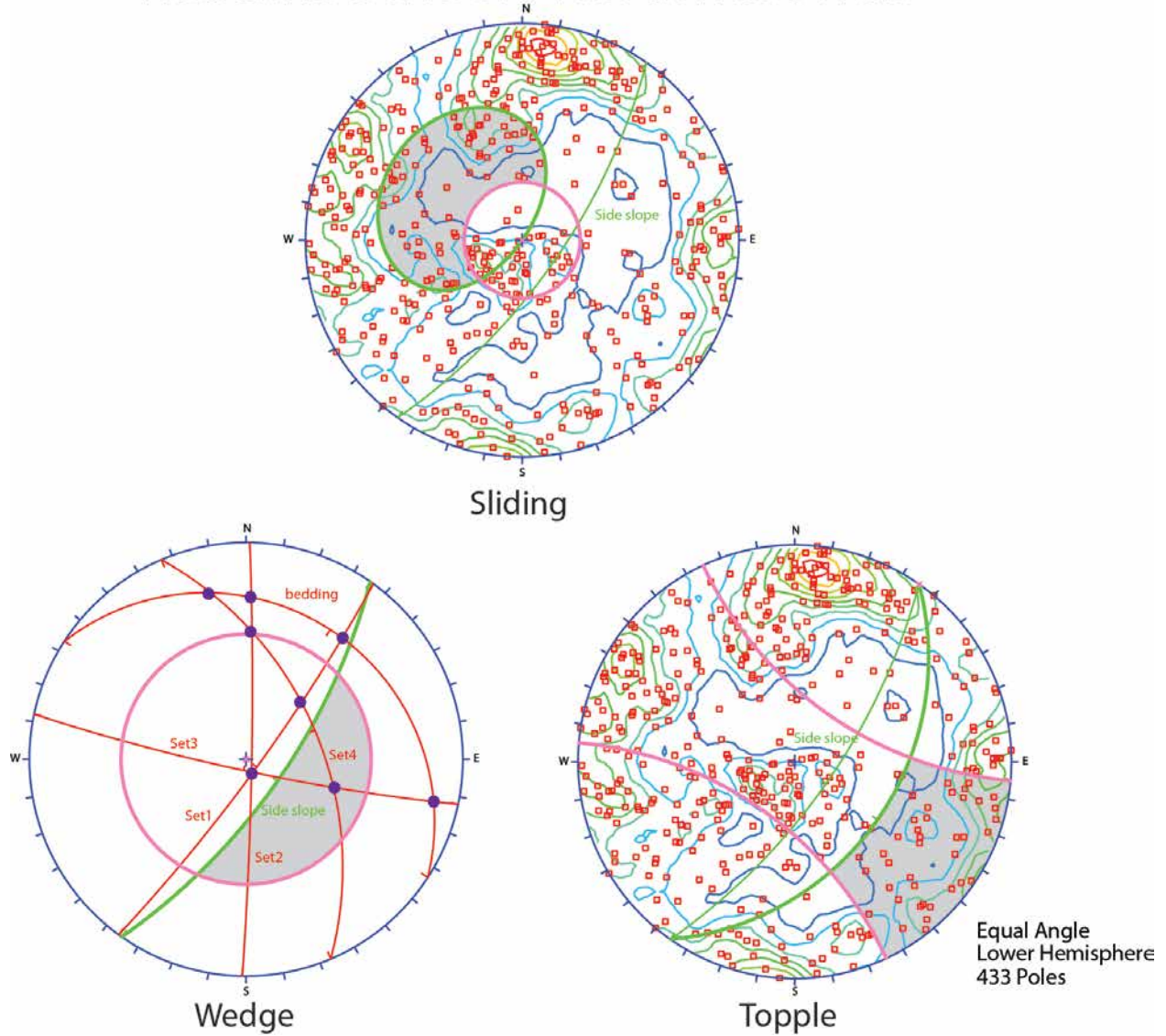
Preliminary kinematic analysis of the Redcliffs School. Assumed slope of 70°/055° (dip/dip direction) and friction angle of 30°.

Redcliffs School - Southwest wall



Preliminary kinematic analysis of the Redcliffs School. Assumed slope of 70°/125° (dip/dip direction) and friction angle of 30°.

Redcliffs School - Northwest wall





www.gns.cri.nz

Principal Location

1 Fairway Drive
Avalon
PO Box 30368
Lower Hutt
New Zealand
T +64-4-570 1444
F +64-4-570 4600

Other Locations

Dunedin Research Centre
764 Cumberland Street
Private Bag 1930
Dunedin
New Zealand
T +64-3-477 4050
F +64-3-477 5232

Wairakei Research Centre
114 Karetoto Road
Wairakei
Private Bag 2000, Taupo
New Zealand
T +64-7-374 8211
F +64-7-374 8199

National Isotope Centre
30 Gracefield Road
PO Box 31312
Lower Hutt
New Zealand
T +64-4-570 1444
F +64-4-570 4657